Department of Chemical Engineering

Catalyst Development for Higher Alcohol Synthesis (HAS)

Min Ao

This thesis is presented for the Degree of

Doctor of Philosophy

of

Curtin University

March 2017

Declaration

To the best of my knowledge and belief this thesis contains no material previously published by any other person except where due acknowledgment has been made.

This thesis contains no material which has been accepted for the award of any other degree or diploma in any university.

Signature:.....

Date:2017/03/30.....

To my beloved family

Abstract

The Fischer-Tropsch (F-T) technology is a proven technique for the conversion of syngas to valuable synthetic fuels and chemicals. Higher alcohol — containing 2 or more carbon atoms — represents a very attractive product class of the F-T synthesis and can be widely used in a large array of applications. It is recognised that a successful higher alcohol synthesis (HAS) process requires a highly selective and stable catalyst. HAS catalysts have thus been studied intensively over the past three decades by many industrial and academic researchers. However, none of the HAS catalysts or processes developed to date have been sufficiently active and/or selective to motivate industrial commercialization of HAS *via* the F-T process. Perovskite oxides (ABO_3), particularly $LaCoO_3$, have attracted increasing interest for HAS in the last ten years, due to their unique structure and flexibility in their design and preparation. Many promising results were reported recently by different researchers, unfortunately, the higher alcohols' yields were still too low for any industrial application.

The present study aims to develop stable perovskite catalysts with high activity and selectivity for HAS from syngas. In addition, this research also dedicates to providing insights into the effect of partial substitution of the A- and/or B-site in the perovskite catalyst on the catalyst properties and catalytic performances, using $LaCoO_3$ as model catalyst.

Firstly, this research reported the effect of strontium substitution at the A-site of $LaCoO_3$ perovskite in the F-T synthesis for the first time. It was found that strontium substitution improved $La_{1-x}Sr_xCoO_3$ catalyst's reducibility and increasing strontium substitution beyond a threshold of $x=0.1$ had an inverse effect on the catalytic performance in the syngas conversion. For $x\leq0.1$, the catalysts exhibited a stable rhombohedral structure, which led to a good dispersion of active centre of Co^0 during the reduction process, and displayed a high catalytic activity. For $x>0.1$, the catalyst structure was gradually changed from a rhombohedral to a less stable cubic structure, and led to Co^0 sintering, as well as the formation of inactive $SrCO_3$ during the reaction. The turnover frequency of cobalt atom in the F-T reaction decreased significantly with increasing strontium substitution levels due to the loss of active catalyst surface. Substitution at the A site improved syngas conversion, but no increase on higher

alcohol selectivity was observed. It was also found that the strontium substitution appeared to favour the Boudouard reaction at the beginning of the induction period.

Secondly, this research evaluated the performance of different nickel substitution levels at the B-site of $La_{0.9}Sr_{0.1}Co_{1-y}Ni_yO_3$ perovskite catalysts for HAS from syngas. It was found that nickel substitution also improved the catalyst's reducibility, CO conversion and higher alcohol selectivity. We believe the synergistic effects between the two metal species in the Co-Ni alloy were responsible for the performance improvement. That is, the Co-Ni alloy showed a bi-functionality — chain propagation, leading to the formation of the hydrocarbon precursors, and the subsequent CO insertion, under hydrogenation condition. With high nickel substitution levels (y=0.5), metal nickel also formed and existed outside of the perovskite framework. The extra-lattice nickel species, reduced to metallic nickel, favoured the methanation reaction rather than the formation of higher alcohols. The $La_{0.9}Sr_{0.1}Co_{0.9}Ni_{0.1}O_3$ catalyst showed highly dispersed bimetallic Co-Ni alloy and less extra-lattice Ni^0 phase. This catalyst also demonstrated the highest selectivity toward higher alcohol formation. It was also found that a homogeneous distribution of the bi-metallic Co-Ni alloy is the key factor for both high higher alcohol selectivity and yield in HAS. The reaction temperature was also proven to be a critical factor affecting both alcohol selectivity and yield.

Thirdly, tri-metallic Co-Ni-Cu-based $La_{0.9}Sr_{0.1}Co_{0.8}Ni_{0.1}Cu_{0.1}O_3$ (LSCNC) perovskite oxides were used as catalysts for further investigations into the synergistic effect of the metals at the B-site of perovskites for HAS. With the addition of copper, the CO adsorption ability of the catalyst was reduced, which led to a lower CO conversion and lower total alcohol yield compared to that of Co-Ni-based catalyst ($La_{0.9}Sr_{0.1}Co_{0.9}Ni_{0.1}O_3$) for HAS and catalyst decay occurred beyond 310°C. However, the synergetic effect between the three metals had a positive effect on increasing ethanol selectivity, indicating the tri-metallic LSCNC catalyst had the potential to produce $C_{2+}OH$ at optimal conditions.

The effect of alkali promoters (sodium and potassium) were also studied carefully, and catalytic stability tests were carried out over the LSCNC catalyst. The addition of potassium improved the higher alcohol selectivity and yield in the F-T process significantly. Moreover, K-promoted catalyst showed excellent reaction stability for HAS from syngas, with no deactivation observed after more than 240 h time on stream,

suggesting that potassium is not only a promoter for HAS but also a catalyst stabiliser. In addition, the effect of reaction conditions were also investigated in this study: catalytic activity of K-LSCNC catalyst increased with reaction temperature, and a H_2/CO ratio of 2 was the optimal ratio for higher alcohol formation.

In summary, this work not only presents the development of a series of substituted $LaCoO_3$-based perovskite catalysts for HAS *via* the F-T process, but also proposed a direction in designing perovskite catalysts tailored for the selective production of higher alcohols. The findings in this study can significantly contribute to the future development of perovskite catalysts, HAS process, and other related fields.

Acknowledgements

I would like to express my most enthusiastic gratitude to my principal supervisor, Dr Gia Hung Pham, for providing me the precious opportunity for this research and for his utmost guidance, training, patience, persistent support as well as devotion in supervision during the course of my research. His knowledge, intelligence, and passion for science have always inspired and guided me to move forward, leading to the completion of this PhD project.

Equally, I owe my sincere gratitude to my co-supervisor Dr Valérie Sage from CSIRO for her insightful comments and immense help in every detail in my experiment and writing. I am very thankful for her advice and past experiences that she shared, which have been very valuable to me.

I would also like to thank my co-supervisor, Prof Vishnu Pareek, for all the kind suggestions and supports of my research and career.

Thank you very much for Dr Gia Hung Pham, Dr Valérie Sage, and Prof Vishnu Pareek for their great guidance and warm encouragement. It is a great honour to be one of their students and be part of their amazing research group. Without their help, I would not be able to complete my PhD and thesis.

I gratefully acknowledge the Curtin International Postgraduate Research Scholarship (CIPRS) from Curtin University and partial financial and facility support from CSIRO for making my PhD study possible.

I am thankful to the colleagues in CSIRO for their ongoing support and help. Special thanks go to Dr Nick Burk and Dr Yunxia Yang for reviewing the thesis manuscripts and giving many useful comments. I also thank Mr Philip Hazewinkel, Dr Tejas Bhatelia, Dr Laure Braconnier, and Dr Yong Sun for teaching me a lot in the operation of the Syncat Facility to allow me to gain a better understanding of the reaction process. I also thank Dr Seng Lim, Dr Jim Patel, Dr Liangguang Tang, Dr Chaoen Li, Dr Doki Yamaguchi, Dr Ken Chiang and all the other members in Energy Resource Processing Group for helping review my presentations and giving suggestions. I also appreciate the help from Mr Michael Verrall, who provides invaluable technical assistance in the operation of the XRD and SEM equipment.

In addition, I would like to give my gratitude to the Curtin technician team, Dr Roshanak Doroushi, Mr Xiao Hua, Mr Yu Long, Dr Guanliang Zhou, Ms Karen Haynes, Mr Jason Wright, Mr Araya Abera, Mr Andrew Chan, Ms Ann Carroll, Ms Melina Miralles and Ms Anja Werner for their help and technical support in the lab.

I am also thankful to my friends and colleagues, Mingming, Xin, Fenny, Stacey, Wenran, Ping, Meiwen, Wenjie, Chen, Ting, Yeewen, Junfang, Xiaoguang, Chao, Eugene, Boon, Xujun, Sicheng, Yash, Xiaochen, Chi, Huayang, Hoang, and Nabil. Thank you very much for all your help during my experiments, moral supports and encouragement you all gave me. I cannot imagine my life without you!

And last, but not the least, I would like to express my deepest love to my parents. I truly thank you for your unconditional love and tremendous supports. I cannot go so far without your constant and eternal encouragement. To my husband and best friend, Tianyuan, thank you for being there and taking care of me in every way possible. I'm very lucky to have you in my life. I love you all dearly.

List of Publications

Published Paper:

1. **Min Ao**, Gia Hung Pham, Valérie Sage, Vishnu Pareek, Structure and activity of strontium substituted $LaCoO_3$ perovskite catalysts for syngas conversion. *Journal of Molecular Catalysis A: Chemical* 2016, 416, 96–104.
2. **Min Ao**, Gia Hung Pham, Valérie Sage, Vishnu Pareek, Selectivity enhancement for higher alcohol product in Fischer-Tropsch synthesis over nickel-substituted $La_{0.9}Sr_{0.1}CoO_3$ perovskite catalysts. *Fuel* 2017, 206, 390-400.

Manuscripts in Preparation:

3. **Min Ao**, Gia Hung Pham, Valérie Sage, Vishnu Pareek, Catalytic activity and alkali promoter effect of tri-metallic $La_{0.9}Sr_{0.1}Co_{0.8}Ni_{0.1}Cu_{0.1}O_3$ perovskite catalyst for higher alcohol synthesis from syngas (**In preparation**).

Conferences:

4. **Min Ao**, Gia Hung Pham, Valérie Sage, Vishnu Pareek, Effect of strontium substitution on structure and reduction property of $LaCoO_3$ perovskite catalyst. Chemeca 2014: 28 Sept – 01 Oct 2014, Perth, Australia (**Oral presentation; "*The Chemeca 2014 Prize for Best Student Paper*"**).
5. **Min Ao**, Gia Hung Pham, Valérie Sage, Vishnu Pareek, Behaviour of low Sr-substituted $La_{1-x}Sr_xCoO_3$ perovskite catalyst during induction period in syngas conversion. 11^{th} Natural Gas Conversion Symposium: 6-9 June 2016, Tromsø, Norway (**Poster**).
6. **Min Ao**, Gia Hung Pham, Valérie Sage, Vishnu Pareek, Sr-substituted $La_{1-x}Sr_xCoO_3$ perovskite catalysts for syngas conversion. The 1^{st} Australia-Japan Symposium on Carbon Resource Utilisation: 27-30 November 2016, Melbourne, Australia (**Poster**).

Table of Contents

List of Figures

List of Tables

List of Abbreviations

AC	Active carbons
AMS	Alkali-doped molybdenum sulphide
ASF	Anderson-Schulz-Flory
BET	Brunauer-Emmett-Teller
BPC	Back pressure controller
Bpd	Barrels per day
Btu	British thermal units
$C_{2+}OH$	Higher alcohols including ethanol
C atom %	Carbon atom percentage
CNT	Carbon nanotubes
CSIRO	Commonwealth Scientific and Industrial Research Organisation
DSC	Differential scanning calorimetry
FCC	Face-centred cubic
FID	Flame ionization detector
F-T	Fischer-Tropsch
GC/MS	Gas chromatography/ mass spectroscopy
GHSV	Gas hourly space velocity
GTL	Gas-to-liquids
HAS	Higher alcohol synthesis
HT	High-temperature
ICP-OES	Inductively coupled plasma-optical emission spectroscopy

I.D.	Inner diameter
IFP	Institut Français du Pétrole
JCPDS-ICDD	Joint Committee on Powder Diffraction Standards- International Centre for Diffraction Data
LT	Low-temperature
LNG	Liquefied natural gas
LSCN	$La_{0.9}Sr_{0.1}Co_{0.9}Ni_{0.1}O_3$
LSCNC	$La_{0.9}Sr_{0.1}Co_{0.8}Ni_{0.1}Cu_{0.1}O_3$
MFC	Mass flow controllers
MTBE	Methyl tert-butyl ether
MWCNT	Multi-walled carbon nanotubes
$Mole_{F\ in}$	Moles of gas (CO or H2) in the feed-gases
$Mole_{F\ out}$	Moles of gas (CO or H2) in the out-gases
$Mole_i$	Moles of carbon-containing product i
m_{cat}	Mass of catalyst
n_i	The number of carbon atoms in product i
NP	Nanoparticle
OMC	Ordered mesoporous carbon
P	Pressure
PI	Pressure indicator
r_A	Radius of cation A
r_B	Radius of cation B
r_O	Radius of the anion O

RGA	Refinery gas analyser
S_{BET}	Specific surface area
SEM	Scanning electron microscopy
S_i	Molar selectivity
SN	Sonochemical
SOFCs	Solid oxide fuel cells
STY	Space time yield
T	Temperature
t	Tolerance factor
t	Reaction time
TCD	Thermal conductivity detectors
Tcf	Trillion cubic feet
TGA	Thermogravimetric analysis
TI	Temperature indicator
TOF	Turnover frequency
TOS	Time on stream
TPR	Temperature-programmed reduction
WGS	Water gas shift
WHSV	Weight hourly space velocity
*W*n	Weight fraction
XRD	X-ray diffraction
α	Chain growth probability
Δm	Mass gain

Chapter 1 Introduction

1.1 Background and Motive

Natural gas is the third largest global energy source at present, behind oil and coal. This fossil fuel currently accounts for about 1/5 of the worldwide energy consumption and this ratio is expected to increase substantially in coming decades [1]. The fast-growing consumption of natural gas is attributed to its abundant resources, robust production and somewhat cleaner output than its counterparts, namely coal and oil [2]. Forty to sixty percent of the world's proven natural gas reservoirs are remote or stranded, so transporting natural gas from the reservoir to the end users by pipeline is difficult and expensive [3]. Liquefied natural gas (LNG) is a current solution for natural gas transportation, when pipelines are not an option (*e.g.* overseas export), but the relatively high cost of production process and the expensive infrastructures (*e.g.* cryogenic tanks) have limited its current commercial application to large natural gas resources, rather than the small/stranded ones. Strict transportation requirement, energy security of supply and environmental concerns create a need to look at alternative ways to utilise natural gas resources. Chemically converting this methane-rich feedstock into transport fuels or chemicals, *via* the Gas-to-Liquids (GTL) technology, has been proved to be a promising way for natural gas utilisation.

In the GTL process, methane from the natural gas is first transformed into synthesis gas (syngas, a mixture of CO and H_2), which is then catalytically converted into liquid synthetic fuels or chemicals in a second step *via* the Fischer-Tropsch (F-T) synthesis, before being refined/separated into desired fuels such as gasoline and diesel. Prior to the syngas generation process, during the natural gas clean-up stage, mercury, sulphur, and nitrogen are removed, so the products produced by syngas are virtually free of contaminants such as sulphur and metals. In view of environmental protection and resources utilisation, the catalytic conversion of syngas is generally recognized as a promising route for providing clean fuels and chemicals for the chemical industry. As global energy demand rises by nearly 48% from 2012 to a projected 815 quadrillion British thermal units (Btu) in 2040, syngas will become increasingly important for liquid fuels and chemical synthesis [2].

The F-T technology has proven ability to convert syngas to high-value hydrocarbons (*e.g*. gasoline, diesel and light olefins) and organic oxygenates (*e.g*. methanol, ethanol and mixed higher alcohols) [4]. Since its discovery in the 1920s by German scientists, F-T synthesis has received increasing attention and undergone periods of rapid development due to the depletion of fossil fuel resources, rising crude oil prices, and politico-economic contexts. The F-T synthesis produces a wide range of products by applying various reaction conditions and catalysts. The traditional F-T products are principally hydrocarbons and methanol. Hydrocarbons need further treatment such as cracking to convert them to more useful products, adding to the production costs. Although methanol yield in the F-T process can reach very high level under ideal operating conditions, this process cannot bring any considerable profit as the market price of methanol is low. Thus, producing higher-value products by the F-T process becomes attractive, and higher alcohol synthesis (HAS) from syngas process has been investigated intensively by industrial and academic researchers over the past 30 years.

Higher alcohols — containing 2 or more carbon atoms — can be widely used in industrial chemistry as primary materials. The most useful higher alcohols are C_2 to C_5 alcohols (linear or branched), some of which can also be used directly as transportation fuels, either alone or in gasoline blends, to extend gasoline supplies and enhance octane number, thus improving engine performance [5]. Higher alcohols are usually produced through two major processes in industry: fermentation of sugars derived from corn or sugar cane (mostly ethanol) and hydroformylation of olefins [6, 7]. However, the disadvantages of these processes could not be neglected. Alcohols produced from fermentation need more energy and the cost of production is high. Though sugar from plant material is a renewable resource, it's also an important feed grain for human needs. One of the major limitations for higher alcohol production through hydroformylation is its requirement for high energy input, as the reaction takes place at severe conditions (high temperatures and high pressures). This process also heavily rely on olefins, which is a finite resource based on crude oil. Compared to the above processes, the F-T process is a promising way for HAS from syngas. In F-T process, syngas can be produced from a wide range of resources such as natural gas, coal and biomass, which does not compete with potential food sources.

It is recognised that a successful HAS process requires a highly selective and stable catalyst, so HAS catalysts have been studied intensively over the past three decades by many industrial and academic researchers [6, 8, 9]. Four major catalyst groups have been studied from the early stage of the HAS process: modified methanol synthesis catalyst, modified F-T catalysts, molybdenum-based catalysts and rhodium-based catalysts. Although there have been various catalytic systems developed for HAS from syngas, yields still remains low, and a great effort is still required to improve both stability and selectivity of catalysts. Unfortunately, no commercial F-T process for HAS exists as of today, and all published research results are from bench scale.

Perovskite oxide (ABO_3) was found to be a good catalyst precursor for different chemical reactions. This structure can be formed easily with a wide range of A- and B- site metal, which facilitate catalyst design and preparation. This catalyst type has attracted increasing interest for HAS in the last ten years. Many promising results were reported recently by different researchers, but unfortunately, the targeted products' yields were still too low for any industrial application. Some questions about the effect of perovskite structure and the type of metal atoms on the catalytic activity, such as active centre dispersion, the synergistic effect between metal atoms and reduction properties, still remain. The mentioned knowledge gaps are the main motives of this research.

1.2 Scope and Objectives

The present study aims to develop stable perovskite catalysts with high activity and selectivity for HAS from syngas. In addition, this research also dedicates to provide insights into the effect of partial substitution of lanthanum and cobalt atom in $LaCoO_3$ perovskite on the catalyst properties and catalytic performances. To this end, comprehensive studies integrating catalyst design and characterization, catalytic reaction and stability test were implemented. The specific objectives of this study are as follows:

- To design, prepare and characterize ABO_3 substituted perovskite catalysts ($A_{1,1-x}A_{2,x}B_{1,1-y-z}B_{2,y}B_{3,z}O_3$).
- To investigate the effect of partial substitution of the A- and B-sites of perovskite catalysts for HAS from syngas in F-T synthesis.

- To examine the effect of alkali promoters and reaction conditions over prepared perovskite catalysts for higher alcohol formation.
- To test the catalyst performance over the catalysts mentioned above in HAS process, and assess the catalyst stability and lifetime.

1.3 Thesis Outline

This thesis consists of 7 chapters including the current chapter. Each chapter in this thesis is outlined below:

- Chapter 1 introduces the background and objectives of the current research.
- Chapter 2 provides an up-to-date literature review on the development of HAS process from syngas, a classification of HAS catalysts and catalyst characteristics effect for HAS selectivity, finally leading to the identification of existing research gaps and catalyst candidates for the present study.
- Chapter 3 provides an overview of the research methodology employed to achieve the research objectives and detailed descriptions on the sample preparation, experimental setups, and analytical instruments involved.
- Chapter 4 studies the structure and activity effect of strontium-substituted $LaCoO_3$ perovskite catalysts for syngas conversion. Behaviour of $La_{1-x}Sr_xCoO_3$ perovskite catalysts during the induction period in syngas conversion is also included.
- Chapter 5 investigates the effect of nickel substitution in $La_{0.9}Sr_{0.1}CoO_3$ perovskite catalysts for HAS in F-T synthesis.
- Chapter 6 examines the performance of alkali-promoted Co-Ni-Cu-based perovskite catalysts for HAS from syngas. The effects of reaction conditions were studied and catalytic stability tests were carried out over the selected catalyst.
- Chapter 7 concludes on the meaningful findings in this study and lists out recommendations for future work.

References

[1] I. Wender, Fuel Processing Technology, 48 (1996) 189-297.

[2] J. Conti, P. Holtberg, J. Diefenderfer, A. LaRose, J.T. Turnure, L. Westfall, U.S. Energy Information Administration, (2016) 1-275.

[3] C. System, Nexant, (2005) 1-14.

[4] M.E. Dry, Catalysis Today, 71 (2002) 227-241.

[5] G.A. Mills, Fuel, 73 (1994) 1243-1279.

[6] V. Subramani, S.K. Gangwal, Energy & Fuels, 22 (2008) 814-839.

[7] P.L. Spath, D.C. Dayton, National Renewable Energy Laboratory, (2003) 1-140.

[8] K. Xiao, Z. Bao, X. Qi, X. Wang, L. Zhong, K. Fang, M. Lin, Y. Sun, Chinese Journal of Catalysis, 34 (2013) 116-129.

[9] V.R. Surisetty, A.K. Dalai, J. Kozinski, Applied Catalysis A: General, 404 (2011) 1-11.

Chapter 2 Literature Review

2.1 Introduction

The modern world's fuels and valuable chemicals production is currently based predominantly on petroleum crude oil as a feedstock. Figure 2-1 illustrates the energy consumption worldwide by energy source. However, interest is now shifting towards finding alternative sources to power the world and produce fuels and industrial chemicals due to depleting crude oil reserves and increasing environmental issues.

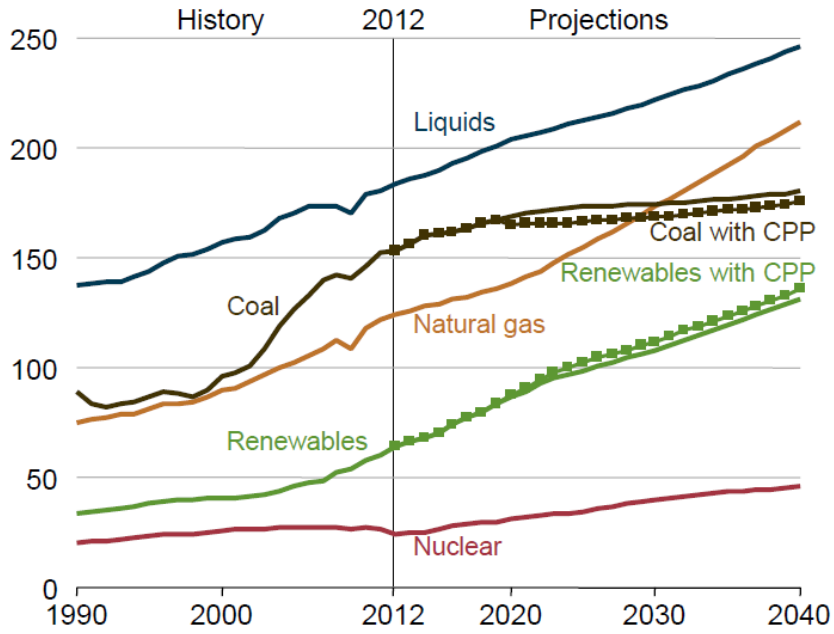

Figure 2-1. World energy consumption by energy source from 1990 to 2040 (quadrillion British thermal units) [1]. Note: Dotted lines for coal and renewables show projected effects of the U.S. Clean Power Plan.

Natural gas is viewed more and more as an alternative and transitional feedstock, and the ability to convert it to a wide range of fuels and chemicals has attracted interest since the 1920s. 130 trillion cubic feet (Tcf) of natural gas are currently produced annually all over the world, with 50.7 Tcf used in the industrial sector for the production of organic chemicals, plastics, detergents, and cosmetics [1].

The most common uses for natural gas are power generation, transportation fuels, and transformation to chemical feedstocks [2]. The Gas-to-Liquids (GTL) process is recognised as one of the major routes that chemically converts natural gas to liquid

fuels (or other chemicals), which could help to satisfy growing global demand for high-quality liquid products. In a typical GTL process, natural gas (cleaned up to methane) is first converted to synthesis gas (syngas), a mixture of hydrogen and carbon monoxide, by partial oxidation, steam reforming, or dry reforming (or combinations thereof). Syngas is then catalytically converted into different liquid products *via* the Fischer-Tropsch (F-T) synthesis, which is recognised as an effective process to generate valuable products from natural gas, *via* syngas production [3, 4]. Oxygenates, and alcohols in particular, represent a very attractive product class of the F-T synthesis [2, 5]. Alcohols can be added to gasoline to improve combustion efficiency by increasing the oxygen content. Also, alcohols promote complete fuel combustion, thereby reducing carbon monoxide emission and toxic tailpipe pollution. Methanol has been successfully produced through this route in large scale — over 90 methanol plants worldwide have a combined production capacity of about 110 million metric tons annually [6]. However, there has been intensive research focused on shifting the synthesis away from methanol and toward higher alcohols ($C_{2+}OH$) over the past three decades. Higher alcohols are used in a large array of applications, such as alternative fuels, fuel additives, and raw materials in industry or intermediates for value added chemicals.

The objective of this chapter is to review the development and current status of catalysts used for higher alcohol synthesis (HAS) from syngas from 1980 to date. Due to the large number of reports and the many different impact factors on the catalysts' performance, it is impossible to review all of them in this chapter. This review concentrates on the important factors such as catalyst types, supports, promoters, and catalyst preparation methods for HAS. The review starts with a short introduction on F-T synthesis (Section 2.2) and its use to produce alcohols (Section 2.3), and then moves on to review different catalyst types used for HAS (Section 2.4). The performances of the catalysts (conversion and selectivity) in relation to their characteristics (supports, promoters, preparation methods, *etc*.) are also analysed and discussed in Section 2.5. The advantages and disadvantages of all the listed HAS catalysts are then evaluated in Section 2.6. In addition, a particular emphasis on perovskite catalysts is made in Section 2.7 as it is considered a most promising catalysts for HAS from syngas. Lastly, this chapter identifies the challenges, perspectives and objectives of this study in Section 2.8.

2.2 Fischer-Tropsch Synthesis

Since the discovery of the F-T synthesis in the 1920s and its first industrial application in 1936 for the production of fuels from coal, both in Germany, F-T synthesis has received intermittent attention and undergone some periods of rapid development and growth, generally linked to political and economic factors [5, 7-9]. Nowadays, the F-T process is used industrially mostly for the production of liquid fuels from natural gas. There are a few large-scale F-T plants in operation today, for gasoline and diesel fuels production from natural gas, such as the Shell plants in Malaysia (Bintulu GTL, 14,700 barrels per day (bpd)) and Qatar (Pearl GTL, 140,000 bpd), the Sasol plants in Qatar (Oryx GTL, with Qatar Gas, 24,000 bpd) and South Africa (Mossel Bay GTL, with PetroSA, 36,000 bpd), and the Chevron plants in Nigeria (Escravos GTL, with Nigerian National Petroleum Company and Sasol, 36,000 bpd) [10-13].

In the F-T process, a number of hydrocarbons can be produced from syngas, with paraffin and olefin generally the main desired products, synthesised according to Equation (2-1) and (2-2) respectively (see reviews [14, 15]).

Paraffin production: $(2n+1)\,H_2 + n\,CO \rightarrow C_nH_{2n+2} + n\,H_2O$ (2-1)

Olefin production: $2n\,H_2 + n\,CO \rightarrow C_nH_{2n} + n\,H_2O$ (2-2)

One of the most accepted mechanism of F-T synthesis for hydrocarbon formation is a CO adsorption and dissociation mechanism to for CH_x* group, follow by chain growth and hydrogenation (see Figure 2-2). However, side reactions also take place during the F-T synthesis, resulting in the formation of methane (Equation (2-3)), carbon dioxide (Equation (2-4)), and carbon (Equation (2-5)).

Methanation: $2\,H_2 + CO \rightarrow CH_4 + H_2O$ (2-3)

Water gas shift reaction: $CO + H_2O \leftrightarrow CO_2 + H_2$ (2-4)

Boudouard reaction: $CO + CO \rightarrow CO_2 + C$ (2-5)

Since methane is the most thermo-dynamically favoured product in the F-T synthesis, the catalyst and reaction conditions need to be designed to suppress its formation in order to increase the selectivity and yield of the target products [16]. The

water gas shift (WGS) is an important side reaction, which affects the H_2/CO ratio during the reaction as it produces hydrogen along with carbon dioxide. Therefore, the WGS reaction is desirable for feeds containing a low H_2/CO ratio (*e.g.* syngas from biomass or coal) but undesirable with high H_2/CO ratio (*e.g.* with syngas derived from methane steam reforming). In addition, the Boudouard reaction leads to the catalyst deactivation via carbon deposition on the catalyst surface [17].

The hydrocarbon product distribution in F-T synthesis can be described as a chain polymerisation process and follows the Anderson–Schulz–Flory (ASF) distribution, defined by Equation (2-6) [15]. Ideally, the weight fraction (W*n*) of a single hydrocarbon product with a carbon number of *n* depends on the chain growth probability (α).

$$W_n/n=(1-\alpha)^2\alpha^{(n-1)} \quad (2\text{-}6)$$

In an ideal case, the resulting F-T product distribution, depicted as a plot of the logarithm of W*n*/*n versus n*, is a straight line with the slope of the line giving the α value. A small α value (α <0.5) results in the formation of lighter (C_1-C_4) hydrocarbons, while a large α value (α >0.95) leads to heavier hydrocarbons (above C_{22}), and the valuable C_5–C_{22} liquid hydrocarbons becomes the main product when the α value is in the range of 0.7-0.875 [15, 18]. However, deviations from the linear ASF distribution are reported frequently, due to either a superposition of two ASF distributions resulting from multiple reaction paths or growth sites, or secondary reaction processes (olefin readsorption and chain grow) [19, 20]. The most common deviation is C_1 (methane) and C_2 (ethane) — C_1 is measured higher than that predicted value according to the ASF distribution, while a much lower C_2 is usually produced.

The F-T synthesis has several notable advantages. Firstly, the F-T synthesis can produce a mixture of hydrocarbons from different carbonaceous feedstocks, such as natural gas, coal, and biomass. Although the first step of the process to generate syngas will vary depending on the feedstock (*e.g.* reforming or partial oxidation of natural gas, and gasification for coal and biomass), any syngas can then be converted to synthetic fuels *via* the F-T synthesis. Secondly, F-T products can be stored and transported by the same means as petroleum products because of their similar function and composition. In addition, F-T fuels are largely compatible with current vehicles and infrastructure, and can be blended with current petroleum fuels, such as jet fuels, motor

gasoline, and diesel [21]. Thirdly, F-T products are of high quality, being free of sulphur and containing very few aromatics and other contaminants typically found in petroleum products, thus they burn cleaner than conventional fuels and reduce local emissions [22].

However, drawbacks also exist in the F-T synthesis: in most cases, F-T products, especially waxes — the very long chain hydrocarbon products (> C_{20-25}) — usually need to be converted to more valuable chemicals and transportation fuels. In general, the heavy products (wax) must be cracked into the middle distillate range through wax hydrocracking, catalytic cracking, or steam/thermal cracking [23, 24]. This cracking process is an additional production cost to the F-T process. The high capital, operation, and maintenance costs of the process, as well as the price of gas and oil, are some of the constraints that influenced the commercialisation and competitiveness of the GTL F-T synthesis compared to the conventional refinery.

Despite the disadvantages of F-T synthesis, the depletion of fossil fuel resources and rising crude oil prices still make it an important route for crude oil replacement in the 21st century, as an alternative source of fuels and chemicals. Thus, future research will continue and be more focused on reducing the production costs, improving process efficiency, and producing new valuable products to make the F-T process more economical.

2.3 Higher Alcohol Synthesis from Syngas

2.3.1 Introduction

Among all the F-T products, alcohols are attractive targets as they can be used as transport fuels, fuel additives, and as intermediates for high-value chemicals in areas such as medicine, cosmetics, chemicals, and polyester production [25, 26]. Furthermore, as previously stated, alcohol synthesis *via* the F-T technology using natural gas or biomass as feedstock is now expected to become a more attractive pathway to reduce the crude oil dependence.

As mentioned above, methanol (CH_3OH) can also be produced *via* the F-T process, according to Equation (2-7).

Methanol production: $2\ H_2 + CO \rightarrow CH_3OH$ (2-7)

Though there is still debate on the mechanism of methanol formation from syngas, it is generally considered that the CO_2 generated from the WGS reaction (Equation (2-4)) is the "real" reactant, followed by hydrogenation to form methanol [27, 28].

Methanol is the simplest alcohol and an important feedstock for the production of a range of chemicals including acetic acid, formaldehyde, di-methyl-ether, and olefins [29-34]. It is also a platform chemical, being widely used in a number of industrial applications. However, methanol is not ideal as a fuel or fuel additive because its presence in transport fuels can promote engine wear through oxidation. Another major disadvantage of using methanol as a fuel additive is its limited miscibility with current gasoline (less than 10% at room temperature and pressure). Phase separation thus occurs when temperatures decrease, and methanol, separated from the gasoline, settles at the bottom of the tank and becomes corrosive to the engines [35, 36].

For approximately the last 37 years, there has been intensive research focused on shifting the synthesis away from methanol and toward higher alcohols [37]. Higher alcohols containing 2 or more carbon atoms — ($C_{2+}OH$) — are valuable natural gas derivatives and can also be synthesised through reforming and F-T reactions. The most useful higher alcohols are C_2 to C_5 alcohols, which can be used directly as transportation fuels or blended in current fossil fuels for octane number enhancement without phase separation problems. As fuel additives, higher alcohols can extend gasoline supplies and enhance overall energy efficiency, thus improving engine performance and reducing greenhouse gas emissions [5, 35]. In addition to their potential applications as transportation fuels, higher alcohols have been widely considered as a feedstock for the synthesis of primary materials in industrial chemistry, such as fragrance compounds, precursors of surfactants, plasticizers, *etc.* [38, 39].

In industry, ethanol is mostly produced through a biological treatment process, by fermentation of sugars derived from grain starches (wheat and corn), sugar beets, sugar crops using microorganisms, or by fermentation of non-sugar lignocelluloses fractions of crops (grasses and trees) [40, 41]. C_{3+} alcohols can be produced through homologation of methanol and subsequent alcohols from syngas. However, the currently favoured route involves the hydroformylation of olefins, which are the cracking fractions of the distilled crude oil [17, 42, 43]. SaBuCo butanol plant of Saudi

Butanol Company at Jubail (Saudi Arabia) is currently the biggest butanol plant in the world, which began its commercial operations in March 2016. This butanol plant produces 330,000 ton per year of *n*-butanol and 11,000 ton per year of *iso*butanol [44]. In addition, Chemical group Oxea scheduled to open a propanol plant with the capacity to produce 150,000 ton per year of *n*-propanol in Bay City, Texas in 2017 [45].

Compared to these processes, the F-T technology is a promising way for higher alcohol synthesis from syngas. It can use natural gas, coal or biomass as feedstock to produce higher alcohols (*via* syngas) and does not compete with the feed grains available for human consumption [35] or depend on crude oil. Alcohols are generally formed from syngas according to Equation (2-8) [26]:

$$2n\ H_2 + n\ CO \rightarrow C_nH_{2n+1}OH + (n-1)\ H_2O \qquad (2\text{-}8)$$

Since the early development of HAS from syngas, various theories about the underlying reaction mechanisms have been proposed. The CO insertion mechanism proposed by Xu *et al*. [46] is widely accepted for HAS process. In general, the above alcohol reaction mechanism includes CO dissociation, CO insertion, carbon chain growth, and hydrogenation steps, as shown in Figure 2-2.

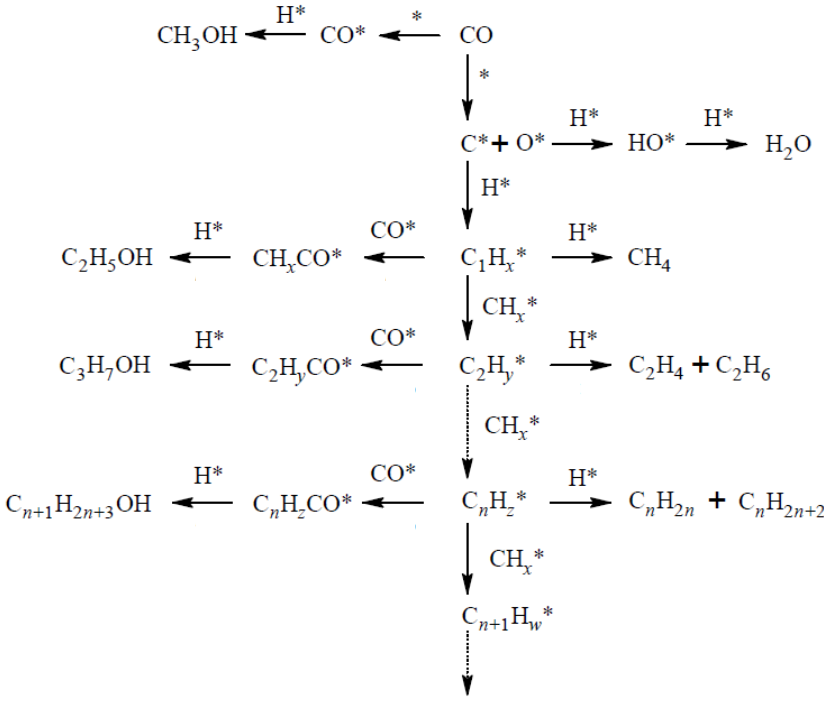

Figure 2-2. Hydrocarbons and alcohol formation through CO insertion mechanism (adapted from Xiao *et al*.[28]).

The reaction scheme starts with the CO adsorption and dissociation to form adsorbed $C_1H_x^*$ group, then the carbon-chain growth of this alkyl group is propagated via CH_x^* addition. For higher alcohol formation, the adsorbed CO^* molecule inserts between the metal site and the alkyl group to give an acyl intermediate ($C_nH_zCO^*$) which can form C_{n+1} alcohol by hydrogenation. In parallel, the alkyl groups can be directly hydrogenated to form paraffin products. Note that the methanol formation *via* CO insertion is different from the mechanism mentioned above, that is, the adsorbed CO^* molecule is directly hydrogenated to from methanol. Based on this CO insertion mechanism, the alcohols produced from HAS reaction also follow a linear ASF distribution.

Because of their importance, the synthesis of higher alcohols from syngas *via* the F-T process has been intensively investigated and reported in the literature by industrial and academic research organisations. The number of reports on HAS has increased significantly since 1980. The driving force behind this interest in HAS from alternative feedstocks started during the oil crises in the 1970s, which initiated the search for alternative fuels. However, none of the higher alcohol F-T synthesis catalysts or processes developed to date have been sufficiently active and/or selective to motivate industrial commercialization of the F-T process for HAS. Consequently, there are no higher alcohol F-T production plants in operation today. Most of the reported results of this process are based on experimental works at laboratory bench scale.

Many authors have summarised a large number of reports and literatures on higher alcohol synthesis from syngas [16, 25, 26, 28, 35, 38, 39, 46-48]. However, there are many factors affecting the HAS process, not only regarding the catalysts (catalyst types, supports, promoters, and catalyst preparation methods) but also reactor design and operating conditions (temperature, pressure, feed composition, flow, *etc*.), and different studies have used different conditions to test catalysts and report their findings. It is thus challenging to truly compare different catalysts reported by different researchers, and draw any solid conclusion regarding catalytic activity, product selectivity and optimum conditions of the process. The next sections will review in detail various catalysts used for HAS in F-T synthesis, as reported in the literature.

2.3.2 HAS Catalysts Types

The development of stable catalysts with high activity is the key element in HAS from syngas. In the period 1980-2016, a wide range of catalysts for HAS have been reported by many industrial and academic researchers. According to the available reports in the literature, typical HAS catalysts can be divided into 5 groups [28, 35]:

1. Modified methanol synthesis catalysts
2. Modified F-T synthesis catalysts
3. Molybdenum (Mo)-based catalysts
4. Rhodium (Rh)-based catalysts
5. Perovskite catalysts

Figure 2-3 illustrates the evolution of the number of found publications for each catalyst type with time.

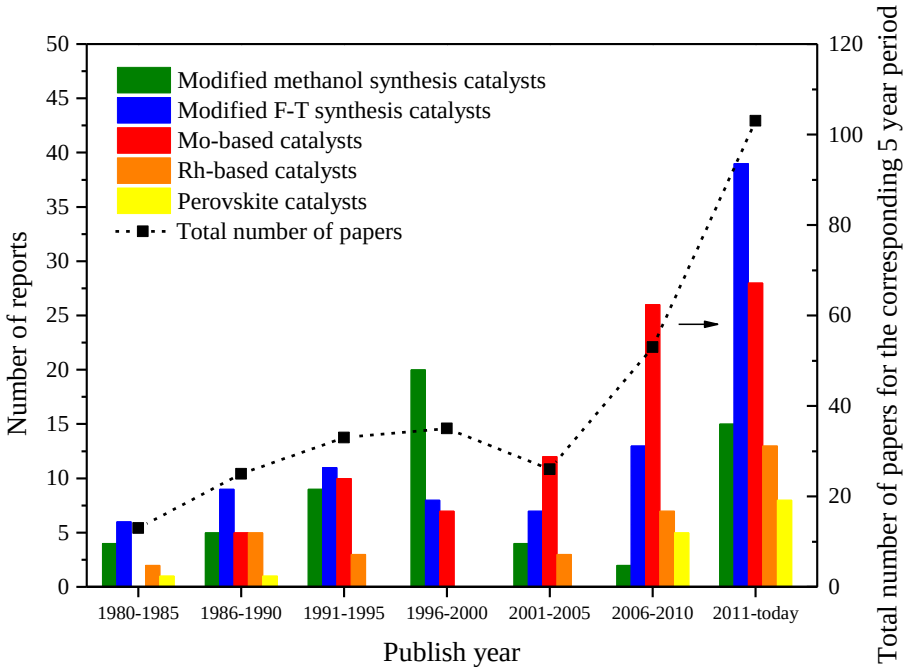

Figure 2-3. Number of reports related to different HAS catalyst types published with time.

It shows that the total publication numbers changed very little between 1980 and 2005, and stayed below 40 per five year period. Post 2005, the total report number increased significantly and reached 103 for the five year period between 2011 and 2016. These results indicate that HAS has been a very attractive research area over the past 10 years. Modified F-T synthesis catalysts and Mo-based catalysts are the

most researched catalyst types for HAS, attracting growing interest in the last 2 decades. Recently, perovskite catalysts have emerged and have attracted some interest. Each catalyst group will be reviewed and discussed in detail in later sections of this chapter. The following sections discuss the all-important issues of catalyst conversion, selectivity, and yield to HAS.

2.3.3 Syngas Conversion over HAS Catalysts

The evolution of CO conversion with time, reported for all the different types of catalysts mentioned in Section 2.3.2 (Figure 2-3), is plotted in Figure 2-4. It can be noted that a wide range of CO conversion levels were reported, even for the same catalyst type. This is because the experiments were carried out by different researchers using different reactor systems and reaction conditions. It was assumed that the reported CO conversion was the optimal value for the studied process.

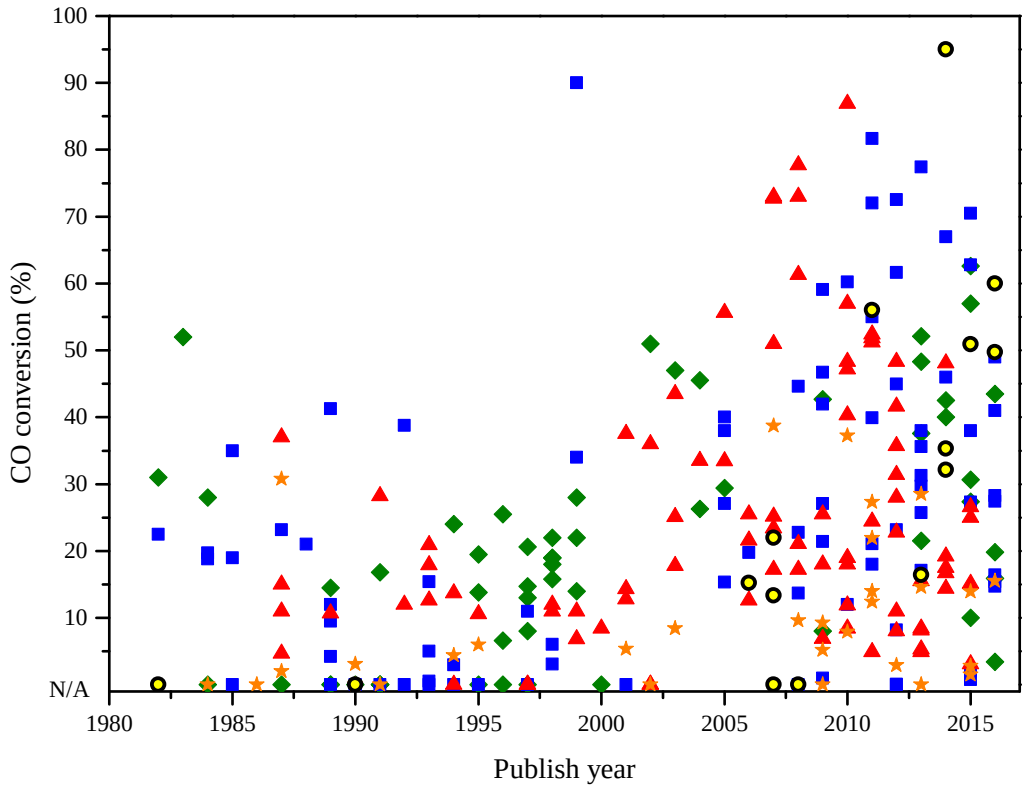

Figure 2-4. Reported optimal CO conversion in HAS from syngas for different types of catalysts between 1980 and 2016: (♦) Modified methanol synthesis catalysts, (■) Modified F-T synthesis catalysts, (▲) Mo-based catalysts, (★) Rh-based catalysts, and (○) Perovskite catalysts.

The reported data summarised in Figure 2-4 show that the maximum CO conversion for all catalyst types has generally increased with the HAS process

development time. In the early years of HAS development, CO conversion stayed low for all catalyst types, with a maximum of 52% reported by Smith *et al*. in 1983, using a Cu/ZnO catalyst promoted with 0.5% K_2CO_3 — a modified methanol synthesis catalyst [49]. However, the CO conversion of modified methanol synthesis catalysts has improved less than 8% since that report. From the beginning of this century, CO conversions have largely improved for the modified F-T synthesis catalysts and Mo-based catalysts, reaching conversion well above 60-70%, from 30-40% in the 1980s. Although Rh-based catalysts have been investigated intensively over the past 37 years, very little catalytic activity improvement was reported and the CO conversion level remains very low (around 40%). The highest CO conversion reported to this date was by Fang *et al*. in 2014, using a $CuO/LaCoO_3$ perovskite catalyst (95% CO conversion) [50].

2.3.4 Higher Alcohol Selectivity over HAS Catalysts

High product selectivity is the main target of HAS catalyst development, to encourage commercialization of F-T HAS. Figure 2-5 shows the reported higher alcohol selectivity (as C atom % on a CO_2-free basis) of HAS over different catalyst systems from 1980 to date.

In order to use selectivity figures consistent and comparable across the literature, carbon atom percentage (C atom %) was used to indicate selectivity in this work. C atom % of a carbon containing product (for example C_2H_5OH) is defined as the selectivity of this product based on the carbon atom of the total carbon-containing products formed from consumed CO. It is impossible to avoid the WGS reaction (Equation (2-4)), a side reaction in F-T synthesis. Thus, C atom % on a CO_2-free basis, to exclude the effect of the WGS reaction, has often been used for alcohol and hydrocarbon selectivity calculations in the literature. For comparison purposes, the higher alcohol selectivity in the present review is also reported as C atom% on a CO_2-free basis. Necessary recalculations were applied in some cases where the reported literature data were not appropriate to compare. Instead of higher alcohol selectivity, some authors reported the total alcohol (including methanol) selectivity in their work. Because of the lack of necessary information for higher alcohol selectivity recalculation, these reports were not included for discussion on selectivity in this review.

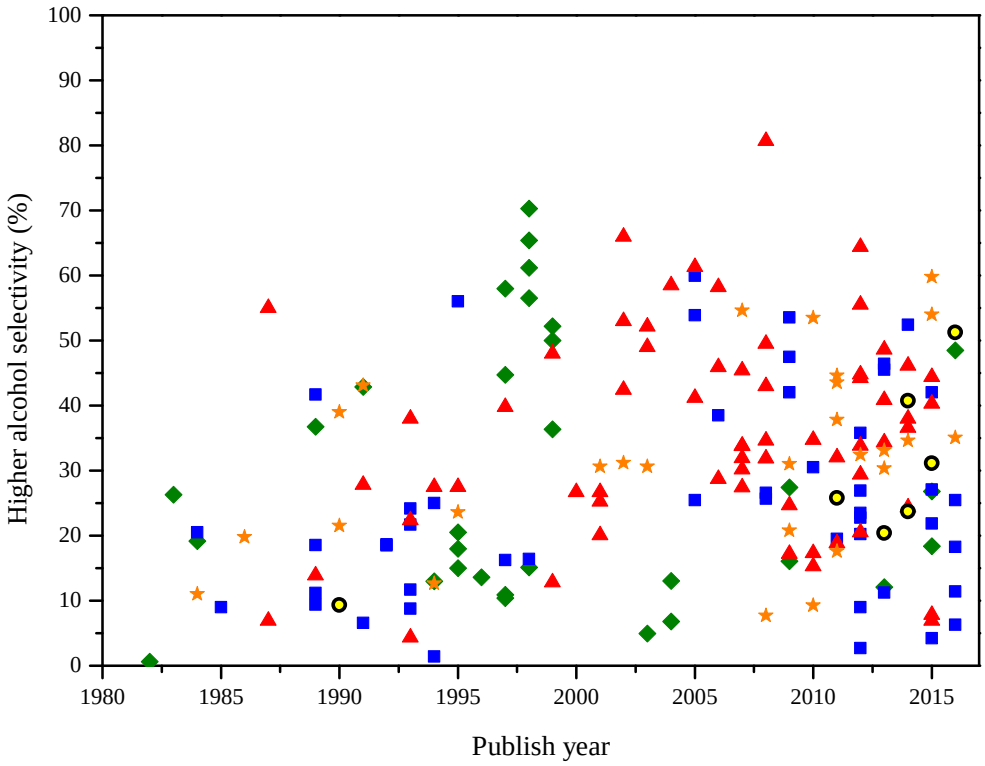

Figure 2-5. Reported higher alcohol selectivity of HAS from syngas over different types of catalysts from 1980 to 2016: (♦) Modified methanol synthesis catalysts, (■) Modified F-T synthesis catalysts, (▲) Mo-based catalysts, (★) Rh-based catalysts, and (○) Perovskite catalysts.

All five catalyst types detailed in this review showed potential for quite high $C_{2+}OH$ selectivity (>50%) in the timeframe investigated (see Figure 2-5). In the short period of 1997-1999, a number of Zn/Cr-based modified methanol synthesis catalysts were developed that presented relatively high $C_{2+}OH$ selectivity (50-70%) [51-58]. However, not much further progress on selectivity for these catalysts had been made since then. In the later time, this catalyst type becomes less attractive (Figure 2-3), with lower $C_{2+}OH$ selectivity compared to other catalysts. The modified F-T synthesis catalysts, despite being the most studied HAS catalyst type, have shown no significant improvement in higher alcohol selectivity in the last two decades. The higher alcohol selectivity of Mo-based catalysts increased with the HAS development time up to recent years, as did the selectivity of Rh-based catalysts, although less studied over the last 37 years. However, for all the catalysts mentioned above, it seems that despite very noticeable improvement in conversion in the last decade (Figure 2-4), less progress has been achieved in higher alcohol selectivity in the same period, as shown in Figure 2-5. In contrast, perovskite catalysts show a different trend. Though these catalysts started to attract attention only in the last 10 years and fewer reports are

available, their reported CO conversion and $C_{2+}OH$ selectivity increased progressively with development time. They should thus be considered as promising catalysts in recent years, with considerable opportunities for further improvements.

2.3.5 Higher Alcohol Yield over HAS Catalysts

CO conversion and higher alcohol selectivity are the main factors usually reported to evaluate catalysts (or operating conditions) in HAS. As shown in Figure 2-6, these two factors are generally following opposite trends over HAS, with the catalysts exhibiting high selectivity at low conversion (blue square) or low selectivity at high conversion (pink square). What's more, most of the catalysts discussed in this chapter show low CO conversion (less than 40%) and low higher alcohol selectivity (less than 55%) (overlap of blue and pink square).

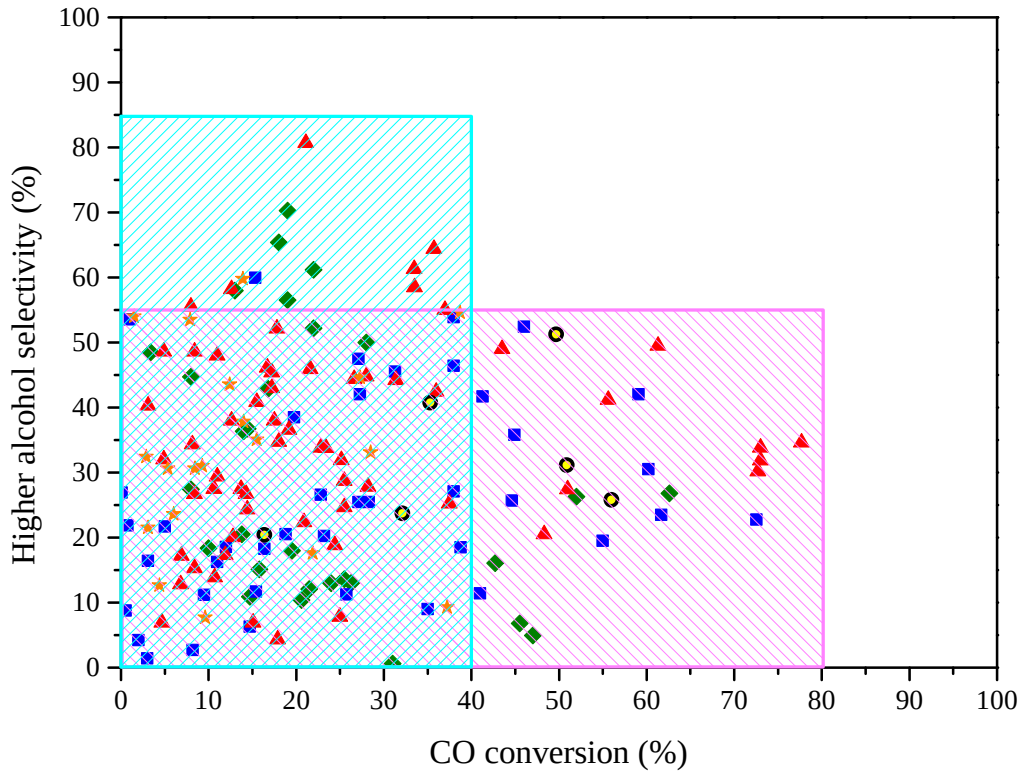

Figure 2-6. Higher alcohol selectivity evolve with conversion over different types of catalyst: (♦) Modified methanol synthesis catalysts, (■) Modified F-T synthesis catalysts, (▲) Mo-based catalysts, (★) Rh-based catalysts, and (○) Perovskite catalysts.

Thus, comparing higher alcohol yield is essential to evaluate process and catalyst performances. The yields of higher alcohols obtained from the catalysts discussed in this review were calculated based on Equation (2-9) and are presented in Figure 2-7.

$$\text{Higher alcohol yield (\%)} = \frac{\text{CO conversion (\%)} \times \text{Higher alcohol selectivity (\%)}}{100\%} \quad (2\text{-}9)$$

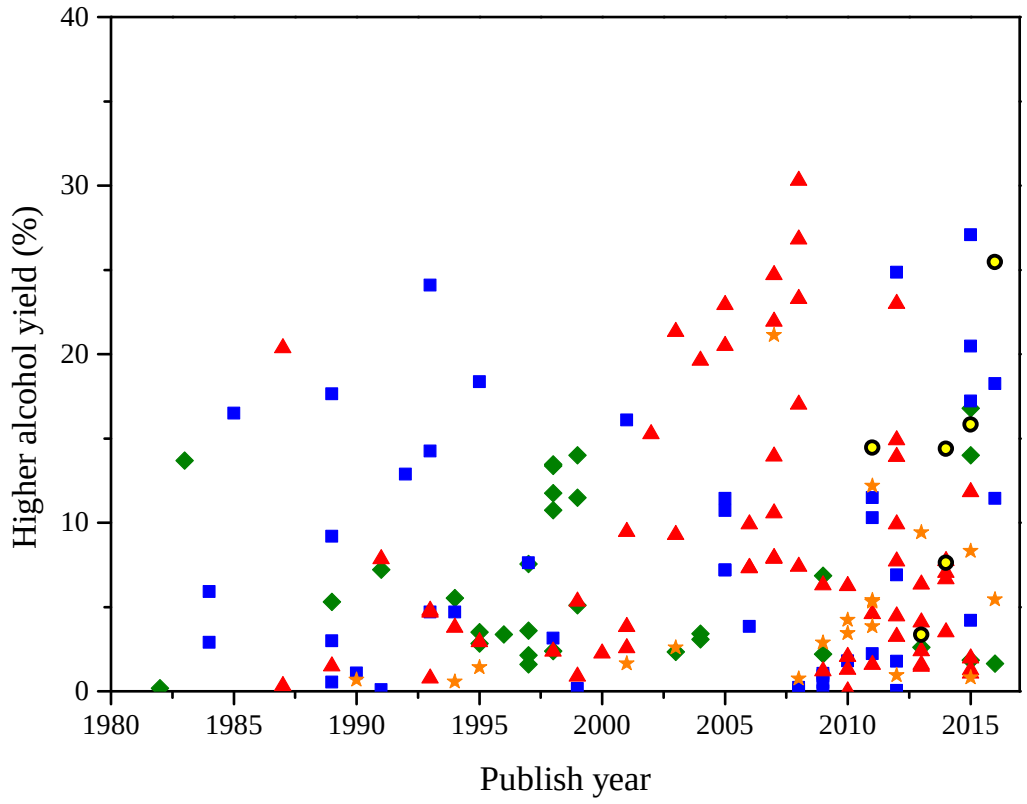

Figure 2-7. Reported higher alcohol yield for HAS from syngas from 1980 to 2016: (♦) Modified methanol synthesis catalysts, (■) Modified F-T synthesis catalysts, (▲) Mo-based catalysts, (★) Rh-based catalysts, and (○) Perovskite catalysts.

Over the last 37 years, great efforts have been made to improve the higher alcohol yield. Figure 2-7 shows that higher alcohol yield has improved with process development time. To date, a maximum of 30% higher alcohol yield was reached by using Mo-based catalysts [59]. Other catalysts types have also shown their potential to form higher alcohols, reaching yields between 10% and 28%. Among all the reported catalyst types, only perovskite catalysts showed a sharp increase in higher alcohol yield within a short period of development time.

2.4 Catalysts for Fischer-Tropsch Higher Alcohol Synthesis

2.4.1 Modified Methanol Synthesis Catalysts

There are two types of modified methanol synthesis catalysts that have been employed in HAS research: high-temperature (HT) and low-temperature (LT) modified methanol synthesis catalysts [35].

2.4.1.1 High-temperature Modified Methanol Synthesis Catalysts

Typical HT modified methanol synthesis catalysts are alkali promoted ZnO/Cr_2O_3 catalysts, which produce a mixture of methanol and branched alcohols as major alcohol products, with a small amount of ethanol [51-58, 60-68]. Among branched alcohols, *iso*butanol was the main component, which is also a very important material to form methyl tert-butyl ether (MTBE)—a common oxygenated additive found in gasoline [64]. However, MTBE fell out of favour in 2000 when it was found to contaminate groundwater [69]. To the best of our knowledge, the highest $C_{2+}OH$ selectivity for HT modified methanol synthesis catalysts was reported by Minahan *et al*. at 70.3% using a Zn/Cr-based spinel catalyst containing excess ZnO and promoted with palladium and caesium (HAS carried out at 440 °C and 6.9 MPa) [54]. They found that the addition of palladium to HT modified methanol synthesis catalysts not only enhanced the *iso*butanol production rate but also contributed to a reduction in the optimum reaction pressure, which is economically favourable. Alkali elements such as potassium and caesium are often used as additives to promote the HAS reaction. It has been found that the increase of the potassium and caesium concentration results in increased higher alcohol selectivity (mostly *iso*butanol selectivity) [52, 53]. Though caesium was proved to be a better promoter of Zn/Cr-based catalysts for *iso*butanol synthesis compared to potassium [53, 54], the latter is still used in many studies because of its low-cost and availability [56-58].

Reaction conditions also play an important role in the HAS process. The reaction temperatures and pressures used in most experiments with HT modified methanol synthesis catalysts were higher than that used for the other catalyst types, with temperatures as high as 400-450 °C and pressures in the range of 6-15 MPa [51-58, 60-68]. However, HT modified methanol synthesis catalysts show on average lower CO conversion compared to LT catalysts, as shown in Figure 2-8. What's more, large

amounts of hydrocarbons were produced at high operation temperatures together with alcohol products, as high reaction temperatures favour the reactions in the decreasing order: F-T reaction > HAS > methanol synthesis [46, 66].

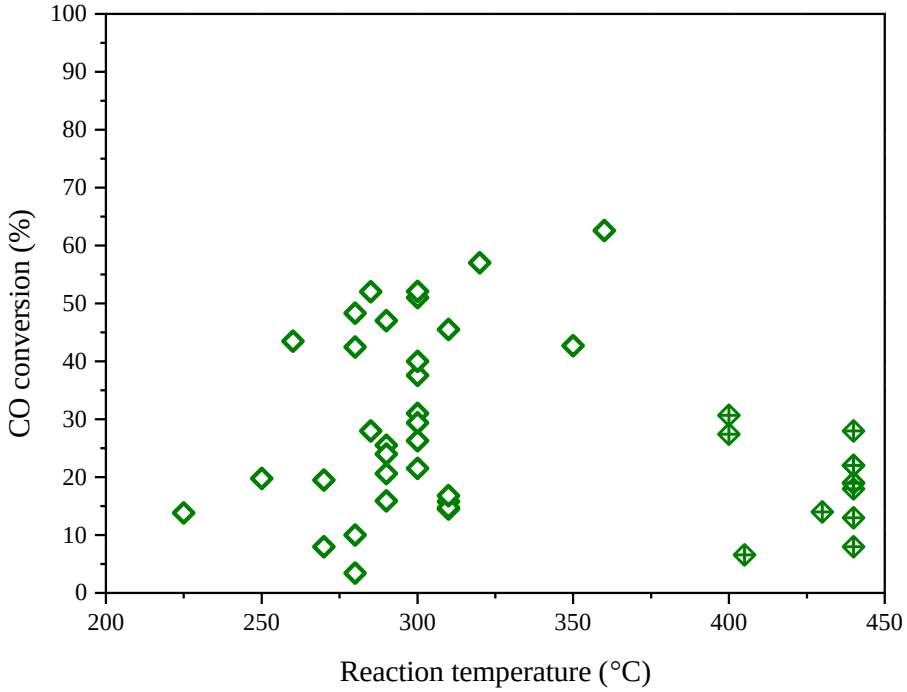

Figure 2-8. CO conversion *versus* reaction temperatures over (◈) HT modified methanol synthesis catalysts and (◇) LT modified methanol synthesis catalysts.

Moreover, these catalysts require high operating temperatures and pressures and show lower activity towards higher alcohol formation compared to other catalysts. As a result, HT modified methanol catalysts lost their attractiveness after 2000, and research turned to other types of catalysts to form higher alcohols. Higher attention was then placed on low-temperature modified methanol catalysts.

2.4.1.2 Low-temperature Modified Methanol Synthesis Catalysts

Typical LT modified methanol synthesis catalysts are copper-based catalysts — Cu/Zn, Cu/Zn/Al or Cu/Zn/Cr — promoted with alkali metals, and have been studied continuously since the 1980s [49, 70-110]. The presence of copper enables alcohol production at lower operating temperatures (250-300 °C) and pressures (2-10 MPa) [35] compared to HT modified methanol synthesis catalysts. Although the bi-metal Cu/Zn catalyst is active in HAS, a third component, either Al_2O_3 or Cr_2O_3, is always added in order to stabilise the catalyst against sintering [79, 92, 103, 109]. In addition,

alkali promoters such as lithium, sodium, potassium, and caesium are very often found in LT modified methanol synthesis catalysts and are reported to promote the production of higher alcohols [49, 51-58, 62-66, 79-94]. Despite LT modified methanol synthesis catalysts yielding high CO conversion at lower temperatures (see Figure 2-8), methanol remained the dominant alcohol product and the selectivity towards higher alcohols stayed low [108]. Smith and co-workers studied the HAS process over Cu/ZnO catalysts promoted with cerium at 310 °C and 6.0 MPa, using a H_2/CO ratio of 0.45 and a GHSV of 3265 h^{-1} [83]. The alcohol product selectivity did not follow the ASF distribution — methanol was the main product (39.0%), with small amounts of ethanol (5.5%) and propanol (10.3%). The higher alcohol selectivity reached 42.9% in total, with a relatively abundant amount of *iso*butanol included (13.1%). They reported that the low selectivity towards ethanol was because of the fast C-C chain growth of the C_2 surface intermediate over the Cs-promoted catalysts.

As mentioned above, reaction conditions, including syngas feed composition, play a role in higher alcohol selectivity. Low H_2/CO ratio (less or equal to 1) favoured the higher alcohol formation over LT modified methanol synthesis catalysts [68, 79, 82, 83, 103]. According to Equation (2-8), a H_2/CO ratio of 2 is ideal for alcohol formation. However, higher alcohols are favoured with a CO-rich feed gas (ratio less than 2) [25]. This is because high CO partial pressure promotes the carbon chain growth, while high H_2 partial pressure favours the hydrogenation of C_1 intermediate to methanol, thus inhibiting the chain growth to higher alcohols [49, 104, 107].

Catalyst deactivation by copper sintering is the main drawback of the LT modified methanol synthesis catalysts, and it was found that the Cu-based catalysts cannot be used at temperatures greater than 300 °C [46]. Although much effort from different research groups has been made, the higher alcohol selectivity is still low for these types of catalysts, with a maximum of *ca.* 48.5% reached for a 1.2 *wt.*% Na-doped Co-modified Cu/ZnO/Al_2O_3 catalyst (280 °C, 6.0 MPa, and 9600 h^{-1} GHSV)) [92].

2.4.2 Modified F-T Synthesis Catalysts

Modified F-T synthesis catalysts have played an important role in HAS from early development time until now. The traditional F-T catalysts, mainly based on cobalt and iron metal supported on silica or alumina, produce long chain hydrocarbons, and only small amounts of oxygenates (including alcohols) as by-products. Simple

modifications of F-T catalysts, such as promotion with transition metals (Cu, Ni, Mo, Mn, Re, Ba, *etc*.) and/or alkali cations (Li, Na, K, Cs, *etc*.), can significantly increase the selectivity and yield of higher alcohols at moderate reaction conditions [111-134]. The alcohol products obtained from modified F-T catalysts are generally straight-chain primary alcohols and obey the ASF distribution. In this catalytic system, the copper-modified F-T synthesis catalysts have been extensively studied because of their high selectivity and activity toward higher alcohols.

Since 1978, the Institut Français du Pétrole (IFP) has patented and developed a series of Cu-Co-based catalysts, which reached a high range of $C_{2+}OH$ selectivity (24-50%) in comparison with other catalyst types [46]. These encouraging results have attracted many researchers' attention and this catalyst type has been extensively studied [135-169]. Cobalt is used for the synthesis of long-chain paraffin in F-T reaction, while copper is selective in methanol synthesis from syngas [152, 158, 167, 168]. It has been reported that the Cu-Co bimetallic sites were involved in the formation of higher alcohols [136, 146, 169]. The interactions between the highly dispersed metallic copper and cobalt particles cause cobalt species to reduce more easily, in other words, the synergetic effect of Cu-Co is very important in catalytic activity towards HAS [144, 165, 166]. In order to get further insights into the active sites for HAS, Subramanian and co-workers studied the unsupported Cu-Co bimetallic nanoparticles as catalysts for HAS at 270 °C and 2.0 MPa [152]. Under such reaction conditions, the higher alcohol selectivity increased with the Cu/Co atomic ratio, and the highest ethanol and C_{2+} oxygenates (including acetaldehyde and acetone) selectivity was achieved (22.3% and 53.5%, respectively) for the Cu-Co-based catalyst with a high ratio (Cu/Co=24:1). The higher Cu/Co ratio led to higher ethanol and C_{2+} oxygenates selectivity but suppressed the hydrocarbon formation, thus the activity of this Cu-Co-based catalyst was low. As a result, the Cu/Co ratio needs to be chosen to achieve a proper balance between catalyst activity and selectivity to obtain a high yield of higher alcohols. However, the insufficient stability of Cu-Co-based catalysts, mainly due to the sintering of copper as mentioned in Section 2.4.1.2, represents one of the major problems for larger industrial applications [35, 46].

Cu-Fe-based F-T synthesis catalysts were also investigated by some researchers [170-197]. Similar to elemental cobalt, iron species including α-Fe, Fe_3O_4, and FeC_x are the active centres for the C-C chain growth and hydrogenation [170, 173]. Xiao *et*

al. proved that the synergistic effect between copper and iron ions benefited higher alcohol formation [191, 197]. However, this synergism only exists on Cu-Fe bimetallic nanoparticles, and the agglomeration of one site or the separation of the copper and iron phases would lead to a decrease in higher alcohol selectivity [46]. To the best of our knowledge, a potassium promoted $Cu_{20}Fe_{30}$ catalyst on SiO_2-SiO_2 bimodal pore support reported by Ding *et al.* exhibited the highest $C_{2+}OH$ selectivity (52.4%) among all the Cu-Fe-based modified F-T synthesis catalysts [186]. The high specific surface area (107 $g \cdot m^{-2}$) and unique biomodal porous structure enhanced the dispersion of Cu-Fe active centres, improved the diffusion efficiency of products, and promoted the catalytic activity and higher alcohol selectivity.

For modified F-T synthesis catalysts, Co- or Fe-based catalysts show high CO conversion at low reaction temperatures (see Figure 2-9).

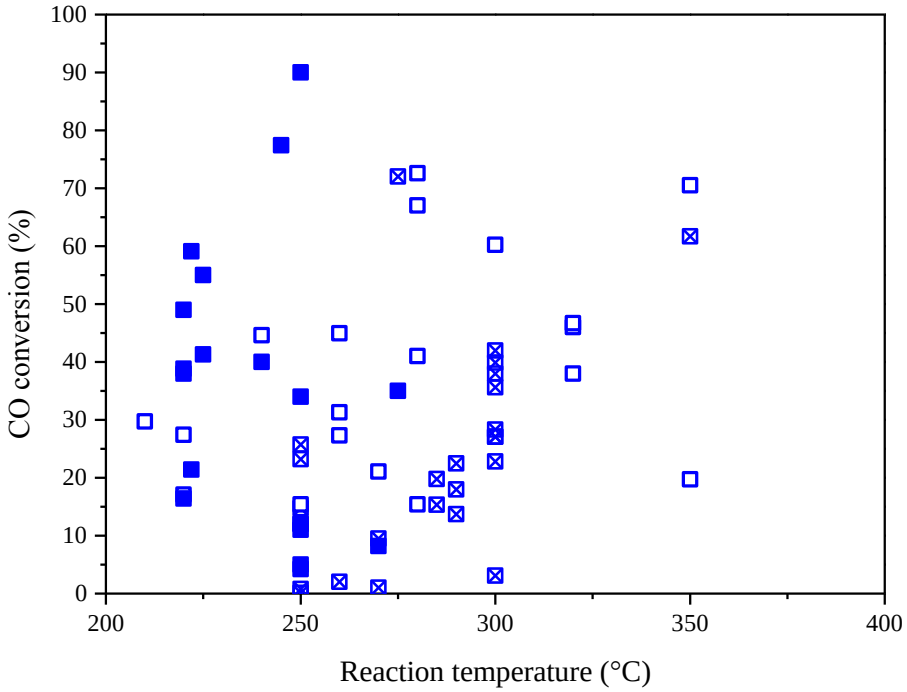

Figure 2-9. CO conversion *versus* reaction temperatures over modified F-T synthesis catalysts: (⊠) Cu-Co-based modified F-T synthesis catalysts, (□) Cu-Fe-based modified F-T synthesis catalysts, and (■) Co-or Fe-based modified F-T synthesis catalysts.

With the addition of copper, the catalysts can be tested at relatively high reaction temperatures (250-350 °C) but the CO conversion decreased greatly following the order of Co- or Fe-based catalysts (mono-metal catalysts) > Cu-Fe-based catalysts > Cu-Co-based catalysts. This effect likely came from the modification of the electronic

structure of cobalt or iron species upon alloying with copper, resulting in a decrease of the CO dissociation ability of these two species in Cu-Fe and Cu-Co catalysts, thus leading to lower CO conversion [158]. Furthermore, Xiao *et al*. proved that there was weak or even no Cu-Fe interaction in the reduced Cu-Fe-based catalysts, thus the ability of original iron elements to convert CO was largely retained. For Cu-Co-based catalysts, however, a Cu-Co alloy was found after the reduction, which reduced the CO activation ability of cobalt elements [166]. Furthermore, Cu-Fe-based catalysts are more favourable for converting syngas with low H_2/CO ratio (0.67-1, such as syngas obtained from coal or biomass gasification) because of the higher WGS activity of iron species [174, 175, 185].

However, most of these modified F-T synthesis catalysts produced hydrocarbons (including methane) as the major products with a hydrocarbon/alcohol ratio of 1 or higher. In order to achieve a high activity and selectivity towards higher alcohols for industrial applications, this catalyst type needs further investigations on the catalyst design to stabilize the active centres during the reaction.

2.4.3 Molybdenum (Mo)-based Catalysts

Molybdenum (Mo)-based catalysts have been considered to be the most attractive catalysts for HAS, as they show on average higher $C_{2+}OH$ selectivity in comparison with the other types of catalyst (see Figure 2-5). Mo-based catalysts produce mainly linear primary alcohols, with selectivity to alcohols following the ASF distribution. In addition to their excellent sulphur resistance, they present high activity for the WGS reaction and a slow rate of coking [198, 199]. According to the literature, Mo-based catalysts can be divided into three classes: molybdenum oxide (Mo-oxide) catalysts, molybdenum carbide (Mo_2C)-based catalysts and molybdenum sulphide (MoS_2)-based catalysts.

2.4.3.1 Molybdenum Oxide Catalysts

Though molybdenum has relatively low activity for syngas conversion and mainly produces hydrocarbons, Mo-oxide catalysts modified with alkali metals, especially potassium [200, 201], or Group VIII metals, in particular F-T elements such as cobalt and nickel [202-204], showed high selectivity to higher alcohols. Recent research results showed that newly developed multi-walled carbon nanotubes (MWCNTs)

[203-205] and carbon nanotubes (CNTs) [199, 206-209] as catalyst supports or promoters have positive effects on the higher alcohol formation. Common catalyst supporters, such as active carbons (AC) [201, 210, 211], silica [200, 212-215], and alumina [216-224], were also tested intensively for this catalyst class, to improve higher alcohol formation. Co-decorated MWCNTs promoted K-Co-Mo catalysts were developed by Wu *et al*. for HAS from syngas [204]. Their $Co_1Mo_1K_{0.05}$-12% (4.2%Co/MWCNTs) catalyst, tested under relatively mild conditions (290 °C, 5.0 MPa, H_2/CO ratio=2, and GHSV=8000 h^{-1}) showed the highest $C_{2+}OH$ selectivity reported to date (80.7%) amongst all catalyst types, to the best of our knowledge. It was reported that the addition of a minor amount of Co-decorated MWCNTs into the Co-Mo-K catalyst led to an increase in the surface concentration of active centres for HAS ($CoO(OH)/Co_3O_4$ and Mo^{4+}). Moreover, the Co-decorated MWCNTs favoured the stationary-state concentration of hydrogen-adsorbed species on the catalyst surface, which would considerably increase the surface hydrogenation reaction rate, inhibit WGS reaction and enhance the main product selectivity.

2.4.3.2 Molybdenum Carbide-based Catalysts

Molybdenum carbides are recognised as active catalysts for light-hydrocarbon formation from syngas (see reviews [28, 48]). However, with a minor amount of alkali metal oxides and transition metals as promoters, Mo_2C-based catalysts showed the ability to convert syngas to form alcohols, especially methanol and ethanol under high reaction pressures [225-243]. Furthermore, this type of catalyst also exhibits higher carbon deposition resistance. When used for syngas conversion, Mo_2C-based catalysts show a high catalytic activity with excellent stability over prolonged period (over 150 h) [228-230]. This was probably due to the elimination of both surface and deposited carbon over the catalyst during the induction period of the reaction [244, 245]. Part of the surface oxygen on the Mo_2C-based catalyst likely reacted with carbidic carbon and was removed from the top surface layer, thus minimising carbon formation.

CO conversion of Mo_2C-based catalysts was generally found to be higher compared to that of the other types of Mo-based catalysts in the same reaction temperature range (see Figure 2-10). However, the majority of the products over Mo_2C-based catalysts are hydrocarbons, especially at higher reaction temperatures.

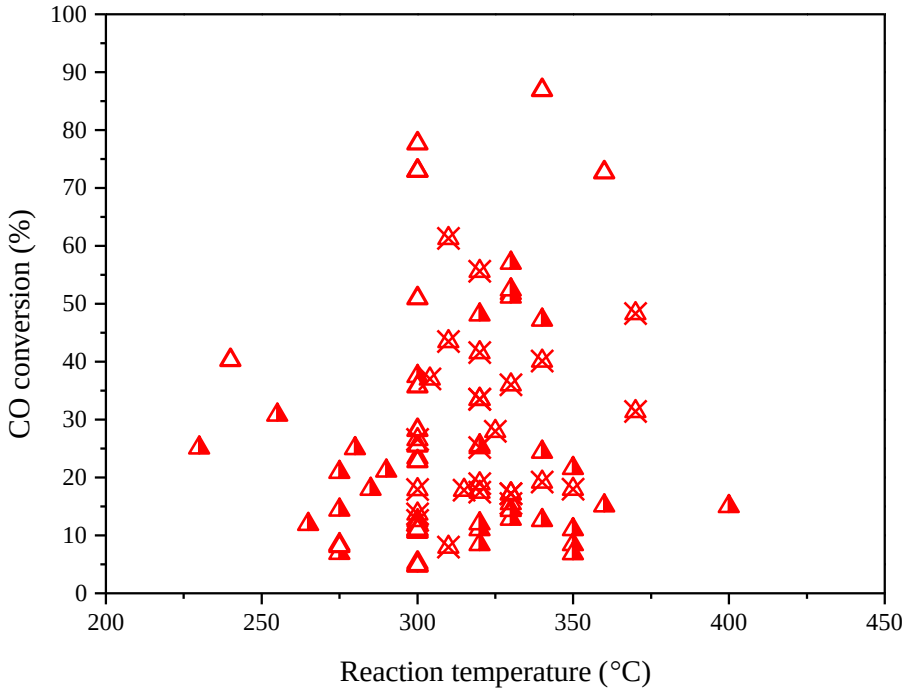

Figure 2-10. CO conversion *versus* reaction temperatures over Mo-based catalysts: (◭) Mo-oxide catalysts, (△) Mo_2C-based catalysts, and (※) MoS_2-based catalysts.

Though vanadium was less investigated as a promoter for catalysts for HAS, a K/V-Mo_2C catalyst, reported by Chiang *et al.*, showed relativity high $C_{2+}OH$ selectivity (60.4%) compared to other Mo_2C-based catalysts [239]. In the K/V-Mo_2C catalyst, potassium was thought to be responsible for shifting the product distribution from paraffins to alcohols, and although vanadium has a strong ability for hydrogenation, its addition further increased the catalyst selectivity toward higher alcohols, especially ethanol, due to the synergistic effect of vanadium and potassium [246].

2.4.3.3 Molybdenum Sulphide -based Catalyst

The MoS_2-based catalysts for HAS were first developed by Dow Chemical Company [247] and Union Carbide Company [248] in 1984 and 1985, respectively. By far, most of the interest in Mo-based catalysts for HAS from syngas has been focused on alkali-doped molybdenum sulphide (AMS) catalysts, as they demonstrate higher sulphur resistance [59, 198, 249-284] and sometimes even need 50 to 100 ppm of hydrogen sulphide in the syngas mixture to maintain the stability of the catalysts [267, 275, 285]. The effect of H_2S-containing feed in the HAS from syngas over MoS_2-based catalysts was reported by Andersson *et al.* [254] and Christensen *et al.* [277].

These authors found that the presence of hydrogen sulphide in the syngas feed decreased the higher alcohol selectivity by greatly increasing hydrocarbon selectivity. The role of hydrogen sulphide in syngas was to replenish the hydrogen adsorption sites, which enhanced the hydrogenation activity of the catalyst, thereby increasing hydrocarbon formation. However, it was also observed that the addition of hydrogen sulphide favoured chain growth of alcohol products, and thus shifted the alcohol distribution to higher alcohols. Although the reasons for this promotional effect remained unclear, it was hypothesised that the concentration of H_2S affected both the number and the nature of active sites over the catalyst [277]. It should be noted that some organic sulphur compounds were also found in the products [238]. MoS_2-based catalysts are also less sensitive to CO_2 and show significant resistance to deactivation caused by coke deposition [38, 278]. These not only make MoS_2-based catalysts more suitable for carbon monoxide-deficient syngas (a low H_2/CO ratio of less than 2) but also save on the cost of deep desulphurization of the feed gas and water separation, which are attractive on a commercial aspect. A La-promoted $Ni/K_2CO_3/MoS_2$ catalyst was investigated by Li and co-workers for the conversion of syngas to higher alcohols and reached a high $C_{2+}OH$ selectivity of 58.5% with a low hydrocarbon selectivity at 34.0% [256]. The nickel promoter in this catalyst showed a promotional effect on the activity towards higher alcohol synthesis due to its strong ability for CO insertion in syngas reactions. Furthermore, the addition of lanthanum restrained the congregation of nickel and resulted in more highly dispersed nickel, thus suppressing the methanation reaction and improving the formation of higher alcohols. The congregated NiS_x particles were recognised as the active centres for hydrocarbon formation while the highly dispersed nickel species promoted the higher alcohol formation.

All Mo-based catalysts discussed here only show high $C_{2+}OH$ selectivity when promoted with alkali metals and/or Group VIII metals. Also, a relatively long induction period of HAS process was observed over Mo-based catalysts. Due to the complexity of the promoted Mo-based catalysts, the exact nature of the active sites on the catalyst surface still remained unclear, and progress is still required to develop a highly selective and active catalyst for industrial application.

2.4.4 Rhodium-based Catalysts

Rhodium-based catalysts have been known to directly convert syngas to ethanol and higher alcohols as early as 1978 and are still being studied now [286]. Among all the Group VIII metals, rhodium is unique because of its special position in the periodic table, that is, it lies between copper and iron elements that favour CO dissociation and hydrocarbon formation, and palladium, platinum, and iridium that do not dissociate CO and produce methanol (see review [47]). Due to their ability to catalyse both CO dissociation and CO insertion, Rh-based catalysts showed the highest ethanol selectivity (above 50%) among all the HAS catalysts reported to date [287-289]. For most of the Rh-based catalysts, HAS experiments were conducted at relatively lower reaction temperatures compared to other catalysts types (180 to 320 °C), as shown in Figure 2-11 [246, 287-316].

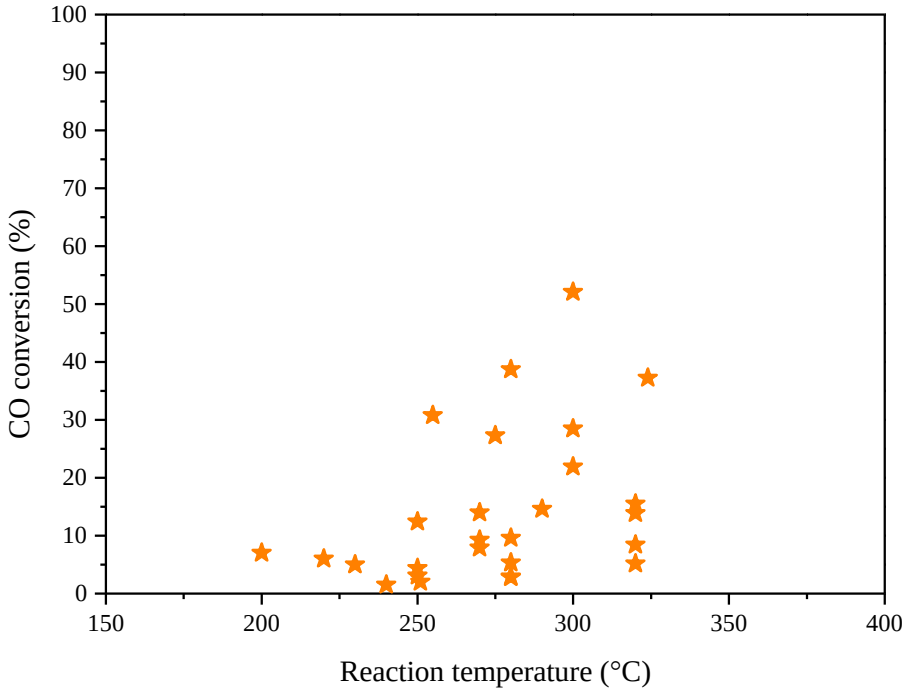

Figure 2-11. CO conversion *versus* reaction temperatures over Rh-based catalysts.

Methane is generally the main by-product of HAS process from syngas over Rh-based catalysts [310, 313]. Hu *et al*. found that relatively low reaction temperature, high operating pressure, and low H_2/CO ratio could partially inhibit methane formation [288]. They reported 56.1% selectivity to ethanol over Rh-Mn/SiO_2 catalyst in a microchannel reactor at reaction conditions of 280 °C, 5.4 MPa, 3750 h^{-1} GHSV, and a H_2/CO ratio of 2, with a relatively low methane selectivity of 38.4%, compared to

54% when the reaction was carried out at 300 °C, 3.8 MPa, 3750 h^{-1} GHSV and a H_2/CO ratio of 3. Furthermore, the addition of promoters to Rh-based catalysts, such as manganese, lanthanum, vanadium, and iron, is another effective way to decrease methane selectivity and enhance ethanol selectivity [287, 293, 295, 317]. Subramanian and co-workers found that with the doubly promoted La-V-Rh/SiO_2 catalyst, the ethanol selectivity reached a maximum at 51.8% while methane selectivity was only 15.4% [287]. The synergistic effect of lanthanum and vanadium promoted ethanol formation by increasing both CO dissociation and CO insertion rates [293, 307].

The support used for Rh-based catalysts also significantly affects the activity and selectivity of the HAS reaction. Gronchi and co-workers investigated the catalyst performance of 1 *wt*.% rhodium supported on lanthanum oxide, thoria, zirconia, and vanadium(III) oxide under the same reaction conditions (220 °C and 0.1 MPa) [313]. They found that zirconia gave the highest selectivity of ethanol at 52% but with low CO conversion (2%). Although the support influence on ethanol selectivity was not discussed in detail, it was hypothesised by Gronchi *et al.* that the support affects the dispersion of the rhodium species, which then affects the catalytic performances.

However, Rh-based catalysts are not attractive for commercial application because of the limited availability and high cost of rhodium, and great efforts have been made by academic and industrial researchers to find less expensive HAS catalysts with higher $C_{2+}OH$ activity and selectivity.

2.4.5 Perovskite Catalysts

Perovskite catalysts for HAS from syngas were developed and reported for the first time in 1982 [318]. In the early stage of perovskite catalyst development for HAS, limited reports were available, with catalysts exhibiting low higher alcohol selectivity. In 1990, Bourzutschky *et al*. reported that a $LaMn_{0.5}Cu_{0.5}O_3$ perovskite catalyst exhibited high methanol selectivity (79.9%) and low $C_{2+}OH$ selectivity (9.3%) in the HAS process (300 °C, 10.6 MPa, GHSV=12000 h^{-1}, and H_2/CO ratio at 2) [319]. From 2006, perovskite catalysts started to attract more attention [50, 319-331] because their special structures offer many advantages compared to the other HAS catalysts discussed above (see Section 2.7).

Recently, Tien-Thao *et al*. investigated a series of $LaCo_{1-x}Cu_xO_3$ perovskite catalysts for HAS [320-325]. $LaCo_{0.7}Cu_{0.3}O_3$ perovskite catalyst showed higher $C_{2+}OH$ selectivity compared to that of unsubstituted $LaCoO_3$ perovskite catalyst (27.3 *wt*. % vs. 13.6 *wt*. %) at 275 °C, 6.9 MPa, GHSV=5000 h^{-1} and H_2/CO ratio at 2 [321]. This result was consistent with previous findings on modified F-T synthesis catalysts (see Section 2.4.2), demonstrating that a Cu-Co alloy is effective for HAS due to the strong synergetic effect between copper and cobalt. The addition of alkali metals, especially potassium, was found to further increase the $LaCo_{0.7}Cu_{0.3}O_3$ perovskite catalyst selectivity towards higher alcohols (37.5 *wt*.%), with the optimum content in the range of 0.1–0.3 *wt*.% [322].

As discussed earlier, the catalyst support play an essential role in higher alcohol formation. Liu and co-workers found that when supported on zirconia, $LaCo_{0.7}Cu_{0.3}O_3$ perovskite exhibited excellent $C_{2+}OH$ selectivity (40.7% at 310 °C, 3.0 MPa, GHSV=3900 h^{-1}, and H_2/CO ratio at 2) [329]. According to He *et al*., zirconia is active for the formation of higher alcohols (mainly ethanol and *iso*butanol) from syngas [332], thus the strong interaction between zirconia and the highly dispersed Cu-Co alloy of the perovskite resulted in the high selectivity for C_{2+} alcohols.

As shown in Figure 2-12, most of the perovskite catalysts were tested around 300 °C for HAS from syngas. The highest reported CO conversion (95%) was obtained over a 7.5 *wt*.% CuO/$LaCoO_3$ perovskite catalyst at 300 °C with a total alcohol selectivity of 31% [50]. The authors suggested that the presence of copper ions outside the perovskite structure facilitated methane and carbon dioxide formation from CO (methanation and WGS), hence the high CO conversion, and the interactions between metallic copper and cobalt carbide were necessary for alcohol formation.

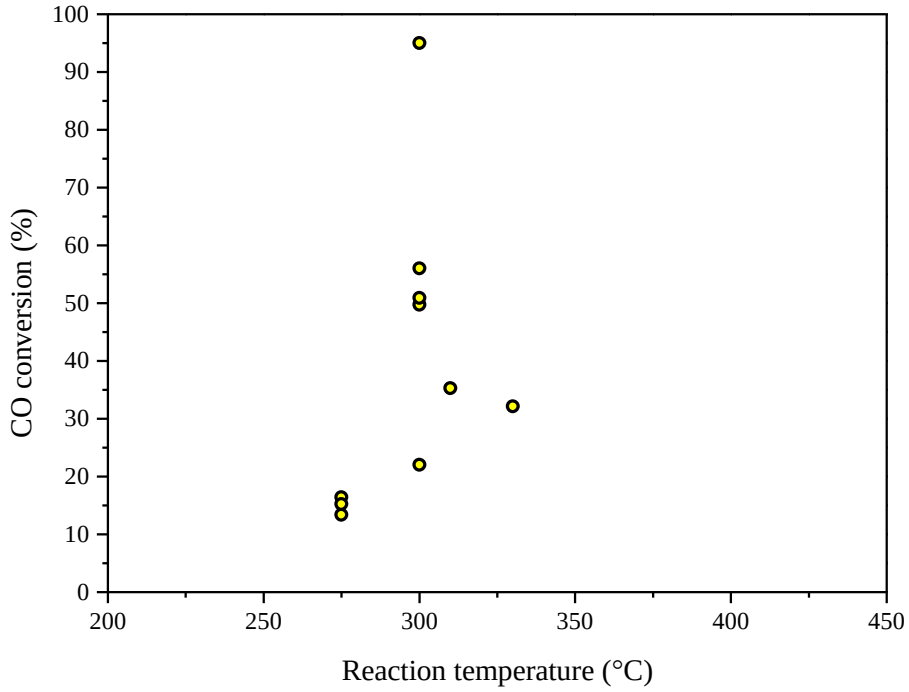

Figure 2-12. CO conversion *versus* reaction temperatures over Cu-Co based perovskite catalysts.

Although perovskite catalysts are only recently being investigated for HAS, with a limited number of reports available, this catalyst system demonstrated potential for high CO conversion and higher alcohol selectivity in HAS process and are considered promising.

2.5 Effect of Catalyst Characteristics for HAS

2.5.1 Effect of Catalyst Supports

Catalyst activity and selectivity are very much dependent on the catalyst support. In general, the catalyst support is considered as a solid material with high surface area, which promotes the distribution of the active metal components. The nature of the support such as surface acidity and texture not only affect the metal dispersion but also influence the interaction between active elements and support. Typical catalyst supports, such as various kinds of zeolite, alumina, silica, zirconia, and carbon have been widely used for catalytic conversion of syngas to higher alcohols (see reviews [16, 35, 48, 333]).

2.5.1.1 Influence of Surface Acidity

Bian and co-workers studied the effect of catalyst support over molybdenum-based catalysts doped with potassium and found that the alcohol yield increased in the order Al_2O_3<SiO_2<un-supported (supports calcination at 500 °C), inverse to the support surface acidity [221]. It has been proved that acidic elements on the catalyst surface favour alcohol dehydration [96, 201]. Thus, part of formed alcohol products are decomposed immediately on these active sites to form hydrocarbons. As a result, the acidity of the supports enhances hydrocarbon selectivity while suppressing the formation of alcohols. Avlia *et al*. also reported that the alcohol selectivity over K/Mo-based catalysts increased in the order of ZrO_2<$ZnCr_2O_4$<Cr_2O_3<ZnO, with the decrease in surface acidity [334]. It is thus reasonable to claim that acidic supports are not particularly suitable for HAS from syngas. In general, higher alcohol formation from syngas requires neutral or basic catalyst supports, such as MgO, ZnO, ZrO_2, CeO_2, La_2O_3,Cr_2O_3, TiO_2, and ThO_2 [86, 243, 249, 298, 309, 329, 332, 334].

However, acidic supports such as alumina and silica are widely used in HAS catalysts due to their high specific surface area, ample porosity, good stability, low-cost, and high availability [16, 38, 140, 298]. In order to improve the selectivity of higher alcohols over these metal oxide support catalysts, a key point is to reduce or eliminate the strong acidity of the catalyst surface. One possible solution, largely used in the literature as noted above, is to modify the supports by introducing alkali promoters to make the catalyst surface neutral or basic [71, 115, 187, 218-221, 278, 288, 302, 332]. Another way to solve this problem is to increase the calcination temperature of the catalyst. Fu *et al.* reported that with high calcination temperature (800 °C), the interactions between the active species of K/Mo-based catalysts and the Al_2O_3 support were strengthened and the number of acidic sites decreased [224]. As a result, both the higher alcohol selectivity and yield were remarkably enhanced along with increasing calcination temperature.

2.5.1.2 Influence of Surface Texture

To further enhance the catalyst performance, new types of catalyst supports can be used in HAS. Carbon nanotubes, including multi-walled carbon nanotubes, have been recognised as a kind of novel nano-carbon support for HAS catalysts [139, 148, 151, 154, 203-208, 279, 311]. CNTs-supported and MWCNTs-supported catalysts

have several advantages over traditional supports, such as high specific surface area that allow greater dispersion of the active sites, resistance to acidic/basic conditions, stability at high temperatures and an inert graphitic surface [203, 280]. Moreover, MWCNTs catalysts provide some unique characteristics that make them suitable as catalytic supports, including highly graphitized tube walls and nano-sized channels, which favour diffusion of reactants and products and maximize metallic dispersion (see review [35]). They are also less prone to sintering of the active phases and coke formation during the catalytic process [207]. Zhang and co-workers have reported that CNT-based materials (including MWCNTs) promoted by cobalt and nickel could act as a novel support of catalysts for HAS [204-206]. They found that the MWCNTs caused little change in the apparent activation energy for the HAS, but improved the concentration of active centres for alcohol formation. The transition metal (Co/Ni) decorated on the CNTs could further enhance the CNTs' capability of adsorbing and activating H_2, and thus, their promoter action was more remarkable. However, the complicated synthesis procedure and high cost of MWCNTs and CNTs somehow limit their applications as catalysts support in HAS process.

2.5.2 Effect of Catalyst Promoters

Promoters are substances added to a catalyst to improve its catalytic activity, even though they have little or no catalytic effect by themselves. In most cases, the promoters interact with the active species of the catalysts and thereby change their electronic and crystal structures, as well as affect the active metal-support interaction, which in turn affect the catalyst reducibility and catalytic performances. Commonly used promoters in HAS are metallic ions, such as alkali metals, F-T elements (copper, iron, nickel *etc*.), and other metallic ions.

2.5.2.1 Effect of Alkali Promoters

Alkali promoters have been widely used for HAS reactions in order to enhance the activity and selectivity towards higher alcohols as well as the stability of catalysts (see numerous examples mentioned above). As mentioned before, these basic promoters neutralize the acidity of the catalyst supports and thus inhibit undesired reactions such as methanation, alcohol dehydration and coke formation [38, 88, 138, 322]. In addition, alkali metals have been shown to promote chain growth and shift the

selectivity from hydrocarbons to alcohols by increasing the rate of CO insertion and decreasing the rate of hydrogenation of alkyl species [64, 71, 105, 231, 274, 279, 283].

It has been shown that the alkali promoters performance over HAS catalysts follows the general trend Li < Na < K < Rb < Cs, in accordance with the increasing alkali atomic size and basicity [16]. Caesium has been reported to be the best alkali promoter for modified methanol synthesis catalysts for branched higher alcohol synthesis [16, 35, 51, 52]. The addition of caesium provides strong basic sites and neutralise the acidic supports (*e.g.* Cr_2O_3 and Al_2O_3) of modified methanol synthesis catalysts. Furthermore, caesium was reported to significantly promote the selectivity towards branched higher alcohols because it favoured the base-catalysed β carbon-addition of the growing alcohol intermediates [335]. However, it is less effective for linear primary alcohol formation over modified F-T synthesis catalysts, Mo-based catalysts, and perovskite catalysts, where lithium, sodium, and potassium are more effective [138, 141, 186, 204, 239, 268]. Compared to lithium and sodium, the addition of potassium promoted higher selectivity towards $C_{2+}OH$ because of its relatively higher basicity [89, 274, 322].

Nevertheless, the HAS catalytic performance not only depends on the basicity of the alkali promoters but also relates to the concentration of the promoters. Due to the differences in catalysts' acidity and properties, the amount of promoters should be varied and optimised according to a given type of catalyst. Anton *et al*. investigated the effect of sodium addition on the cobalt-modified $Cu/ZnO/Al_2O_3$ catalysts for higher alcohol formation from syngas [92]. With low sodium loadings ($\leq$ 0.6 *wt*. %), bulk metallic copper particles, metallic cobalt, and species resulting from the close contact between metallic copper and cobalt were detected on the catalyst surface. The selectivity to $C_{2+}OH$ alcohols gradually increased during the first 10 h TOS indicating enhanced Cu-Co surface alloy formation during the reaction, considered as the active sites for HAS. However, probably due to the highly exothermic methanation (promoted by Co^0), coking of metallic cobalt occurred and contributed to the strong initial deactivation of the catalyst. With high sodium loadings ($\geq$ 0.8 *wt*. %), deactivation did not occur and constant CO conversion and product distribution was observed. Carbonization of metallic cobalt was favoured, resulting in the formation of bulk Co_2C. The Co_2C-Co^0 interfaces, which is known to facilitate CO adsorption [336], was considered as an additional active site for HAS in this catalyst. According to the

literature, the $Cu/ZnO/Al_2O_3$ catalyst promoted with 1.2 *wt*.% sodium showed the highest selectivity for higher alcohol (48.5% at 280 °C, 6.0 MPa). Surisetty *et al*. studied the promotional effect of potassium over MoS_2 catalysts supported on MWCNTs for HAS (310 °C and 6.9 MPa) [279]. It has been confirmed that increased potassium loadings (from 3 to 9 *wt*. %) clearly increased the higher alcohol selectivity (from 7.6% to 21.2%) while having little effect on CO conversion. Increasing the amount of potassium increased the K-Mo-O interactions that are responsible for HAS, but decreased the availability of MoS_2 sites that are responsible for H_2 activation. Higher levels of alkali promoter loading could reduce the catalytic activity significantly by blocking the active centres on the catalyst surface (see review [16]).

2.5.2.2 Effect of F-T Elements in HAS

F-T metals have been used as promoters in HAS catalysts frequently. The selection of promoters largely depends on the catalyst types. Cobalt and nickel have been reported as promoters to increase the higher alcohol selectivity of Mo-based catalysts [202-204, 225, 251, 253, 254], while iron is often used in modified methanol synthesis catalysts and Rh-based catalysts [70, 181, 289, 295, 299, 300].

It is well confirmed that cobalt promotes carbon chain growth of hydrocarbons in the F-T process [202, 253]. Xiang *et al*. claimed that for K/Mo_2C-based catalysts, the addition of cobalt caused a strong promotion of carbon chain growth, especially for the methanol to ethanol step (see Figure 2-2). The presence of Co resulted in an increased selectivity towards higher alcohols and the Co/Mo mole ratio of the catalyst had a significant effect on the catalyst performance (with a maximum $C_{2+}OH$ selectivity at 27.4% when Co/Mo=1/6) [225].

In the F-T process, nickel is generally considered the active element for methanation [274, 337]. However, recent investigations revealed that when nickel was used as a promoter, it has the potential to promote carbon chain growth due to its strong ability for CO insertion [257, 274]. Li *et al*. found that the nickel modified K/MoS_2 catalyst increased the selectivity of the catalyst towards higher alcohols, especially ethanol [251, 259, 268]. At Ni/Mo molar ratio of 0.33, the methanol selectivity decreased sharply from 22.5% to 6.2% and higher alcohol selectivity increased from 28.8% to 41.2% compared to the non-promoted catalyst [259].

The 3*d* transition metal iron also has a positive influence in HAS due to its combined effect of suppressing methanation and enhancing ethanol production [289]. Xu *et al*. found that addition of iron to $CuMnZrO_2$ catalyst (Cu:Mn:Zr:Fe molar ratio=1:0.5:2:0.1) significantly improved the alcohol distribution towards ethanol from about 6.0 *wt*.% to 24.4 *wt*.% at 300 °C, 8.0 MPa and 8000 h^{-1} GHSV [181]. Similar findings were published where iron was used as a promoter over Rh-based catalysts [289, 295, 300, 306]. Haider *et al*. studied higher alcohol formation using iron promoted Rh-based catalysts and reported that with 2.5 *wt*.% addition of iron to 2 *wt*.% Rh/TiO_2 catalyst, the ethanol selectivity increased from 11.1% (2 *wt*.% Rh/TiO_2 catalyst) and reached a maximum at 31% (270 °C, 2.0 MPa, and H_2/CO ratio of 1) [299].

2.5.2.3 Effect of Other Elements

The introduction of other metals such as lanthanum, manganese, and palladium in HAS catalysts can also promote the catalytic selectivity to higher alcohols. Yang *et al*. investigated the effect of lanthanum addition on $K/Co/MoS_2$ catalyst and found that lanthanum increased the ethanol selectivity from 32.7% without lanthanum to 40.0% with La/Mo molar ratio at 0.2 and decreased the selectivity towards hydrocarbons from 28.9% to 24.8% [250]. The strong interaction between lanthanum and cobalt inhibited the formation of CoS_x crystal particles, thereby enhancing the dispersion of cobalt species and the concentration of Mo-Co-S mixed phases over the catalyst surface. Qi *et al*. found that the addition of manganese to $K/Ni/MoS_2$ catalysts suppressed the formation of methane by inhibiting the sintering of nickel over the catalyst surface [257], thus the higher alcohol formation promoted by nickel became favourable. As a result, the synergetic effect of manganese and nickel improved the selectivity towards higher alcohols (See Section 2.4.3.3, [256]). Palladium is another metal often reported as a promoter for HT modified methanol synthesis catalysts, namely Zr/Cr-based catalysts [51, 54, 58]. Epling *et al*. reported that when Zr/Cr-based catalysts were doped with palladium, the higher alcohol production rate increased significantly, especially that of *iso*butanol [52, 55]. Palladium was added to facilitate the catalyst reducibility and improve the activation of H_2 and CO.

2.5.2.4 Effect of Multi-promoters

It has been found that a mixture of both alkali and non-alkali promoters can be more effective for HAS, such as addition of caesium and palladium over Zn/Cr-based catalysts [52, 55], potassium and lanthanum over Cu-Fe-based catalysts [174, 175], and potassium, nickel, and lanthanum/manganese over MoS_2-based catalysts [256, 257]. Yin *et al*. studied a series of Rh/SiO_2 based catalysts promoted with lithium, manganese, and iron for the catalytic conversion of syngas to ethanol [297], and the results are summarised in Table 2-1. It is clear from Table 2-1 that CO conversion and ethanol formation improved with multi-metal addition to the Rh-based catalyst.

Table 2-1. Effect of different components on the reaction performance of catalysts for CO hydrogenation over Rh/SiO_2 catalyst [297].

Catalyst	CO Conversion (%)[a]	Selectivity (%)			
		Methanol	Ethanol	C_{2+} oxy.	HC
Rh/SiO_2	2.6	4.5	12.3	4	79.2
$Fe/Rh/SiO_2$	2.9	11.8	12.9	7.5	67.8
$Mn/Rh/SiO_2$	8.7	0.3	23	11.9	64.8
$Fe/Mn/Rh/SiO_2$	9.0	1.6	22.7	17.5	58.2
$Li/Mn/Rh/SiO_2$	6.7	1.4	35.5	21.2	41.9
$Fe/Li/Mn/Rh/SiO_2$	8.4	1.6	27.4	28.9	42.7

[a] reaction conditions: T = 320 °C, P = 3.0 MPa, GHSV = 12000 h^{-1}, and $H_2/CO = 2$.

2.5.3 Effect of Catalyst Preparation Method

As mentioned before, catalytic activity and selectivity are affected by the catalyst properties, and the preparation method of the catalyst also plays an important role in its performance in HAS. Most of the catalysts discussed in this chapter were prepared *via* two major methods: precipitation (or co-precipitation) and impregnation. Precipitation is widely used in catalyst preparation, with the main advantages being the possibility of creating very pure materials and the flexibility of the process with respect to the final product composition suitable for small scale research (see reviews [338-340]). Precursor deposition by impregnation is also an important and frequently used method, in which a dry porous support is contacted with a solution containing the dissolved precursors (see review [339]). In addition, mechanical methods such as reactive grinding and ball milling are also used in some studies to prepare catalysts with high catalytic activity [320-323].

In recent years, some research focused on the development of modern catalyst preparation methods to further improve the catalyst performances. Gupta *et al*. prepared Mn/Cu-ZnO nano-wires by electrodeposition method and used it as catalyst for HAS [99]. This method has the ability to control the surface properties of multi-metallic catalysts, which is not possible with conventional catalyst preparation methods such as co-precipitation and impregnation. Zhang *et al*. investigated Cu-Fe-based catalysts for HAS prepared by plasma-assisted method [180]. Compared to conventional catalysts, the catalyst prepared by plasma-assisted method exhibited higher activity and selectivity towards higher alcohols, due to increased specific surface area, higher dispersion of active components (Fe, Cu), and smaller particle size. By using silica sol and silica gel, Ding *et al*. prepared a multi-functional silica-silica bimodal pore catalyst support through incipient-wetness impregnation method [187]. This bimodal support had more surface area and less pore volume, but a higher number of small pores compared to the original silica gel. The good dispersion of the active metal sites (copper and iron) and the high diffusion efficiency of the products inside the bimodal pore structures favoured the catalyst activity and selectivity of higher alcohols. Li *et al*. synthesised a highly homogeneous and dispersed K/Ni/MoS_2 catalyst by ultrasonic technology under non-water environment [268]. This catalyst showed higher $C_{2+}OH$ selectivity compared with the corresponding catalyst prepared by co-precipitation method (61% vs. 44%). The high homogeneity of this K/Ni/MoS_2 catalyst suppressed the formation of nickel sulphides, thus inhibiting methanation. París *et al*. investigated the influence of K/Ni/MoS_2 catalysts preparation route for HAS [274]. A novel catalyst prepared by co-precipitation in micro-emulsion outperformed its counterpart prepared by the conventional method in term of selectivity and yield of higher alcohols, which was attributed to the higher concentration of promoters over the catalyst surface and a lower degree of catalyst crystallinity. Kim *et al*. prepared a structurally well-defined ordered mesoporous carbon (OMC)-supported rhodium nanoparticle (NP) catalysts with low rhodium content (<1 *wt*.%) by sonochemical (SN) method [311]. Compared to the catalyst prepared *via* simple incipient wetness method, the SN catalyst increased the higher alcohol selectivity (from 20.6% to 58.9%) and decreased methane formation (from 65.2% to 24.1%) at 320 °C, 3.0 MPa, 12000 h^{-1} GHSV, and H_2/CO ratio of 2. This is because the uniform size of rhodium NPs in the OMC supports enhanced both the CO insertion and chain growth reactions.

Figure 2-13 displays the differences in higher alcohol selectivity for different catalysts, prepared by different novel methods, compared to conventional methods. It is noticeable that the catalysts prepared by new techniques exhibited higher $C_{2+}OH$ selectivity compared to the catalyst prepared by conventional methods. In general, new preparation techniques enhanced the higher alcohol selectivity because of higher catalyst surface area, more uniform particle size and distribution of active centres. However, such novel methods have their limitations for HAS application, such as high cost, complicated synthesis conditions and reproducibility issue, and difficulty in scale-up procedures.

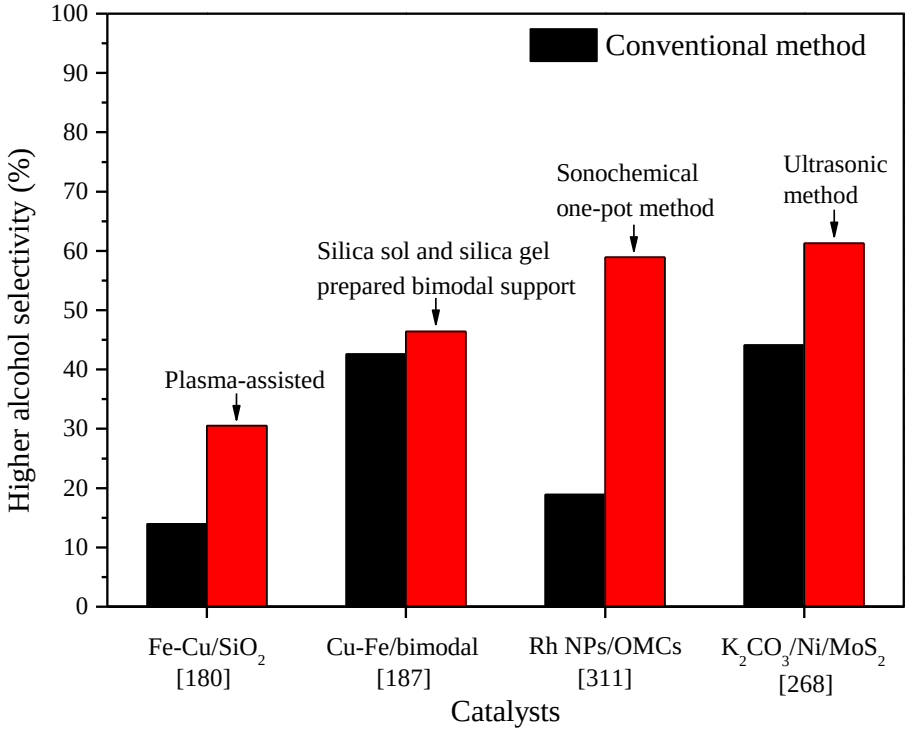

Figure 2-13. Higher alcohol selectivity over different catalysts, prepared by conventional and new methods.

2.6 Evaluation of Different HAS Catalysts

Table 2-2 summarised the typical reaction parameters and resulting yields range of each type of HAS catalyst discussed in Section 2.4, as well as the highest reported yield.

Table 2-2. Comparison of catalysts and reaction parameters for HAS.

Catalyst Type	**Catalyst Formula**	**T (°C)**	**P (MPa)**	**H_2/CO Ratio**	**GHSV (h^{-1})**	**C_{2+}OH Yield (%)[1]**	**Highest Reported C_{2+}OH Yield (%)[2]**
Modified methanol synthesis catalysts	Zn/Cr spinels (HT)	400-440	7-11	1/1	8000-12000	3-13.5	13.5% [55]
	Cu/Zn/Cr oxides (LT)	275-310	8	9/20	3000-5000	2-7.2	7.2% [83]
	Cu/Zn/Al oxides (LT)	250-360	2-8	1/1-2/1	3000-10000	1-14	16.8% [90]
Modified F-T synthesis catalysts	Co-based catalysts	220-290	1-5	1/1-2/1	250-24000	1-17.2	24.9% [114]
	Cu-Co-based catalysts	250-350	2-9	1/1-2/1	3000-18000	1-14.5	20.5% [151]
	Cu-Fe-based catalysts	220-320	3-6	1/1-2/1	4000-6000	3-20	24.1% [186]
Mo-based catalysts	Mo-oxide catalysts	270-360	1.6-10	1/1-2/1	4000-10000	1-10	26.3% [204]
	Mo_2C-based catalysts	275-300	3-10	1/1-2/1	2000-5000	2-24	26.8% [230]
	Mo_2S-based catalysts	290-370	1.5-13	1/1-2/1	1000-6000	1-23	30.3% [59]
Rh-based catalysts	Rh-based catalysts	180-320	0.1-5	2/1-3/1	5000-20000	0.5-12	21.1% [288]
Perovskite catalysts	Perovskite catalysts	275-310	3-7	2/1	3900-5000	3-15	25.5% [326]

[1] General range of higher alcohol yield;

[2] Highest reported higher alcohol yield was sometimes not repeatable.

It can be seen from Table 2-2 and all the catalyst studies mentioned in the sections above that despite intensive work in HAS in the last 37 years, the higher alcohol product yields remain too low for commercial applications at this stage. Some modifications of the catalysts need to be applied to increase the higher alcohol selectivity and yield.

In order to enhance the HAS process, it is important to identify the best catalyst candidates from the previous study and use it as a base to develop future highly active, selective and stable catalysts for HAS. As discussed above, different types of catalysts have been investigated for HAS in the last 37 years, each with their advantages and disadvantages, which are summarised in Table 2-3.

Table 2-3. Advantages and disadvantages of HAS catalysts.

Catalyst Type	**Advantages**	**Disadvantages**
HT Modified methanol synthesis catalysts	– High *iso*butanol selectivity	– High operation temperatures and pressures – Low CO conversion – Low interest currently in *iso*butanol production
LT Modified methanol synthesis catalysts	– Low operation temperatures and pressures – High CO conversion	– Methanol as the main product
Modified F-T synthesis catalysts	– Moderate operation temperatures and pressures – Low H_2/CO ratio in feed (Cu-Fe-based catalysts)	– Low $C_{2+}OH$ selectivity – High hydrocarbon selectivity – Catalyst deactivation caused by copper sintering
Mo-based catalysts	– High $C_{2+}OH$ selectivity – Sulphur resistance (Mo_2S) – Deactivation resistance	– Relatively high reaction temperatures and pressures – Sulphur contamination of the produced alcohols (MoS_2-based catalysts) – Long induction period
Rh-based catalysts	– High selectivity towards ethanol – Low operation temperatures and pressures	– limited availability and high cost of rhodium – Relatively lower higher alcohol yield – High methane selectivity
Perovskite catalysts	– Unique structure and properties of perovskite catalysts (tuneable catalyst) – Huge amount of different compositions	– Low $C_{2+}OH$ selectivity – Not fully studied yet

HT modified methanol synthesis catalysts might not been considered as attractive catalysts anymore for large scale HAS process. The high reaction temperatures lead to methanation instead of the higher alcohol formation, and the high operation temperatures and pressures are less preferred for commercialisation. Besides, the main product formed with HT modified methanol synthesis catalyst (*iso*butanol) has lost attractiveness due to the environmental restriction on MTBE (see Section 2.4.1.1). LT modified methanol synthesis catalysts also might not be suitable for future HAS study because methanol remains the dominant alcohol product. Modified F-T catalysts provide moderate higher alcohol selectivity but hydrocarbon formation is dominant, especially methane. What's more, the catalyst deactivation caused by copper sintering is another drawback. Even though MoS_2-based catalysts have been studied intensively in recent years, it has been reported that these catalysts would cause sulphur contamination of the produced alcohols, which is a critical drawback for MoS_2-based catalysts [190, 328]. In addition, HAS with Mo-based catalysts must be carried out at relatively high reaction temperatures and pressures, and usually have a long induction period [96].

Despite their advantages, Rh-based catalysts could be eliminated from further consideration for commercial application of HAS from syngas, due to the limited availability and high cost of rhodium. The generally lower higher alcohol yield compared to the other catalyst types also makes Rh-based catalysts less attractive for commercial application.

Compared to the catalysts listed above, perovskite catalysts have become an attractive option for the future and commercial application of HAS. Though only limited studies have been reported until now, the unique structure and properties of perovskite catalysts open a new research pathway to a highly active and selective HAS process. Over the last 10 years, important progresses have been made regarding the CO conversion (from 15% to 95%) as well as higher alcohol selectivity (from 10% to 50%). These have led to assumptions that F-T elements substituted into the perovskite catalysts would increase the higher alcohol selectivity. Therefore this research will focus on the development of perovskite catalysts and their catalytic performance for higher alcohol synthesis from syngas.

2.7 Perovskite Catalysts

2.7.1 Introduction

Gustav Rose discovered a calcium titanium oxide mineral with the chemical formula $CaTiO_3$ in the Ural Mountains of Russia in 1839 and named it Perovskite after Russian mineralogist, Count Lev Alexevich Von Perovskt (1792-1856) [341]. Any compound that has the same ABO_3 structure as the original perovskite mineral is now labelled as a perovskite structure. Perovskites started to be reported as catalysts in the 1950s, and from then, many fundamental and applied studies have been carried out for different reactions (see book [342]).

2.7.2 Perovskite Structure

Perovskite oxides have an ABO_3 type crystal structure, ideally cubic, as depicted in Figure 2-14, where A- and B-sites can be occupied by a board range of metallic cations of different sizes and oxidation states. The larger cation A is 12-fold coordinated with oxygen anions and formed a face-centred cubic (FCC) lattice. The smaller cation B is 6-fold coordinated and occupied the octahedral sites in this FCC lattice [342, 343].

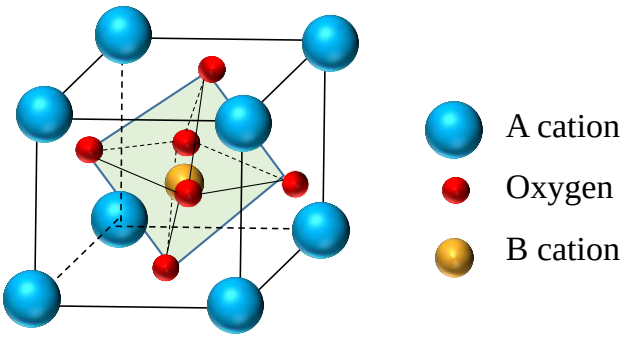

Figure 2-14. Ideal cubic ABO_3 perovskite structure.

The perovskite structure is very tolerant to changes in the ionic radii of A and B cations. In general, the stability and distortion of perovskite structure can be described by the tolerance factor (t), as shown in Equation (2-10) [344]:

$$t = (r_A + r_O)/\sqrt{2}(r_B + r_O) \qquad (2\text{-}10)$$

Where r_A is the radius of cation A, r_B the radius of cation B, and r_O the radius of the anion O. The perovskite structure is maintained when t is between 0.75 and 1.0,

and the ideal cubic structure with *t*=1. However, only a small number of perovskites actually display the cubic structure, and they often exhibit a slight distortion of the lattice, such as rhombohedral, orthorhombic or tetragonal symmetry [345].

In addition to the tolerance factor, the charges of A and B cations have to balance the oxygen anion charge [346]. This means that perovskites of different charge distributions are possible, *e.g.* $A^{1+}B^{5+}O^{3}$, $A^{2+}B^{4+}O^{3}$ or $A^{3+}B^{3+}O^{3}$. Thus the perovskite structure can tolerate significant non-stoichiometric and partial substitution. By introducing one or more elements in each of the A- and B-site, a large variety of perovskites could be designed and prepared to obtain several desired physico-chemical properties. Furthermore, oxygen vacancies can also exist, which results in defective ABO_{3-x} perovskites, with different effect on activity (positive or negative), depending on the process in which the perovskites are used [347, 348]. For example, the partial substitution of La^{3+} by Sr^{2+} in $LaFeO_3$ perovskite creates $La_{1-x}Sr_xFe_{1-x}^{3+}Fe_x^{4+}O_3$. With increasing strontium substation, oxygen vacancies are formed by releasing oxygen ($La_{1-x}Sr_xFe_{1-x+2\delta}^{3+}Fe_{x-2\delta}^{4+}O_{3-\delta}$) [342].

2.7.3 Perovskite Properties

The thermal stability of ABO_3 perovskite oxides is determined by the cations at the A- and B- sites and most perovskites are thermally stable at high temperatures [342]. Many perovskite oxides also exhibit basic properties which make them promising for many reactions, such as oxidative coupling of methane and HAS reactions [342, 345]. In addition, perovskite oxides display several interesting physical properties, such as magnetism, electrical conductivity, and optical properties. Furthermore, the relatively low manufacturing cost of perovskite oxide attracted interest in their applications [349].

In order to take advantage of perovskites as catalysts, an appropriate selection of the A and B cations is necessary. In ABO_3 perovskites, the large cation A can be lanthanide metals (La, Sm, and *etc*.) and/or alkaline earth metals (Ca, Sr, Ba, and *etc*.), and the small cation B can be selected from a wide range of transition metals (Cu, Co, Ni, Fe, Cr, Al, and *etc*.) and noble metals [350-352].

Appropriate attention should be paid to the role of the A- and B-site cations on the catalytic properties of perovskite catalysts in the catalyst design. Previous studies

reported that the partial substitution of the A-site cation affects not only the structure of perovskite but also the oxygen non-stoichiometry and mobility, which will influence the catalytic reducibility and the stability of the perovskite [345, 353, 354]. Falcón *et al*. found that for $LnNiO_3$ (Ln= Pr, Sm, Eu) perovskite catalysts, the orthorhombic phase increased in the order of Pr < Sm < Eu and the reducibility reduced in the same order. With the partial substitution of the A-site Ln cation with strontium, the $Pr_{0.95}Sr_{0.05}NiO_3$ perovskite showed further enhanced reducibility, which led to an increase in activity for CO oxidation due to the relative ease of oxygen removal and the existence of oxygen vacancies [355]. On the other hand, the B-site cation significantly affected the catalytic properties [350, 353, 356]. As mentioned before, the combination of cobalt and copper in $LaCo_{1-x}Cu_xO_3$ perovskites show higher $C_{2+}OH$ selectivity in HAS compared to the unsubstituted $LaCoO_3$ catalyst (27.3 wt. % vs. 13.6 *wt*. %, respectively) [321]. The combination of two different elements at the B-site results in great enhancement of catalytic activity due to synergistic effects, similar to what has already been discussed for other catalysts (Section 2.4). In general, A-site elements affect the perovskite structure which in turn influences the catalyst reducibility, while B-site cations are the reducible species. Thus, the perovskite oxides are promising candidates for many reactions due to their rigid structure, flexible composition, thermal stability, and low cost.

2.7.4 Applications of Perovskite Catalysts

Perovskite oxides can be applied in a wide range of chemical processes. Some examples are provided below.

$SrTiO_3$- and $NaTaO_3$-based perovskite catalysts exhibit high activity and excellent stability as photocatalysts for water splitting under visible-light irradiation [357]. To further optimise the whole reaction process and improve the catalyst performances, many different modification strategies were applied in these ABO_3 structure catalysts, such as incorporation of upconversion luminescent agents (*e.g*. Er^{3+}, Em^{3+}, and Tm^{3+}) and employing appropriate perovskite preparation methods [358, 359].

$LaCoO_3$- and $LaMnO_3$-based perovskites have been recognised as promising catalysts for methane combustion, which is often used to remove exhaust gas from automobiles [360, 361]. With partial substitution at the A- and /or B-site of the perovskite structure, the catalysts show higher catalytic performance due to the non-

stoichiometry of the oxygen and the existence of lattice defects [362]. Due to the properties mentioned above, partially-substituted $La_{1-x}A_xMO_{3-\delta}$ (A=Sr or alkali metals, M=Co or Mn) perovskite catalysts are also widely used to control the emission of soot from diesel engines through soot combustion [363-365].

Comprehensive investigations were applied to study the production of hydrogen over $LaCoO_3$- and $LaFeO_3$-based perovskite catalysts, including dry reforming of methane [366, 367] and ethanol steam reforming [368, 369]. This is because the perovskite catalysts have a rigid crystal structure and show excellent thermal stability. Besides, appropriate substitution at the A- and/or B-site of perovskite catalysts (*e.g.* cerium and/or nickel) also improved the catalytic performance and suppressed the coke formation [366].

Furthermore, there is a great interest in using perovskites as solid oxide fuel cells (SOFCs) due to their excellent oxygen mobility and permeation [370, 371]. Sr-substituted $La_{1-x}Sr_xMnO_{3-\delta}$ perovskite is one of the most commonly used cathode materials in SOFCs, while $LaAlO_3$-based perovskites have been studied as the SOFCs' electrolyte and anode materials [370, 372].

Perovskite catalysts show higher catalytic performances in the above chemical processes due to their unique structure and special properties. Appropriate substitution at the A- and/or B-site of perovskite catalysts further optimise the whole reaction process. As a result, perovskites are promising candidates for HAS, as shown in Section 2.4.5.

2.8 HAS Catalysts Opportunities

2.8.1 Challenges

Catalytic conversion of syngas to higher alcohols is of great interest at the moment due to the global energy crisis, increasing environmental concerns, and the high demand for gasoline additives (see Section 2.3). However, HAS from syngas suffers from low yields and poor selectivity towards the targeted $C_{2+}OH$ products, which significantly limit its potential commercial application. Until now, there is no commercial plant that exists solely for the production of higher alcohols from syngas. Although great efforts have been made for the improvement of the HAS process over

the last three decades, many uncertainties and challenges still exist. This section explores some of these challenges.

The first major technical challenge for HAS process is to break down the "seesaw" effect of higher alcohol selectivity and CO conversion (as shown in Figure 2-6), namely, to achieve high $C_{2+}OH$ selectivity and high CO conversion to get high yields, which are critical for the commercial production of mixed alcohols. Secondly, the selectivity of HAS by-products, such as hydrocarbons (mostly methane) and carbon dioxide, need to be minimised to achieve better carbon efficiency. Thirdly, the stability of the catalysts is one of the key parameters for HAS commercialisation, and the deactivation behaviours of the catalysts should be further studied to prolong the catalyst lifetime. Lastly, the relatively high reaction conditions for HAS process (high temperatures and pressures) need to be reduced to lower the process costs and improving the efficiency.

Future research & development work should focus on the development of highly efficient catalysts for higher alcohol synthesis and optimisation of the reaction process to achieve economic viability for HAS from syngas and meet the market demands.

2.8.2 Potential of Perovskite Catalysts for HAS

A brief summary of the A- and B-site characteristics and functions in the ABO_3 perovskite is presented in Table 2-4.

Table 2-4. Basic functions of both A- and B-site of ABO_3 perovskite catalysts.

	A-site	B-site
Elements	Rare-earth, alkaline-earth or other large ions	Transition metals of first row in periodic table
Atomic radius	R(A)>0.90 Å	R(B)>0.51 Å
Effects on catalyst properties	Structure of perovskite Stability of perovskite Oxygen vacancy and mobility Reducibility of perovskite	Synergistic effects with multiple elements Reducibility of perovskite
Hypothesis effects on HAS Process	CO conversion	Higher alcohol selectivity
Candidates	La (3+) High activity for HAS Easy to form perovskite structure Suppress hydrocarbon formation	Co (3+) Good for carbon chain grows
	Sr (2+) High activity for HAS Generate structural defects	Cu (2+) Good for methanol formation
		Ni (3+) Good for CO insertion Sever methanation

Lanthanum is a good candidate for the A-site for HAS perovskite catalysts as it easily forms the perovskite structure with different B-site metals, such as in $LaCoO_3$, $LaFeO_3$, $LaNiO_3$, $LaMnO_3$, and *etc*. As mentioned in Section 2.5.2.3, lanthanum provides excellent catalytic selectivity for HAS from syngas due to its strong interaction with cobalt and nickel species, which led to the high dispersion of these F-T elements over the catalyst surface [250, 256]. In addition, lanthanum oxide can act as a promoter in Co-contained catalysts for HAS. The increased higher alcohol selectivity was attributed to the formation of new active sites — cobalt carbides (Co_2C) —promoted by lanthanum oxide [113, 122]. Furthermore, the basicity of lanthanum oxide is ideal for CO conversion to form higher alcohols [156]. Substitution at the A-site with a different valence cation, such as strontium, not only influenced the structure and stability of perovskite oxides but also affected the catalytic activity for many reactions, such as oxidation of carbon monoxide [373] and hydrocarbons [374], and steam reforming [374]. Though the effect of strontium substitution has not been

studied in HAS process, it is reasonable to deduce that the Sr-substituted perovskite catalysts would affect the catalyst activity.

As for the B-site cation, cobalt, nickel and copper are good candidates (as a single metal, or partially substituted), as they are active metals (F-T elements) for higher alcohol formation [138, 354]. Cobalt is a very active metal catalyst in F-T synthesis to produce hydrocarbons (paraffin and olefin), while copper tends to form methanol and other alcohols [47, 82, 138]. Nickel is often used as a promoter to increase catalysts' activity and higher alcohol selectivity [251, 256, 259, 268]. Due to the synergistic effect of combined metals, the partial substitution of the B-site in the perovskite structure should be taken into consideration. Some considerations for partial substitution of the A- and B-site are $A_{1,1-x}A_{2,x}BO_{3\pm\delta}$, $A_{1,1-x}A_{2,x}B_{1,1-y}B_{2,y}O_{3\pm\delta}$ or $A_{1,1-x}A_{2,x}B_{1,1-y-z}B_{2,y}B_{3,z}O_{3\pm\delta}$, with A_1=La, A_2=Sr, B_1=Co, B_2=Ni, and B_3=Cu.

Alkali ions (*e.g.*, Li, Na, K, Rb, and Cs) can also be introduced into the perovskite catalysts as promoters to improve the higher alcohol selectivity due to the relatively higher alcohol selectivity of catalysts containing an equal atomic amount of alkali promoters, which increases in the order 0 < Li < Na (≈Rb) < K [375].

2.8.3 Objective of Current Study

A number of research challenges for HAS, in particular the catalysts, have been identified. The objective of the current study focuses on the development of stable perovskite catalysts with high activity and selectivity for HAS from syngas. According to the discussion above, perovskite catalysts are considered as promising catalysts for higher alcohol synthesis from syngas. The unique structure and special properties of perovskite offer a huge range of different compositions for tailor made catalysts, to suit the HAS process [345]. This research also aims to provide insights into the effect of partial substitution on the catalyst properties and reaction performance, as well as on the changes of catalyst structures during the reaction.

The main objectives of the current study are listed below:

- To design, prepare and characterize partially-substituted perovskite catalysts $A_{1,1-x}A_{2,x}B_{1,1-y-z}B_{2,y}B_{3,z}O_{3\pm\delta}$.
- To investigate the effect of partial substitution at the A- and/or B-sites of perovskite catalysts for higher alcohol formation from syngas in F-T synthesis.

- To examine the effect of alkali promoters and reaction conditions over prepared perovskite catalysts for higher alcohol formation.
- To test the performance of the catalysts mentioned above in HAS process, and assess their stability.

2.9 Conclusion

Development of effective catalysts with high selectivity and activity towards higher alcohols, and good stability under moderate reaction conditions are highly desirable goals in HAS from syngas. In this chapter, different catalyst designs and process developments on modified methanol synthesis catalysts, modified F-T synthesis catalysts, Mo-based catalysts, Rh-based catalysts, and perovskite catalysts have been reviewed and assessed in respect of their potential to render the HAS process commercially attractive. This chapter also discusses the effects of various catalyst supports, promoters, and catalyst preparation methods on the performance of HAS catalysts. It was found that the improvement of active centre dispersion over the catalyst surface leads to an increase of the higher alcohol selectivity and yield. While some progress has been made accordingly, improvements in the development of HAS catalysts are still required to achieve a higher yield of $C_{2+}OH$ alcohols for commercialisation. Compared with other HAS catalysts, perovskites are promising for the synthesis of higher alcohols from syngas. As a result, a systematic experimental process for perovskite catalysts development is needed to improve the higher alcohol synthesis from syngas. The objective of the current study is to provide such a systematic study that will offer guidance on the development of perovskite catalysts for HAS.

References

[1] J. Conti, P. Holtberg, J. Diefenderfer, A. LaRose, J.T. Turnure, L. Westfall, U.S. Energy Information Administration, (2016) 1-275.

[2] H. John H, R.W. Koch, A.J. Rezaiyan, U.S.Department of Energy, (1995).

[3] J.R.H. Ross, A.N.J.v. Keulen, M.E.S. Hegarty, K. Seshan, Catalysis Today, 30 (1996) 193-199.

[4] D.J. Wilhelm, D.R. Simbeck, A.D. Karp, R.L. Dickenson, Fuel Processing Technology, 71 (2001) 139-148.

[5] G.A. Mills, Fuel, 73 (1994) 1243-1279.

[6] Methanol Institute, The methanol industry, (2016) Retrieved from http://www.methanol.org/the-methanol-industry/.

[7] D. Leckel, Energy & Fuels, 23 (2009) 2342-2358.

[8] M.E. Dry, Catalysis Today, 71 (2002) 227-241.

[9] J.J.C. Geerlings, J.H.Wilson, G.J. Kramer, H.P.C.E. Kuipers, A.Hoek, H.M. Huisman, Applied Catalysis A: General, 186 (1999) 27-40.

[10] Qatar Petroleum, Oryx GTL, (2015) Retrieved from https://www.qp.com.qa/en/QPActivities/pages/subsidiariesandjointventuresdetails.aspx?aid=37.

[11] Shell Global, Shell-Pearl GTL-an overview, (2016) Retrieved from http://www.shell.com/about-us/major-projects/pearl-gtl/pearl-gtl-an-overview.html.

[12] PetroSA, The Petroleum Oil and Gas Corporation of South Africa (SOC) Ltd, (2016) 1-7.

[13] Hydrocarbons Technology, Escravos Gas-to-Liquids Project, Niger Delta, Nigeria, (2009) Retrieved from http://www.hydrocarbons-technology.com/projects/escravos/.

[14] A.K. Dalai, B.H. Davis, Applied Catalysis A: General, 348 (2008) 1-15.

[15] H. Jahangiri, J. Bennett, P. Mahjoubi, K. Wilson, S. Gu, Catalysis Science & Technology, 4 (2014) 2210-2229.

[16] M. Gupta, M.L. Smith, J.J. Spivey, ACS Catalysis, 1 (2011) 641-656.

[17] P.L. Spath, D.C. Dayton, National Renewable Energy Laboratory, (2003) 1-140.

[18] K.K. Ramasamy, M. Gray, H. Job, Y. Wang, Chemical Engineering Science, 135 (2015) 266-273.

[19] K.D. Kruit, D. Vervloet, F. Kapteijn, J.R. van Ommen, Catalysis Science & Technology, 3 (2013) 2210-2213.

[20] C.H. Bartholomew, R.J. Farrauto, Fundamentals of Industrial Catalytic Processes, Wiley, (2010).

[21] T. Takeshita, K. Yamaji, Energy Policy, 36 (2008) 2773-2784.

[22] M.J.A. Tijmensen, A.P.C. Faaij, C.N. Hamelinck, M.R.M.v. Hardeveld, Biomass and Bioenergy, 23 (2002) 129-152.

[23] A.d. Klerk, Industrial & Engineering Chemistry Research 46 (2007) 5516-5521.

[24] S. Gamba, L.A. Pellegrini, V. Calemma, C. Gambaro, Catalysis Today, 156 (2010) 58-64.

[25] J.J. Spivey, A. Egbebi, Chemical Society reviews, 36 (2007) 1514-1528.

[26] K. Fang, D. Li, M. Lin, M. Xiang, W. Wei, Y. Sun, Catalysis Today, 147 (2009) 133-138.

[27] X. Liu, G.Q. Lu, Z. Yan, J. Beltramini, Industrial & Engineering Chemistry Research, 42 (2003) 6518-6530.

[28] K. Xiao, Z. Bao, X. Qi, X. Wang, L. Zhong, K. Fang, M. Lin, Y. Sun, Chinese Journal of Catalysis, 34 (2013) 116-129.

[29] K.A. Ali, A.Z. Abdullah, A.R. Mohamed, Renewable and Sustainable Energy Reviews, 44 (2015) 508-518.

[30] Y. Jeong, I. Kim, J.Y. Kang, H. Jeong, J.K. Park, J.H. Park, J.C. Jung, Journal of Molecular Catalysis A: Chemical, 400 (2015) 132-138.

[31] F. Collignon, R. Loenders, J. Martens, P. Jacobs, G. Poncelet, Journal of Catalysis, 182 (1999) 302-312.

[32] M. Xu, J.H. Lunsford, D.W. Goodman, A. Bhattacharyya, Applied Catalysis A: General, 149 (1997) 289-301.

[33] Z. Chu, H. Chen, Y. Yu, Q. Wang, D. Fang, Journal of Molecular Catalysis A: Chemical, 366 (2012) 48-53.

[34] C.J. Yoo, Y.K. Hong, K.Y. Lee, D.J. Moon, 23rd North American Catalysis Society Meeting, (2013).

[35] V.R. Surisetty, A.K. Dalai, J. Kozinski, Applied Catalysis A: General, 404 (2011) 1-11.

[36] C. Yao, C.S. Cheung, C. Cheng, Y. Wang, T.L. Chan, S.C. Lee, Energy Conversion and Management, 49 (2008) 1696-1704.

[37] R.G. Herman, Catalysis Today, 55 (2000) 233-245.

[38] V. Subramani, S.K. Gangwal, Energy & Fuels, 22 (2008) 814-839.

[39] V.S. Dorokhov, M.A. Kamorin, N.N. Rozhdestvenskaya, V.M. Kogan, Comptes Rendus Chimie, 19 (2016) 1184-1193.

[40] H.U. Masaaki Umeda, Plant Physiology, 106 (1994) 1015-1022.

[41] J.-S. Kim, B.-G. Kim, C.-H. Lee, S.-W. Kim, H.-S. Jee, J.-H. Koh, A.G. Fane, Journal of Cleaner Production, 5 (1997) 263-267.

[42] J. Lodgsdon, Encyclopedia of chemical technology, 9 (1994) 812-860.

[43] G.M. Torres, R. Frauenlob, R. Franke, A. Börner, Catalysis Science & Technology, 5 (2015) 34-54.

[44] Chemicals-Technology, SaBuCo Butanol Plant, Jubail, Saudi Arabia, (2016) Retrieved from http://www.chemicals-technology.com/projects/sabuco-butanol-plant-jubail.

[45] Chemical Week, Oxea gets preliminary approval to build 150,000 m.t./year n-propanol plant at Bay City, TX, (2015) Retrieved from http://www.chemweek.com/markets/basic_chemicals/petrochemicals/oxoalcohols/Oxea-gets-preliminary-approval-to-build-150000-m-t-year-n-propanol-plant-at-Bay-City-TX_75177.html.

[46] X. Xu, E.B.M. Doesburg, J.J.F.Scholten, Catalysis Today, 2 (1987) 125-170.

[47] P. Forzatti, E. Tronconi, I. Pasquon, Catalysis Reviews, 33 (1991) 109-168.

[48] S. Zaman, K.J. Smith, Catalysis Reviews, 54 (2012) 41-132.

[49] K.J. Smith, R.B. Anderson, The Canadian Journal of Chemical Engineering, 61 (1983) 40-45.

[50] Y. Fang, Y. Liu, W. Deng, J. Liu, Journal of Energy Chemistry, 23 (2014) 527-534.

[51] D.M. Minahan, W.S. Epling, G.B. Hoflund, Catalysis Letters, 50 (1998) 199-203.

[52] W.S. Epling, G.B. Hoflund, D.M. Minahan, Applied Catalysis A: General, 183 (1999) 335-343.

[53] D.M. Minahan, W.S. Epling, G.B. Hoflund, Applied Catalysis A: General, 166 (1998) 375-385.

[54] D.M. Minahan, W.S. Epling, G.B. Hoflun, Journal of Catalysis, 179 (1998) 241-257.

[55] W.S. Epling, G.B. Hoflund, D.M. Minahan, Journal of Catalysis, 175 (1998) 175-184.

[56] G.B. Hoflund, W.S. Epling, D. M.Minahan, Catalysis Letters, 45 (1997) 135-138.

[57] W.S. Epling, G.B. Hoflund, W.M. Hart, D.M. Minahan, Journal of Catalysis, 169 (1997) 438-446.

[58] G.B. Hoflund, W.S. Epling, D.M. Minahan, Catalysis Today, 52 (1999) 99-109.

[59] J. Bao, Y.-L. Fu, G.-Z. Bian, Catalysis Letters, 121 (2008) 151-157.

[60] W. Keim, W. Falter, Catalysis Letters, 3 (1989) 59-64.

[61] E. Troncon, G. Groppi, Applied Catalysis A: General, 79 (1991) 181-190.

[62] K.A.N. Verkerk, B. Jaeger, C.-H. Finkeldei, W. Keim, Applied Catalysis A: General, 186 (1999) 407-431.

[63] E. Tronconi, N. Ferlazzo, P. Forzatti, I. Pasquon, Industrial & Engineering Chemistry Research, 26 (1987) 2122-2129.

[64] L. Tan, G. Yang, Y. Yoneyama, Y. Kou, Y. Tan, T. Vitidsant, N. Tsubaki, Applied Catalysis A: General, 505 (2015) 141-149.

[65] E. Tronconi, L. Lietti, P. Forzatti, I. Pasquon, Applied Catalysis, 47 (1989) 317-333.

[66] A.B. Stiles, F. Chen, J.B. Harrison, X. Hu, D.A. Storm, H.X. Yang, Industrial & Engineering Chemistry Research 30 (1991) 811-821.

[67] S. Tian, S. Wang, Y. Wu, J. Gao, Y. Bai, P. Wang, H. Xie, Y. Han, Y. Tan, Journal of Molecular Catalysis A: Chemical, 404-405 (2015) 139-147.

[68] A. Beretta, Q. Sun, R.G. Herman, K. Klier, Industrial & Engineering Chemistry Research 35 (1996) 1534-1542.

[69] R. Johnson, J. Pankow, D. Bender, C. Price, J. Zogorski, Environmental Science & Technology, 34 (2000) 210A-217A.

[70] J.A. Sibilia, M. Dominguez, R.G. Herman, K. Klier, Prepr Div Fuel Chem, 29 (1984) 261-268.

[71] A. Cosultchi, M. Pérez-Luna, J.A. Morales-Serna, M. Salmón, Catalysis Letters, 142 (2012) 368-377.

[72] R. Xu, W. Wei, W.H. Li, T.D. Hu, Y.H. Sun, Journal of Molecular Catalysis A: Chemical, 234 (2005) 75-83.

[73] E.Ramaroson, R.Kieffer, A.Kiennemann, Applied Catalysis, 4 (1982) 281-286.

[74] Q. Zhu, R. Zhang, D. He, Tsinghua University, (2010) 1-2.

[75] N. Zhao, R. Xu, W. Wei, Y. Sun, Reaction Kinetics and Catalysis Letters, 75 (2002) 297-304.

[76] C.R. Apesteguia, S. Fe, Argentina, S.L. Soled, S. Miseo, N. Pittstown, Exxon Research and Engineering Company, 5,508,246 (1996).

[77] W. Chu, R. Kieffer, A. Kiennemann, J.P. Hindermann, Applied Catalysis A: General, 121 (1995) 95-111.

[78] R. Xu, Z. Ma, C. Yang, W. Wei, Y. Sun, Reaction Kinetics and Catalysis Letters, 81 (2004) 91-98.

[79] J.G. Nljnan, R.G. Herman, K. Klier, Journal of Catalysis, 116 (1989) 222-229.

[80] A.-M. Hilmen, M. Xu, M.J.L. Gines, E. Iglesia, Applied Catalysis A: General, 169 (1998) 355-372.

[81] A. Beretta, Q. Sun, R.G. Herman, K. Klier, Preprints of Papers, American Chemical Society, Division of Fuel Chemistry, (1995) 142-147.

[82] J.M. Campos-Martin, J.L.G. Fierro, A. Guerrero-Ruiz, R.G. Herman, K. Klierz, Journal of Catalysis, 163 (1996) 418-428.

[83] K.J. Smith, C.W. Young, R.G. Herman, K. Klier, Industrial & Engineering Chemistry Research 30 (1991) 61-71.

[84] J.G. Nunan, C.E. Bogdan, K. Klier, K.J. Smith, C.-W. Young, R.G. Herman, Journal of Catalysis, 116 (1989) 195-221.

[85] E.M. Calverley, K.J. Smith, Journal of Catalysis, 130 (1991) 626-626.

[86] E. Heracleous, E.T. Liakakou, A.A. Lappas, A.A. Lemonidou, Applied Catalysis A: General, 455 (2013) 145-154.

[87] J.C. Slaa, J.G.v. Ommen, J.R.H. Ross, Topics in Catalysis, 2 (1995) 79-89.

[88] I. Boz, Catalysis Letters, 87 (2003) 187-194.

[89] I. Boz, M. Sahibzada, I.S. Metcalfe, Industrial & Engineering Chemistry Research, 33 (1994) 2021-2028.

[90] Y. Wu, H. Xie, S. Tian, N. Tsubaki, Y. Han, Y. Tan, Journal of Molecular Catalysis A: Chemical, 396 (2015) 254-260.

[91] M.M. Burcham, R.G. Herman, K. Klier, Industrial & Engineering Chemistry Research, 37 (1998) 4657-4668.

[92] J. Anton, J. Nebel, H. Song, C. Froese, P. Weide, H. Ruland, M. Muhler, S. Kaluza, Journal of Catalysis, 335 (2016) 175-186.

[93] K.M. Walter, M. Schubert, W. Kleist, J.-D. Grunwaldt, Industrial & Engineering Chemistry Research, 54 (2015) 1452-1463.

[94] M. Xu, M.J.L. Gines, A.-M. Hilmen, B.L. Stephens, E. Iglesia, Journal of Catalysis, 171 (1997) 130-147.

[95] Y. Liu, K. Murata, M. Inaba, I. Takahara, K. Okabe, Fuel, 104 (2013) 62-69.

[96] J.H. Lee, K.H. Reddy, J.S. Jung, E.-H. Yang, D.J. Moon, Applied Catalysis A: General, 480 (2014) 128-133.

[97] H. Guo, F. Peng, H. Zhang, L. Xiong, S. Li, C. Wang, B. Wang, X. Chen, Y. Chen, International Journal of Hydrogen Energy, 39 (2014) 9200-9211.

[98] H. Guo, S. Li, H. Zhang, F. Peng, L. Xiong, J. Yang, C. Wang, X. Chen, Y. Chen, Industrial & Engineering Chemistry Research, 53 (2014) 123-131.

[99] M. Gupta, J.J. Spivey, Catalysis Today, 147 (2009) 126-132.

[100] Y.-J. Liu, Z.-J. Zuo, C.-B. Liu, C. Li, X. Deng, W. Huang, Fuel Processing Technology, 144 (2016) 186-190.

[101] Y. Liu, C. Liu, C. Li, W. Huang, Catalysis Communications, 76 (2016) 29-32.

[102] J. Anton, J. Nebel, H. Song, C. Froese, P. Weide, H. Ruland, M. Muhler, S. Kaluza, Applied Catalysis A: General, 505 (2015) 326-333.

[103] J.M.Campos-Martin, A.Guerrero-Ruiz, J.L.G.Fierro, Journal of Catalysis, 156 (1995) 208-218.

[104] K.J. Smith, R.B. Anderson, Journal of Catalysis, 85 (1984) 428-426.

[105] R. Xu, S. Zhang, C.B. Roberts, Industrial & Engineering Chemistry Research, 52 (2013) 14514-14524.

[106] X. Ning, Z. An, J. He, Journal of Catalysis, 340 (2016) 236-247.

[107] L. Majocchi, L. Lietti, A. Beretta, P. Forzatti, E. Micheli, L. Tagliabue, Applied Catalysis A: General, 166 (1998) 393-405.

[108] D.J. Elliott, F. Pennella, Journal of Catalysis, 114 (1988) 90-99.

[109] J.C. Slaa, J.G.v. Ommen, J.R.H. Ross, Catalysis Today, 15 (1992) 129-148.

[110] M. Xu, E. Iglesia, Journal of Catalysis, 188 (1999) 125-131.

[111] J.F. Knifton, J.J. Linb, D.A. Stern, S. Wang, Catalysis Today, 18 (1993) 355-384.

[112] N. Kumar, M.L. Smith, J.J. Spivey, Journal of Catalysis, 289 (2012) 218-226.

[113] G. Jiao, Y. Ding, H. Zhu, X. Li, J. Li, R. Lin, W. Dong, L. Gong, Y. Pei, Y. Lu, Applied Catalysis A: General, 364 (2009) 137-142.

[114] G. Jiao, Y. Ding, H. Zhu, X. Li, W. Dong, J. Li, Y. LÜ, Chinese Journal of Catalysis, 30 (2009) 92-94.

[115] T. Matsuzaki, T.-a. Hanaoka, K. Takeuchi, H. Arakawa, Y. Sugi, K. Wei, T. Dong, M. Reinikainen, Catalysis Today, 36 (1997) 311-324.

[116] K. Fujimoto, T. Oba, Applied Catalysis, 13 (1985) 289-293.

[117] T. Matsuzaki, K. Takeuchi, T.-a. Hanaoka, H. Arawaka, Y. Sugi, Applied Catalysis A: General, 105 (1993) 159-184.

[118] A. Loaiza-Gil, J. Arenas, M. Villarroel, F. Imbert, H. del Castillo, B. Fontal, Journal of Molecular Catalysis A: Chemical, 228 (2005) 339-344.

[119] A.E. Colley, M.J. Betts, R.G. Copperthwaite, G.J. Hutchings, N.J. Coville, Journal of Catalysis, 134 (1992) 186-203.

[120] T. Ishida, T. Yanagihara, X. Liu, H. Ohashi, A. Hamasaki, T. Honma, H. Oji, T. Yokoyama, M. Tokunaga, Applied Catalysis A: General, 458 (2013) 145-154.

[121] K.T.T. Matsuzaki, H. Arakawa, T. Hanaoka, Y. Sugi, Applied Catalysis, 48 (1989) 149-157.

[122] V.M. Lebarbier, D. Mei, D.H. Kim, A. Andersen, J.L. Male, J.E. Holladay, R. Rousseau, Y. Wang, The Journal of Physical Chemistry C, 115 (2011) 17440-17451.

[123] M. Blanchard, H. Derule, P. Canesson, Catalysis Letters, 2 (1989) 319-322.

[124] Y. Pei, Y. Ding, H. Zhu, H. Du, Chinese Journal of Catalysis, 36 (2015) 355-361.

[125] K. Takeuchi, T. Matsuzaki, T.-a. Hanaoka, H. Arakawa, Y. Sugi, Journal of Molecular Catalysis, 55 (1989) 361-370.

[126] H. Du, H. Zhu, X. Chen, W. Dong, W. Lu, W. Luo, M. Jiang, T. Liu, Y. Ding, Fuel, 182 (2016) 42-49.

[127] E.B. Pereira, G.-A. Martin, Applied Catalysis A: General, 115 (1994) 135-146.

[128] S.S.C. Chuang, S.-I. Pien, K. Ghosal, Applied Catalysis, 70 (1991) 101-114.

[129] S. Uchiyama, Y. Obayashi, M. Shibata, T. Uchiyama, N. Kawata, T. Konishi, Journal of the Chemical Society, Chemical Communications, (1985) 1071-1072.

[130] M. Inoue, T. Miyake, Y. Takegami, T. Inui, Applied Catalysis, 11 (1984) 103-116.

[131] H. Ono, K. Fujiwara, M. Hashimoto, H. watanabe, K. Yoshida, Journal of Molecular Catalysis, 58 (1990) 289-297.

[132] M. Inoue, T. Miyake, S. Yonezawa, D. Medhanavyn, Y. Takegami, T. Inui, Journal of Molecular Catalysis, 45 (1988) 111-126.

[133] M.A. Fraga, E. Jordao, Reaction Kinetics and Catalysis Letters 64 (1998) 331-336.

[134] E.B. Pereira, G.-A. Martin, Applied Catalysis A: General, 103 (1993) 291-309.

[135] R. Kieffer, M. Fujiwara, L. Udron, Y. Souma, Catalysis Today, 36 (1997) 15-24.

[136] J.A. Dalmona, P. Chaumetteb, C. Mirodatosa, Catalysis Today, 15 (1992) 101-127.

[137] H.-B. Zhang, X. Dong, G.-D. Lin, X.-L. Liang, H.-Y. Li, Chemical Communications, (2005) 5094-5096.

[138] P. Courty, D. Durand, E. Freund, A. Sugier, Journal of Molecular Catalysis, 17 (1982) 241-254.

[139] X. Dong, X.-L. Liang, H.-Y. Li, G.-D. Lin, P. Zhang, H.-B. Zhang, Catalysis Today, 147 (2009) 158-165.

[140] V. Mahdavi, M.H. Peyrovi, M. Islami, J.Y. Mehr, Applied Catalysis A: General, 281 (2005) 259-265.

[141] A.D.d. Aquino, A.J.G. Cobo, Catalysis Today, 65 (2001) 209-216.

[142] P. Chaumette, P. Courty, Topics in Catalysis, 2 (1995) 117-126.

[143] X. Mo, Y.-T. Tsai, J. Gao, D. Mao, J.G. Goodwin, Journal of Catalysis, 285 (2012) 208-215.

[144] J.E. Baker, R. Burch, S.J. Hibble, P.K. Loader, Applied Catalysis, 65 (1990) 281-292.

[145] R.T. Figueiredo, M.L. Granados, J.L.G. Fierro, L. Vigas, P.R.d.l. Piscina, N. Homs, Applied Catalysis A: General, 170 (1998) 145-157.

[146] J. Wang, P.A. Chernavskii, A.Y. Khodakov, Y. Wang, Journal of Catalysis, 286 (2012) 51-61.

[147] S. Deng, W. Chu, H. Xu, L. Shi, L. Huang, Journal of Natural Gas Chemistry, 17 (2008) 369-373.

[148] L. Shi, W. Chu, S. Deng, Journal of Natural Gas Chemistry, 20 (2011) 48-52.

[149] P. Mohanty, K.K. Pant, J. Parikh, D.K. Sharma, Fuel Processing Technology, 92 (2011) 600-608.

[150] J.E. Baker, R. Burch, S.E. Golunski, Applied Catalysis, 53 (1989) 279-297.

[151] H.B. Zhang, X. Dong, G.D. Lin, X.L. Liang, H.Y. Li, Chem Commun (Camb), (2005) 5094-5096.

[152] N.D. Subramanian, G. Balaji, C.S. Kumar, J.J. Spivey, Catalysis Today, 147 (2009) 100-106.

[153] D. Mahajan, P. Vijayaraghavan, Fuel, 78 (1999) 93-100.

[154] P. Wang, Y. Bai, H. Xiao, S. Tian, Z. Zhang, Y. Wu, H. Xie, G. Yang, Y. Han, Y. Tan, Catalysis Communications, 75 (2016) 92-97.

[155] Y. Yang, X. Qi, X. Wang, D. Lv, F. Yu, L. Zhong, H. Wang, Y. Sun, Catalysis Today, 270 (2015) 101-107.

[156] Z. Wang, J.J. Spivey, Applied Catalysis A: General, 507 (2015) 75-81.

[157] P. Chaumette, P. Courty, A. Kiennemann, R. Kieffer, S. Boujana, G.A. Martin, J.A. Dalmon, P. Meriaudeau, C. Mirodatos, B. Holhein, D. Mausbeck, A.J. Hubert, A. Germain, A. Noels, Industrial & Engineering Chemistry, 33 (1994) 1460-1467.

[158] J. Su, Z. Zhang, D. Fu, D. Liu, X.-C. Xu, B. Shi, X. Wang, R. Si, Z. Jiang, J. Xu, Y.-F. Han, Journal of Catalysis, 336 (2016) 94-106.

[159] W. Feng, Q. Wang, B. Jiang, P. Ji, Industrial & Engineering Chemistry Research, 50 (2011) 11067-11072.

[160] D. Lü, Y. Zhu, Y. Sun, Chinese Journal of Catalysis, 34 (2013) 1998-2003.

[161] L. Shi, W. Chu, S. Deng, H. Xu, Journal of Natural Gas Chemistry, 17 (2008) 397-402.

[162] H. Xu, W. Chu, L. Shi, H. Zhang, S. Deng, Journal of Fuel Chemistry and Technology, 37 (2009) 212-216.

[163] A. Sugier, E. Freund, Institut Francais du Petrole, France, 4122110 (1978).

[164] J. Wang, P.A. Chernavskii, Y. Wang, A.Y. Khodakov, Fuel, 103 (2013) 1111-1122.

[165] J. Llorca, N. Homs, O. Rossell, M. Seco, J.-L.G. Fierro, P.R.d.l. Piscina, Journal of Molecular Catalysis A: Chemical, 149 (1999) 225-232.

[166] K. Xiao, X. Qi, Z. Bao, X. Wang, L. Zhong, K. Fang, M. Lin, Y. Sun, Catalysis Science & Technology, 3 (2013) 1591-1602.

[167] G. Prieto, S. Beijer, M.L. Smith, M. He, Y. Au, Z. Wang, D.A. Bruce, K.P. de Jong, J.J. Spivey, P.E. de Jongh, Angewandte Chemie, 53 (2014) 6397-6401.

[168] N. Mouaddib, V. Perrichon, G.A. Martin, Applied Catalysis A: General, 118 (1994) 63-72.

[169] Y. Xiang, R. Barbosa, N. Kruse, ACS Catalysis, 4 (2014) 2792-2800.

[170] M.Pijolat, V.Perrichon, Applied Catalysis, 13 (1985) 321-333.

[171] P. Johnston, G.J. Hutchings, N.J. Coville, K.P. Finch, J.R. Moss, Applied Catalysis A: General, 186 (1999) 245-253.

[172] X. Zhang, Z. Li, Q. Guo, H. Zheng, K. Xie, Fuel Processing Technology, 91 (2010) 379-382.

[173] L.D. Mansker, Y. Jin, D.B. Bukur, A.K. Datye, Applied Catalysis A: General, 186 (1999) 277-296.

[174] W. Mao, H. Ma, H. Zhang, Q. Sun, W. Ying, D. Fang, Catalysis Letters, 142 (2012) 1098-1106.

[175] W. Mao, Q. Sun, W. Ying, D. Fang, World Academy of Science, Engineering and Technology, 59 (2011) 2459-2468.

[176] M. Ding, M. Qiu, J. Liu, Y. Li, T. Wang, L. Ma, C. Wu, Fuel, 109 (2013) 21-27.

[177] Y. Su, YingliWang, Z. Liu, Journal of Natural Gas Chemistry, 17 (2008) 327-331.

[178] M. Lin, K. Fang, D. Li, Y. Sun, Catalysis Communications, 9 (2008) 1869-1873.

[179] M. Ding, M. Qiu, T. Wang, L. Ma, C. Wu, J. Liu, Applied Energy, 97 (2012) 543-547.

[180] H. Zhang, W. Chu, H. Xu, J. Zhou, Fuel, 89 (2010) 3127-3131.

[181] R. Xu, C. Yang, W. Wei, W.-h. Li, Y.-h. Sun, T.-d. Hu, Journal of Molecular Catalysis A: Chemical, 221 (2004) 51-58.

[182] A. Kiennemann, A. Barama, S. Boujana, M.M.Bettahar, Applied Catalysis A: General, 99 (1993) 175-194.

[183] A. Razzaghi, J.-P. Hindermann, A. Kiennemanna, Applied Catalysis, 13 (1984) 193-210.

[184] Y. Lu, F. Yu, J. Hu, J. Liu, Applied Catalysis A: General, 429-430 (2012) 48-58.

[185] Y. Lu, B. Cao, F. Yu, J. Liu, Z. Bao, J. Gao, ChemCatChem, 6 (2014) 473-478.

[186] M. Ding, J. Tu, J. Liu, N. Tsubaki, T. Wang, L. Ma, Catalysis Today, 234 (2014) 278-284.

[187] M. Ding, J. Liu, Q. Zhang, N. Tsubaki, T. Wang, L. Ma, Catalysis Communications, 28 (2012) 138-142.

[188] H. Zhang, X. Yang, L. Zhou, Y. Su, Z. Liu, Journal of Natural Gas Chemistry, 18 (2009) 337-340.

[189] M. Ding, J. Tu, M. Qiu, T. Wang, L. Ma, Y. Li, Applied Energy, 138 (2015) 584-589.

[190] B. Hou, X. Han, M. Lin, K. Fang, Journal of Fuel Chemistry and Technology, 44 (2016) 217-224.

[191] K. Xiao, Z. Bao, X. Qi, X. Wang, L. Zhong, K. Fang, M. Lin, Y. Sun, Journal of Molecular Catalysis A: Chemical, 378 (2013) 319-325.

[192] Z. Bao, K. Xiao, X. Qi, X. Wang, L. Zhong, K. Fang, M. Lin, Y. Sun, Journal of Energy Chemistry, 22 (2013) 107-113.

[193] H. Guo, H. Zhang, F. Peng, H. Yang, L. Xiong, C. Wang, C. Huang, X. Chen, L. Ma, Applied Catalysis A: General, 503 (2015) 51-61.

[194] C. Sun, D. Mao, L. Han, J. Yu, Catalysis Communications, 84 (2016) 175-178.

[195] H. Du, H. Zhu, Z. Zhao, W. Dong, W. Luo, W. Lu, M. Jiang, T. Liu, Y. Ding, Applied Catalysis A: General, 523 (2016) 263-271.

[196] H. Du, H. Zhu, T. Liu, Z. Zhao, X. Chen, W. Dong, W. Lu, W. Luo, Y. Ding, Catalysis Today, 281 (2016) 549-558.

[197] K. Xiao, Z. Bao, X. Qi, X. Wang, L. Zhong, M. Lin, K. Fang, Y. Sun, Catalysis Communications, 40 (2013) 154-157.

[198] R. Suárez París, M. Boutonnet, S. Järås, Catalysis Communications, 67 (2015) 103-107.

[199] A. Tavasoli, S. Karimi, M. Davari, N. Nasrollahi, T. Nematian, Journal of Industrial and Engineering Chemistry, 20 (2014) 674-681.

[200] T. Tatsumi, A. Muramatsu, K. Yokota, H.-o. Tominaga, Journal of catalysis, 115 (1989) 388-398.

[201] Z. Li, Y. Fu, M. Jiang, T. Hu, T. Liu, Y. Xie, Journal of Catalysis, 199 (2001) 155-161.

[202] Y. Zhang, Y. Sun, B. Zhong, Catalysis Letters, 76 (2001) 249-253.

[203] C. Ma, H. Li, G. Lin, H. Zhang, Catalysis Letters, 137 (2010) 171-179.

[204] X. Wu, Y. Guo, J. Zhou, G. Lin, X. Dong, H. Zhang, Applied Catalysis A: General, 340 (2008) 87-97.

[205] X. Ma, G. Lin, H. Zhang, Catalysis Letters, 111 (2006) 141-151.

[206] C. Ma, H. Li, G. Lin, H. Zhang, Applied Catalysis B: Environmental, 100 (2010) 245-253.

[207] X. Ma, G. Lin, H. Zhang, Chinese Journal of Catalysis, 27 (2006) 1019-1027.

[208] J.-J. Wang, J.-R. Xie, Y.-H. Huang, B.-H. Chen, G.-D. Lin, H.-B. Zhang, Applied Catalysis A: General, 468 (2013) 44-51.

[209] J. Bao, Y. Fu, Z. Sun, C. Gao, Chemical Communications, (2003) 746-747.

[210] Z. Li, Y. Fu, J. Bao, M. Jiang, T. Hu, T. Liu, Y. Xie, Applied Catalysis A: General, 220 (2001) 21-30.

[211] E.T. Liakakou, E. Heracleous, K.S. Triantafyllidis, A.A. Lemonidou, Applied Catalysis B: Environmental, 165 (2015) 296-305.

[212] A. Muramatsu, T. Tatstmi, H.-o. Tominaga, The Journal of Physical Chemistry, 96 (1992) 1334-1340.

[213] E.C. Alyea, D. He, J. Wang, Applied Catalysis A: General, 104 (1993) 77-85.
[214] T. Tatsumi, A. Muramatsu, H.-o. Tominaga, Applied Catalysis, 34 (1987) 77-88.
[215] T. Tatsumi, A. Muramatsu, K. Yokota, H.-O. Tominaga, Journal of Molecular Catalysis, 41 (1987) 385-389.
[216] Z. Li, Y. Fu, M. Jiang, Applied Catalysis A: General, 187 (1999) 187-198.
[217] Z. Li, Y. Fu, M. Jiang, M. Meng, Y. Xie, T. Hu, T. Liu, Catalysis Letters, 65 (2000) 43-48.
[218] G.-z. Bian, Y.-l. Fu, Y.-s. Ma, Catalysis Today, 51 (1999) 187-193.
[219] M. Jiang, G.-Z. Bian, Y.-L. Fu, Journal of Catalysis, 146 (1994) 144-154.
[220] G.-z. Biana, L. Fanb, Y.-l. Fua, K. Fujimoto, Applied Catalysis A: General, 170 (1998) 255-268.
[221] G.-z. Bian, L. Fan, Y.-l. Fu, K. Fujimoto, Industrial & Engineering Chemistry Research, 37 (1998) 1736-1743.
[222] M. Inoue, T. Miyake, Y. Takegami, T. Inui, Applied Catalysis, 29 (1987) 285-294.
[223] M. Inoue, A. Kurusu, H. Wakamatsu, K. Nakajima, T. Inui, Applied Catalysis, 29 (1987) 361-374.
[224] Y.-l. Fu, K. Fujimoto, P.-y. Lin, K. Omata, Y.-s. Yu, Applied Catalysis A: General, 126 (1995) 273-285.
[225] M. Xiang, D. Li, W. Li, B. Zhong, Y. Sun, Catalysis Communications, 8 (2007) 503-507.
[226] Q. Wu, J.M. Christensen, G.L. Chiarello, L.D.L. Duchstein, J.B. Wagner, B. Temel, J.-D. Grunwaldt, A.D. Jensen, Catalysis Today, 215 (2013) 162-168.
[227] L. Zhao, K. Fang, D. Jiang, D. Li, Y. Sun, Catalysis Today, 158 (2010) 490-495.
[228] N. Wang, K. Fang, D. Jiang, D. Li, Y. Sun, Catalysis Today, 158 (2010) 241-245.
[229] M. Xiang, D. Li, H. Xiao, J. Zhang, H. Qi, W. Li, B. Zhong, Y. Sun, Fuel, 87 (2008) 599-603.
[230] M. Xiang, D. Li, H. Xiao, J. Zhang, W. Li, B. Zhong, Y. Sun, Catalysis Today, 131 (2008) 489-495.
[231] M. Xiang, D. Li, H. Qi, W. Li, B. Zhong, Y. Sun, Fuel, 86 (2007) 1298-1303.
[232] M. Xiang, D. Li, W. Li, B. Zhong, Y. Sun, Fuel, 85 (2006) 2662-2665.

[233] H.C. Woo, K.Y. Park, Y.G. Kim, I.-S. Nam, J. Shik, Chung, J.S. Lee, Applied Catalysis, 75 (1991) 267-280.

[234] M. Xiang, D. Li, W. Li, B. Zhong, Y. Sun, Catalysis Communications, 8 (2007) 513-518.

[235] M. Xiang, D. Li, W. Li, B. Zhong, Y. Sun, Catalysis Communications, 8 (2007) 88-90.

[236] J.S. Lee, S. Kim, Y.G. Kim, Topics in Catalysis, 2 (1995) 127-140.

[237] H. Shou, L. Li, D. Ferrari, D.S. Sholl, R.J. Davis, Journal of Catalysis, 299 (2013) 150-169.

[238] S.-H. Chai, V. Schwartz, J.Y. Howe, X. Wang, M. Kidder, S.H. Overbury, S. Dai, D.-e. Jiang, Microporous and Mesoporous Materials, 170 (2013) 141-149.

[239] S.-W. Chiang, C.-C. Chang, J.-L. Shie, C.-Y. Chang, D.-R. Ji, J.-Y. Tseng, Journal of the Taiwan Institute of Chemical Engineers, 43 (2012) 918-925.

[240] J.M. Christensen, L.D.L. Duchstein, J.B. Wagner, P.A. Jensen, B. Temel, A.D. Jensen, Industrial & Engineering Chemistry Research, 51 (2012) 4161-4172.

[241] H. Shou, D. Ferrari, D.G. Barton, C.W. Jones, R.J. Davis, ACS Catalysis, 2 (2012) 1408-1416.

[242] H. Shou, R.J. Davis, Journal of Catalysis, 282 (2011) 83-93.

[243] H. Okatsu, M.R. Morrill, H. Shou, D.G. Barton, D. Ferrari, R.J. Davis, P.K. Agrawal, C.W. Jones, Catalysis Letters, 144 (2014) 825-830.

[244] A. Griboval-Constant, J.-M. Giraudon, G. Leclercq, L. Leclercq, Applied Catalysis A: General, 260 (2004) 35-45.

[245] W. Wu, Z. Wu, C. Liang, X. Chen, P. Ying, C. Li, The Journal of Physical Chemistry B, 107 (2003) 7088-7094.

[246] H.Y. Luo, W. Zhang, H.W. Zhou, S.Y. Huang, P.Z. Lin, Y.J. Ding, L.W. Lin, Applied Catalysis A: General, 214 (2001) 161-166.

[247] Q.J. Quarderer, G.A. Cochram, 0,119,609 (1984).

[248] N.E. Kinkade, PCT Int. Pat. Publication No. WO 85/03073, (1985).

[249] M.R. Morrill, N.T. Thao, P.K. Agrawal, C.W. Jones, R.J. Davis, H. Shou, D.G. Barton, D. Ferrari, Catalysis Letters, 142 (2012) 875-881.

[250] Y. Yang, Y. Wang, S. Liu, Q. Song, Z. Xie, Z. Gao, Catalysis Letters, 127 (2008) 448-455.

[251] D. Li, C. Yang, N. Zhao, H. Qi, W. Li, Y. Sun, B. Zhong, Fuel Processing Technology, 88 (2007) 125-127.

[252] W.P. Dianis, Applied Catalysis, 30 (1987) 99-121.

[253] J. Iranmahbooba, D.O. Hill, Catalysis Letters, 78 (2002) 49-55.

[254] R. Andersson, M. Boutonnet, S. Järås, Fuel, 115 (2014) 544-550.

[255] V.R. Surisetty, A.K. Dalai, J. Kozinski, Applied Catalysis A: General, 381 (2010) 282-288.

[256] D. Li, C. Yang, H. Qi, H. Zhang, W. Li, Y. Sun, B. Zhong, Catalysis Communications, 5 (2004) 605-609.

[257] H. Qi, D. Li, C. Yang, Y. Ma, W. Li, Y. Sun, B. Zhong, Catalysis Communications, 4 (2003) 339-342.

[258] H.C. Woo, I.-S. Nam, J.S. Lee, J.S. Chung, Y.G. Kim, Journal of Catalysis, 142 (1993) 672-690.

[259] D. Li, C. Yang, W. Li, Y. Sun, B. Zhong, Topics in Catalysis, 32 (2005) 233-239.

[260] J. Iranmahboob, H. Toghiani, D.O. Hill, Applied Catalysis A: General, 247 (2003) 207-218.

[261] J. Iranmahboob, D.O. Hill, H. Toghiani, Applied Catalysis A: General, 231 (2002) 99-108.

[262] Z. Liu, X. Li, M.R. Close, E.L. Kugler, J.L. Petersen, D.B. Dadyburjor, Industrial & Engineering Chemistry Research, 36 (1997) 3085-3093.

[263] V.R. Surisetty, I. Eswaramoorthi, A.K. Dalai, Fuel, 96 (2012) 77-84.

[264] R. Andersson, M. Boutonnet, S. Järås, Applied Catalysis A: General, 417-418 (2012) 119-128.

[265] J.S. Lee, S. Kima, K.H. Leea, I.-S. Nama, J.S. Chung, Y.G. Kim, H.C. Woob, Applied Catalysis A: General, 110 (1994) 11-25.

[266] H.C. Woo, J.C. Kim, I.-k. Nam, J.S. Lee, J.S. Chung, Y.G. Kim, Applied Catalysis A: General, 104 (1993) 199-214.

[267] D. Ferrari, G. Budroni, L. Bisson, N.J. Rane, B.D. Dickie, J.H. Kang, S.J. Rozeveld, Applied Catalysis A: General, 462-463 (2013) 302-309.

[268] D. Li, N. Zhao, H. Qi, W. Li, Y.H. Sun, B. Zhong, Catalysis Communications, 6 (2005) 674-678.

[269] J.E. Hensley, S. Pylypenko, D.A. Ruddy, Journal of Catalysis, 309 (2014) 199-208.

[270] M.J. Menart, J.E. Hensley, K.E. Costelow, Applied Catalysis A: General, 437-438 (2012) 36-43.

[271] R. Andersson, M. Boutonnet, S. Jaras, Journal of Chromatography A, 1247 (2012) 134-145.

[272] Y. Yang, Y. Wang, S. Liu, Q. Song, Z. Xie, Z. Gao, Chinese Journal of Catalysis, 28 (2007) 1028-1030.

[273] J. Iranmahboob, H.T. b, D.O. Hill, F. Nadim, Fuel Processing Technology, 79 (2002) 71-75.

[274] R. Suárez París, V. Montes, M. Boutonnet, S. Järås, Catalysis Today, (2014) 294-303.

[275] M.A. Portillo Crespo, A.L. Villanueva Perales, F. Vidal-Barrero, M. Campoy, Fuel Processing Technology, 134 (2015) 270-274.

[276] H. Xiao, D. Li, W. Li, Y. Sun, Fuel Processing Technology, 91 (2010) 383-387.

[277] J.M. Christensen, P.M. Mortensen, R. Trane, P.A. Jensen, A.D. Jensen, Applied Catalysis A: General, 366 (2009) 29-43.

[278] C. Liu, M. Virginie, A. Griboval-Constant, A. Khodakov, Applied Catalysis A: General, 504 (2015) 565-575.

[279] V.R. Surisetty, A. Tavasoli, A.K. Dalai, Applied Catalysis A: General, 365 (2009) 243-251.

[280] V.R. Surisetty, A.K. Dalai, J. Kozinski, Applied Catalysis A: General, 385 (2010) 153-162.

[281] V.R. Surisetty, J. Kozinski, A.K. Dalai, International Journal of Chemical Reactor Engineering, 9 (2011) 1-18.

[282] V.R. Surisetty, Y. Hu, A.K. Dalai, J. Kozinski, Applied Catalysis A: General, 392 (2011) 166-172.

[283] V.R. Surisetty, A.K. Dalai, J. Kozinski, Applied Catalysis A: General, 393 (2011) 50-58.

[284] L. Gang, Z. Chengfang, C. Yanqing, Z. Zhibin, N. Yianhui, C. Linjun, Y. Fong, Applied Catalysis A: General, 150 (1997) 243-252.

[285] V.R. Surisetty, A.K. Dalai, J. Kozinski, industrial & Engineering Chemistry Research, 49 (2010) 6959-6963.

[286] T.P. Wilson, W.J. Bartley, P.C. Ellgen, Proceedings of Symposium, (1982).

[287] N.D. Subramanian, J. Gao, X. Mo, J.G. Goodwin Jr, W. Torres, J.J. Spivey, Journal of Catalysis, 272 (2010) 204-209.

[288] J. Hu, Y. Wang, C. Cao, D.C. Elliott, D.J. Stevens, J.F. White, Catalysis Today, 120 (2007) 90-95.

[289] R.M. Palomino, J.W. Magee, J. Llorca, S.D. Senanayake, M.G. White, Journal of Catalysis, 329 (2015) 87-94.

[290] D. Jiang, Y. Ding, Z. Pan, W. Chen, H. Luo, Catalysis Letters, 121 (2008) 241-246.

[291] M.W. Balakos, S.S.C. Chaung, Fuel Science and Technology International, 9 (1991) 793-810.

[292] H. Orita, S. Naito, K. Tamaru, Journal of Catalysis, 90 (1984) 183-193.

[293] J. Gao, X. Mo, A.C.-Y. Chien, W. Torres, J.G. Goodwin Jr, Journal of Catalysis, 262 (2009) 119-126.

[294] Y. Wang, J. Li, W. Mi, Reaction Kinetics and Catalysis Letters 76 (2002) 141-150.

[295] E. Guglielminotti, F. Pinna, M. Rigoni, G. Strukul, L. Zanderighi, Journal of Molecular Catalysis A: Chemical, 103 (1995) 105-116.

[296] J. Yu, D. Mao, L. Han, Q. Guo, G. Lu, Fuel Processing Technology, 112 (2013) 100-105.

[297] H. Yin, Y. Ding, H. Luo, H. Zhu, D. He, J. Xiong, L. Lin, Applied Catalysis A: General, 243 (2003) 155-164.

[298] L. Han, D. Mao, J. Yu, Q. Guo, G. Lu, Catalysis Communications, 23 (2012) 20-24.

[299] M.A. Haider, M.R. Gogate, R.J. Davis, Journal of Catalysis, 261 (2009) 9-16.

[300] J. Wang, Q. Zhang, Y. Wang, Catalysis Today, 171 (2011) 257-265.

[301] G. Chen, C.-Y. Guo, X. Zhang, Z. Huang, G. Yuan, Fuel Processing Technology, 92 (2011) 456-461.

[302] A. Benedetti, A. Carimati, S. Marengo, S. Martinengo, F. Pinna, R. Tessari, G. Strukul, T. Zerlia, L. Zanderighi, Journal of Catalysis, 122 (1990) 330-345.

[303] V. Abdelsayed, D. Shekhawat, J.A. Poston, J.J. Spivey, Catalysis Today, 207 (2013) 65-73.

[304] Y. Liu, K. Murata, M. Inaba, I. Takahara, K. Okabe, Catalysis Today, 164 (2011) 308-314.

[305] D. Mei, R. Rousseau, S.M. Kathmann, V.-A. Glezakou, M.H. Engelhard, W. Jiang, C. Wang, M.A. Gerber, J.F. White, D.J. Stevens, Journal of Catalysis, 271 (2010) 325-342.

[306] H. Ngo, Y. Liu, K. Murata, Reaction Kinetics, Mechanisms and Catalysis, 102 (2010) 425-435.

[307] X. Mo, J. Gao, N. Umnajkaseam, J.G. Goodwin Jr, Journal of Catalysis, 267 (2009) 167-176.

[308] J.Thivolle-cazat, Applied Catalysis, 24 (1986) 211-218.

[309] J.R. Katzer, A.W. Sleight, P. Gajardo, J.B. Michel, E.F. Gleason, S. Mcmillan, Faraday Discussions of the Chemical Society, 72 (1981) 121-133.

[310] J. Lim, H.-G. Park, T.-W. Kim, D. Kim, K.-S. Ha, Fuel, 169 (2016) 25-32.

[311] T.-W. Kim, M.-J. Kim, H.-J. Chae, K.-S. Ha, C.-U. Kim, Fuel, 160 (2015) 393-403.

[312] J. Yu, D. Mao, L. Han, Q. Guo, G. Lu, Fuel Processing Technology, 106 (2013) 344-349.

[313] P. Gronchi, E. Tempesti, C. Mazzocchia, Applied Catalysis A: General, 120 (1994) 115-126.

[314] A. Henrion, H. Ewald, H. Miessner, Applied Catalysis, 62 (1990) 23-34.

[315] B.J. Kip, P.A.T. Smeets, J.v. Grondelle, R. Prins., Applied Catalysis, 33 (1987) 181-208.

[316] Z. Fan, W. Chen, X. Pan, X. Bao, Catalysis Today, 147 (2009) 86-93.

[317] S.C. Chuang, Y.H. Tian, J.G. Goodwin, I. Wender, Journal of Catalysis, 96 (1985) 396-407.

[318] P.R. Watson, G.A. Somorjai, Journal of Catalysis, 74 (1982) 282-295.

[319] J. A. Brown Bourzutschky, N.Homs, AT.Bell, Journal of Catalysis, 124 (1990) 52-72.

[320] N. Tien-Thao, M.H. Zahedi-Niaki, H. Alamdari, S. Kaliaguine, Applied Catalysis A: General, 326 (2007) 152-163.

[321] N. Tien-Thao, H. Alamdari, M.H. Zahedi-Niaki, S. Kaliaguine, Applied Catalysis A: General, 311 (2006) 204-212.

[322] N. Tien-Thao, M. Hassanzahediniaki, H. Alamdari, S. Kaliaguine, Journal of Catalysis, 245 (2007) 348-357.

[323] N. Tien-Thao, H. Alamdari, S. Kaliaguine, Journal of Solid State Chemistry, 181 (2008) 2006-2019.

[324] T. Nguyen, M. Zahedi-Niaki, H. Alamdari, S. Kaliaguine, International Journal of Chemical Reactor Engineering, 5 (2007) art. A82.

[325] N.T. Thao, Asian Journal of Chemistry, 25 (2013) 8082-8086.

[326] T. Niu, G.L. Liu, Y. Chen, J. Yang, J. Wu, Y. Cao, Y. Liu, Applied Surface Science, 364 (2016) 388-399.

[327] G. Liu, D. Pan, T. Niu, A. Cao, Y. Yue, Y. Liu, RSC Advances, 5 (2015) 31637-31647.

[328] G. Liu, T. Niu, A. Cao, Y. Geng, Y. Zhang, Y. Liu, Fuel, 176 (2016) 1-10.

[329] G. Liu, Y. Geng, D. Pan, Y. Zhang, T. Niu, Y. Liu, Fuel Processing Technology, 128 (2014) 289-296.

[330] Y. Fang, Y. Liu, L. Zhang, Applied Catalysis A: General, 397 (2011) 183-191.

[331] G. Liu, T. Niu, D. Pan, F. Liu, Y. Liu, Applied Catalysis A: General, 483 (2014) 10-18.

[332] D. He, Y. Ding, H. Luo, C. Li, Journal of Molecular Catalysis A: Chemical, 208 (2004) 267-271.

[333] H.-B. Zhang, X.-L. Liang, X. Dong, H.-Y. Li, G.-D. Lin, Catalysis Surveys from Asia, 13 (2009) 41-58.

[334] Y. Avila, C. Kappenstein, S. Pronier, J. Barrault, Applied Catalysis A: General, 132 (1995) 97-109.

[335] J.G. Nunan, C.E. Bogdan, K. Klier, K.J. Smith, C.-w. Young, R.G. Herman, Journal of Catalysis, (1989) 195-221.

[336] Y.-P. Pei, J.-X. Liu, Y.-H. Zhao, Y.-J. Ding, T. Liu, W.-D. Dong, H.-J. Zhu, H.-Y. Su, L. Yan, J.-L. Li, W.-X. Li, ACS Catalysis, 5 (2015) 3620-3624.

[337] K. Shimura, T. Miyazawa, T. Hanaoka, S. Hirata, Journal of Molecular Catalysis A: Chemical, 407 (2015) 15-24.

[338] G. Ertl, H. Knözinger, J. Weitkamp, Preparation of solid catalysts, Wiley, (2008).

[339] A.Y. Khodakov, W. Chu, P. Fongarland, Chemical Reviews 107 (2007) 1692-1744.

[340] J.A. Schwarz, C. Contescu, A. Contescu, Chemical Reviews, 95 (1995) 477-510.

[341] A. Manan, Y. Iqbal, M.u. Rahman, M. Khan, Journal of The Pakistan Materials Society, 2 (2008) 15-20.

[342] M. Misono, Studies in Surface Science and Catalysis, 176 (2013) 67-95.

[343] A. Chroneos, R.V. Vovk, I.L. Goulatis, L.I. Goulatis, Journal of Alloys and Compounds, 494 (2010) 190-195.

[344] V.M. Goldschmidt, Naturwissenschaften, 14 (1926) 477-485.

[345] M.A. Peña, J.L.G. Fierro, Chemical Reviews, 101 (2001) 1981-2017.

[346] D.M. Smyth, Annual Review of Materials Science, 15 (1985) 329-357.

[347] S. Aasland, H. Fjellvasg, B.C. Hauback, Journal of Solid State Chemistry, 135 (1998) 103-110.

[348] P. Porta, S.D. Rossi, M. Faticanti, G. Minelli, I. Pettiti, L. Lisi, M. Turco, Journal of Solid State Chemistry, 146 (1999) 291-304.

[349] T. Ishihara, Structure and Properties of Perovskite Oxides, Springer, (2009).

[350] L. Tejuca, J. Fierro, Properties and applications of perovskite-type oxides, Marcel Dekker, (2000).

[351] H. Tanaka, I. Tan, M. Uenishi, M. Kimura, K. Dohmae, Topics in Catalysis, 16/17 (2001) 63-70.

[352] R. Van Grieken, J. Pena, A. Lucas, G. Calleja, M. Rojas, J. Fierro, Catalysis Letters, 8 (1991) 335-344.

[353] H. Tanaka, M. Misono, Current Opinion in Solid State and Materials Science, 5 (2001) 381-387.

[354] K.L. Cottbus, Technical University of Berlin, Doctor of philosophy (2012) 108.

[355] H.Falcon, M.J. Martınez-Lope, J.A. Alonso, J.L.G. Fierro, Solid State Ionics, 131 (2000) 237-248.

[356] Y. Bu, Q. Zhong, D. Xu, W. Tan, Journal of Alloys and Compounds, 578 (2013) 60-66.

[357] J. Shi, L. Guo, Progress in Natural Science: Materials International, 22 (2012) 592-615.

[358] J. Shi, J. Ye, L. Ma, S. Ouyang, D. Jing, L. Guo, Chemistry, 18 (2012) 7543-7551.

[359] H. Husin, W.-N. Su, H.-M. Chen, C.-J. Pan, S.-H. Chang, J. Rick, W.-T. Chuang, H.-S. Sheu, B.-J. Hwang, Green Chemistry, 13 (2011) 1745.

[360] T. Seiyama, Catalysis Reviews, 34 (1992) 281-300.

[361] L. Marchetti, L. Forni, Applied Catalysis B: Environmental, 15 (1998) 179-187.

[362] H. Arandiyan, Methane Combustion Over Lanthanum-based Perovskite Mixed Oxides, Springer, (2015).

[363] X. Wang, Y. Zhang, Q. Li, Z. Wang, Z. Zhang, Catalysis Science & Technology, 2 (2012) 1822-1824.

[364] N. Russo, S. Furfori, D. Fino, G. Saracco, V. Specchia, Applied Catalysis B: Environmental, 83 (2008) 85-95.

[365] D.H. Prasad, S.Y. Park, E.-O. Oh, H. Ji, H.-R. Kim, K.-J. Yoon, J.-W. Son, J.-H. Lee, Applied Catalysis A: General (2012) 100-106.

[366] R. Thalinger, M. Gocyla, M. Heggen, R. Dunin-Borkowski, M. Grünbacher, M. Stöger-Pollach, D. Schmidmair, B. Klötzer, S. Penner, Journal of Catalysis, 337 (2016) 26-35.
[367] G. Valderrama, A. Kiennemann, M.R. Goldwasser, Catalysis Today, 133-135 (2008) 142-148.
[368] S.Q. Chen, Y.D. Li, Y. Liu, X. Bai, International Journal of Hydrogen Energy, 36 (2011) 5849-5856.
[369] F. Ma, Z. Ding, W. Chu, S. Hao, T. Qi, Chinese Journal of Catalysis, 35 (2014) 1758-1778.
[370] C.A. da Silva, P.E.V. de Miranda, International Journal of Hydrogen Energy, 40 (2015) 10002-10015.
[371] N. Sun, H. Liu, Z. Yu, Z. Zheng, C. Shao, Solid State Ionics, 268 (2014) 125-130.
[372] J. Wang, M. Saccoccio, D. Chen, Y. Gao, C. Chen, F. Ciucci, Journal of Power Sources, 297 (2015) 511-518.
[373] K. Rida, A. Benabbas, F. Bouremmad, M. Peña, A. Martinez-Arias, Catalysis Communications, 7 (2006) 963-968.
[374] M. Morales, M. Segarra, Applied Catalysis A: General, 502 (2015) 305-311.
[375] M. Dry, J. Anderson, M. Boudart, Anderson, JR, Boudart, M., Ed, 1 (1981) 159.

Chapter 3 Research Methodology and Analytical Techniques

3.1 Introduction

This chapter provides the overall research methodology employed to achieve the thesis objectives outlined in Chapter 1. The experimental and analytical techniques are described in detail in the following sections.

3.2 Methodology

A methodical approach was pursued to develop the best possible perovskite catalysts for higher alcohol synthesis (HAS), within the parameters of this work. An overview of the research methodology followed in this study is illustrated in Figure 3-1. As reflected in this flow diagram, the study has 3 main sections, catalysts design and preparation, catalysts characterization, and catalysts testing in HAS, all of which are detailed below.

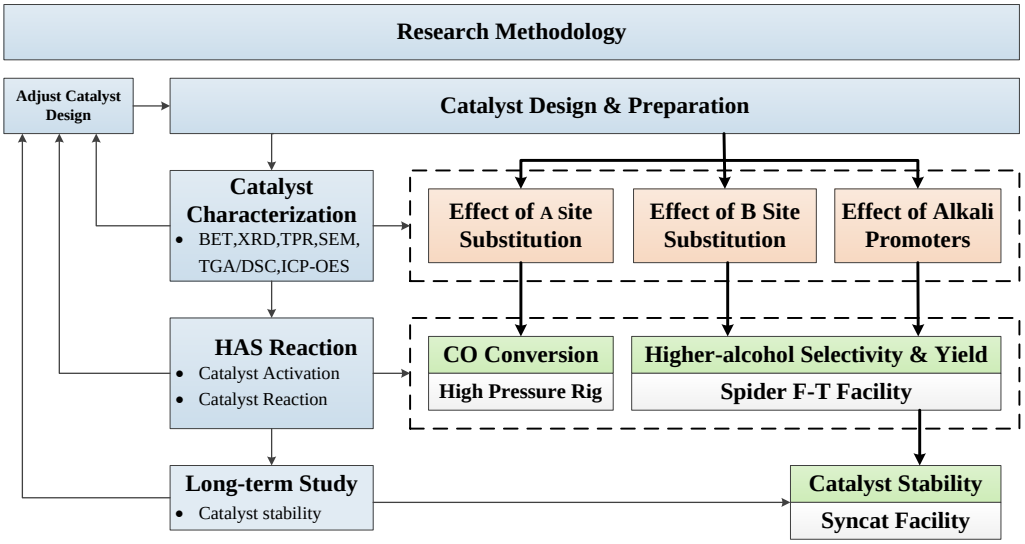

Figure 3-1. Research methodology.

3.3 Catalyst Design and Preparation

3.3.1 Catalyst Design

It has been proven that among perovskites (ABO_3), $LaCoO_3$ is a promising base material for its use as a catalyst in Fischer-Tropsch (F-T) process because of its high activity, high selectivity to hydrocarbons and low water gas shift (WGS) activity [1-3]. Following the extensive literature review presented in Chapter 2, Section 2.9.2, strontium was selected as a substitution element of cation A (lanthanum) in $LaCoO_3$ perovskite, while nickel and copper were good candidates for B site metals substitution. In this study, the possible formulas of the perovskite catalysts is $La_{1-x}Sr_xCo_{1-y-z}Ni_yCu_zO_3$. A series of alkali promoted multi-metal La/Sr/Co/Ni/Cu perovskite catalysts (with different composition and contents of cation A and B) have also been designed and prepared for conversion of syngas into higher alcohols.

3.3.2 Catalyst Preparation Method

3.3.2.1 Co-precipitation Method

$La_{1-x}Sr_xCo_{1-y-z}Ni_yCu_zO_3$ perovskite catalysts were prepared by co-precipitation. The required amount of the appropriate metal nitrates, lanthanum nitrate ($La(NO_3)_3 \cdot 6H_2O$, 99.9%), strontium nitrate ($Sr(NO_3)_2$, 99%), cobalt nitrate ($Co(NO_3)_2 \cdot 6H_2O$, 98%), nickel nitrate ($Ni(NO_3)_2 \cdot 6H_2O$, 98.5%) and copper nitrate ($Cu(NO_3)_2 \cdot 6H_2O$, 98%), obtained from Sigma-Aldrich, were used as reagents and ammonia water (35% mass fraction, Aldrich) was used as a precipitation agent. The metal precursors were weighed in stoichiometric proportions and dissolved successively in distilled water to get 1mol/L solution for both A and B site metal elements. Ammonia water was added to the aqueous solution dropwise under vigorous stirring until a pH of 9 was reached. The precipitate was then filtered and dried at 120 °C overnight. The dried material was calcined in a muffle furnace under air atmosphere. The detailed drying and calcination procedure of perovskite catalysts prepared in this study is presented in Figure 3-2.

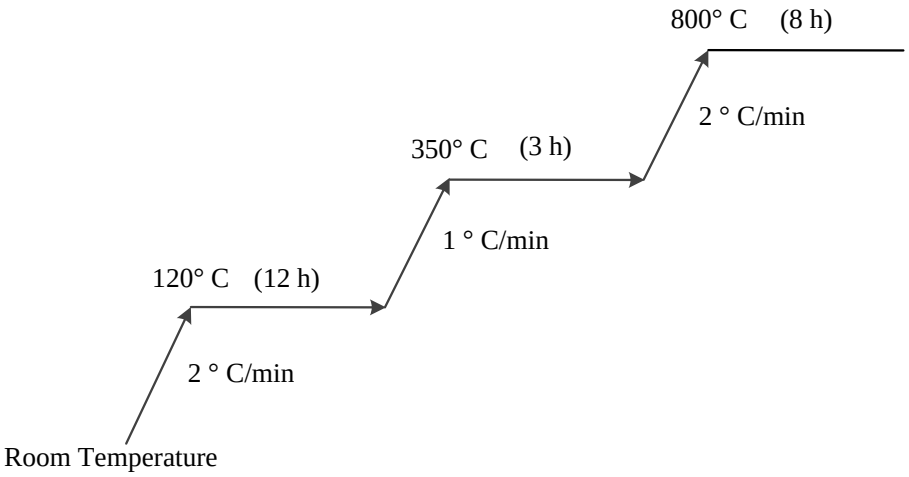

Figure 3-2. Drying and calcination procedure of $La_{1-x}Sr_xCo_{1-y-z}Ni_yCu_zO_3$ perovskite catalysts.

3.3.2.2 Impregnation Method

To load alkali metals on the catalyst surface, incipient-wetness impregnation method was employed. The total amount of promoter metal was fixed at 1 wt. % for all samples. A certain volume of alkali carbonate (Na_2CO_3 or K_2CO_3, 99%, Sigma-Aldrich) solution (0.217 and 0.128 mol/L, respectively) was added to the calcined perovskites to reach incipient wetness. After aging for 24 h at room temperature, the paste was dried for 8 h at 110°C and then calcined in a muffle furnace with air flow at 800°C for 6 h with a ramping rate of 2°C/min.

3.4 Analysis Techniques for Catalyst Characterization

Catalyst characterisation provides important information about the structure and properties of perovskite catalysts. It not only allows identification of the active sites for HAS reaction but also reveals possible routes for optimisation of the catalyst structure. Figure 3-3 provides an overall picture of the analytical techniques used to characterise the perovskite catalysts in this study.

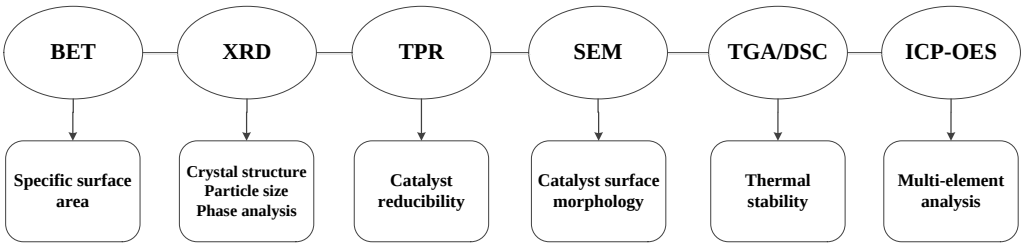

Figure 3-3. Analysis techniques for catalyst characterisation.

3.4.1 Specific Surface Area

The specific surface area is an important parameter of catalysts, which related to the catalysts' activity. Specific surface area measurements of the catalysts were carried out on a Micro Tristar II apparatus at liquid nitrogen temperature using the Brunauer–Emmett–Teller (BET) method. The samples were degassed by evacuation at 250 °C for 12 h before N_2 adsorption measurements.

3.4.2 X-ray Diffraction Analysis

X-ray diffraction (XRD) is a characterisation method of solids, which is commonly used to analyse the phases and to determine the particle size of perovskite catalysts. In this study, XRD analyses were performed on a Bruker D8 Advance X-ray diffractometer with Co *K*α radiation (λ=1.78897 nm) operating at 40 kV. The spectra were obtained between the 2θ ranges of 20 and 80° at a scanning speed of 1°/min for prepared catalysts and 5°/min for reduced and used catalysts at room temperature. The patterns recorded were identified by reference to the powder diffraction data (JCPDS-ICDD) with the standard spectra software.

3.4.3 Hydrogen Temperature-programmed Reduction Analysis (H_2-TPR)

Hydrogen temperature-programmed reduction (TPR) experiments were carried out to study the catalyst redox properties. H_2-TPR experiments were performed using a ChemBET 3000 equipment. In each analysis, 0.1 g or 0.3 g of sample in the form of a powder was placed in a quartz cell. The sample was outgassed at 300 °C for 1 h with 20 ml/min flowing nitrogen through the cell to remove the contaminants on the surface of the sample and then cooled down to room temperature. The sample was then reduced with a 5% H_2/N_2 gas mixture at a total flow of 20 ml/min. The temperature was increased at 5 °C/min from room temperature to 800 °C.

3.4.4 Scanning Election Microscopy (SEM)

Scanning electron microscopy (SEM) was used to obtain the samples' surface morphology and composition. SEM images were recorded using a Field Emission Zeiss Ultra Plus unit, with an acceleration voltage of 5 kV.

3.4.5 Thermogravimetric Analysis and Differential Scanning Calorimetry (TGA/DSC)

Thermogravimetric analysis and Differential scanning calorimetry (TGA/DSC) of catalyst precursors and used catalysts were performed on a Mettler Toledo TGA/DSC instrument, from 25 to 950 °C at a heating rate of 10 °C /min and under an air flow of 60 ml/min.

3.4.6 Inductively Coupled Plasma Optical Emission Spectrometry (ICP-OES)

The atomic compositions of the perovskite catalysts were determined by inductively coupled plasma optical emission spectroscopy (ICP-OES) using a Perkin Elmer Optima 8300 ICP-OES Spectrometer. The concentrations of the components obtained in parts per million were converted into atomic concentrations using the atomic weights of the metals.

3.5 Higher Alcohol Synthesis from Syngas

3.5.1 Instruments for Catalyst Performance Test

In this study, the HAS reactions from syngas were tested on three different fixed-bed reactor systems, each offering different performances.

3.5.1.1 High Pressure Rig

The catalytic tests for syngas conversion study were carried out in a high-pressure experimental unit which consists of three parts: gas feeding system, reaction system and separation and analysis system (Figure 3-4).

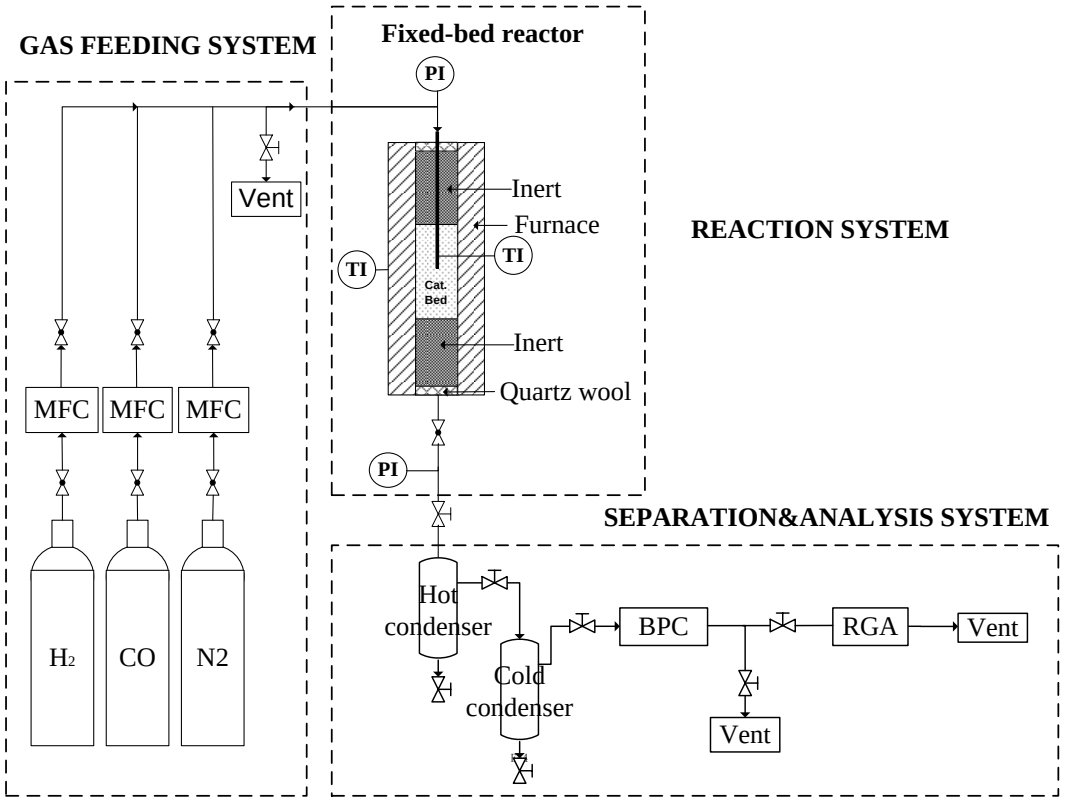

Figure 3-4. Schematic diagram of the high-pressure experimental unit for syngas conversion (MFC: mass flow controller; BPC: back pressure controller; RGA: refiner gas analyser; PI: pressure indicator; TI: temperature indicator).

The stainless-steel fixed-bed reactor (I.D. = 12.7 mm, L = 385 mm) was packed with 1 g of catalyst (66–150 μm) diluted with alumina (1:10 ratio) in the middle of the reactor, between inert beds of alumina spheres (I.D. 1mm) at both ends of the reactor. The reaction temperature was monitored by a thermocouple, which was inserted in the middle of the catalytic bed. Three calibrated mass flow controllers (MFC) were used to regulate the flow of the inlet gases (H_2 and N_2 with purity of 99.999%, CO purity 99.5%). The reactor pressure was controlled by a back pressure controller (BPC). The pressures at the inlet and outlet of the reactor were recorded during the reaction, to ensure the pressure drop across the catalyst bed was known and could be continually monitored. To avoid condensation of oxygenates and long chain hydrocarbon products (only present in a small amount) leaving the reactor, the transfer lines downstream of the reactor were heated to 130 °C.

The inlet (using a reactor by-pass) and outlet gases (carbon monoxide, hydrogen, nitrogen, carbon dioxide, methane and C_1–C_5 hydrocarbons) were analysed on-line with a PerkinElmer CLARUS 580 refinery gas analyser (RGA) equipped with one

flame ionization detector (FID) and two thermal conductivity detectors (TCD), and a combination of packed columns (HayeSep N 60/80 mesh, HayeSep T 60/80 mesh, Molecular Sieve 80/100 mesh and Molecular Sieve 5A 80/100 mesh). The run time for each experiment was about 24 h. The feed gas conversion and other gaseous products were monitored continuously with a time interval of 8 min. The liquid products (aqueous and organics) were collected at the end of the run and analysed off-line after being carefully separated by condensation on an Agilent 7890 GC/MS equipped with an HP-5 MS capillary column (30 m×0.32 mm×0.25 μm) and a FID detector.

3.5.1.2 Spider F-T Facility

Higher alcohol selectivity studies over the perovskite catalysts were performed in a high-flow fixed-bed reactor (Spider 3F-T instrument, AMTech, Germany), as shown in Figure 3-5. The set-up was similar to the high pressure rig (Section 3.5.1.1).

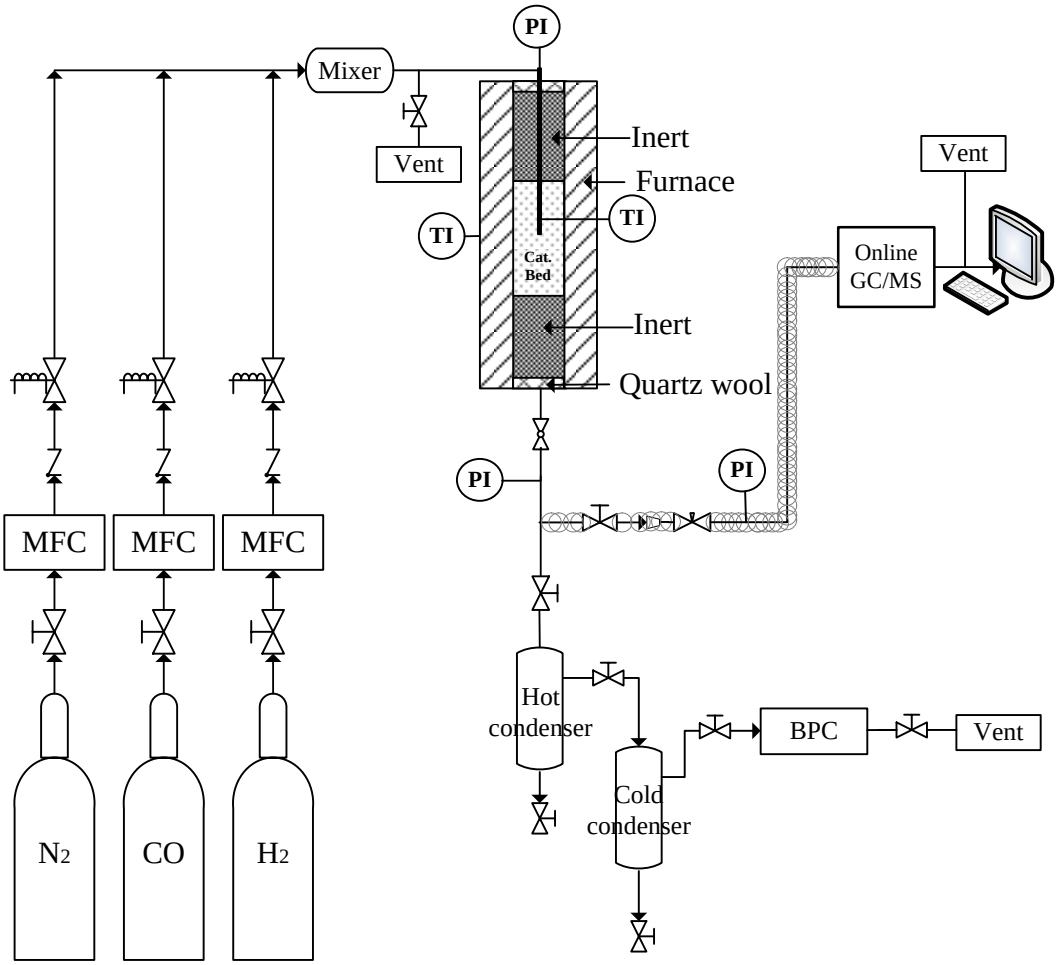

Figure 3-5. Schematic diagram of Spider F-T instrument for higher alcohol synthesis.

The reactor was made up of an Inconel tube (I.D. = 12.7 mm, L = 200 mm). 0.5 gram of catalyst, diluted with 1.5 gram of alumina (pellet size: 53-105 μm), were used in each test. Inert alumina spheres (I.D. 1mm) were packed on both ends of the reactor. The feed gases were sent to a GC/MS via a bypass line for analysis. The products were analysed directly without any treatment using an online Agilent 7890 GC/MS and the temperature of the transfer line between the reactor outlet and the GC valves were kept at 200 °C in order to avoid any product condensation.

The permanent gases (CO, H_2, N_2, CH_4, CO_2 and CH_4) were separated using a TDX-01 packed column (2 m×80/100 mesh) connected to a TCD detector. Quantitative and qualitative analysis of all organic products was carried out using an MS HP-5 column (30 m×0.32 mm×0.25 µm) connected to the mass spectrometer. The experiments were carried out for 24h and the data obtained from each experiment were the average of measurements over the steady-state period.

3.5.1.3 Syncat Facility

In order to confirm the laboratory research outcomes, long-term tests of the catalyst stability were performed using one of the gas processing rigs of CSIRO SynCat Facility. The long term HAS reactions were carried out in a down flow fixed-bed stainless steel reactor (I.D. = 19 mm, L = 500 mm), fitted with a ¼″ thermal well, which includes 5 thermocouples. A simplified experimental set-up schematic is shown in Figure 3-6.

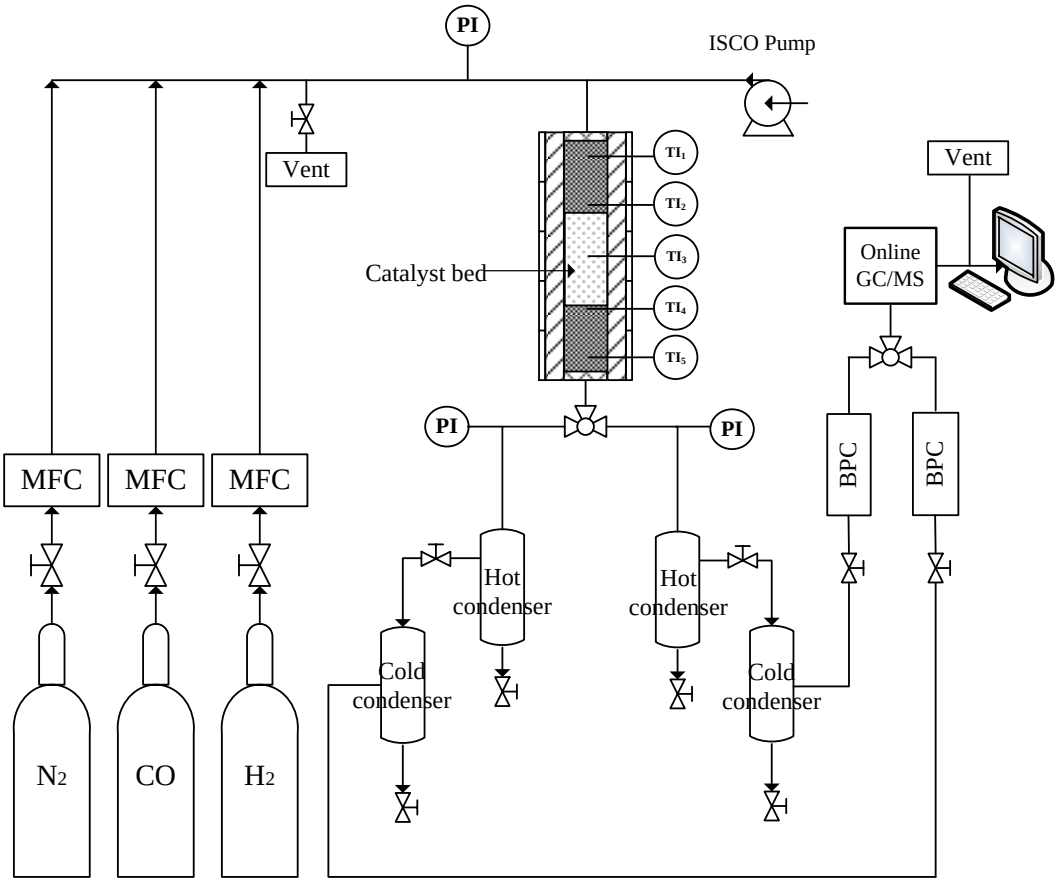

Figure 3-6. Simplified piping and instrumentation diagram of the Syncat gas processing rig.

In a typical experiment, the reactor was loaded with *ca.* 5 g of catalyst with a particle size of 53-105 μm. The catalyst was diluted with alumina (3 parts alumina to 1part catalyst) to prevent hot spots forming along the reactor and ensure a more uniform temperature in the catalyst bed. The outlet gases were depressurised through a BPC and continuously analysed on-line by Agilent RGA after passing through a hot trap (120°C) and a cold trap (15°C) to condense any liquid products. The RGA was equipped with a FID and two TCD, using HP-AL/S, Molsieve 5A 60/80 mesh, and HayeSep Q 80/100 mesh columns respectively. N_2 was used as internal standard.

3.5.2 Higher Alcohol Synthesis

Similar procedures were followed for testing the perovskite catalysts in HAS on all the test rigs described above.

Prior to the HAS, the catalyst was reduced *in situ* using a gas mixture of 20% H_2 in N_2 at a flow rate of 100 ml/min under ambient pressure. The reactor temperature

was slowly increased from room temperature to 450 ℃ and held at this temperature overnight.

After the *in situ* reduction of the catalyst, the reactor was cooled down to reaction temperature and pressurised to reaction conditions with nitrogen. A syngas mixture composition of $H_2/CO/N_2$= 2:1:3 was used as feed for all experiments in this work. N_2 acted as an internal calibration standard. The syngas feed was introduced through the reactor at the appropriate gas hourly space velocities (GHSV). The HAS reaction was carried out at steady state under the reaction conditions for the required period of time.

After the reaction, nitrogen was introduced to purge the reactor system and depressurized to ambient pressure. The used catalysts were collected after the reactor was cooled down to room temperature under the nitrogen atmosphere.

3.5.3 Calculation Methods

Using N_2 as an internal standard, the feed gas conversion X_F was calculated as in Equation (3-1):

$$X_{\mathrm{F}} = \frac{Mole_{\mathrm{F\ in}} - Mole_{\mathrm{F\ out}}}{Mole_{\mathrm{F\ in}}} \times 100\% \qquad (3\text{-}1)$$

Where $Mole_{\mathrm{F\ in}}$ and $Mole_{\mathrm{F\ out}}$ are the moles of gas (CO or H_2) in the feed-gases and out-gases, respectively.

The molar selectivity S_i of each carbon-containing product i was calculated as in Equation (3-2):

$$S_{\mathrm{i}} = \frac{Mole_{\mathrm{i}} \times n_i}{Mole_{\mathrm{co\ react}}} \times 100\% \qquad (3\text{-}2)$$

$Mole_i$, n_i represent the moles of carbon-containing product *i* and the number of carbon atoms in product *i*, respectively.

The specific selectivity (related to alcohol distribution in subsequent chapters) of alcohol product S_A with n_A carbon number, in the total alcohol product, was obtained by Equation (3-3):

$$S_A = \frac{Mole_A \times n_A}{\sum Mole_A \times n_A} \times 100\% \quad (3\text{-}3)$$

$Mole_A$, n_A represent the moles of alcohol product *A* and the number of carbon atoms in alcohol *A*, respectively.

The space time yield (STY) of alcohol product R_A ($mg \cdot g_{cat}^{-1} \cdot h^{-1}$) was calculated according to Equation (3-4):

$$R_A = \frac{m_A}{m_{cat} \times t} \times 100\% \quad (3\text{-}4)$$

Here, m_A is the mass of alcohol *A* (mg), m_{cat} is the mass of catalyst (g) and *t* represents reaction time (h).

References

[1] L. Huang, M. Bassir, S. Kaliaguine, Applied Surface Science, 243 (2005) 360-375.
[2] N. Tien-Thao, H. Alamdari, M.H. Zahedi-Niaki, S. Kaliaguine, Applied Catalysis A: General, 311 (2006) 204-212.
[3] N. Tien-Thao, H. Alamdari, S. Kaliaguine, Journal of Solid State Chemistry, 181 (2008) 2006-2019.

Chapter 4: Behaviour of Low Strontium Substituted $La_{1-x}Sr_xCoO_3$ Perovskite Catalysts in Syngas Conversion

4.1 Introduction

As reviewed in Chapter 2, Section 2.2, the Fischer-Tropsch (F-T) synthesis has proven its ability for the conversion of syngas to high value hydrocarbons (*e.g.* gasoline, diesel and light olefins) and organic oxygenates (*e.g.* methanol and other higher alcohols) [1]. Cobalt and iron oxides are the most common catalysts for F-T synthesis and have been thoroughly investigated (see Chapter 2, Section 2.4.2). Recently, perovskite catalysts with an ABO_3 type structure, where A and B represent different metallic elements, have been investigated for F-T synthesis, due to the flexibility in their design and preparation (see Chapter 2, Section 2.8). It is envisaged that their tailorable compositions and structures could be used to target specific desirable products of syngas conversion, such as higher alcohols [2-12]. In addition, their high thermal stability and excellent redox properties also make perovskite oxides ideal candidates for the F-T reaction. For example, a series of $La(CoFe)O_3$ perovskite catalysts have been reported to show high C_2-C_4 olefins selectivity [3, 4]. Tien-Thao and co-workers investigated the performance and stability of the $LaCo_{1-x}Cu_xO_3$ perovskite catalysts (x=0-0.4) for syngas conversion, reporting its high selectivity towards higher alcohol formation [6-10].

Partial substitution at the A or/and B sites of the perovskite (ABO_3) leads to changes in the perovskite structure, the oxygen mobility and the redox properties of the perovskite, which affects the catalytic activity. The effects of partial substitution of La^{3+} by lower oxidation state ions such as Sr^{2+} in $LaCoO_3$ perovskites have been widely investigated for both fundamental research and industrial applications such as batteries [13], thermoelectric materials [14] or as a catalyst for steam and hydrocarbon reforming [15]. The catalytic properties of $La_{1-x}Sr_xCoO_3$ perovskites have also been studied for the oxidation of carbon monoxide [16, 17], hydrocarbons [18-20] and soots [21, 22]. It was found that the changes in the perovskite structure of $LaCoO_3$ with partial substitution of La^{3+} by Sr^{2+} positively and significantly affected the catalytic activity in the above-mentioned applications.

However, despite the extensive research, large gaps between the fundamental understanding of these catalysts and their activity still remain. To date, no information is available on how Sr^{2+} modified the perovskite structure and the reduction processes. Furthermore, there is no general agreement about the maximum amount of Sr^{2+} that can be substituted in $LaCoO_3$ for it to maintain its initial perovskite structure. In addition, to the best of our knowledge, there is no specific study about the effect of strontium substitution in $LaCoO_3$ perovskite catalysts for syngas conversion. Although other perovskite catalysts for HAS from syngas have been investigated intensively to date, product yields still remain too low for commercial applications, with reagent conversion and product selectivity following opposite trends (high selectivity at low conversion and *vice versa*) [6-12]. Moreover, investigation on perovskite catalyst behaviours during its induction period in F-T synthesis has never been reported before. It is not very clear what changes occurred in the perovskite catalysts during the induction period and how these changes influence the catalyst behaviour and activity in F-T reaction.

The main objective of this chapter is thus to gain some insights into the effect of strontium substitution on $LaCoO_3$ perovskites structure and reduction properties. The effect of strontium substitution on the catalytic activity of $LaCoO_3$ perovskites in syngas conversion will also be investigated, with an added focus on the induction period in F-T synthesis. To this end, $La_{1-x}Sr_xCoO_3$ perovskite catalysts (x=0 to 0.4) were prepared using the co-precipitation technique and their activities were tested in F-T synthesis at different reaction conditions, in a fixed bed reactor. All the catalysts were thoroughly characterised by several techniques (described in Chapter 3, Section 3.4). The result of this work is an important step in the design of catalysts tailored for specific reactions and products, such as the F-T process for HAS from syngas.

4.2 Effect of Strontium Substitution on Structure and Reduction Properties of $LaCoO_3$ Perovskite Catalysts

4.2.1 Structure of $La_{1-x}Sr_xCoO_3$ Perovskites

$La_{1-x}Sr_xCoO_3$ perovskite samples (x=0 to 0.4) were prepared according to the co-precipitation method described in Chapter 3, Section 3.3.2, and analysed by thermogravimetric analysis and differential scanning calorimetry (TGA/DSC),

Brunauer-Emmett-Teller (BET) method and X-ray diffraction (XRD) (Chapter 3, Section 3.4).

The TGA/DSC diagram of the unsubstituted $LaCoO_3$ perovskite material before calcination is shown in Figure 4-1.

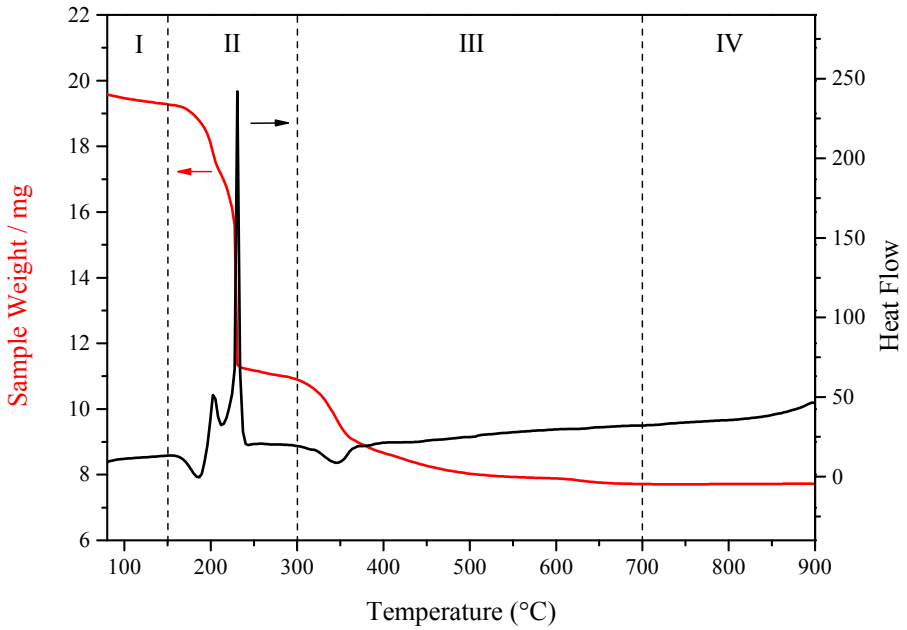

Figure 4-1. Sample weight (TGA) (—) and heat flow (DSC) (—) profiles of $LaCoO_3$ material before calcination.

The TGA signal shows that weight loss appears to take place in four steps. The first weight loss step (I) below 150 °C was mostly due to the desorption of adsorbed or hydration water, with a weight loss of 4%. The second step (II) represented a significant weight loss between 150 and 300 °C, related to an exothermic process displaying a sharp peak on the DSC, with a maximum at 250 °C. The experimental weight loss (41%) was related to the decomposition of the ammonium nitrate in the powder precursor, as observed by Biamino *et al*. [23]. The following weight loss step (III), between 300 and 700 °C, corresponded to the formation of perovskite oxide. The sharp weight loss (7.2%) at about 350 °C, associated with an endothermic peak in the DSC, was related to the decomposition of metal hydroxide in the material, accompanied by the loss of H_2O. At temperatures higher than 700 °C (step IV), no further weight loss was observed for $LaCoO_3$, suggesting that the $LaCoO_3$ perovskite structure, expected to be produced upon the decomposition of the precursors, was finally formed at that temperature, in agreement with literature results [24]. The TGA

results indicated that the calcination temperature used in this work (800 °C) was thus suitable for perovskite formation.

The specific surface areas (S_{BET}) of the prepared $La_{1-x}Sr_xCoO_3$ perovskite samples are given in Table 4-1.

Table 4-1. BET surface area and mean particle size of $La_{1-x}Sr_xCoO_3$.

Samples	x	S_{BET} (m^2 /g)	Crystal domain size (nm)[a]
$LaCoO_3$	0	2.4	39
$La_{0.9}Sr_{0.1}CoO_3$	0.1	4.7	36
$La_{0.8}Sr_{0.2}CoO_3$	0.2	4.5	34
$La_{0.7}Sr_{0.3}CoO_3$	0.3	5.0	30
$La_{0.6}Sr_{0.4}CoO_3$	0.4	5.5	27

[a] Calculated from XRD results with Scherrer equation: $D=k\lambda/(\beta\cos\theta)$ applied to the (0 2 4) diffraction peak (see Figure 4-2).

The results in Table 4-1 showed that the S_{BET} of the prepared catalysts were low relative to most catalysts and the partial substitution of lanthanum by strontium doubled the catalysts' surface areas, with a slightly increasing trend with increasing strontium substitution. However, these trends should be considered with caution, allowing for the experimental error at these low S_{BET} values. It is well known that the specific surface area of perovskite is affected by the calcination temperature [25]. The surface area of $LaCoO_3$ perovskite prepared in this work (2.4 m^2/g with calcination at 800°C) is in agreement with the result reported by Lee *et al.* for the same material, at similar calcination temperature (2.8 m^2/g, for calcination at 850°C) [26]. The surface areas of the $La_{1-x}Sr_xCoO_3$ perovskites prepared in this study were lower than those reported by Gao and Wang (10.0 m^2/g for x=0.1; 7.4 m^2/g for x=0.3), who however used a lower calcination temperature (700°C) [18].

The crystalline structure of a perovskite catalyst is an important factor that affects its catalytic activity for different reactions. For example, it was reported in the literature that the partial substitution of La^{3+} by monovalent Ag^+ turned the rhombohedral structure of $La_{1-x}Ag_xMn_{0.9}Co_{0.1}O_3$ catalyst to an orthorhombic structure, which, according to Pecchi *et al*. is a more suitable structure for the *n*-hexane combustion reaction [27]. The XRD patterns of the prepared $La_{1-x}Sr_xCoO_3$ perovskite oxides with different strontium substitution levels are presented in Figure 4-2.

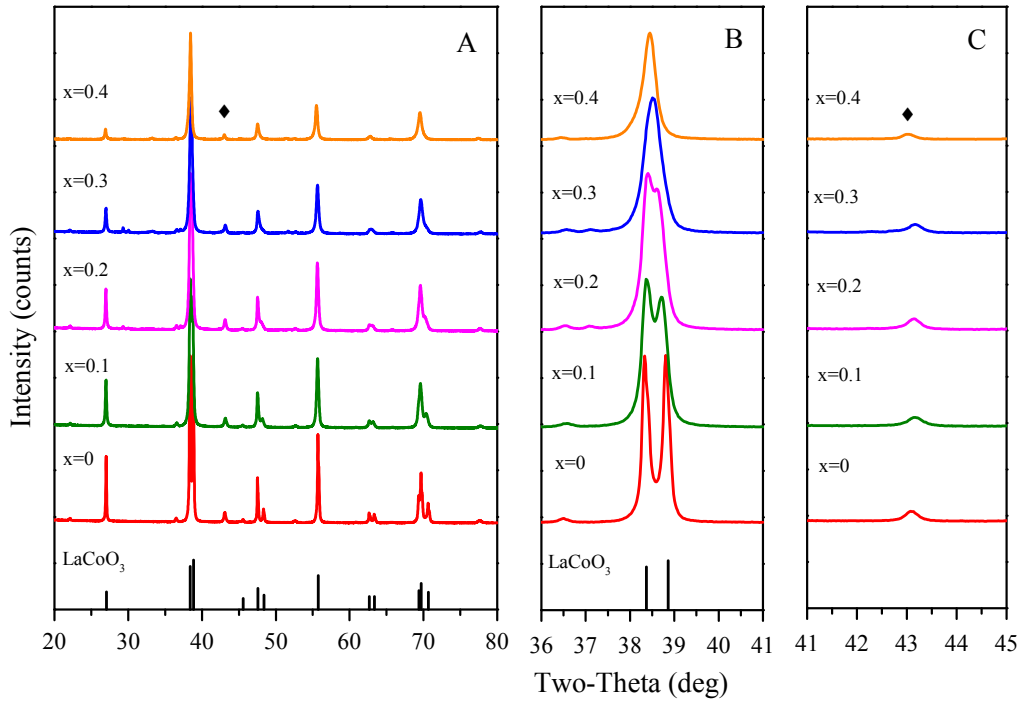

Figure 4-2. X-ray diffraction patterns of $La_{1-x}Sr_xCoO_3$ perovskites calcined at 800°C for x=0 to x=0.4: (A) full pattern, (B) zoom in the perovskite peak range and (C) zoom on the Co_3O_4 phase (♦).

The perovskite structure is recognisable in the XRD patterns, as it exhibits two typical doublets of rhombohedral structure: a first sharp and highly intense one at $2\theta \approx 38\text{-}39°$, and a second broader and less intense one with a shoulder around $2\theta = 70°$ [5, 27]. The data in Figure 4-2 reveal that the $La_{1-x}Sr_xCoO_3$ materials exhibit the strong reflections of $LaCoO_3$ (JCPDS-ICDD 48-0123) perovskite structure (Figure 4-2. B), suggesting that the adopted calcination temperature of 800 °C was suitable for perovskite formation. This supports the TGA/DSC results presented above. The diffraction profiles reveal that a well-defined rhombohedral structure was obtained for the $La_{1-x}Sr_xCoO_3$ materials without or with low strontium substitution ($x \leq 0.1$), with the clearly distinct doublet peak at $2\theta \approx 38\text{-}39°$ [14]. With the increase in strontium substitution levels ($x \geq 0.2$), the typical doublet peak indicative of the rhombohedral structure became weaker and gradually evolved to a singlet peak indicating cubic symmetry [28, 29]. In addition, Co_3O_4 (JCPDS-ICDD 80-1541) phase was found in all samples, with very low peak intensity [30].

Due to the high tolerance of the perovskite structure to distortion by metallic elements of different sizes and oxidation states, substitution of La^{3+} with a higher ionic radius cation, Sr^{2+} (1.36 Å and 1.44 Å, respectively [31]) into the A site of $LaCoO_3$

maintained the rhombohedral structure of $La_{1-x}Sr_xCoO_3$ materials at low strontium substitution levels ($x \leq 0.1$). At higher strontium substitution levels ($x \geq 0.2$), the symmetry of the crystal structure changed from rhombohedral to cubic [28, 29]. Furthermore, due to the difference in ionic radii, the diffraction lines of $La_{1-x}Sr_xCoO_3$ progressively shifted to lower 2θ values with increasing x. As a result, the crystalline domain sizes were markedly diminished from 39 to 27 nm according to the Scherrer equation [14, 22] (see Table 4-1). The slight shift of the peaks observed indicates that the strontium ions have entered into the perovskite lattice, as proposed in the literature [25]. The ability of strontium to substitute lanthanum in the $LaCoO_3$ perovskite lattice has been reported in the literature differently. Schmal *et al.* [32] suggested that 5 mol % of strontium (x=0.05) was the maximum limit to form the single phase related to the $LaCoO_3$ perovskite, while Hueso *et al*. [29] proved that even with x=0.5, the partially substituted $La_{1-x}Sr_xCoO_3$ materials were still able to maintain the perovskite structure. In this work, the XRD results confirmed that a perovskite structure was obtained for all $La_{1-x}Sr_xCoO_3$ materials up to x=0.4, while the initial rhombohedral crystal structure of $LaCoO_3$ perovskite was maintained in $La_{1-x}Sr_xCoO_3$ perovskites with strontium substitution only up to x=0.1. If $x \geq 0.2$, the initial rhombohedral crystal structure starts to disappear and give place to a cubic structure.

4.2.2 Reduction Properties of $La_{1-x}Sr_xCoO_3$ Perovskites

In order to investigate the effect of strontium substitution on the reducibility of $La_{1-x}Sr_xCoO_3$ perovskites, hydrogen temperature-programmed reduction (TPR) was carried out from room temperature to 800 °C. The H_2-TPR profiles of the prepared $La_{1-x}Sr_xCoO_3$ perovskite materials are displayed in Figure 4-3. The partial substitution of lanthanum by strontium in $La_{1-x}Sr_xCoO_3$ perovskites gives rise to significant differences in the H_2-TPR profiles compared to $LaCoO_3$ perovskite. All the reduction peaks visible in the temperature range (100 °C to 800 °C) of the H_2-TRP profiles in Figure 4-3 can be assigned to the reduction of Co species, as La^{3+} and Sr^{2+} are not reduced under such experimental conditions [33].

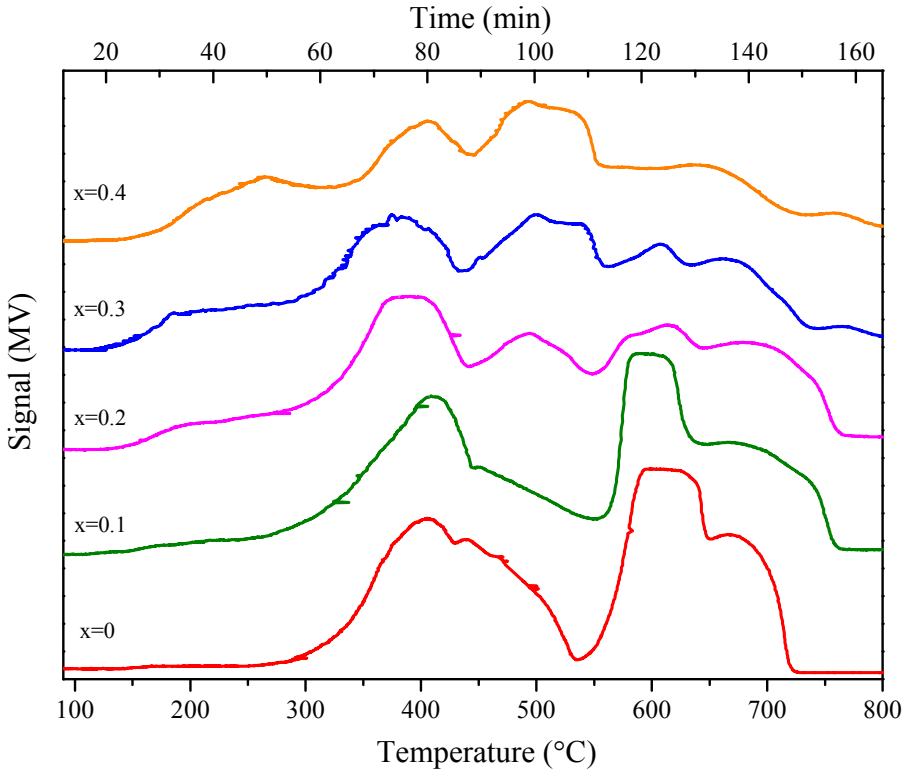

Figure 4-3. TPR profiles of $La_{1-x}Sr_xCoO_3$ (x=0 to 0.4) calcined at 800 °C.

For $LaCoO_3$, two main reduction peaks were observed, suggesting two main reduction steps. The reduction steps can be described as follows:

$$2\ LaCoO_3 + H_2 \rightarrow 2\ LaCoO_{2.5} + H_2O \quad (4\text{-}1)$$

$$LaCoO_3 + y\ H_2 \rightarrow LaCo_{1-z}O_{3-y} + z\ Co^0 + y\ H_2O \quad (4\text{-}2)$$

$$2\ LaCoO_{2.5} + 2\ H_2 \rightarrow La_2O_3 + 2\ Co^0 + 2\ H_2O \quad (4\text{-}3)$$

The first peak at *ca.* 400 °C corresponds to the reduction of Co^{3+} to Co^{2+} (Equation (4-1)), in good agreement with the literature [34, 35]. A small shoulder was also observed on that peak at higher temperature (430 °C), which, according to the literature, suggests that a small amount of cobalt was directly reduced to Co^0 (Equation (4-2)) [11, 36, 37]. The second peak between 600°C and 750 °C relates to the complete reduction of Co^{2+} to Co^0 (Equation (4-3)) [33]. The small shoulder at 670 °C might come from the further reduction of the $LaCo_{1-z}O_{3-y}$ species. A similar reduction behaviour was also observed for catalyst x=0.1. With the increase of strontium content in the perovskites, the number of reduction peaks continuously increased while the reduction temperatures of the different cobalt species were decreased significantly. For

higher strontium substituted catalysts (x≥0.2), the two main reduction peaks shifted to lower temperatures compared to that for x≤0.1 sample: the reduction of Co^{3+} to Co^{2+} and, to a lesser extent, to Co^0, occurred at 200-450°C with two peaks at 250°C and 400°C, while the main peak of Co^{2+} to Co^0 shifted to 500°C. This is in accordance with the literature, which showed that strontium substitution shifted the reduction peaks of $La_{1-x}Sr_xCoO_3$ materials to lower temperatures [15, 38]. The partial substitution of La^{3+} by Sr^{2+} generates oxygen vacancies to compensate and preserve the electroneutrality of the perovskite, which promotes the mobility of lattice oxygen to the surface and favoured its removal by the reducing gas [38].

In order to investigate the phase changes of the $La_{1-x}Sr_xCoO_3$ perovskites during reduction, all samples were reduced at 450°C in 5% H_2/N_2 for 1 hour before XRD analysis. The reduced catalysts were cooled down to room temperature under the nitrogen atmosphere and then tested in XRD to make sure no oxidation happened. The XRD patterns of the $La_{1-x}Sr_xCoO_3$ perovskites after reduction are shown in Figure 4-4. It should be noted that the perovskite samples were only partially reduced at 450°C according to Figure 4-3.

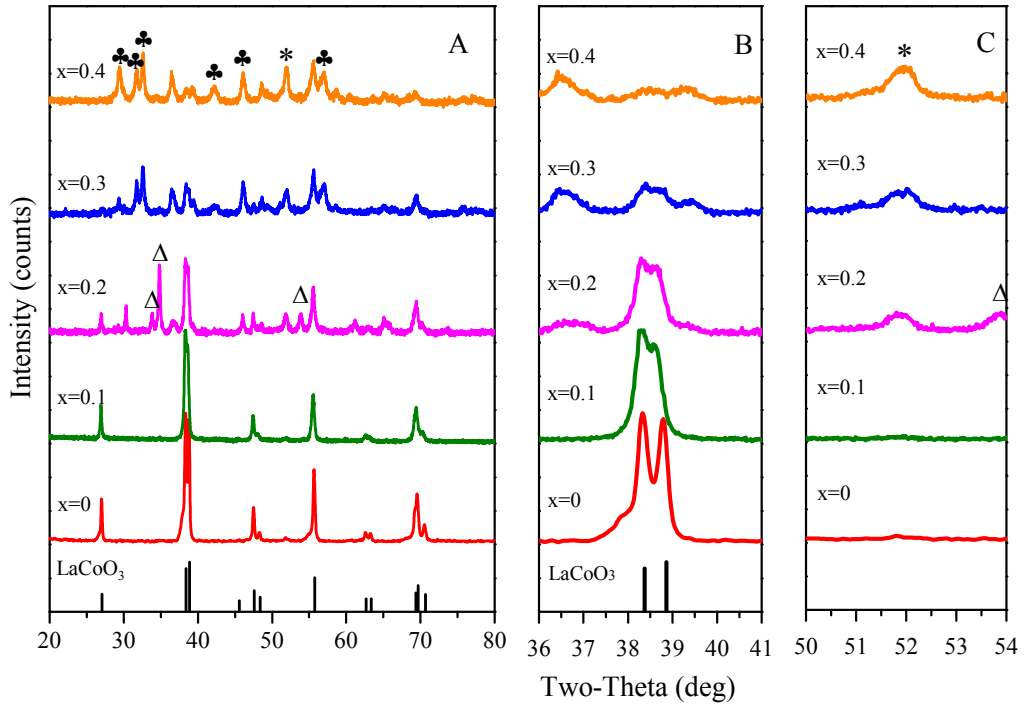

Figure 4-4. X-ray diffraction patterns of $La_{1-x}Sr_xCoO_3$ perovskites after reduction at 450°C for 1 h (5% H_2/N_2), for x=0 to x=0.4: (A) full pattern, (B) zoom in the perovskite peak range and (C) zoom on the Co^0 peak. Phase: (Δ) La_2O_3, (♣) La_2SrO_x, (*) Co^0.

For the low strontium substituted samples (x=0 and 0.1), the perovskite rhombohedral structure remained after reduction at 450 °C with H_2 (Figure 4-4. B). However, the typical diffraction peaks at $2\theta \approx 38\text{-}39°$ were weaker in intensity and broader compared to the fresh catalysts (Figure 4-2. B), suggesting that the crystalline structure partly collapsed during the reduction. For the samples with $x \geq 0.2$, the higher the substitution level, the more decomposed the cubic perovskite structure, indicating that they had less thermal resistance under reducing atmosphere than rhombohedral perovskites. It is postulated that the progressive substitution of La^{3+} by divalent Sr^{2+} not only changed the structure symmetry and generated structure defects in $La_{1-x}Sr_xCoO_3$ perovskites, but also destabilized the structure by the mismatch of the cation size between La^{3+} and Sr^{2+} (1.36 Å and 1.44 Å respectively), affecting their capacity to maintain their structure under reductive atmosphere.

After reduction at 450 °C, La_2O_3 (JCPDS-ICDD 74-2430), La_2SrO_x (JCPDS-ICDD 42-0343) and metallic Co^0 (JCPDS-ICDD 15-0806) were formed in samples with a high strontium content ($x \geq 0.2$). From Figure 4-4. C, the existence of Co^0 at lower reduction temperature confirmed the one-step reduction mechanism of Co^{3+} to Co^0 in $La_{1-x}Sr_xCoO_3$ (Equation (4-2)), as the complete reduction of Co^{2+} to Co^0 takes place at temperature above 500 °C (Equation (4-3), Figure 4-3). As the atomic ratio of (La+Sr)/Co in all $La_{1-x}Sr_xCoO_3$ materials was equal to 1, the reduction of Co^{3+} in $La_{1-x}Sr_xCoO_3$ occurred concomitantly with the formation of La_2O_3 and La_2SrO_x to preserve the electroneutrality of the perovskite. Furthermore, the strong Co^0 diffraction lines observed in higher strontium substituted perovskites ($x \geq 0.2$) indicate that the reduced Co^0 mainly resulted from the collapsed cubic perovskite structure. However, there was no obvious diffraction lines for Co^0, La_2O_3 and La_2SrO_x found in samples with x=0 and 0.1, indicating that the partial reduction of the rhombohedral structure at 450 °C most likely resulted in Co^0 and related components being highly dispersed over the catalyst surface [3, 36].

The quantification of the total H_2-TPR reduction peak areas can be taken as an indication of H_2 consumption for cobalt reduction in the perovskite structure. The results in Table 4-2 show a positive relationship between the relative H_2-TPR peak area of $La_{1-x}Sr_xCoO_3$ perovskite at 800°C and the strontium substitution levels. With increasing strontium substitution, the perovskites exhibited a higher cobalt molar

content due to the relative atomic mass of strontium being lower than that of lanthanum (87.62 g/mol and 138.91 g/mol, respectively), hence an increase in H_2 consumption and relative TPR peak area.

Table 4-2. Relative total peak area of H_2-TPR reduction peaks of $La_{1-x}Sr_xCoO_3$ perovskites.

Samples	x	Relative TPR peak area/g_{cat}*	Relative Co molar concentration/g_{cat}
$LaCoO_3$	0	100	100.0
$La_{0.9}Sr_{0.1}CoO_3$	0.1	102	102.1
$La_{0.8}Sr_{0.2}CoO_3$	0.2	105	104.4
$La_{0.7}Sr_{0.3}CoO_3$	0.3	109	106.7
$La_{0.6}Sr_{0.4}CoO_3$	0.4	114	109.1

* The H_2-TPR peak areas were integrated to 800°C and calculated as: H_2-TPR peak area of $La_{1-x}Sr_xCoO_3$/TPR peak area of $LaCoO_3$×100, per gram of catalyst.

The relative H_2-TPR peak areas per mole of cobalt were thus calculated for two different temperature ranges (25°C to 450°C and 25°C to 800°C), and are presented in Figure 4-5 as a function of the strontium substitution level. It can be observed that the relative TPR peak areas per mole of cobalt increased with increasing strontium substitution levels, and that the increase is much higher at 450°C in comparison to 800°C. In addition, the results in Figure 4-4 and Figure 4-5 indicate that the $LaCoO_3$ perovskite had the lowest cobalt reduction level compared to other catalysts. This is mainly due to its stable rhombohedral structure, leading to highly dispersed metallic cobalt after reduction at 450°C, and it may not be fully reduced even at 800°C.

As mentioned previously, strontium substitution modifies the $LaCoO_3$ perovskite to produce a less stable structure and lower the reduction temperature. The XRD results in Figure 4-4 show that the Co^0 peak in the $La_{1-x}Sr_xCoO_3$ perovskite with x=0.4 was stronger and broader than in the other materials. What's more, the TPR results in Figure 4-5 further proved that this perovskite had a slower reduction process and it exhibited a lower relative peak area per mole cobalt at 450°C. It is thus reasonable to deduce that the $La_{1-x}Sr_xCoO_3$ perovskite with x=0.4 has a higher tendency to sinter. However, following reduction at 800 °C, the $La_{0.6}Sr_{0.4}CoO_3$ perovskite was believed to be fully reduced and thus showed a higher relative H_2-TPR peak area compared to other samples.

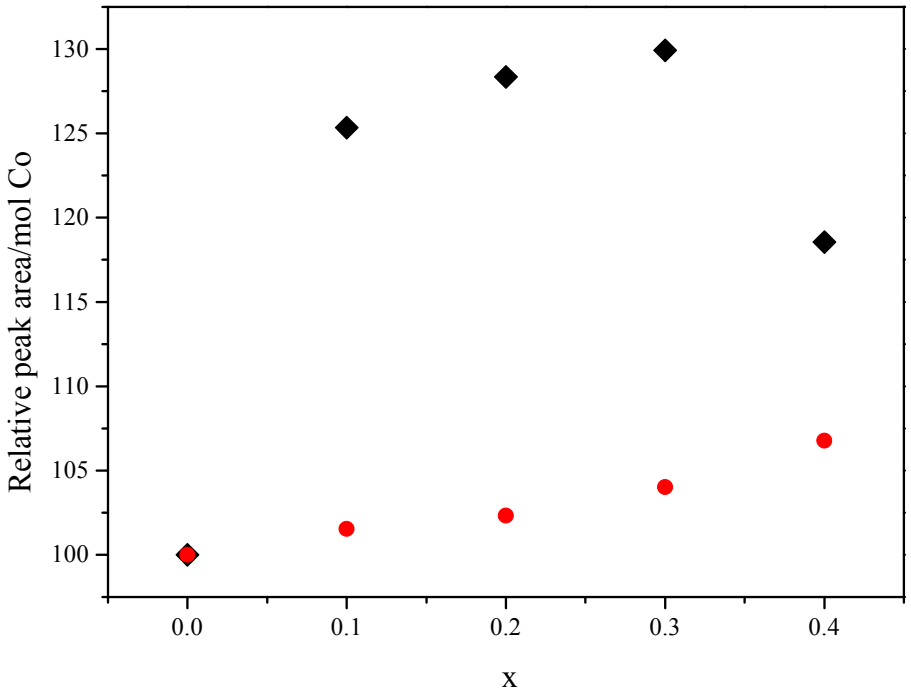

Figure 4-5. Relative peak area per mole Co of $La_{1-x}Sr_xCoO_3$ perovskites after reduction at (♦) 450 °C and (•) 800 °C. The H_2-TPR peak areas were integrated to 450 °C or 800 °C and calculated as: H_2-TPR peak area of $La_{1-x}Sr_xCoO_3$/TPR peak area of $LaCoO_3$×100, per mole of Co.

It is postulated that the partial strontium substitution facilitates the reducibility of the $La_{1-x}Sr_xCoO_3$ perovskite catalysts not only by lowering the reduction temperature but also by increasing the cobalt reduction level [39]. Thus it is expected that strontium substitution in $La_{1-x}Sr_xCoO_3$ perovskites will alter the catalytic activity in F-T synthesis.

4.3 Catalytic Activity of Sr-substituted $LaCoO_3$ Perovskite Catalysts in Syngas Conversion

The catalytic activity of the prepared $La_{1-x}Sr_xCoO_3$ perovskites (x=0 to 0.4) in F-T synthesis for HAS was investigated. The F-T reactions were carried out at steady state under the same reaction conditions for each catalyst: 300°C to 350 °C, 3.0 MPa and a gas hourly space velocity (GHSV) of 3500 h^{-1} (without considering N_2) (See Chapter 3, Sections 3.5.1.1). The experiments were carried out for 24h and the data obtained from each experiment were the average of measurements over the steady-state period (at least 10 measured values) with a carbon mass balance error less than 4%.

4.3.1 Catalyst Activity in Syngas Conversion

The catalytic activity of the prepared $La_{1-x}Sr_xCoO_3$ perovskites for F-T synthesis was investigated. The conversion of the reactants (CO or H_2) was monitored frequently during the experimental time period. A typical CO conversion as a function of the reaction time is given in Figure 4-6.

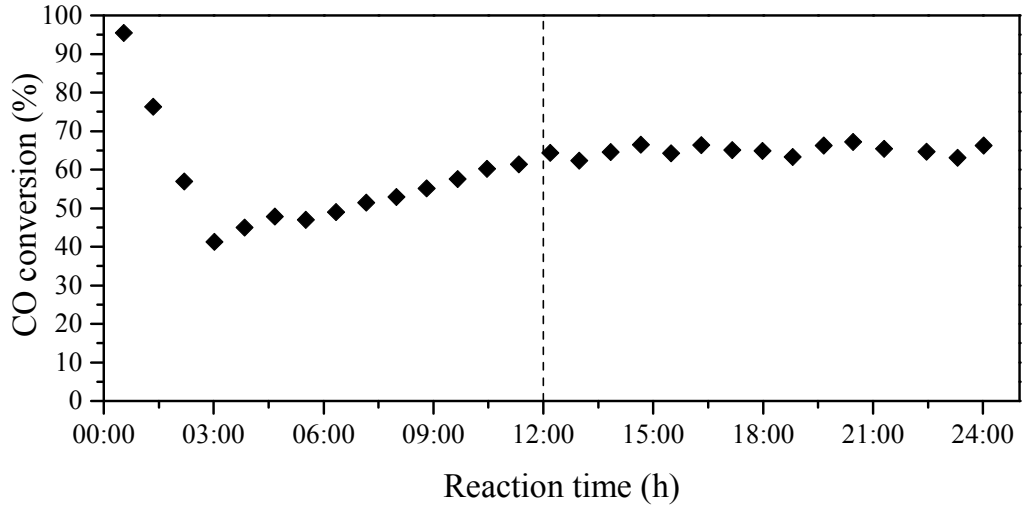

Figure 4-6. Evolution of CO conversion with reaction time for catalyst x = 0.1 at 300 °C, P=3.0 MPa, GHSV = 3500 h^{-1}, and $H_2/CO/N_2$= 2:1:3.

After a catalyst induction period of about 12 h, CO conversion was stable for the remaining of the experiment, with unnoticeable catalyst deactivation within a 24 h period reaction time. The mean conversion values during the stable period (after *ca.* 12 h) were used as reactant conversion in this work.

CO and H_2 conversion over the prepared $La_{1-x}Sr_xCoO_3$ catalysts as a function of strontium substitution and at different reaction temperatures are displayed in Figure 4-7. As expected, the results show that CO and H_2 conversion in the F-T reaction over the prepared $La_{1-x}Sr_xCoO_3$ catalysts increased with the reaction temperature. CO conversion was slightly higher than H_2 conversion at high reaction temperatures (T=325°C and 350°C), indicating that the water gas shift reaction (Equation 2-4) was more prevalent at the higher temperature, although only to a small extent overall. The catalytic results showed that the substitution by strontium had an inverse effect on the catalytic activity of $La_{1x}Sr_xCoO_3$ beyond x=0.1. CO and H_2 conversions increased only

for low strontium substitution levels ($x \leq 0.1$) and then quickly decreased with increasing x values.

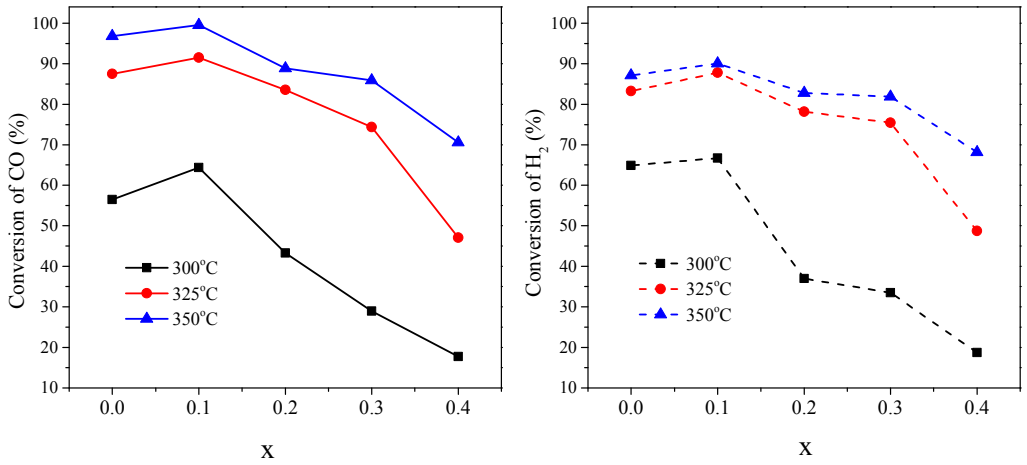

Figure 4-7. CO (left) and H_2 (right) conversion as a function of strontium substitution for $La_{1-x}Sr_xCoO_3$ catalysts at different reaction temperatures. F-T synthesis conditions: P=3.0 MPa, GHSV=3500h^{-1}, and $H_2/CO/N_2$=2:1:3.

The F-T synthesis with the $La_{1-x}Sr_xCoO_3$ perovskite catalysts produced mostly light hydrocarbons (C_1 to C_5, in the gas phase) and liquid oxygenated products (C_1 to C_9 alcohols), with a small portion of heavier hydrocarbons (C_6 to C_{14}) present in the liquid phase. In order to simplify the discussion on product selectivity, the products were grouped into four main groups: carbon dioxide, methane, light hydrocarbons (C_2-C_5) and oxygenates (which also includes C_{5+} hydrocarbons, produced in very small amounts). The product selectivity of syngas conversion over the prepared catalysts at 300 °C as a function of strontium substitution is given in Figure 4-8.

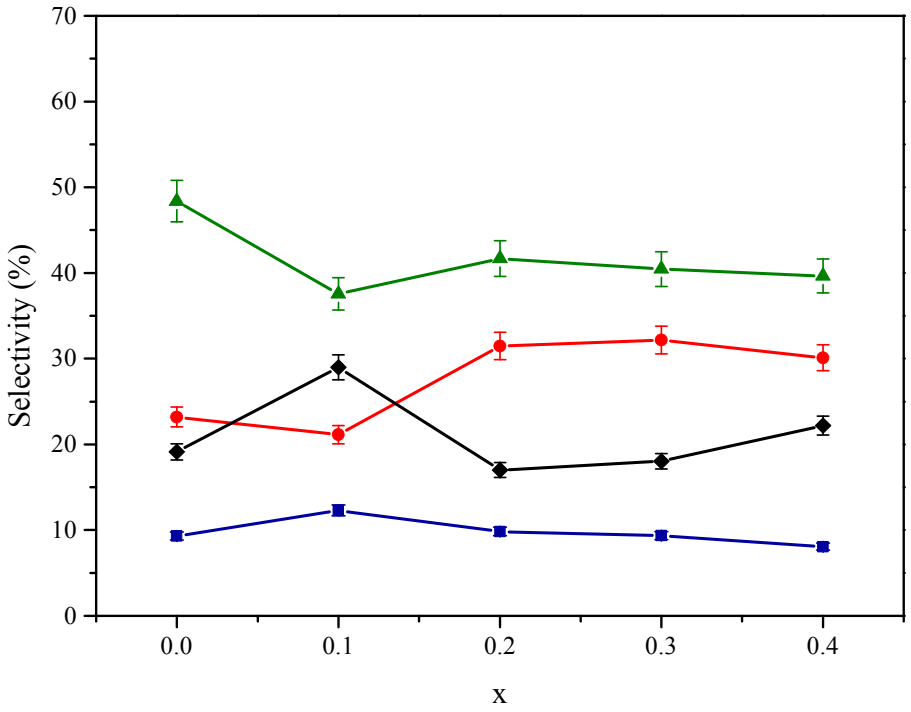

Figure 4-8. Product selectivity (■) CO_2, (▲) CH_4, (●) C_2-C_5 and (♦) C_{5+}/Oxygenates for $La_{1-x}Sr_xCoO_3$ catalysts. F-T synthesis conditions: T=300 °C, P=3.0 MPa, GHSV=3500h^{-1}, and $H_2/CO/N_2$=2:1:3.

With any amount of strontium substitution, the catalysts selectivity toward methane decrease slightly compared to the selectivity obtained for the $LaCoO_3$ catalyst, while the selectivity towards higher hydrocarbons (C_2-C_5) increased (except for the catalyst with x=0.1). Over all of the five catalysts with different strontium substitutions, except for the one with x=0.1, there were no remarkable changes in the oxygenates product selectivity (less than 5%). It can be deduced that the strontium substitution of $La_{1-x}Sr_xCoO_3$ has mild effects on the higher alcohol product selectivity at 300°C, considering the small uncertainties that may be present in the measurements.

This is in agreement with previous findings presented in the literature, that while substitution at the A site influence CO conversion, the product selectivity in F-T synthesis is mainly affected by the B site substitution in perovskite catalysts [6, 10], which will be investigated in Chapter 5.

4.3.2 Catalyst Structure after Reaction

In this study, the used catalysts after a 24 h catalytic performance test were investigated by XRD analysis and the results are given in Figure 4-9.

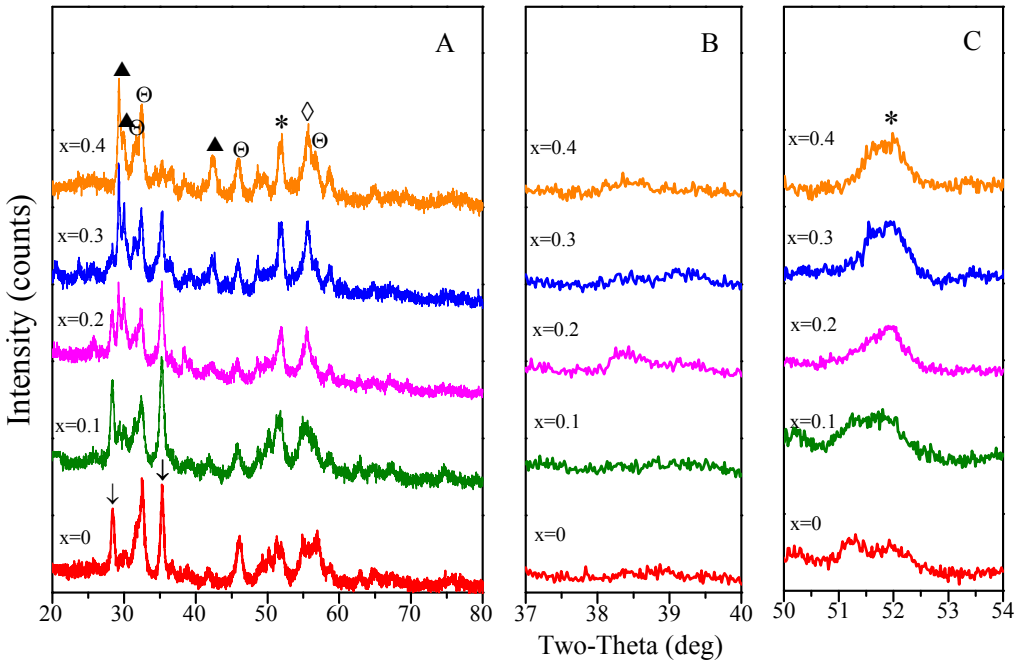

Figure 4-9. X-ray diffraction patterns of $La_{1-x}Sr_xCoO_3$ perovskites after 24 hours reaction. (A) full pattern, (B) zoom in the perovskite peak range and (C) zoom on the Co^0 peak. Phase: (↓) $LaCO_3OH$, (Θ) $La(OH)_3$, (▲) $SrCO_3$, (◊) $La_2O_2CO_3$ and (*) Co^0.

The XRD results show that the typical diffraction peak(s) associated with the perovskite structure in the range $2\theta \approx 38\text{-}39°$ could not be detected for any of the used catalysts, and new phases corresponding to $LaCO_3OH$ (JCPDS-ICDD 26-0815), LaO_2CO_3 (JCPDS-ICDD 22-0642), $La(OH)_3$ (JCPDS-ICDD 83-2034) and $SrCO_3$ (JCPDS-ICDD 74-1491) were observed. Compared to the XRD analysis of the catalysts after reduction (Figure 4-4), where no Co^0 could be detected on the catalysts with low strontium levels (x=0 and 0.1), Co^0 peaks was observed on these 2 catalysts after reaction (Figure 4-9). These catalysts were thus further reduced and their rhombohedral structure collapsed during the F-T synthesis, due to the presence of a reducing atmosphere (H_2) that promoted the formation of active Co^0 sites. In parallel, La_2O_3 and La_2SrO_x formed during the reduction (see Figure 4-4) further reacted with F-T side products H_2O or/and CO_2 to produce $LaCO_3OH$, $La(OH)_3$ and $La_2O_2CO_3$ (Equations (4-4), (4-5), and (4-6), respectively) .

$$La_2O_3 + 2\,CO_2 + H_2O \rightarrow 2\,LaCO_3OH \qquad (4\text{-}4)$$

$$La_2O_3 + 3\,H_2O \rightarrow 2\,La(OH)_3 \qquad (4\text{-}5)$$

$$La_2O_3 + 2\,CO_2 \leftrightarrow La_2O_2CO_3 \qquad (4\text{-}6)$$

$SrCO_3$ was formed by the reaction between La_2SrO_x and CO_2 produced during the F-T reaction [15]. As expected, with increasing strontium substitution, the peak intensity of Co^0 and $SrCO_3$ gradually increased, due to improved reducibility and higher strontium content, respectively. However, the peak intensity of $LaCO_3OH$ decreased significantly with increasing x, due to the decrease in lanthanum concentration in the catalysts.

Figure 4-10 shows the Scanning electron microscope (SEM) images of the fresh (left) and used (right) $La_{1-x}Sr_xCoO_3$ perovskite catalysts with different strontium substitution levels.

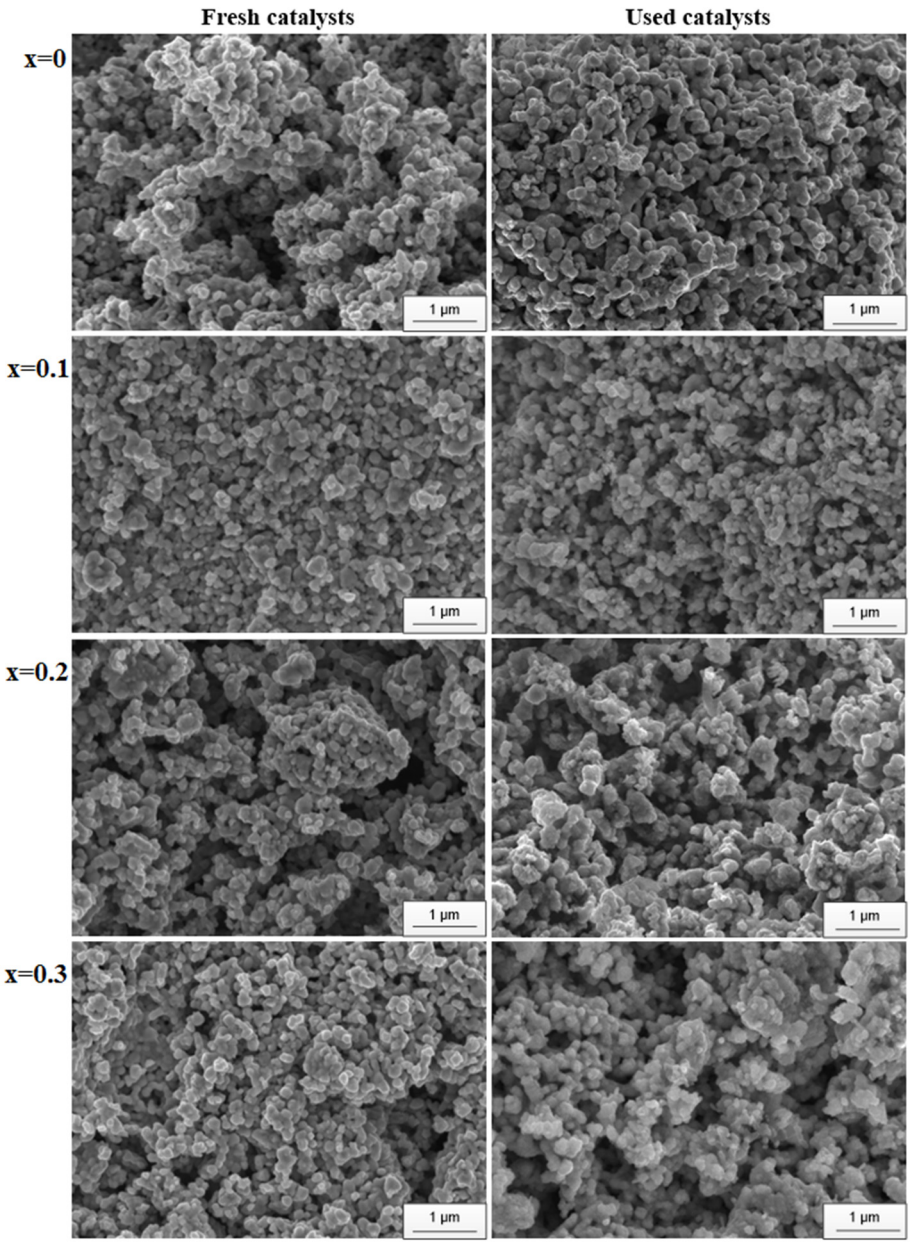

Figure 4-10. SEM images of fresh (left) and used (right) $La_{1-x}Sr_xCoO_3$ samples.

The SEM micrographs of the fresh $La_{1-x}Sr_xCoO_3$ perovskite samples (Figure 4-10 (left)) do not show large morphological differences with different strontium substitution: the dominant morphologies are polyhedral grains, with a non-homogeneous size distribution. The $LaCoO_3$ powder showed a wide range of particle size from 50 to 300 nm (measured from SEM pictures, based on the average measurement of ~100 particles), with 80% of the powder diameter between 150 and 250 nm. In contrast, the particle size distributions of the strontium substituted catalysts were much narrower (100-200 nm), with smaller average particle diameters compared to the unsubstituted one. The similar particle size distributions observed for the

substituted catalysts would thus not affect their surface areas significantly, in accordance with the BET results (Table 4-1).

One the other hand, the SEM analyses show some variations in the morphologies of the $La_{1-x}Sr_xCoO_3$ perovskite catalysts after reaction (Figure 4-10 (right)). The $La_{1-x}Sr_xCoO_3$ perovskite catalysts with $x \leq 0.1$ were less affected by sintering as they retained their crystal size after reaction (100-200 nm). However, for catalysts with $x \geq 0.2$, the main particle size was increased from 100-200 nm before reaction, to 200-300 nm after reaction.

4.3.3 Relationship between Perovskite Structure and Catalytic Activity

In order to explain the change in catalytic activity with strontium substitution, the physical and chemical characteristics of the catalysts need to be understood. In this study, as shown above, the catalysts' specific surface areas only slightly increased with different level of strontium substitution, while the particle size was narrower (Figure 4-10). It is generally expected that both CO and H_2 conversions would increase with increasing surface area. However, the perovskites surface areas were very low and the results in Figure 4-7 showed that a significant drop of catalytic activity was observed with $La_{1-x}Sr_xCoO_3$ catalysts with $x>0.1$. This thus suggest that the crystal structure might be responsible for the drop in catalytic activity, and that the catalysts' surface area and morphologies will have little or no effect on the catalyst activity.

Both TPR and XRD analysis (Figure 4-3 and Figure 4-4, respectively) demonstrated that the substitution of trivalent La^{3+} by divalent and bigger Sr^{2+} in $LaCoO_3$ perovskite sample promotes the catalyst's reducibility. The catalytic activity of the F-T catalysts is related to the effectiveness of the active centre (metallic cobalt) [3, 4]. According to Table 4-2 and Figure 4-5, more metallic cobalt was formed during reduction of the $La_{1-x}Sr_xCoO_3$ perovskite catalysts with higher strontium substitution levels. The higher the Sr^{2+} substitution, the easier for $La_{1-x}Sr_xCoO_3$ perovskites to be reduced at 450°C and the more metallic cobalt is available on the catalyst surface. This should in theory, facilitate CO adsorption to form complexes with the Co^0 active centres, and initiate the F-T reaction. Thus a higher catalytic activity could be expected for the catalysts with higher strontium substitution. However, the reverse effect was observed in this study. In order to explain the experimental results, the turnover

frequency of the active centre cobalt of the catalysts was calculated (TOF, defined as mole of CO converted per mole of cobalt atom per second). The results are given in Figure 4-11. These show that the TOF values increased with increasing strontium substitution at low levels ($x \leq 0.1$), then decreased significantly with x higher than 0.1, while the molar concentration of cobalt in the catalyst increased, due to the lower molar mass of strontium compared to lanthanum. This suggests that not all reduced cobalt acted as active centres for the F-T reaction.

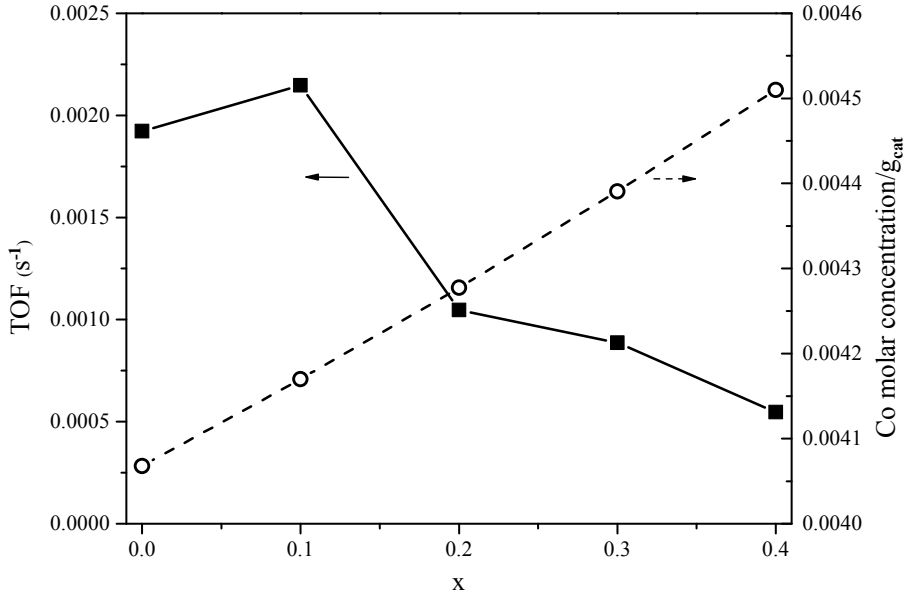

Figure 4-11. TOF of $La_{1-x}Sr_xCoO_3$ catalysts (same reaction conditions as for Figure 4-8).

The XRD results in Figure 4-4 and Figure 4-9 confirm that the stable rhombohedral structure led to a better dispersion of the active site Co^0 over the catalyst surface, and thus the higher TOF value observed for x=0 and 0.1. In addition, $SrCO_3$ was found on the surface of the catalysts after reaction, and the XRD peak intensity of this compound increased with increasing x (see Figure 4-9). It was reported that this compound is inactive in F-T synthesis and hinders CO's access to the active sites by covering the catalyst surface [15], which has a negative effect on the catalytic activity and progressively partially inhibits the F-T reaction with increasing strontium substitution.

The $La_{0.9}Sr_{0.1}CoO_3$ catalyst proved to have the optimal strontium substitution level for $La_{1-x}Sr_xCoO_3$ catalysts in the F-T process, displaying the best compromise between low active site Co^0 sintering and reducibility improvement by strontium substitution.

For these reasons, this catalyst showed the highest catalytic performance in syngas conversion compared with the other catalysts in this study. A comparison of the catalytic activity of several catalysts (including perovskite catalysts and Co-based catalyst) with different chemical compositions in the F-T synthesis, in terms of specific reaction rates is listed in Table 4-3. Taking the catalyst activity (CO reaction rate) and reaction conditions into consideration, the $La_{0.9}Sr_{0.1}CoO_3$ perovskite catalyst prepared in this study reached a moderate level of catalytic activity compared to other reported catalysts.

Table 4-3. Catalyst performance of some representative catalysts reported in the literature.

Catalyst	**Ref.**	**Temp. (°C)**	**H_2:CO[a]**	**Pressure (MPa)**	**GHSV (h^{-1})**	**CO rate [b] ($\mu mol.g_{cat}^{-1}.s^{-1}$)**
$La_{0.9}Sr_{0.1}CoO_3$	This work	300	2:1	3.0	3500	8.53
$LaCo_{0.7}Cu_{0.3}O_3$	[7]	300	2:1	6.9	5000	4.16
7.5%CuO/$LaCoO_3$	[11]	300	2:1	3.0	3900	14.02
$LaCo_{0.7}Cu_{0.3}O_3/ZrO_2$	[12]	310	2:1	3.0	3900	5.21
6%Co_3O_4/$LaFe_{0.7}Cu_{0.3}O_3$	[25]	300	2:1	3.0	3900	8.27
CuCo/SiO_2 [c]	[40]	300	2:1	5.0	6000	5.18
Fe-Cu-Co/Pal-B21[c, d]	[41]	350	2:1	5.5	6000	14.2

[a] Molar ratio

[b] CO conversion rate : calculated based on the data in the literature

[c] For comparison purpose, Co-based catalyst for F-T reaction tested under similar conditions.

[d] H_2SO_4-activated palygorskite (Pal) supported Cu–Fe–Co based catalysts

4.4 Behaviour of $La_{1-x}Sr_xCoO_3$ Perovskite Catalysts during the Induction Period in Syngas Conversion

It is very common for F-T synthesis catalysts to have an induction period prior to achieving steady state. In general, the F-T synthesis induction period varies from minutes to hundreds of hours depending on the nature of the catalysts and the reaction conditions [42-46]. However, a complete explanation of this period is currently lacking and catalyst evaluations in the literature are generally based on the data collected at steady state. The more accepted hypothesis to explain the induction period is that the catalyst undergoes a transformation before being fully active. In order to gain a deeper insight into the catalyst performance, the catalyst behaviours during both the induction period and the steady state stage of the F-T reaction should be taken into consideration. In this section, the induction periods for Sr-substituted perovskite catalysts La_{1-}

$_xSr_xCoO_3$ (x=0, 0.1 and 0.2) were obtained under the same operation conditions of T=300°C, P=3.0 MPa and GHSV=3500 h^{-1}. A mixture of gas (H_2/CO/N_2=2:1:3) was used as feed gas.

The variations in the CO and H_2 conversion as a function of time on stream (TOS) for $La_{1-x}Sr_xCoO_3$ perovskite catalysts are shown in Figure 4-12. An induction period (about 12 h) was necessary for all the Sr-substituted perovskite catalysts to achieve steady state in F-T reaction, which is much shorter than for standard supported Co/SiO_2 catalysts reported in the literature (over 24 h) [42].

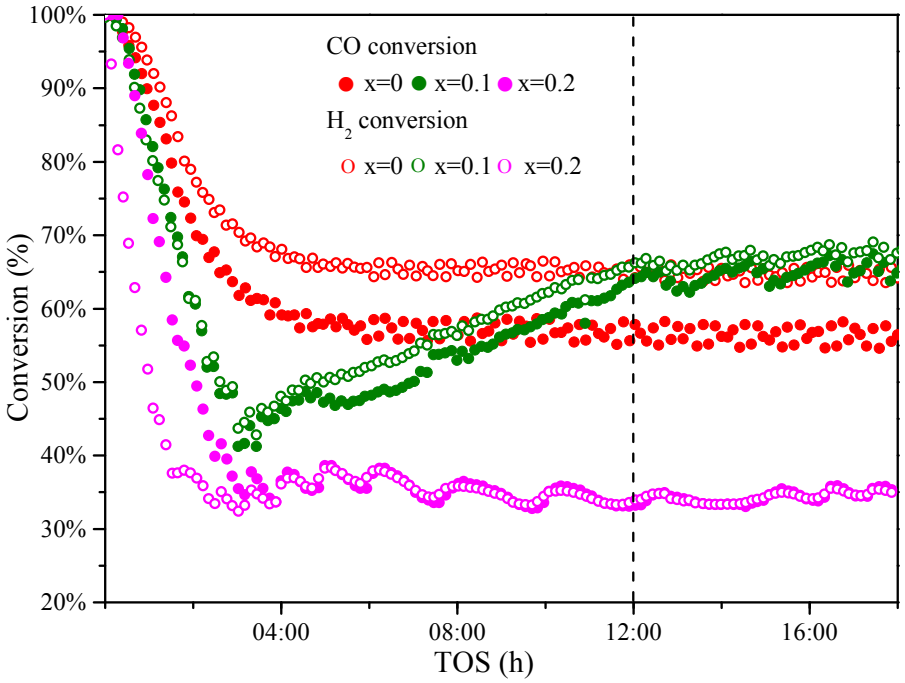

Figure 4-12. Evolution of CO and H_2 conversion with the time on stream in F-T synthesis for $La_{1-x}Sr_xCoO_3$ perovskite catalysts (x=0, 0.1 and 0.2).

The perovskite catalysts with different strontium substitution levels showed different ratio *R* between H_2 and CO conversions during the induction period (Equation (4-7)).

$$R = H_2 \text{ conversion / CO conversion} \qquad (4\text{-}7)$$

In Figure 4-13, during the first 4 hours of the reaction, the activity of $LaCoO_3$ catalyst (x=0) towards H_2 conversion was considerably higher than for CO conversion, with a conversion ratio *R* increasing from 1.01 to 1.12. When strontium was substituted in the catalysts ($La_{1-x}Sr_xCoO_3$, x=0.1 and 0.2), a different behaviour was observed

during the induction period, with first a quick decrease of *R* for the first hour, followed by an increase, to reach the equilibrium of *R*~1 after *ca*. 4 h. This trend was more drastic for x=0.2 than for x=0.1.

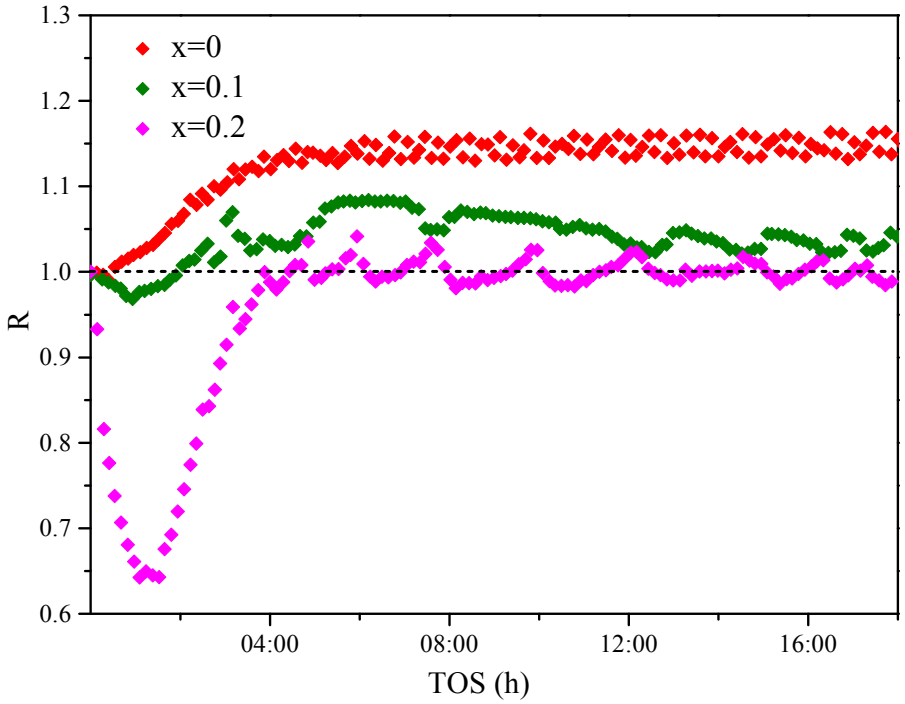

Figure 4-13. Ratio between H_2 and CO conversions (*R*) with the time on stream in F-T synthesis for $La_{1-x}Sr_xCoO_3$ perovskite catalysts.

In F-T reaction, the main reaction is the formation of hydrocarbons (and water) from CO and H_2 (see Equation (4-8) and (4-9)).

$$(2n+1)\ H_2 + n\ CO \rightarrow C_nH_{2n+2} + n\ H_2O \qquad (4\text{-}8)$$

$$2n\ H_2 + n\ CO \rightarrow C_nH_{2n} + n\ H_2O \qquad (4\text{-}9)$$

However, during the initial stage of the induction period, the CO conversion for $La_{0.8}Sr_{0.2}CoO_3$ catalyst was much higher compared to H_2 conversion. Both the water gas shift reaction (Equation (4-10)) and the Boudouard reaction (Equation (4-11)) are common side reactions in the F-T synthesis, that would yield this effect [47, 48]. Both these reactions also result in the formation of CO_2.

$$CO + H_2O \leftrightarrow CO_2 + H_2 \qquad (4\text{-}10)$$

$$CO + CO \rightarrow CO_2 + C \qquad (4\text{-}11)$$

Since no water was introduced into the system, and its formation was limited to the F-T synthesis reactions (mainly Equation 2-1 and 2-2), the Boudouard reaction was believed to be the predominant side reaction that took place at the beginning of the F-T reaction. Figure 4-14 shows that in the initial stage of the induction period (first 4 hours), the CO_2 selectivity gradually increased for all catalysts, and was higher for the catalyst with x=0.2 than that for x=0 and 0.1.

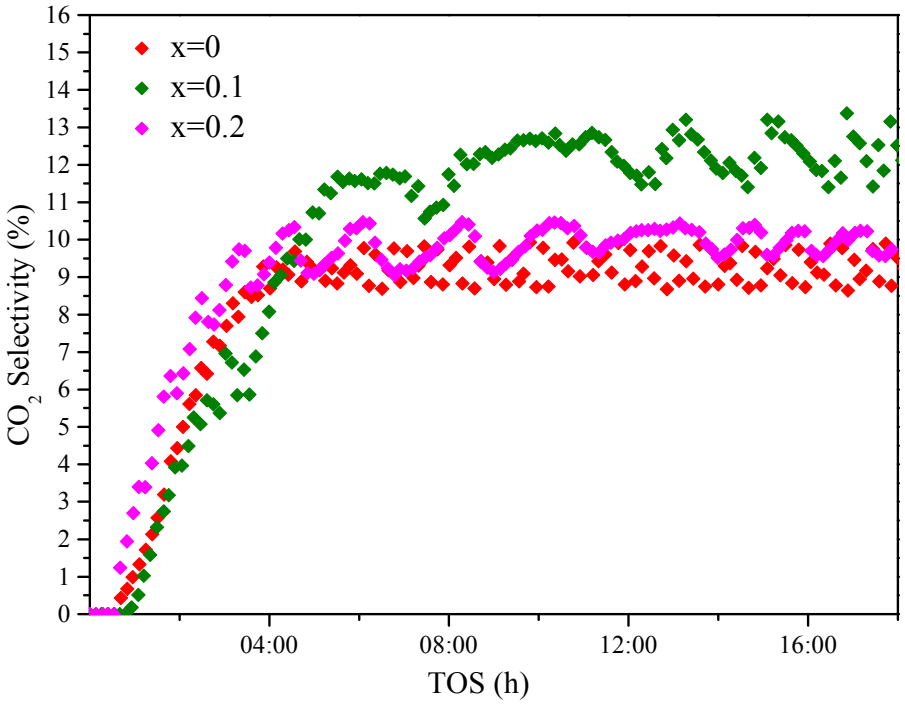

Figure 4-14. CO_2 selectivity with the time on stream in F-T synthesis for $La_{1-x}Sr_xCoO_3$ perovskite catalysts.

Table 4-4 shows the mass gain (Δm) of the used $La_{1-x}Sr_xCoO_3$ catalysts analysed by TGA. The mass gains were caused by carbon formed during the reaction, which are combusted during TGA. As all the used catalysts were treated under the same condition, it could be assumed that the amount of residual F-T products was similar for all catalysts, and that the relative difference in mass gains could be essentially attributed to the carbon formation over different catalysts. The addition of strontium was proved to have high affinity for CO_2 [49], hence $SrCO_3$ was formed easily during the reaction and its peak intensity increased with strontium substitution (see Figure

4-9). Both these results indicate that the strontium substitution might favour the Boudouard reaction and its extent increased with strontium substitution.

Table 4-4. Mass gain of used $La_{1-x}Sr_xCoO_3$ catalysts after reaction.

Catalyst	x	Δm (mg_{carbon}/g_{cat})
$LaCoO_3$	0	126.4
$La_{0.9}Sr_{0.1}CoO_3$	0.1	192.2
$La_{0.8}Sr_{0.2}CoO_3$	0.2	217.9

It is reasonable to deduce that the carbon formation caused by the Boudouard reaction mainly took place in the first 4 hours of the F-T reaction because of the dramatic increase of CO_2 selectivity. After that, the WGS reaction become more prominent than the Boudouard reaction with time on stream because of the presence of water, produced in F-T reactions. Indeed, for the $La_{1-x}Sr_xCoO_3$ catalyst with x=0.1, the higher CO conversion (Figure 4-12) and CO_2 selectivity (Figure 4-14) observed after *ca.* 4 h TOS together with the higher *R* ratio, compared to the catalyst with x=0.2, indicate a higher extent of the WGS reaction. In Figure 4-12, the catalyst with x=0.2 shows the lowest CO conversion in the steady state, which indicates that in addition to catalyst structure, carbon formation during the induction period also leads to the decrease of catalytic activity. The unsubstituted $LaCoO_3$ catalyst exhibited the highest *R* ratio and the lowest amount of carbon and CO_2 were formed. As both the WGS and Boudouard reactions were less prominent, this catalyst might favoured the methanation reaction, as confirmed by the highest selectivity towards methane observed in Figure 4-8.

4.5 Conclusion

Sr-substituted $La_{1-x}Sr_xCoO_3$ perovskite catalysts, active in the F-T synthesis, were successfully synthesised by co-precipitation. Increasing the partial substitution of lanthanum by strontium beyond x = 0.1 modified the stable rhombohedral structure of $La_{1-x}Sr_xCoO_3$ perovskites towards a less stable cubic symmetry, which was easier to reduce but favoured cobalt sintering during the reduction process. At high strontium substitution levels ($x \geq 0.2$), the inactive $SrCO_3$ compound, which is suspected to cover the catalyst surface, was also formed, further affecting the activity of $La_{1-x}Sr_xCoO_3$ perovskite catalysts. As a consequence the catalytic activity of $La_{1-x}Sr_xCoO_3$ perovskites decreased in the F-T reaction for $x \geq 0.2$. At low strontium substitution

level (x = 0.1) the catalytic activity in F-T reaction was improved compared to $LaCoO_3$ perovskite due to the improvement in reducibility, without the negative effect on Co^0 active site dispersion and sintering. In addition, $La_{1-x}Sr_xCoO_3$ perovskite catalysts exhibited a shorter induction period compared to other types of Co-based catalysts for syngas conversion. However, strontium substitution favoured the Boudouard reaction in the initial reaction stage and the amount of carbon formed on the catalyst increased with increasing strontium substitution. The optimal strontium substitution for $La_{1-x}Sr_xCoO_3$ perovskite catalysts for syngas conversion was thus evaluated at x = 0.1, for which the catalyst exhibited a good compromise between reducibility, sintering and activity.

This work represents the first step in designing perovskite catalysts tailored for the selective production of higher alcohol in the Fischer-Tropsch process. In the next chapter, the catalyst selectivity will be further investigated with B site substitution effects on $La_{0.9}Sr_{0.1}CoO_3$ perovskites in F-T synthesis, and its effect on higher alcohol selectivity.

4.6 References

[1] M.E. Dry, Catalysis Today, 71 (2002) 227-241.

[2] J. A. Brown Bourzutschky, N.Homs, AT.Bell, Journal of Catalysis, 124 (1990) 52-72.

[3] L. Bedel, A.C. Roger, C. Estournes, A. Kiennemann, Catalysis Today, 85 (2003) 207-218.

[4] L. Bedel, A. Roger, J. Rehspringer, Y. Zimmermann, A. Kiennemann, Journal of Catalysis, 235 (2005) 279-294.

[5] N. Escalona, S. Fuentealba, G. Pecchi, Applied Catalysis A: General, 381 (2010) 253-260.

[6] N. Tien-Thao, H. Alamdari, S. Kaliaguine, Journal of Solid State Chemistry, 181 (2008) 2006-2019.

[7] N. Tien-Thao, M.H. Zahedi-Niaki, H. Alamdari, S. Kaliaguine, Applied Catalysis A: General, 326 (2007) 152-163.

[8] N. Tien-Thao, M. Hassanzahediniaki, H. Alamdari, S. Kaliaguine, Journal of Catalysis, 245 (2007) 348-357.

[9] T. Nguyen, M. Zahedi-Niaki, H. Alamdari, S. Kaliaguine, International Journal of Chemical Reactor Engineering, 5 (2007) art. A82.

[10] N. Tien-Thao, H. Alamdari, M.H. Zahedi-Niaki, S. Kaliaguine, Applied Catalysis A: General, 311 (2006) 204-212.

[11] Y. Fang, Y. Liu, W. Deng, J. Liu, Journal of Energy Chemistry, 23 (2014) 527-534.

[12] G. Liu, Y. Geng, D. Pan, Y. Zhang, T. Niu, Y. Liu, Fuel Processing Technology, 128 (2014) 289-296.

[13] N. Sun, H. Liu, Z. Yu, Z. Zheng, C. Shao, Solid State Ionics, 268 (2014) 125-130.

[14] A.J. Zhou, T.J. Zhu, X.B. Zhao, Materials Science and Engineering: B, 128 (2006) 174-178.

[15] M. Morales, M. Segarra, Applied Catalysis A: General, 502 (2015) 305-311.

[16] K.S. Chan, J. Ma, S. Jaenicke, G.K. Chuah, Applied Catalysis A: General, 107 (1994) 201-227.

[17] H.M. Reichenbach, P.J. McGinn, Applied Catalysis A: General, 244 (2003) 101-114.

[18] Z. Gao, R. Wang, Applied Catalysis B: Environmental, 98 (2010) 147-153.

[19] S. Irusta, M.P. Pina, M. Men´endez, J. Santamar´ıa, Journal of Catalysis, 179 (1998) 400-412.

[20] J. Hueso, J. Cotrino, A. Caballero, J. Espinos, A. Gonzalezelipe, Journal of Catalysis, 247 (2007) 288-297.

[21] D.H. Prasad, S.Y. Park, E.-O. Oh, H. Ji, H.-R. Kim, K.-J. Yoon, J.-W. Son, J.-H. Lee, Applied Catalysis A: General (2012) 100-106.

[22] J. Hueso, A. Caballero, M. Ocana, A. Gonzalezelipe, Journal of Catalysis, 257 (2008) 334-344.

[23] S. Biamino, C. Badini, Journal of the European Ceramic Society, 24 (2004) 3021-3034.

[24] K. Rida, M.A. Peña, E. Sastre, A. Martinez-Arias, Journal of Rare Earths, 30 (2012) 210-216.

[25] Y. Fang, Y. Liu, L. Zhang, Applied Catalysis A: General, 397 (2011) 183-191.

[26] M.-J. Lee, J.-H. Jun, J.-S. Jung, Y.-R. Kim, S.-H. Lee, Bulletin of the Korean Society, 26 (2005) 1591-1596.

[27] G. Pecchi, C.M. Campos, M.G. Jiliberto, E.J. Delgado, J.L.G. Fierro, Applied Catalysis A: General, 371 (2009) 78-84.

[28] N.M.L.N.P. Closset, R.H.E.v. Doorn, H. Kruidhof, J. Boeijsma, Powder Diffraction, 11 (1995) 31-34.

[29] J.L. Hueso, J.P. Holgado, R. Pereñíguez, S. Mun, M. Salmeron, A. Caballero, Journal of Solid State Chemistry, 183 (2010) 27-32.

[30] J.A. Villoria, M.C. Alvarez-Galvan, S.M. Al-Zahrani, P. Palmisano, S. Specchia, V. Specchia, J.L.G. Fierro, R.M. Navarro, Applied Catalysis B: Environmental, 105 (2011) 276-288.

[31] R.D. Shannon, Acta Crystallographica Section A: Crystal Physics, (1976) 751-767.

[32] M. Schmal, C.A.C. Perez, R.N.S.H. Magalhães, Topics in Catalysis, 57 (2014) 1103-1111.

[33] L. Huang, M. Bassir, S. Kaliaguine, Applied Surface Science, 243 (2005) 360-375.

[34] B. Levasseur, S. Kaliaguine, Applied Catalysis A: General, 343 (2008) 29-38.

[35] S. Royer, F. Bérubé, S. Kaliaguine, Applied Catalysis A: General, 282 (2005) 273-284.

[36] F. Ma, W. Chu, L. Huang, X. Yu, Y. Wu, Chinese Journal of Catalysis, 32 (2011) 970-977.

[37] C.A. Chagas, F.S. Toniolo, R.N.S.H. Magalhães, M. Schmal, International Journal of Hydrogen Energy, 37 (2012) 5022-5031.

[38] R. Pereñíguez, J.L. Hueso, F. Gaillard, J.P. Holgado, A. Caballero, Catalysis Letters, 142 (2012) 408-416.

[39] T. Nakamura, M. misono, Y. Yoneda, Journal of Catalysis, 83 (1983) 151-159.

[40] S. Deng, W. Chu, H. Xu, L. Shi, L. Huang, Journal of Natural Gas Chemistry, 17 (2008) 369-373.

[41] H. Guo, H. Zhang, F. Peng, H. Yang, L. Xiong, C. Huang, C. Wang, X. Chen, L. Ma, Applied Clay Science, 111 (2015) 83-89.

[42] S. Bai, C. Huang, J. Lv, Z. Li, Catalysis Communications, 22 (2012) 24-27.

[43] H. Ono, K. Fujiwara, M. Hashimoto, H. watanabe, K. Yoshida, Journal of Molecular Catalysis, 58 (1990) 289-297.

[44] S.-H. Chai, V. Schwartz, J.Y. Howe, X. Wang, M. Kidder, S.H. Overbury, S. Dai, D.-e. Jiang, Microporous and Mesoporous Materials, 170 (2013) 141-149.

[45] N. Wang, K. Fang, D. Jiang, D. Li, Y. Sun, Catalysis Today, 158 (2010) 241-245.

[46] H. Xiao, D. Li, W. Li, Y. Sun, Fuel Processing Technology, 91 (2010) 383-387.

[47] D. Dasgupta, T. Wiltowski, Fuel, 90 (2008) 174-181.

[48] H. Jahangiri, J. Bennett, P. Mahjoubi, K. Wilson, S. Gu, Catalysis Science & Technology, 4 (2014) 2210-2229.

[49] G. Valderrama, A. Kiennemann, M.R. Goldwasser, Journal of Power Sources, 195 (2010) 1765-1771.

Chapter 5 Nickel-substituted $La_{0.9}Sr_{0.1}CoO_3$ Perovskite Catalysts for Higher Alcohol Production in Fischer-Tropsch Synthesis

5.1 Introduction

In Chapter 4, it was demonstrated that low level substitution of strontium at the A site of the $LaCoO_3$ perovskite catalysts increased the syngas conversion due to improvements in reducibility and dispersion of the Co^0 active centres on the catalyst surface, but no effect on higher alcohol ($C_{2+}OH$) selectivity was noticed [1]. However, a highly selective catalyst towards $C_{2+}OH$ alcohols is essential for the success of the higher alcohol synthesis (HAS) process.

Partial substitution at the B site of the perovskites was found to be an effective method for improving the product selectivity in F-T synthesis (see Chapter 2, Section 2.8). Tien-Thao *et al*. reported on a series of copper-substituted $LaCo_{1-x}Cu_xO_3$ perovskite catalysts in HAS from syngas [2-5]. These perovskite catalysts showed higher $C_{2+}OH$ selectivity compared to the unsubstituted $LaCoO_3$ perovskite catalyst (up to 27.3 wt.% for x=0.3, *vs*. 13.6 wt.%) [2]. Liu and co-workers found that for a Co-Cu-doped $LaFeO_3$ perovskite, the alcohol selectivity during CO hydrogenation decreased with the Co/Cu molar ratio, and the highest $C_{2+}OH$ selectivity (33%) was achieved for the 2% $Co_3O_4/LaFe_{0.7}Cu_{0.3}O_3$ perovskite catalyst with a low ratio (Co/Cu molar ratio=0.19) [6]. It has been reported that the synergism between cobalt and copper favoured the formation of higher alcohols, which can be explained in mechanistic terms. According to the mechanisms mentioned in Chapter 2 (Section 2.3.1), the formation of alcohols in the F-T synthesis includes CO dissociation, CO insertion, carbon chain growth, and hydrogenation. The F-T element cobalt is active for CO dissociation and chain propagation, while copper promotes the insertion of adsorbed CO into the carbon chain and subsequent alcohol formation [7-9].

The transition metal nickel is well known as an active catalyst for methane formation from syngas [7, 10]. However, if nickel is used as a promoter in other metal-based catalysts, then the catalyst becomes more active towards higher alcohol

synthesis. Li *et al.* found that nickel is an effective promoter for K_2CO_3/MoS_2 catalyst and enhances higher alcohol production [11-13]. Recent research on Ni-containing catalysts such as Cu-Mn-Ni, K-Ni-MoS_2, and Ni-Cu/CeO_2 suggested that nickel had the potential to promote higher alcohol synthesis due to its strong ability for CO insertion [10, 14, 15]. Since then nickel has been considered as a promising candidate for HAS from syngas.

The synergism of the bifunctional active centres, with one metal active site preferentially catalysing CO dissociation and carbon chain growth and the other promoting CO insertion, benefits the higher alcohol formation (see review [16]). It is thus reasonable to deduce that a perovskite catalyst with a Co-Ni bimetallic combination would be a good candidate for HAS because cobalt promotes chain propagation and nickel has a strong ability for CO insertion, thus promoting CO conversion and higher alcohol selectivity. Indeed, the perovskite structure is very tolerant to the partial substitution of B site elements (see Chapter 2, Section 2.8.3). Besides, the unique structure of perovskite leads to high metallic dispersion once the catalysts are reduced, as demonstrated in Chapter 4 [2, 17]. This represents an advantage compared to the impregnation method commonly used to prepare Co-Ni bi-metal catalysts [18], with its well-known difficulty in controlling the active components distribution, which led to inhomogeneous active materials over the catalysts [19]. In addition, it has previously been established in the literature that during the reduction process of bimetallic Co-Ni perovskite catalysts, a Co-Ni alloy was formed [20-22]. Both XRD and TPR analysis proved that metal-metal interactions took place due to the close vicinity and electronic interaction between Co^{3+} and Ni^{3+} sites.

To the best of our knowledge, there is no investigation of HAS over Co-Ni bimetal catalysts to date. The aim of this chapter is to further improve the activity of the $La_{0.9}Sr_{0.1}CoO_3$ perovskite catalysts developed in Chapter 4, using nickel substitution at the B site ($La_{0.9}Sr_{0.1}Co_{1-y}Ni_yO_3$) to improve their selectivity toward higher alcohols in HAS.

5.2 Effect of Nickel Substitution on Structure and Reduction Properties of $La_{0.9}Sr_{0.1}CoO_3$

5.2.1 Structure of $La_{0.9}Sr_{0.1}Co_{1-y}Ni_yO_3$ Perovskites

$La_{0.9}Sr_{0.1}Co_{1-y}Ni_yO_3$ perovskite samples (y=0, 0.1, 0.5, and 1) were prepared according to the co-precipitation method described in Chapter 3, Section 3.3.2, and analysed by Brunauer-Emmett-Teller (BET) method and X-ray diffraction (XRD) (Chapter 3, Section 3.4).

The specific surface area of the prepared $La_{0.9}Sr_{0.1}Co_{1-y}Ni_yO_3$ perovskite catalysts are summarised in Table 5-1. The catalyst surface areas were between 4 and 7 m^2/g, lower than that reported by Valderrama *et al.* for La-Sr-Co-Ni-O based perovskite catalysts (6-15 m^2/g), which were calcined at 750°C [17].

Table 5-1. Specific surface areas of $La_{0.9}Sr_{0.1}Co_{1-y}Ni_yO_3$ perovskite catalysts.

Sample	y	Surface area (m^2/g)
$La_{0.9}Sr_{0.1}CoO_3$	0	4.7
$La_{0.9}Sr_{0.1}Co_{0.9}Ni_{0.1}O_3$	0.1	4.1
$La_{0.9}Sr_{0.1}Co_{0.5}Ni_{0.5}O_3$	0.5	4.7
$La_{0.9}Sr_{0.1}NiO_3$	1	6.3

The relatively low surface areas of the perovskite catalysts are related to the preparation method since the catalysts were calcined at a high temperature (800°C), which might induce the sintering of the solids (see Chapter 4, Section 4.2.1). Because the surface area changed by very small increments with nickel substitution, it is expected that the catalytic activity was not affected by the specific surface area (as explained in Chapter 4, Section 4.3.3).

Figure 5-1 presents the powder XRD patterns of the as-prepared $La_{0.9}Sr_{0.1}Co_{1-y}Ni_yO_3$ perovskite catalysts (before reduction).

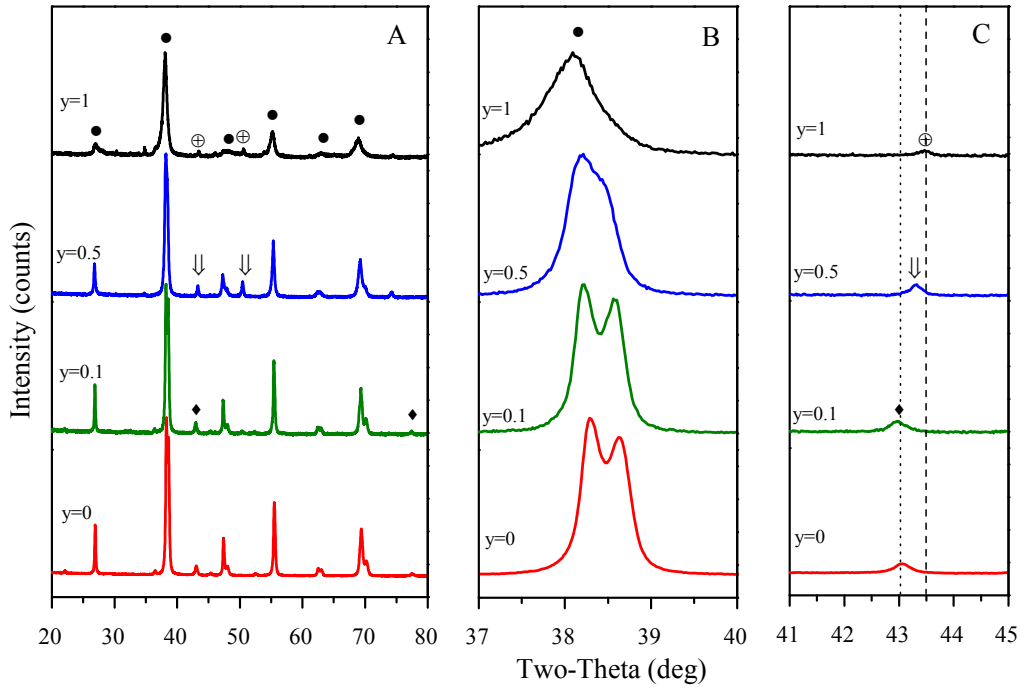

Figure 5-1. XRD patterns of as-prepared $La_{0.9}Sr_{0.1}Co_{1-y}Ni_yO_3$ perovskite catalysts. (A) full pattern, (B) zoom in the perovskite peak range, and (C) zoom in the Co-Ni oxide peak range. Phases: (•) Perovskite (including $La_{0.9}Sr_{0.1}CoO_3$ and $La_{0.9}Sr_{0.1}NiO_3$), (♦) Co_3O_4, (⊕) NiO, and (⇓) Co-Ni oxide.

These results show that all $La_{0.9}Sr_{0.1}Co_{1-y}Ni_yO_3$ catalysts exhibited the perovskite structure for the different substitution levels of nickel (y), as shown by the presence of the typical perovskite diffraction peaks between 38° and 40° [23, 24]. In addition, $La_{0.9}Sr_{0.1}Co_{1-y}Ni_yO_3$ perovskite diffraction peak at 38-39° in Figure 5-1 (B) gradually shifted to lower 2θ with increasing nickel substitution, which indicates that nickel ions have entered into the perovskite structure since the ionic radius of Ni^{3+} (0.56 Å) is higher than that of Co^{3+} (0.52 Å). In Figure 5-1 (C), small fractions of Co_3O_4 (JCPDS-ICDD 80-1541) were found in the catalyst without nickel (y=0), while NiO (JCPDS-ICDD 47-1049) was present in the catalyst without cobalt (y=1). These secondary phases were also observed by other authors [24]. For the low Ni-substituted catalyst (y=0.1), only the Co_3O_4 phase was observed with low peak intensity and the NiO phase was barely visible, indicating that all the nickel elements had entered into the perovskite structure. On the other hand, the Co-Ni oxide phase (JCPDS-ICDD 03-0995) was detected at 43.3° for the Ni-substituted perovskite catalysts with y=0.5. This peak was present between the diffraction lines of Co_3O_4 and NiO, indicating that nickel oxide and cobalt oxide were also potentially present in this catalyst. Due to the close position of the diffraction peaks and the similarities in structure between Co_3O_4, NiO,

and Ni-Co oxide, distinguishing between these three phases is very difficult [25]. The secondary phases Co-Ni oxide and possibly NiO present in the catalyst with y=0.5 suggests that only a limited amount of nickel atoms could enter the $La_{0.9}Sr_{0.1}CoO_3$ perovskite structure.

5.2.2 Reduction Properties of $La_{0.9}Sr_{0.1}Co_{1-y}Ni_yO_3$ Perovskites

The reduction properties of the Ni-substituted $La_{0.9}Sr_{0.1}CoO_3$ perovskites were investigated by H_2-temperature programmed reduction (TPR), as displayed in Figure 5-2. All the TPR peaks can be ascribed to the reduction of Co^{3+} and Ni^{3+}, since La^{3+} and Sr^{2+} are not reduced under such experimental conditions [17, 23].

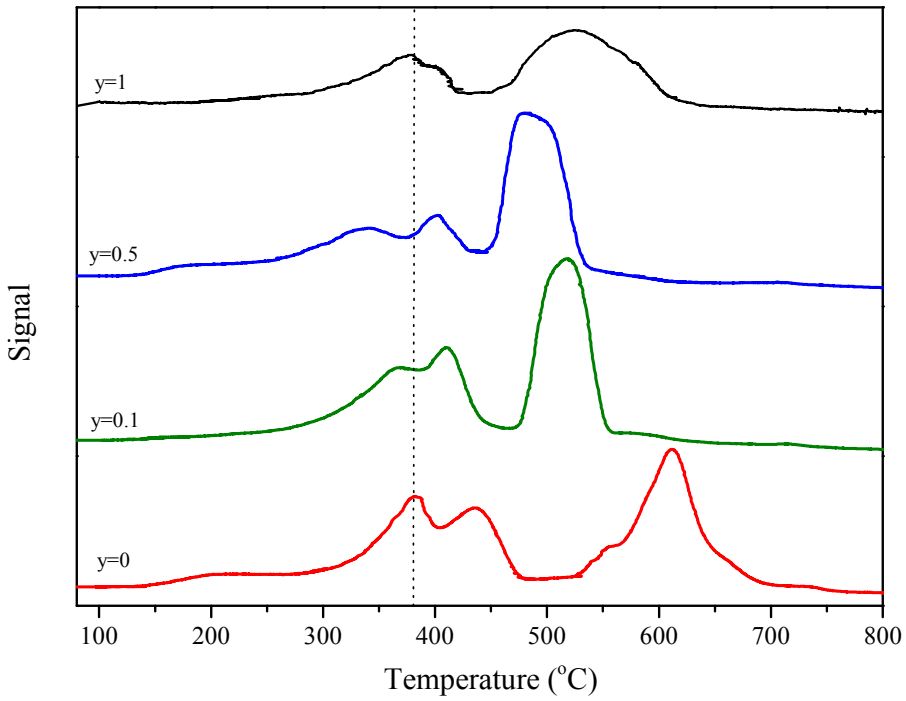

Figure 5-2. TPR profiles of $La_{0.9}Sr_{0.1}Co_{1-y}Ni_yO_3$ perovskite catalysts[1].

As detailed in Chapter 4, Section 4.2.2, the reduction process of $La_{0.9}Sr_{0.1}CoO_3$ perovskite took place in two steps: Co^{3+} was first reduced mostly to Co^{2+} at low temperatures, between ~350-500°C, while the reduction peaks at higher temperatures (500-700°C) corresponded to the formation of Co^0. Few Co^{3+} species were directly

[1] The TPR trace for $La_{0.9}Sr_{0.1}Co_{0.9}Ni_{0.1}O_3$ perovskite in Figure 5-2 appears different from that presented in Figure 4-3 due to a different amount of catalyst used (0.1 g *vs*. 0.3 g). High amount of catalyst consumed more hydrogen and led to the overlap of reduction peaks.

reduced to Co^0, hence the presence of two peaks in the lower temperatures reduction step (350-500°C) [26]. $La_{0.9}Sr_{0.1}NiO_3$ perovskite also presented a two-steps reduction process: the first one, at about 370°C, corresponding to the reduction of Ni^{3+} to Ni^{2+}, and the second step at 520°C leading to Ni^0 formation [23]. The reduction steps can be described as follows:

$$2\ LaNiO_3 + H_2 \rightarrow La_2Ni_2O_5 + H_2O \qquad (5\text{-}1)$$

$$La_2Ni_2O_5 + 2\ H_2 \rightarrow La_2O_3 + 2\ Ni^0 + 2\ H_2O \qquad (5\text{-}2)$$

For Ni-substituted perovskite catalysts (y=0.1 and 0.5), the first two reduction peaks at low temperatures were overlapped (300-450°C) and were attributed to the reduction of Ni^{3+} to Ni^{2+}, Co^{3+} to Co^{2+} and, to a lesser extent, to Co^0. The peak at higher temperatures (450-550°C) was ascribed to the complete reduction of the B site elements (cobalt and nickel). With nickel substitution, the third reduction peak was shifted to lower temperatures. This behaviour indicates that the Co^{2+} and Ni^{2+} species were reduced at lower temperatures when both metals were present, that is, the substitution of nickel in $La_{0.9}Sr_{0.1}CoO_3$ perovskites favoured the reduction of cobalt species. Furthermore, a new broad reduction peak at ~200 °C was also observed for the catalyst with y=0.5, which originated from the reduction of the extra-framework Ni-containing oxide. This observation is consisted with the work of Kotsev *et al.*, who reported the reduction behaviours of a series of NiO samples with different calcination temperatures [27].

To investigate the phase changes of the prepared perovskite catalysts after reduction, the samples were reduced at 450°C in 5% H_2/N_2 for 1 hour before XRD analysis. The XRD patterns are shown in Figure 5-3.

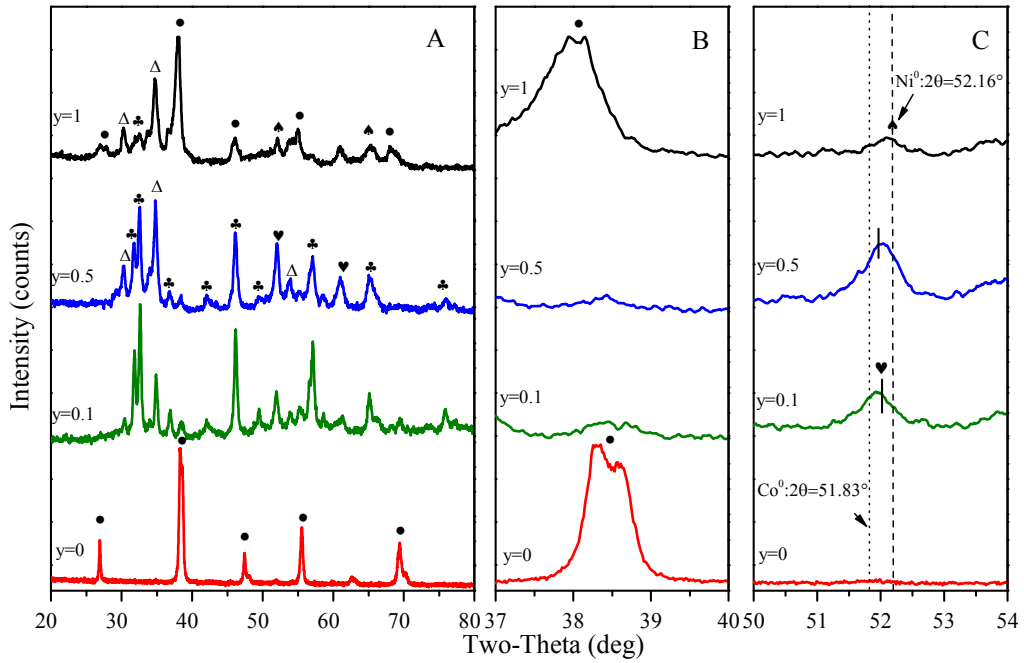

Figure 5-3. XRD patterns of $La_{0.9}Sr_{0.1}Co_{1-y}Ni_yO_3$ perovskite catalysts after reduction at 450 °C. (A) full pattern, (B) zoom in the perovskite peak range and (C) zoom in the metallic peak range. Phases: (●) Perovskite, (Δ) La_2O_3, (♣) La_2SrO_x, (♠) Ni^0 and (♥) Co-Ni alloy.

On reduction at 450 °C, the perovskite structure of the catalysts with only one metal in the B site (y=0 and y=1) was preserved, with the main diffraction peaks at $2\theta \approx 38\text{-}39°$ still present on the spectra, although broader, suggesting a partial collapse of the crystalline structure (see Figure 5-3 (B)). However, the perovskite structure of Ni-substituted catalysts (y=0.1 and 0.5) collapsed after reduction, as the $2\theta \approx 38\text{-}39°$ peaks disappeared for these catalysts. In parallel, new phases such as La_2SrO_x (JCPDS-ICDD 42-0343) and La_2O_3 (JCPDS-ICDD 74-2430) were observed. After reduction at 450°C, the Co^0 diffraction peak (2θ=51.83°) was barely visible for the perovskite catalyst with y=0, due to the high stability of $La_{0.9}Sr_{0.1}CoO_3$ catalyst and the good dispersion of the Co^0 species [1] (See Chapter 4, Section 4.2.2). For catalysts with y=0.1 and 0.5, the small diffraction peak located between 51.38° and 52.16° showed that the Co-Ni alloy was formed during the reduction. This is in agreement with the results of Gallego *et al.* who reported that the partial reduction of $LaNi_{0.9}Co_{0.1}O_3$ perovskite catalyst produced a Co-Ni alloy [20]. The weaker diffraction peak of the Co-Ni alloy for the catalyst with y=0.1 suggests that less bimetallic alloy formed on the catalyst surface, as expected, but with a high dispersion, which was also observed by Wang *et al.* [21]. In particular, the diffraction peak of the Co-Ni alloy slightly

shifted toward the peak of metallic nickel with the increase in nickel substitution as shown in Figure 5-3 (C), suggesting that certain amount of metallic nickel was also formed after reduction. Taking the presence of small amount of Ni-containing oxides in the unreduced catalyst (for y=0.5 and 1) (Figure 5-1 (C)) into account, it is reasonable to assume that such phase was reduced to form Ni^0 at lower temperatures, as suggested by Silva *et.al* [24] and Pereñíguez *et.al* [28]. Furthermore, the Ni^0 diffraction peaks could be clearly observed in the catalyst with y=1. These observations are in agreement with the TPR analysis, suggesting that the partial substitution of cobalt by nickel in the $La_{0.9}Sr_{0.1}CoO_3$ perovskite structure lowered the reduction temperature of the catalysts, and increasing nickel substitution level above 0.5 led to a separation of the extra-framework Ni-containing oxide. Similar behaviours were observed by Tien-Thao *et al*., who reported that the substitution of cobalt by copper in $LaCo_{1-x}Cu_xO_3$ perovskites increased the catalyst reducibility and extra-lattice copper oxide existed with copper substitution higher than 0.5 [2].

In order to compare the reduction ability of the catalysts, the total H_2-TPR peak areas were measured and are presented in Figure 5-4. In theory, the more hydrogen is consumed in TPR, the more metal oxides are reduced and more active centres for the F-T reaction are formed. The results in Figure 5-4 demonstrate that the nickel-substituted $La_{0.9}Sr_{0.1}Co_{1-y}Ni_yO_3$ (y not equal to 1) catalysts consumed a similar amount of hydrogen compared to $La_{0.9}Sr_{0.1}CoO_3$, which suggests that nickel-substituted $La_{0.9}Sr_{0.1}Co_{1-y}Ni_yO_3$ catalysts had a similar number of active centres after reduction. In contrast, $La_{0.9}Sr_{0.1}NiO_3$ catalyst consumed about a third less of hydrogen, which may be attributed to the significant sintering of metallic nickel perovskite catalysts [29]. This agrees with the XRD analysis (Figure 5-3), where the metallic nickel diffraction lines for the catalyst with y=1 were much stronger compared to that of cobalt for the catalyst with y=0. In addition, secondary phases such as Co_3O_4 and NiO were also reduced during the TPR process. Less hydrogen would be consumed to reduce NiO (for y=1) than to reduce Co_3O_4 from Co-containing perovskites, which also contributed to the lower hydrogen consumption of $La_{0.9}Sr_{0.1}NiO_3$.

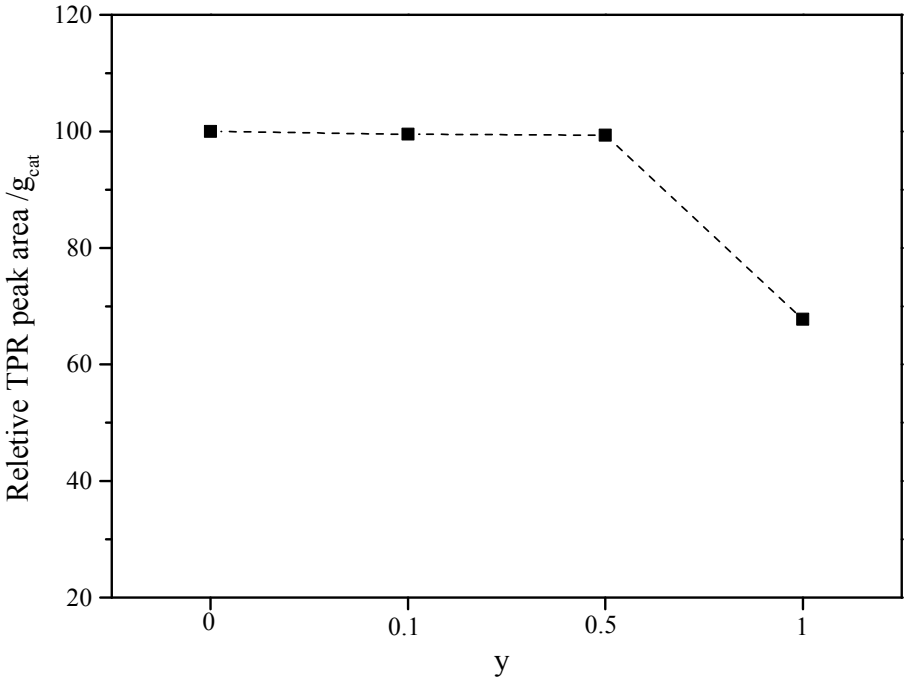

Figure 5-4. Relative total TPR peak area/g_{cat} (TPR peak area of $La_{0.9}Sr_{0.1}Co_{1-y}Ni_yO_3$/TPR peak area of $La_{0.9}Sr_{0.1}CoO_3$×100, per gram of catalyst).

As mentioned above, cobalt and nickel are highly active metals in F-T synthesis, and the mixing of these two active F-T metals has great effects on the reaction activity and selectivity [30]. Thus, metallic cobalt and nickel species, as well as the Co-Ni alloy formed during the reduction of the $La_{0.9}Sr_{0.1}Co_{1-y}Ni_yO_3$ perovskite catalysts can be considered as the active centres for HAS in this study.

5.3 $La_{0.9}Sr_{0.1}Co_{1-y}Ni_yO_3$ Perovskite Catalytic Performance in HAS

5.3.1 Catalyst Activity - CO Conversion

The Ni-substituted perovskites have been tested as catalysts for higher alcohol formation from syngas in the high-flow fixed-bed reactor (Spider F-T facility, see Chapter 3, Section 3.5.1.2). The experiments were carried out at 275°C under 3.0 MPa, GHSV=10995 h^{-1} and H_2/CO=2 for 24 h, for all catalysts. The data obtained from each experiment were the average of measurements over the steady-state period.

The CO and H_2 conversion at 275 °C for the investigated catalysts are given in Figure 5-5. The results show that the catalyst activity changed significantly with the nickel substitution.

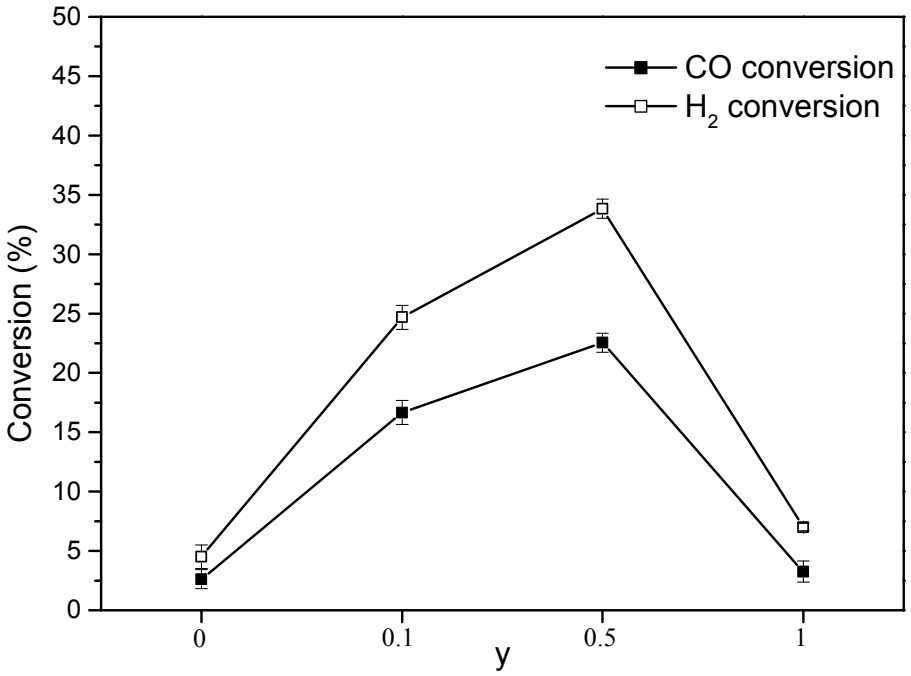

Figure 5-5. CO and H_2 conversion as a function of nickel substitution for $La_{0.9}Sr_{0.1}Co_{1-y}Ni_yO_3$ perovskite catalysts. Reaction condition: T=275 °C, P=3.0 MPa, GHSV=10995 h^{-1}, and H_2/CO=2:1.

The unsubstituted $La_{0.9}Sr_{0.1}CoO_3$ and $La_{0.9}Sr_{0.1}NiO_3$ catalysts showed almost no activity, which was mainly due to the unfavourable operating conditions for mono-metal catalysts used in this experiment. As discussed in Chapter 4, the $La_{0.9}Sr_{0.1}CoO_3$ catalyst exhibited high syngas conversion under relatively high reaction temperatures (≥300 °C) and a low GHSV of 3500 h^{-1} (Chapter 4, Section 4.3). As for the $La_{0.9}Sr_{0.1}NiO_3$ catalyst, though nickel is active for methane formation, the reaction conditions were not optimum for the methanation reaction (typically, T=100-600 °C, P=0.1 MPa, and H_2/CO ratio=3) [25, 31, 32]. However, among the $La_{0.9}Sr_{0.1}Co_{1-y}Ni_yO_3$ perovskites, the bimetallic Co-Ni catalysts with y=0.1 and 0.5 displayed a CO conversion about 5 to 7 times higher than the monometallic B site perovskites (y=0 and 1, respectively). Interestingly, the TPR results (Figure 5-2) suggested that the bimetallic catalysts had a similar number of active centres as $La_{0.9}Sr_{0.1}CoO_3$. These results confirm that nickel substitution improves the catalytic activity of $La_{0.9}Sr_{0.1}CoO_3$ *via* the formation of bi-metallic Co-Ni active centres, which are more active than mono-metallic cobalt active centres.

In order to explain the catalytic activity results, an estimation of the turnover frequency (TOF, defined as moles of CO converted per mole of active centre per second) was performed. Due to the difficulty in determining the exact number of active

centres (Co^0, Ni^0 and Co-Ni alloy) of the catalysts during the reaction, two sets of assumptions were made for the TOF calculation:

- In the first set of assumptions, the "Co-Ni bi-metal" plot in Figure 5-6 (black plot) was calculated based on the hypotheses that (1) all substituted nickel atoms form bimetallic Co-Ni centres and (2) the excess cobalt formed Co^0 active centres and that all metal sites are accessible to the reagent gases.
- In the second set of assumptions, the "separate mono-metal" TOF plot in Figure 5-6 (red plot) was based on the postulations that all B metal sites in the perovskites form separate mono metal active centres (Co^0 and Ni^0) after reduction, thus the total number of active centres in each catalyst is very similar due to the close molecular weight of cobalt and nickel.

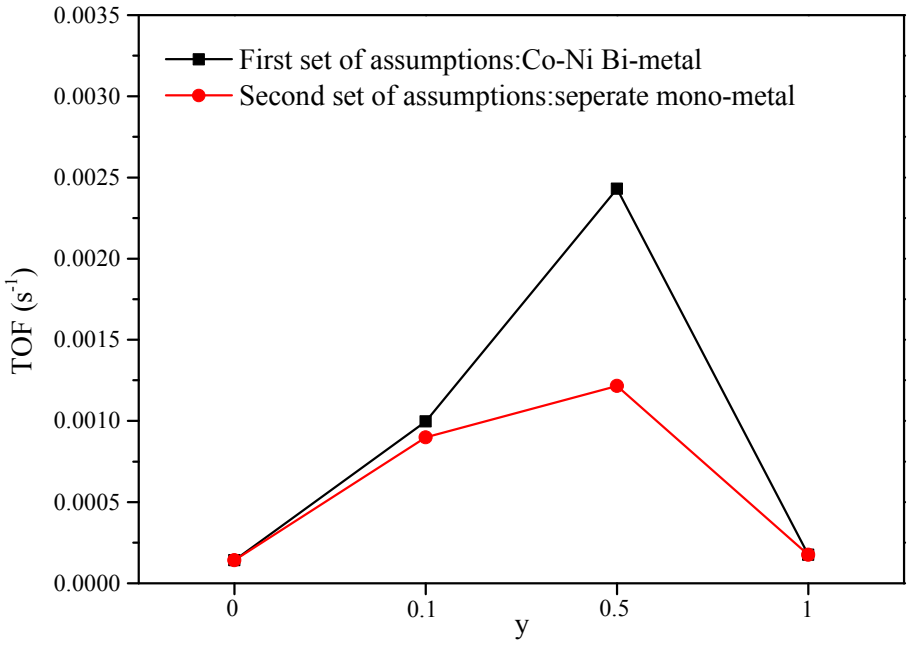

Figure 5-6. TOF of $La_{0.9}Sr_{0.1}Co_{1-y}Ni_yO_3$ perovskite catalysts (same reaction conditions as for Figure 5-5).

Based on this first set of assumptions (Figure 5-6 (black plot)), the results show that the TOF value increased with increasing nickel substitution until y=0.5, thus validating that the Co-Ni alloy centres have a much higher activity than mono-metallic cobalt or nickel active centres, as the higher the nickel substitution level, the lower the theoretical number of bimetallic active centre (for y=0.1 and 0.5). However, it is realistic to presume that in this set of simplified assumptions, a certain amount of

mono-metallic cobalt and nickel active centres do exist in the bimetallic catalysts, thus affecting the real number of active centres. The "separate mono-metal" TOF plot (Figure 5-6 (red plot)) overcame part of this uncertainty and shows the same trend as the "Co-Ni bi-metal" curve.

These selected calculations are based on two extreme and simplified assumptions, and the real TOF for Ni-substituted catalysts would be somewhat in between the two curves. However, the results confirm that nickel substitution improved the catalytic activity of $La_{0.9}Sr_{0.1}Co_{1-y}Ni_yO_3$ catalysts with the formation of Co-Ni bimetal active centres for CO conversion. The results in this work are supported by the reported finding in the literature showing that the alloying of cobalt with nickel strengthened the activity of SiO_2 supported Co-Ni bi-metal catalysts for hydrogen dissociative adsorption, resulting in a higher catalytic activity in CO hydrogenation [33].

The used catalysts after 24 h reaction were analysed by XRD and the results are given in Figure 5-7.

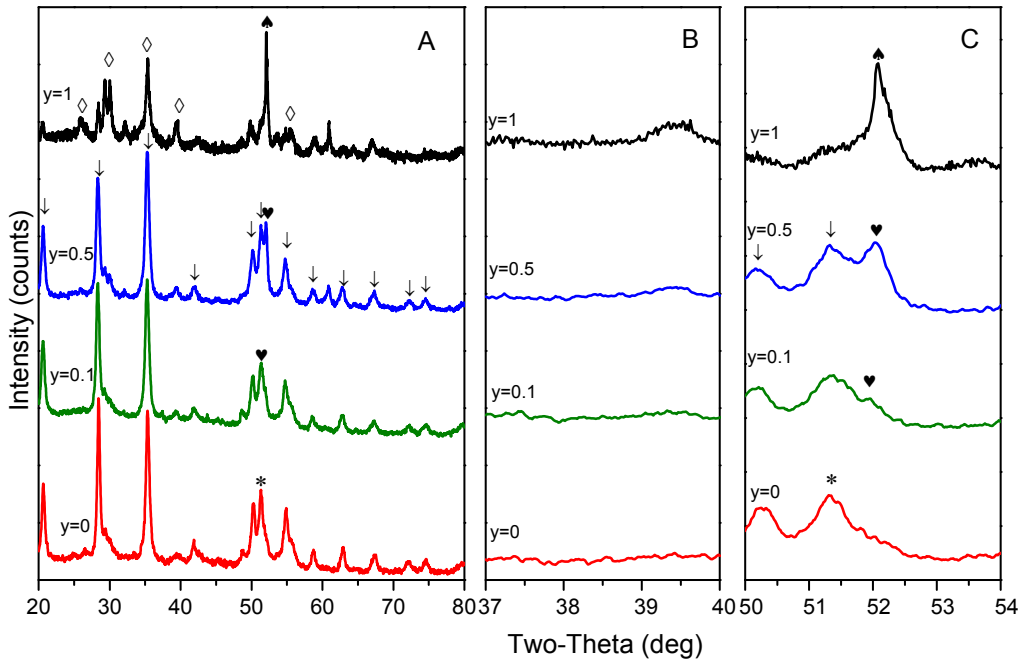

Figure 5-7. XRD patterns of $La_{0.9}Sr_{0.1}Co_{1-y}Ni_yO_3$ perovskite catalysts after reaction. (A) full pattern, (B) zoom in the perovskite peak range and (C) zoom in the metallic peak range. Phases: (♠) Ni^0, (*) Co^0, (♥) Co-Ni alloy, (↓) $LaCO_3OH$, and (◊) $La_2O_2CO_3$.

The diffraction peaks of the perovskite structure at $2\theta \approx 38$-$39°$ have disappeared in all the used catalysts analysed after the F-T reaction (Figure 5-7 (B)), indicating a

collapse of the structure due to the presence of a reducing atmosphere, and possible further reduction. For the Co-containing perovskite catalysts (y=0, 0.1 and 0.5), Co^0 and $LaCO_3OH$ (JCPDS-ICDD 26-0815) were formed during the reaction, in accordance with the observation in Chapter 4 (Section 4.3.2) [1]. La_2SrO_x observed after reduction (see Figure 5-3) was believed to transform into $LaCO_3OH$ and SrO during the HAS reaction (Equation (5-3), with x=4). Although the SrO phase was not detected by XRD, due to possible low concentration and particle size lower than the detection limit of the X-ray analysis, its formation cannot be discarded [17].

$$La_2SrO_x + 2\ CO_2 + H_2O \rightarrow 2\ LaCO_3OH + SrO \quad (5\text{-}3)$$

For Ni-substituted catalysts (y=0.1 and 0.5), the Co-Ni alloy phase could not be detected after reaction due to the impurities (side products) on the surface of the catalyst. Slightly phase separation of the Co-Ni alloy to form Co^0 and Ni^0 atom may be an additional effect to the 2 θ drifting. As expected, the peak intensity of Ni^0 for the catalyst with y=0.5 increased significantly compared to the catalyst with y=0.1. Besides, the 2θ value of the Ni^0 peak slightly shifted to 52.16°, which was closer to the metallic nickel diffraction line. This peak can be associated with the reduction of the extra-framework Ni-containing oxide shown in Figure 5-1. For the catalyst with y=1, the Ni^0 phase was clearly observed, together with the formation of $La_2O_2CO_3$ (JCPDS-ICDD 22-0642) (Equation (5-4)).

$$La_2O_3 + CO_2 \rightarrow La_2O_2CO_3 \quad (5\text{-}4)$$

It has been reported by Maluf *et al.* that the combination of strontium and nickel in La-Sr-Co-Ni-based perovskite structure enhance the water gas shift reaction (WGS) [34]. As a result, the produced water from CO hydrogenation with the $La_{0.9}Sr_{0.1}NiO_3$ catalyst will react preferably with CO to form CO_2 and then form $La_2O_2CO_3$, rather than with La_2SrO_x to form $LaCO_3OH$.

5.3.2 Alcohol Selectivity and Yield

In this section, the effects of nickel substitution on HAS over $La_{0.9}Sr_{0.1}Co_{1-y}Ni_yO_3$ perovskite catalysts are discussed with respect to the following two aspects: (1) the role of nickel in the creation of active sites for HAS and (2) the role of active centres in the formation of higher alcohols.

As discussed thoroughly in the literature, nickel is a good catalyst for methanation because of its strong ability for hydrogenation [7, 10, 35]. As shown in Figure 5-8 (A), the CO methanation reaction rate was much faster than that of the alcohol formation reaction for all Ni-containing catalysts. It should be noted that the lower methane reaction rate observed for the catalyst with y=1 was due to the low conversion of CO (see Figure 5-5)[2]. Thus, as expected, methane selectivity increased significantly with increasing nickel substitution level as shown in Figure 5-8 (B).

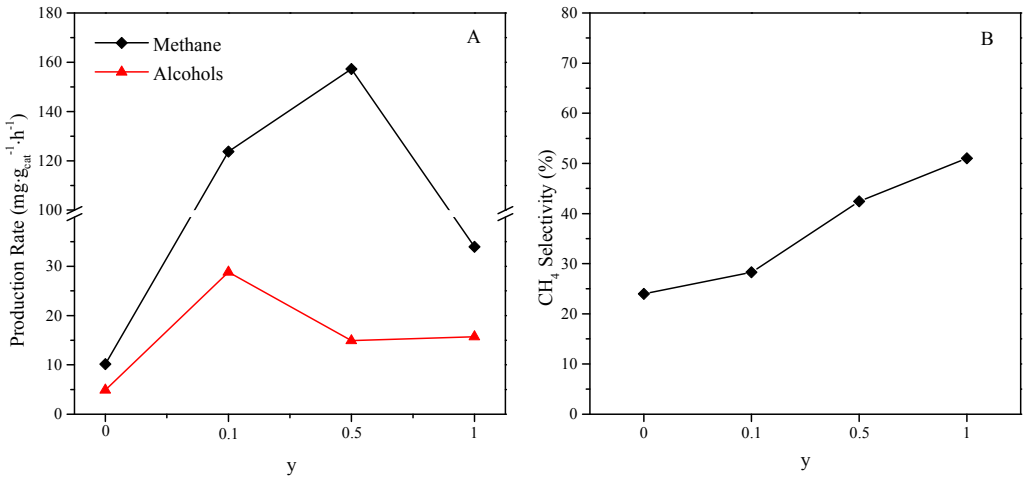

Figure 5-8. Performance of $La_{0.9}Sr_{0.1}Co_{1-y}Ni_yO_3$ perovskite catalysts for higher alcohol formation (same reaction conditions as Figure 5-5): (A) methane and alcohol production rate and (B) methane selectivity.

Figure 5-9 presents the alcohol product distribution (C atom%) and higher alcohol space time yield (STY) over $La_{0.9}Sr_{0.1}Co_{1-y}Ni_yO_3$ perovskite catalysts.

[2] Please note that no experimental data are available for light hydrocarbons, due to the analytical method applied in the tests (single peak in GCMS).

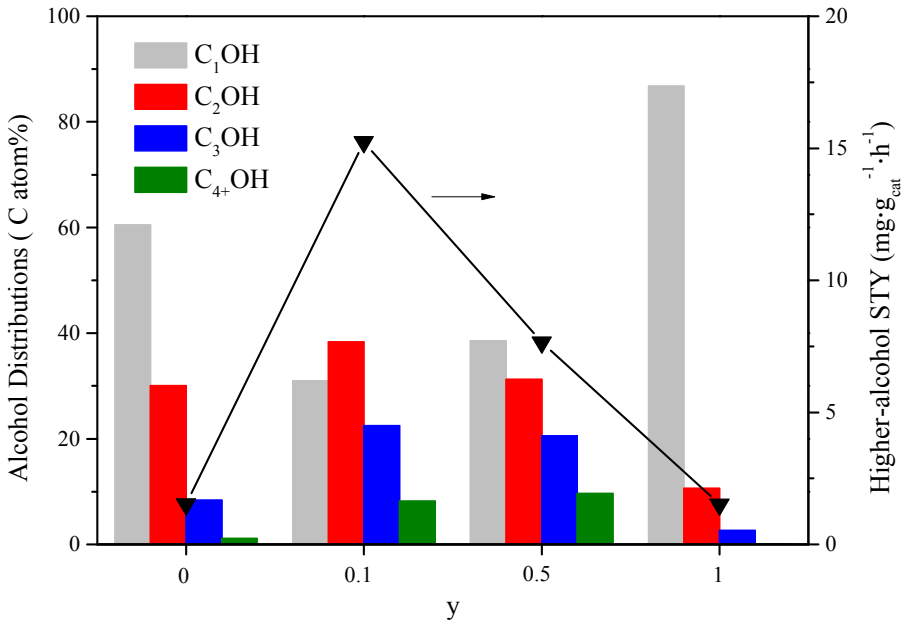

Figure 5-9. Performance of $La_{0.9}Sr_{0.1}Co_{1-y}Ni_yO_3$ perovskite catalysts for higher alcohol formation (same reaction conditions as Figure 5-5).

Figure 5-9 shows the significant effect of the Co-Ni alloy active centres on shifting methanol production towards higher alcohols. At nickel substitution level of 0.1, the amount of methanol decreased significantly to 30.1%, half the value compared to $La_{0.9}Sr_{0.1}CoO_3$ catalyst (60.5%), and the main alcohol product was ethanol, with higher alcohols representing a total of 69.9% of the alcohol products. For catalyst with y=0.5, the higher alcohols were still the main products (61.5%), with the amount of methanol increasing to 38.5%. With further increase in nickel substitution (y=1), methanol became the predominant product (86.7%). In addition, the space time yield of higher alcohols ($C_{2+}OH$) were 15.2 $mg \cdot g_{cat}^{-1} \cdot h^{-1}$ and 7.7 $mg \cdot g_{cat}^{-1} \cdot h^{-1}$ for the catalyst with y=0.1 and y=0.5, respectively, compared to 1.5 $mg \cdot g_{cat}^{-1} \cdot h^{-1}$ for both mono-metallic catalysts (y=0 and 1). These results suggest that the synergistic effect of the Co-Ni alloy not only increase the catalysts activity as discussed above (Section 5.3.1) but also plays a significant role in alcohol production and CO insertion to promote higher alcohol formation. The promotion effect of nickel in HAS from syngas has also been proved by Li *et al.*, who claimed that with the addition of nickel, both the CO conversion and the selectivity toward higher alcohols over alkali-doped molybdenum sulphide catalysts were enhanced greatly (22.5% vs 55.6%, and 28.8% vs. 41.2%, respectively) [13]. However, compared to y=0.1, the higher alcohol STY and higher alcohol selectivity decreased for the catalyst with y=0.5, while methane formation

increased (Figure 5-8), suggesting that the intra- and extra- perovskite lattice nickel atoms play different and competing roles in higher alcohol synthesis. With a high level of nickel substitution (y=0.5), only part of the nickel atoms entered into the perovskite structure to form Co-Ni alloy after reduction to act as active centres for higher alcohol formation. The rest remained in oxide form that reduced to Ni^0 during the reduction process and existed outside the perovskite framework (see Section 5.2.2), which promoted methanation.

Comparing the ratio of each $C_{2+}OH$ alcohol over methanol (C_1OH) for each value of y (Figure 5-10) provides evidence of the ability of nickel substitution in $La_{0.9}Sr_{0.1}Co_{1-y}Ni_yO_3$ perovskite catalysts to promote carbon chain propagation. For catalysts with y=0.1 and 0.5, the ratio of C_2OH/C_1OH, C_3OH/C_1OH and $C_{4+}OH/C_1OH$ were much higher than that for the unsubstituted catalysts (y=0 and 1). This observation is in accordance with the above discussion, indicating that the bi-metal Co-Ni catalyst favours higher alcohol formation. It should be noted that ethanol was the main alcohol product for the $La_{0.9}Sr_{0.1}Co_{0.9}Ni_{0.1}O_3$ catalyst, with a maximum C_2OH/C_1OH ratio of 1.24.

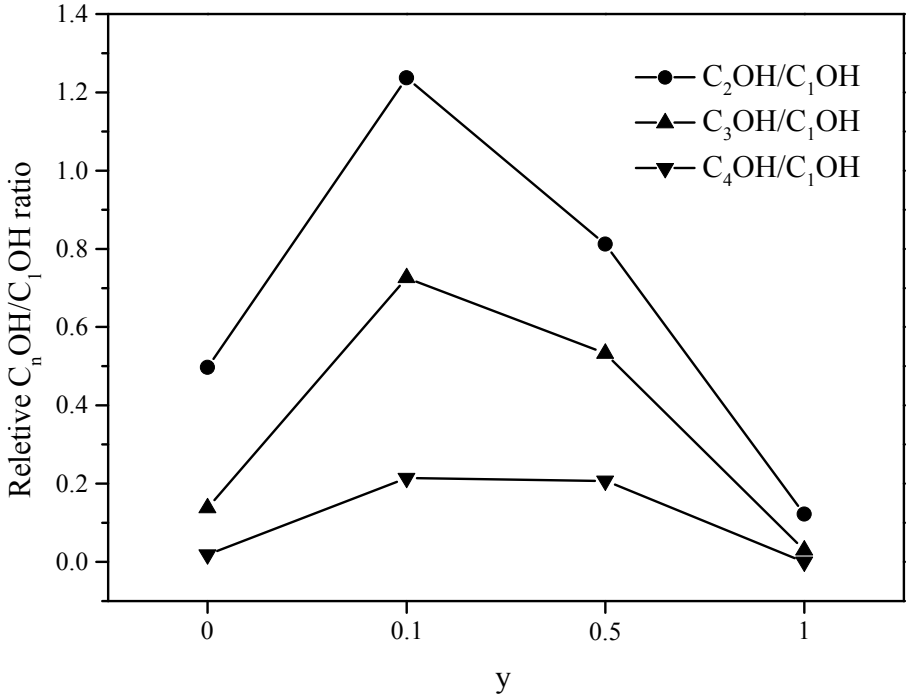

Figure 5-10. C_nOH/C_1OH ratio (with n>1) over $La_{0.9}Sr_{0.1}Co_{1-y}Ni_yO_3$ perovskite catalysts for higher alcohol formation (same reaction conditions as Figure 5-5).

5.3.3 Anderson-Schultz-Flory Distribution of Alcohol Products

As mentioned in Chapter 2, Section 2.3.1, the formation of higher alcohols followed a CO insertion mechanism (most accepted mechanism), that is, insertion of CO into the corresponding hydrocarbon precursors to produce acyl intermediates which are then hydrognetated to alcohol products. The Anderson-Schultz-Flory (ASF) distribution is commonly used to investigate the chain growth of hydrocarbon products in the F-T process (Chapter 2, Section 2.2). This distribution was also employed in several reports to study the mechanism of alcohol (C_1OH to C_5OH) production in the F-T process [2, 3, 12, 13, 15, 36]. A linear ASF distribution (ln W*n*/*n versus n*) is generally expected, indicating a single mechanism or a single type of activation sites. However, deviations from the linear ASF distribution are generally observed, especially for products of low carbon number, due to the superposition of several ASF distributions resulting from multiple growth sites or reaction paths [37-39]. Figure 5-11 presents the ASF plots for alcohol (C_1OH to C_5OH) obtained over the nickel-substituted $La_{0.9}Sr_{0.1}Co_{1-y}Ni_yO_3$ catalysts.

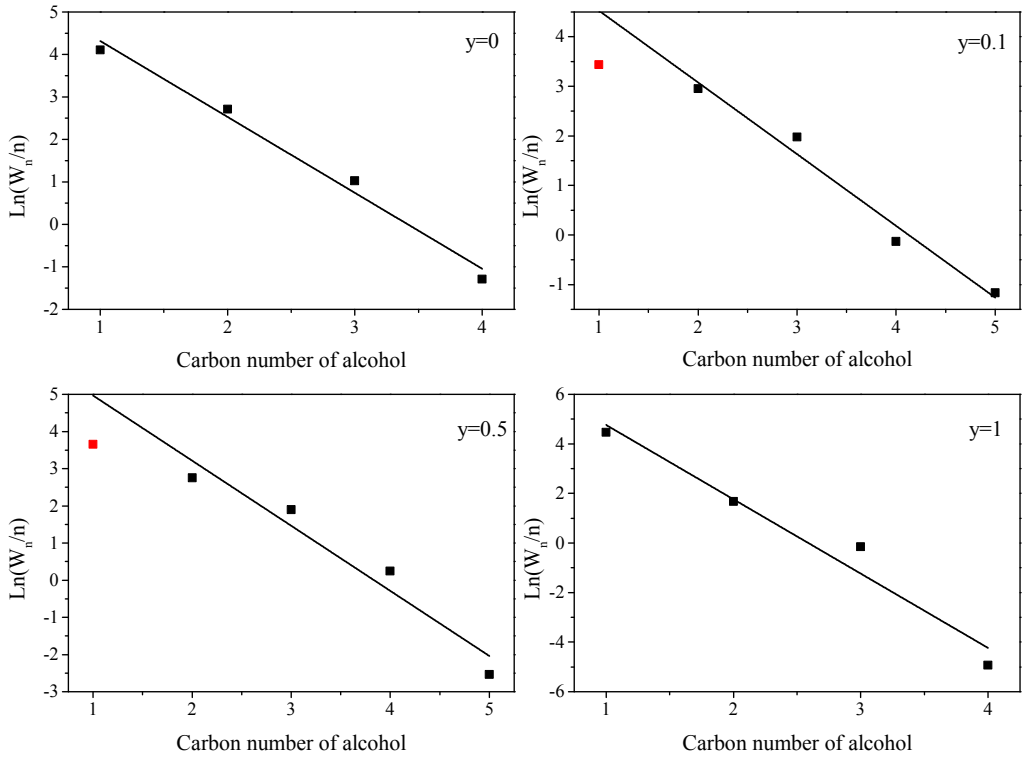

Figure 5-11. ASF plots of alcohols over $La_{0.9}Sr_{0.1}Co_{1-y}Ni_yO_3$ perovskite catalyst with different Ni-substituted level (same reaction condition as in Figure 5-5) (a) y=0, (b) y=0.1, (c) y=0.5 and (d) y=1.

The results in Figure 5-11 show that the chain propagation of alcohol products (C_1OH-C_5OH) over the B site mono-metal catalysts, $La_{0.9}Sr_{0.1}CoO_3$ (y=0) and $La_{0.9}Sr_{0.1}NiO_3$ (y=1), followed the traditional linear ASF distribution. This suggests that there was only one kind of active centre or mechanism over these cataltysts [36]. However, for Ni-substituted $La_{0.9}Sr_{0.1}Co_{1-y}Ni_yO_3$ catalysts (y=0.1 and 0.5), a deviation was observed for methanol in the ASF plots, suggesting that methanol and the higher alcohol formation routes over these two catalysts might be different due to different active centres Co^0, Ni^0 and Co-Ni alloy acting as growth sites [13, 15, 37, 38]. As mentioned in Chapter 2, section 2.3.1, the CO insertion mechanism proposed by Xu *et al*. is widely accepted for HAS from syngas (see Figure 5-12) [40]. According to the discussion above, cobalt is active for CO dissociation, while the Co-Ni alloy catalysis CO insertion and nickel favours methanation. For the catalyst with y=0.1 and 0.5, cobalt and Co-Ni alloy were considered as active centres. During the reaction, CO would either adsorbed on the catalyst surface and then be hydrogenated to form methanol (via CO_2 formation) or be dissociated to form C* for chain propagation. According to this, the ASF distribution of alcohol products should be linear, similar to the catalyst with y=0. However, the presence of the Co-Ni alloy promoted the CO insertion, which increased the formation of higher alcohols. As a result, the selectivity of methanol was relatively less than for mono-metal catalysts, leading to a deviation of methanol in the ASF distribution. In addition, the presence of metallic nickel (y=1 catalyst) favoured methane formation, with more CO dissociated to form C*, which also decrease the formation of methanol.

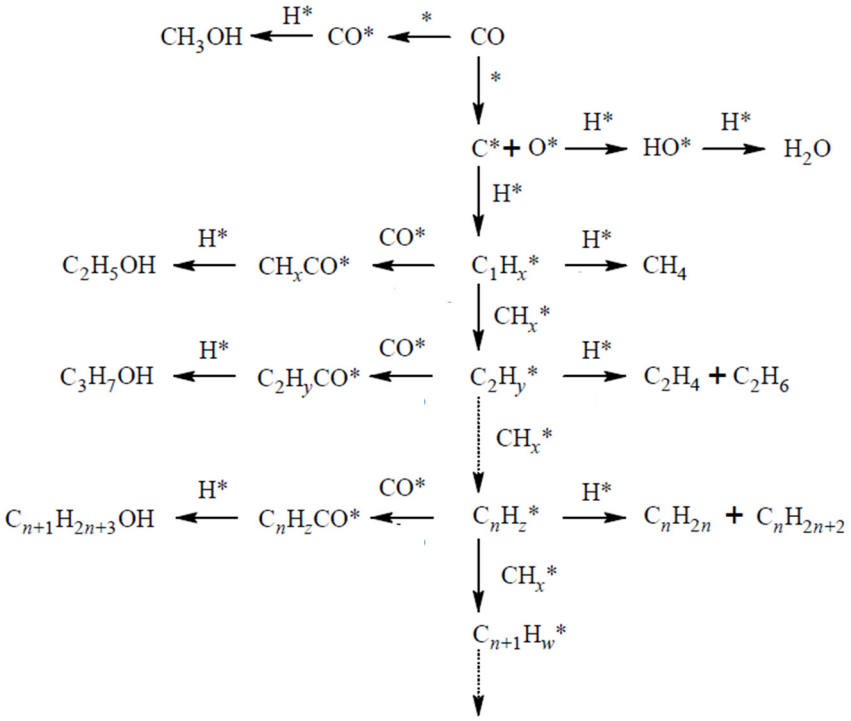

Figure 5-12. Alcohol formation through CO insertion mechanism (adapted from Xiao *et al*.[16]).

The chain growth probability (α), presented in Table 5-2, were calculated using the slope of the straight line for the higher alcohols (see Chapter 2, Equation 2-6), and were higher for both Ni-substituted $La_{0.9}Sr_{0.1}Co_{1-y}Ni_yO_3$ catalysts. For comparison purposes, α value was calculated based on C_2OH-C_4OH data, though C_5OH was observed in catalysts with y=0.1 and 0.5.

Table 5-2. Alcohol chain growth probability of $La_{0.9}Sr_{0.1}Co_{1-y}Ni_yO_3$ perovskite catalysts.

Catalyst	**y**	**α** [a]
$La_{0.9}Sr_{0.1}CoO_3$	0	0.14
$La_{0.9}Sr_{0.1}Co_{0.9}Ni_{0.1}O_3$	0.1	0.21
$La_{0.9}Sr_{0.1}Co_{0.5}Ni_{0.5}O_3$	0.5	0.15
$La_{0.9}Sr_{0.1}NiO_3$	1	0.04

[a] α calculated based on C_2OH -C_4OH.

Confirming the previous results (see Figure 5-10), it is reasonable to claim that nickel substitution, and the presence of a bimetal Co-Ni alloy in the catalyst exerted an positive impact on the chain propagation to produce higher alcohols. Similar results were observed by Li *et al*. when studying HAS in the F-T process over nickel modified K_2CO_3/MoS_2 catalyst [12]. As mentioned before, cobalt favours the dissociation of

CO, thereby promoting the chain growth of hydrocarbons [41], while Ni-based catalysts have a strong ability for CO insertion, favouring alcohol formation [42]. For low nickel substitution catalyst (y=0.1), the Co-Ni alloy exerted the bi-functionality, namely, the formation of the hydrocarbon precusors by chain propagation and the succeeding CO insertion under hydrogenation conditions, hence a higher chain growth probability for higher alcohol formation compared to the catalyst with y=0. However, with the increase in nickel substitution, the $La_{0.9}Sr_{0.1}Co_{0.5}Ni_{0.5}O_3$ catalyst had a lower α value compared to that of the catalyst with y=0.1. The presence of extra-lattice nickel species was favorable to the formation of methane, which exhibited a much faster formation rate than that of alcohols (see Figure 5-8). Without the synergism of the Co-Ni alloy, the catalyst y=1 exihibted a much lower α value than other catalysts due to its high methanation ability [7, 10].

5.4 Effect of Reaction Temperature over $La_{0.9}Sr_{0.1}Co_{0.9}Ni_{0.1}O_3$ Perovskite Catalyst on Higher Alcohol Formation

The $La_{0.9}Sr_{0.1}Co_{0.9}Ni_{0.1}O_3$ catalyst showed the highest catalytic performance in HAS compared with the other catalysts evaluated in this chapter. To provide further insights into the catalyst with y=0.1, and optimise higher alcohol production, the effect of reaction temperature on the synthesis of higher alcohols was investigated. The reactions were carried out in the range of 275°C to 340°C at 3.0 MPa, GHSV=10995 h^{-1}, and $H_2/CO=2$. The measured space time yields of alcohols, methane and carbon dioxide are given in Figure 5-13.

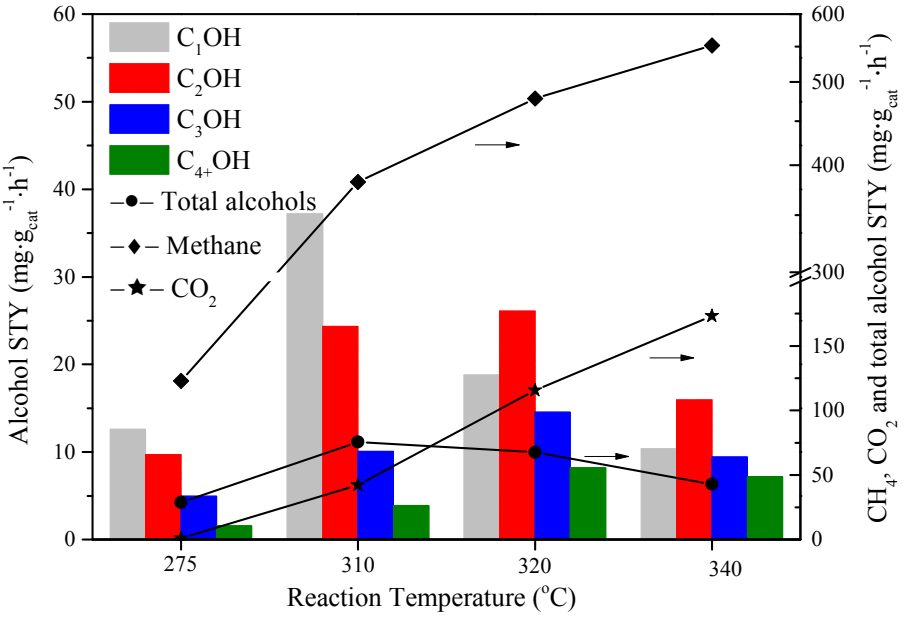

Figure 5-13. The effect of reaction temperature for $La_{0.9}Sr_{0.1}Co_{0.9}Ni_{0.1}O_3$ perovskite catalyst space time yield of alcohols, methane and carbon dioxide. Reaction conditions: T=275-340°C, P=3.0 MPa, GHSV= 10995 h^{-1}, and H_2/CO=2:1.

With increasing reaction temperature, the STY of methanol showed a maximum at 310°C and then decreased, while the STY for C_2OH, C_3OH, and $C_{4+}OH$ showed a maximum at 320°C, with a total higher alcohol STY of 48.9 $mg \cdot g_{cat}^{-1} \cdot h^{-1}$. Indeed, methanol formation is generally favoured at low temperature, while relatively high temperature promotes the higher alcohol formation [43-45]. However, it is well known that CO adsorption and dissociation on the catalyst surface strongly depends on the reaction temperature [3, 4], with CO adsorption inversely proportional to temperature, while higher temperatures kinetically favour the methanation and WGS reactions. The increasing reaction temperature thus increased the methane and carbon dioxide production and suppressed the alcohol production, as also reported by Tien-Thao *et al*. [4] and Liu *et al*. [25]. In parallel, the increase in the extent of the WGS reaction would lead to change in the H_2/CO ratio (increase) and contribute to the decrease in CO insertion and C-C chain growth [40, 46]. As a result, the alcohol STY decreased at higher reaction temperatures (above 320°C).

5.5 Comparison of $La_{0.9}Sr_{0.1}Co_{0.9}Ni_{0.1}O_3$ Perovskite Catalyst with Other HAS Catalysts

The same process conditions for higher alcohol synthesis *via* the F-T process do not exist in the literature for the direct comparison of the performance of the catalysts used in this work with other catalytic systems. However, some catalytic performances of other reported catalysts including cobalt and nickel elements for HAS are summarised in Table 5-3. As expected, different kinds of catalysts and reaction conditions led to different alcohol yields. Generally, higher reaction temperature and pressure, and lower GHSV led to better yields of alcohols, as can be seen in Table 5-3. Taking the catalyst activity and reaction conditions into consideration, the $La_{0.9}Sr_{0.1}Co_{0.9}Ni_{0.1}O_3$ perovskite catalyst prepared in this study reached a high level of CO conversion and higher alcohol selectivity (weight fraction) compared to other catalysts.

Table 5-3. Catalyst performance of some representative catalysts reported in the literature.

Catalyst	Conditions				CO conv. (%)	ROH STY [1]	Alcohol weight fraction (wt.%)		Ref.
	T °C	P MPa	H_2/CO	GHSV h^{-1}			C_1OH	$C_{2+}OH$	
$La_{0.9}Sr_{0.1}Co_{0.9}Ni_{0.1}O_3$	320	3.0	2	10995	49.2	67.7	27.8	72.2	This work
$5Cu15Co/Al_2O_3$	250	2.0	2	4500	30.9	43.8	43.1	56.9	[47]
$Ni/Mn/K/MoS_2$	315	9.5	2	6000	17.8	330	45.8	54.2	[14]
$CsNiCu/CeO_2$	300	3.0	2	2400	37.6	178.4	54.0	46.0	[15]
$LaCo_{0.7}Cu_{0.3}O_3/ZrO_2$	310	3.0	2	3900	35.3	97.3	17.6	82.4	[48]
$LaRhO_3$	300	0.6	1	NA	NA	31.0	51.6	48.4	[46]

[1] ROH STY: $mg \cdot g_{cat}^{-1} \cdot h^{-1}$.

5.6 Conclusions

Ni-substituted $La_{0.9}Sr_{0.1}Co_{1-y}Ni_yO_3$ perovskite catalysts were successfully synthesised by the co-precipitation method. XRD analysis revealed that the perovskite structure was maintained with the substitution of nickel into the $La_{0.9}Sr_{0.1}CoO_3$ catalyst. The close proximity of nickel and cobalt sites in the perovskite lattice promoted the catalyst reducibility. Though the perovskite structure disappeared during the reaction, both the strong interaction between cobalt and nickel and the good

dispersion of the active centres that came from the unique perovskite structure had a positive effect on the catalytic performance for HAS in the F-T process. The interactions between the nickel and cobalt in the perovskite structure generated Co-Ni alloy after reduction, with the synergistic effect between cobalt and nickel responsible for the improvement in CO conversion and higher alcohol selectivity. That is, the Co-Ni alloy showed a bi-functionality—the chain propagation of hydrocarbon precursors and subsequent CO insertion. With higher nickel substitution levels (y=0.5), metallic nickel also formed and existed outside of the perovskite framework. The extra-lattice nickel species, reduced to metallic nickel, favoured the methanation reaction rather than the formation of higher alcohols.

Due to the highly dispersed bimetallic Co-Ni alloy and less extra-lattice Ni^0 phase, the $La_{0.9}Sr_{0.1}Co_{0.9}Ni_{0.1}O_3$ catalyst showed the highest selectivity toward higher alcohol formation. A homogeneous distribution of the bi-metallic Co–Ni alloy is a key characteristic for high yields in the synthesis of higher alcohols. The reaction temperature was also proved to be a critical factor affecting both alcohol yield and selectivity.

References

[1] M. Ao, G.H. Pham, V. Sage, V. Pareek, Journal of Molecular Catalysis A: Chemical, 416 (2016) 96-104.

[2] N. Tien-Thao, H. Alamdari, M.H. Zahedi-Niaki, S. Kaliaguine, Applied Catalysis A: General, 311 (2006) 204-212.

[3] T. Nguyen, M. Zahedi-Niaki, H. Alamdari, S. Kaliaguine, International Journal of Chemical Reactor Engineering, 5 (2007) art. A82.

[4] N. Tien-Thao, M.H. Zahedi-Niaki, H. Alamdari, S. Kaliaguine, Applied Catalysis A: General, 326 (2007) 152-163.

[5] N.T. Thao, Asian Journal of Chemistry, 25 (2013) 8082-8086.

[6] G. Liu, D. Pan, T. Niu, A. Cao, Y. Yue, Y. Liu, RSC Advances, 5 (2015) 31637-31647.

[7] K. Xiao, X. Qi, Z. Bao, X. Wang, L. Zhong, K. Fang, M. Lin, Y. Sun, Catalysis Science & Technology, 3 (2013) 1591-1602.

[8] N.D. Subramanian, G. Balaji, C.S. Kumar, J.J. Spivey, Catalysis Today, 147 (2009) 100-106.

[9] J. Su, Z. Zhang, D. Fu, D. Liu, X.-C. Xu, B. Shi, X. Wang, R. Si, Z. Jiang, J. Xu, Y.-F. Han, Journal of Catalysis, 336 (2016) 94-106.

[10] R. Suárez París, V. Montes, M. Boutonnet, S. Järås, Catalysis Today, (2014) 294-303.

[11] D. Li, N. Zhao, H. Qi, W. Li, Y.H. Sun, B. Zhong, Catalysis Communications, 6 (2005) 674-678.

[12] D. Li, C. Yang, N. Zhao, H. Qi, W. Li, Y. Sun, B. Zhong, Fuel Processing Technology, 88 (2007) 125-127.

[13] D. Li, C. Yang, W. Li, Y. Sun, B. Zhong, Topics in Catalysis, 32 (2005) 233-239.

[14] H. Qi, D. Li, C. Yang, Y. Ma, W. Li, Y. Sun, B. Zhong, Catalysis Communications, 4 (2003) 339-342.

[15] Y. Liu, K. Murata, M. Inaba, I. Takahara, K. Okabe, Fuel, 104 (2013) 62-69.

[16] K. Xiao, Z. Bao, X. Qi, X. Wang, L. Zhong, K. Fang, M. Lin, Y. Sun, Chinese Journal of Catalysis, 34 (2013) 116-129.

[17] G. Valderrama, A. Kiennemann, M.R. Goldwasser, Journal of Power Sources, 195 (2010) 1765-1771.

[18] D.R.M. Godoi, J. Perez, H. Mercedes Villullas, Journal of The Electrochemical Society, 154 (2007) B474.

[19] J.A. Schwarz, C. Contescu, A. Contescu, Chemical Reviews, 95 (1995) 477-510.

[20] G.S. Gallego, C. Batiot-Dupeyrat, J. Barrault, E. Florez, F. Mondragón, Applied Catalysis A: General, 334 (2008) 251-258.

[21] Z. Wang, C. Wang, S. Chen, Y. Liu, International Journal of Hydrogen Energy, 39 (2014) 5644-5652.

[22] O. González, J. Lujano, E. Pietri, M.R. Goldwasser, Catalysis Today, 107-108 (2005) 436-443.

[23] G. Valderrama, A. Kiennemann, M.R. Goldwasser, Catalysis Today, 133-135 (2008) 142-148.

[24] C.R.B. Silva, L. da Conceição, N.F.P. Ribeiro, M.M.V.M. Souza, Catalysis Communications, 12 (2011) 665-668.

[25] K.K. Ramasamy, M. Gray, H. Job, Y. Wang, Chemical Engineering Science, 135 (2015) 266-273.

[26] B. Levasseur, S. Kaliaguine, Applied Catalysis A: General, 343 (2008) 29-38.

[27] N.K. Kotsev, L.I. Ilieva, Catalysis Letters, 18 (1993) 173-176.

[28] R. Pereñíguez, V.M. González-DelaCruz, J.P. Holgado, A. Caballero, Applied Catalysis B: Environmental, 93 (2010) 346-353.

[29] S.Q. Chen, Y. Liu, International Journal of Hydrogen Energy, 34 (2009) 4735-4746.

[30] A. Zare, A. Zare, M. Shiva, A.A. Mirzaei, Journal of Industrial and Engineering Chemistry, 19 (2013) 1858-1868.

[31] D. Hu, J. Gao, Y. Ping, L. Jia, P. Gunawan, Z. Zhong, G. Xu, F. Gu, F. Su, Industrial & Engineering Chemistry Research, 51 (2012) 4875-4886.

[32] A. Zhao, W. Ying, H. Zhang, H. Ma, D. Fang, Catalysis Communications, 17 (2012) 34-38.

[33] T. Ishihara, N. Horiuchi, T. Inoue, K. Eguchi, Y. Takita, H. Arai, Journal of Catalysis, 136 (1992) 232-241.

[34] S. Maluf, E. Tanabe, P. Nascente, E. Assaf, Topics in Catalysis, 54 (2011) 210-218.

[35] K. Shimura, T. Miyazawa, T. Hanaoka, S. Hirata, Journal of Molecular Catalysis A: Chemical, 407 (2015) 15-24.

[36] M. Ding, J. Tu, M. Qiu, T. Wang, L. Ma, Y. Li, Applied Energy, 138 (2015) 584-589.

[37] C.H. Bartholomew, R.J. Farrauto, Fundamentals of Industrial Catalytic Processes, Wiley, (2010).

[38] J. Patzlaff, Y. Liu, C. Graffmann, J. Gaube, Catalysis Today, 71 (2002) 381-394.

[39] A. Cosultchi, M. Pérez-Luna, J.A. Morales-Serna, M. Salmón, Catalysis Letters, 142 (2012) 368-377.

[40] X. Xu, E.B.M. Doesburg, J.J.F.Scholten, Catalysis Today, 2 (1987) 125-170.

[41] Y. Zhang, Y. Sun, B. Zhong, Catalysis Letters, 76 (2001) 249-253.

[42] S. Uchiyama, Y. Ohbayashi, T. Hayasaka, N. Kawata, Applied Catalysis, 42 (1988) 143-152.

[43] J.C. Slaa, J.G.v. Ommen, J.R.H. Ross, Catalysis Today, 15 (1992) 129-148.

[44] M. Gupta, M.L. Smith, J.J. Spivey, ACS Catalysis, 1 (2011) 641-656.

[45] V. Subramani, S.K. Gangwal, Energy & Fuels, 22 (2008) 814-839.

[46] P.R. Watson, G.A. Somorjai, Journal of Catalysis, 74 (1982) 282-295.

[47] J. Wang, P.A. Chernavskii, A.Y. Khodakov, Y. Wang, Journal of Catalysis, 286 (2012) 51-61.

[48] G. Liu, Y. Geng, D. Pan, Y. Zhang, T. Niu, Y. Liu, Fuel Processing Technology, 128 (2014) 289-296.

Chapter 6 Tri-metallic Co-Ni-Cu-based Perovskite Catalysts for Higher Alcohol Synthesis

6.1 Introduction

Although higher alcohol synthesis (HAS) catalysts have been investigated over the past two decades intensively (see Chapter 2), the targeted product yields still remain low under a wide range of different process parameters such as temperature, pressure, contact time and H_2/CO ratio. Until today, there is no HAS process (from syngas) available on a commercial scale [1, 2]. As discussed in Chapter 2, higher alcohols are highly valuable products, so that the HAS process remains a major research topic of many industrial and academic research groups. It is believed that the type of active centre on the catalyst surface is a crucial factor for higher alcohol formation from syngas. In Chapter 4, the mono-metallic $La_{1-x}Sr_xCoO_3$ perovskite catalysts (x=0-0.4) have been investigated for syngas conversion and despite showing CO conversion in the high range compared to other reported catalysts, the higher alcohol yield remained low for commercial application under a wide range of Fischer-Tropsch (F-T) reaction conditions.

It was reported that the synergistic effect between two metal species in a bimetallic alloy can change the physical and chemical properties of the individual metal atoms. This finding was proven by many reported research results using different bi-metal alloy, such as Cu-Co, Cu-Fe, and Cu-Ni for HAS *via* F-T reaction [3-5]. In Chapter 5, the author found and reported for the first time that the bi-metal Co-Ni alloy in $La_{0.9}Sr_{0.1}Co_{1-y}Ni_yO_3$ perovskite catalysts had a positive effect on higher alcohol selectivity and yield, for low nickel substitution level. The experimental results established that the synergistic effect between the two metals in the Co-Ni alloy played a crucial role in enhancing the higher alcohol selectivity.

Based on the reported results in the literature and this work, it is clear that the catalytic activity of bi-metal catalysts for HAS from syngas is heavily affected by the type of each individual metal. Copper is commonly used as an active element for HAS from syngas in various types of catalysts (modified methanol synthesis catalysts, F-T synthesis catalysts, *etc*.), as it displays an ability to form C_{2+} oxygenates [3, 6]. As

mentioned in Chapter 2, Cu-based catalysts containing F-T elements such as cobalt and iron are considered as some of the most promising catalysts in HAS due to their high activity and selectivity to higher alcohols.

To further explore the synergistic effect of metals in multi-metal alloy on targeted product yield, a more complex metal alloy, Co-Ni-Cu, is used in this chapter. To date, only few tri-metallic catalysts for HAS in F-T process have been investigated. Surisetty *et al*. reported that K-promoted tri-metallic Co-Rh-Mo sulphide catalyst showed a higher $C_{2+}OH$ selectivity compared to that of the K-promoted bi-metallic Rh-Mo sulphide catalyst (31.4% vs. 24.6%) in HAS [7]. The tri-metallic catalyst had an increased amount of active centres responsible for the formation of alcohols and exhibited a positive synergistic effect between the metal species. Guo *et al*. investigated the catalytic activity of Fe-Cu-Co based catalysts with palladium promotion for HAS and revealed that the addition of small amounts of cobalt improved the Fe-Cu interaction and dispersion, and then the synergism between iron and copper ions benefited the formation of higher alcohols [8, 9]. The synergism of Fe-Cu was attributed to the formation of dual-site, with copper active for CO insertion, while iron favoured CO dissociation and chain propagation [10].

In addition to metallic effect, other efforts have been made to increase the catalytic activity and higher alcohol selectivity in HAS [11-13]. Alkali element (lithium, sodium or potassium) used as catalyst promoter showed substantial improvements in higher alcohol ($C_{2+}OH$) selectivity, as well as in prolonging the catalyst lifetime [14, 15]. Thus, alkali promoters have been widely used in different catalyst types for HAS from syngas and can even be considered as necessary for HAS [15-18] (see Chapter 2, Section 2.6.2.1). Further optimisation of reaction conditions such as temperature, H_2/CO molar ratio and gas hourly space velocity (GHSV) would also contribute to an increase in catalyst performance for HAS from syngas.

The aim of this chapter is to study the catalytic performance of a tri-metallic catalyst in HAS. In order to take advantages of the perovskite structure and three active catalytic components of F-T synthesis, namely, cobalt, nickel, and copper, a $La_{0.9}Sr_{0.1}Co_{0.8}Ni_{0.1}Cu_{0.1}O_3$ perovskite catalyst was used in this chapter. Furthermore, experimental investigations were performed to evaluate the effect of alkali (sodium and potassium) addition in the $La_{0.9}Sr_{0.1}Co_{0.8}Ni_{0.1}Cu_{0.1}O_3$ perovskite catalyst for HAS.

The most promising catalyst for HAS in this chapter was selected and used for further studies on the catalyst process parameter sensitivity and catalyst stability.

6.2 Catalytic Activity of Co-Ni-Cu-based Perovskite Catalyst for Higher Alcohol Synthesis

A tri-metal alloy $La_{0.9}Sr_{0.1}Co_{0.8}Ni_{0.1}Cu_{0.1}O_3$ perovskite catalyst was synthesised and its activity in HAS compared with the bi-metal $La_{0.9}Sr_{0.1}Co_{0.9}Ni_{0.1}O_3$ perovskite catalyst studied in Chapter 5. Catalytic activity tests were carried out in a high-pressure fixed-bed reactor (Spider 3 F-T instrument, AMTech, Germany). Detailed descriptions of the experimental procedures were given in Chapter 3. For comparison purposes, the reaction conditions were kept the same than for these tests described in Chapter 5, section 5.4 (T=275-340 °C, 3.0 MPa, H_2/CO=2, and GHSV=10995 h^{-1}). For simplified writing purpose, the acronyms LSCNC and LSCN are used in this chapter to represent $La_{0.9}Sr_{0.1}Co_{0.8}Ni_{0.1}Cu_{0.1}O_3$ and $La_{0.9}Sr_{0.1}Co_{0.9}Ni_{0.1}O_3$ catalysts, respectively.

The results in Figure 6-1 present the CO conversions at different temperature (275 to 340 °C) during a 120 hour time on stream (TOS) test for LSCNC perovskite catalyst.

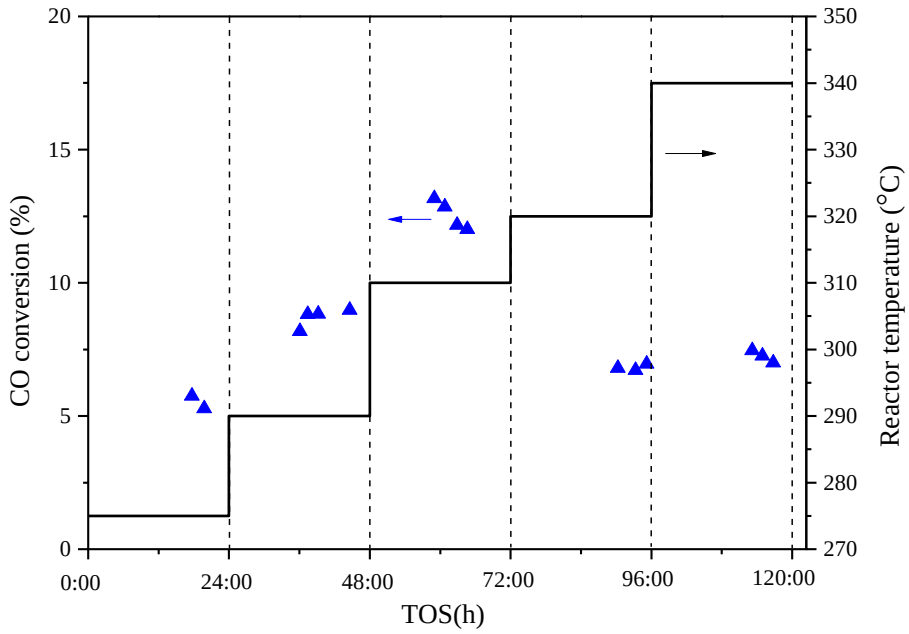

Figure 6-1. CO conversion for HAS with LSCNC perovskite catalyst, at different temperatures. Reaction conditions: P=3.0MPa, GHSV=10995 h^{-1}, and H_2/CO=2:1.

As shown in Figure 6-1, CO conversion in the HAS reaction over the prepared LSCNC perovskite catalyst increased with reaction temperature at temperatures no

more than 310°C. At reaction temperatures higher than 310°C, CO conversion decreased with increasing reaction temperatures. This result suggests that the LSCNC catalyst decayed at high temperatures (≥320°C) under reductive syngas atmosphere. Yang *et al*. [19] and Xiao *et al*. [20] reported a similar catalyst decay in Cu-contained catalysts, namely Cu-Co/TiO_2 catalyst and Cu-Fe bi-metallic catalyst for HAS from syngas, respectively. Based on their research findings, they concluded that copper containing catalysts were not suitable to operate at temperatures higher than 300°C due to the sintering of copper [5, 21]. Because of the catalyst decay, the test results of LSCNC catalyst at high temperature (320-340°C) will be excluded from any further discussions. The results of CO conversion, higher alcohol yield and alcohol distribution (C atom%) of HAS from syngas over LSCNC and LSCN catalysts at 290 and 310°C are listed in Table 6-1.

Table 6-1. Comparison of catalytic performances between LSCNC and LSCN catalysts at 290-310 °C, P=3.0 MPa, GHSV=10995 h^{-1}, and H_2/CO=2:1.

T (°C)	Catalyst	CO conv.%	Selectivity%		ROH STY $mg \cdot g_{cat}^{-1} \cdot h^{-1}$	Alcohol Distribution (C atom %)			
			CH_4	CO_2		C_1OH	C_2OH	C_3OH	$C_{4+}OH$
290	LSCNC	8.7	11.3	4.8	19.7	63.1	29.3	6.8	0.8
	LSCN	34	48.9	3.0	69.2	43.2	32.4	16.0	8.3
310	LSCNC	12.6	26.3	12.1	53.2	40.0	42.5	9.7	7.8
	LSCN	35.8	49.9	3.7	79.5	39.5	36.0	17.1	7.5

The results in Table 6-1 show that CO conversion over LSCNC catalyst (8.7% at 290°C and 12.6% at 310°C, respectively) was lower than that of the bi-metallic LSCN catalyst (34% % and 35.8% respectively). Xiao *et al.* reported a similar result when copper was added to a Co-based catalyst [3]. Due to the modification of the electronic structure of cobalt sites by copper modification, the CO dissociation ability of cobalt in Cu-Co catalyst was decreased, thus leading to lower CO conversion [5, 22]. It is well known that cobalt and nickel are the active centres for methane formation from syngas [23, 24]. As a result, the LSCN catalyst showed high methane selectivity of nearly 50%. Surprisingly, with copper substitution in the B site of the LSCN perovskite catalyst, the methane selectivity decreased dramatically (about 2 to 4 times). Similar results were also observed by Tien-thao *et al*. for Co-based catalyst, when studying higher alcohol formation in F-T process over Cu-substituted $LaCoO_3$ perovksite catalysts [24]. The suppression of methane formation with copper addition was

possibly due to the enhanced stability of the CH_x species on the surface, with copper active for chain termination and alcohol production [22, 25]. However, CO_2 selectivity of LSCNC perovskite catalyst was higher than that of LSCN catalyst, especially at 310 °C. No explanation in the literature could be found about the effect of copper on CO_2 selectivity in HAS at this stage.

As mentioned in Section 6.1, the addition of copper to HAS catalysts is expected to improve their selectivity towards higher alcohols, due to its activity in CO insertion to form alcohols [3, 10]. The ethanol distribution of LSCNC perovskite increased at temperature of 310°C. The above results suggest that the synergism between cobalt, nickel and copper had a positive effect on decreasing the formation of methane and improving the ability for ethanol formation in the F-T process. However, compared to LSCN catalyst, the space time yield (STY) of total alcohols over tri-metallic LSCNC catalyst was 72% lower at 290°C and 33% lower at 310°C. The lower alcohol STY indicates that the slight increase in ethanol formation was not enough to compensate for the decrease of CO activation ability with the addition of copper. As a result, the catalytic performance was not improved with low amount of copper addition (Co/Ni/Cu=8/1/1) as expected. Consequently, further investigations were performed, the results of which are discussed in the following sections.

6.3 Alkali-promoted Tri-metallic LSCNC Perovskite Catalysts for Higher Alcohol Synthesis

As mentioned in Section 6.1 and in Chapter 2, Section 2.6.2.1, alkali promotion is one of the most attractive methods to enhance higher alcohol selectivity and catalyst stability. In the following section, sodium and potassium are used as promoters of LSCNC perovskite catalysts ($La_{0.9}Sr_{0.1}Co_{0.8}Ni_{0.1}Cu_{0.1}O_3$) for HAS from syngas.

6.3.1 Effect of Alkali Promoters on LSCNC Perovskite Properties

In order to study the effect of promoters, the loading of sodium and potassium additives on LSCNC catalyst were kept at the same level (*ca*. 0.65 wt.%) for all tests. The specific surface area (S_{BET}) and measured metal element concentrations of the alkali-promoted perovskite catalysts are listed in Table 6-2. The S_{BET} of all the perovskite samples were rather low (below 5 m^2/g) due to the high calcination temperature (800 °C) [26]. At this low surface area and with only small change in

alkali concentration between sodium and potassium-promoted catalyst, it is expected that the catalysts' performance were not affected by the S_{BET}.

Table 6-2. Physical properties of the perovskite catalysts with/without alkali addition.

Samples	Surface area (m^2/g)	Alkali loading (wt.%)
Na-LSCNC	3.35	0.67
K-LSCNC	1.59	0.64
LSCNC*	1.75	-

* LSCNC exact elemental composition: $La_{0.87}Sr_{0.13}Co_{0.8}Ni_{0.11}Cu_{0.09}O_3$.

The XRD patterns of the fresh alkali-promoted catalysts Na-LSCNC and K-LSCNC and the non-promoted LSCNC catalyst are presented in Figure 6-2. The sharp and clear peaks of the perovskite structure were obtained for all three catalysts after calcination at 800°C, indicating that the alkali additives did not alter the catalysts' crystallographic structure. Only small reflections were found in the perovskite catalysts, which can be assigned to Co_3O_4. No significant reflection lines of alkali metals could be seen in the promoted catalysts, most likely due to the low promoter content, which is below the XRD detection limit.

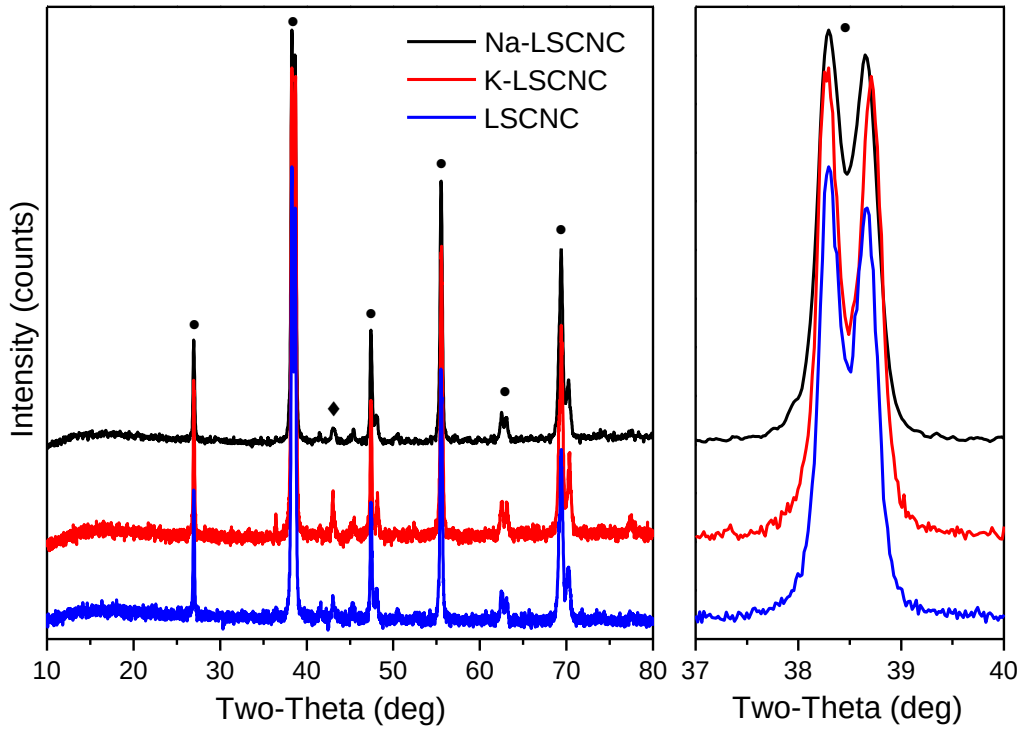

Figure 6-2. X-ray diffraction patterns of alkali-promoted LSCNC perovskite catalysts (left) full pattern, (right) zoom in on the perovskite peak range. Phases: (●) Perovskite, (♦) Co_3O_4.

In order to study the phase change of alkali-promoted LSCNC catalysts in the reduction process, the X-ray patterns of all the samples reduced at 450 °C for 1 h are shown in Figure 6-3.

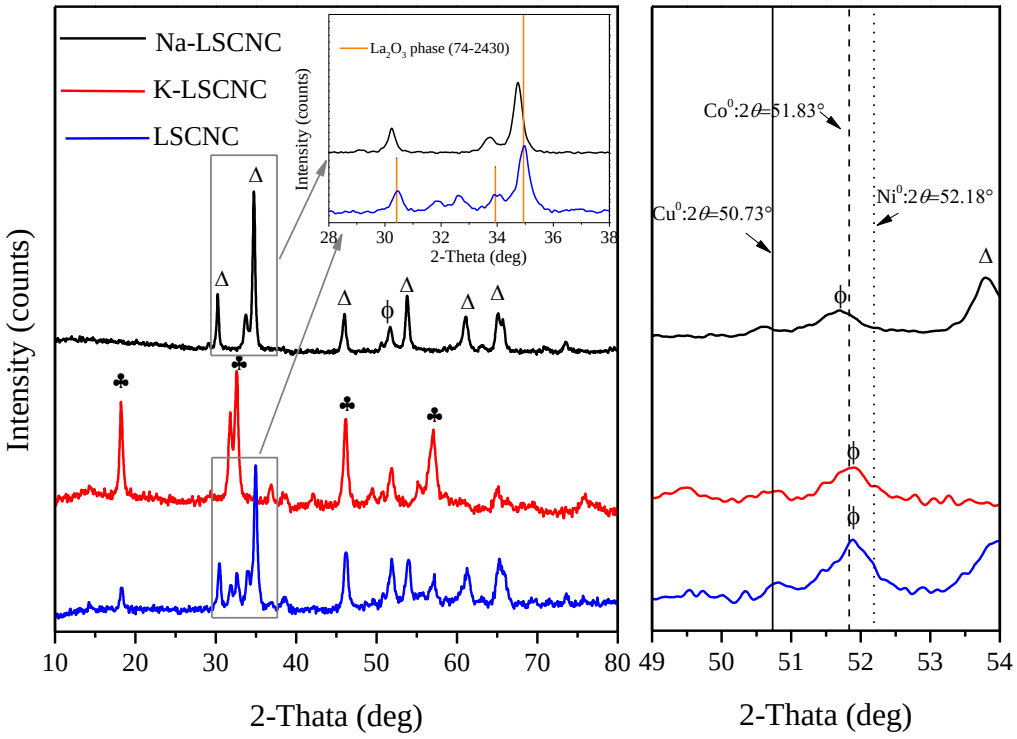

Figure 6-3. X-ray diffraction patterns of alkali-promoted LSCNC perovskite catalysts after reduction at 450 °C (left) full pattern, (right) zoom in on the metallic peak range. Phases: (Δ) La_2O_3, (♣) La_2SrO_x, and (ϕ) Co-Ni-Cu alloy.

Upon reduction at 450 °C, the perovskite structure in the 2θ range of 38-39° had disappeared for all catalysts, and La_2O_3 (JCPDS-ICDD 74-2430) and La_2SrO_x (JCPDS-ICDD 42-0343) phases were formed, as observed in the previous chapter (see Chapters 5, Section 5.2). However, while both phases were observed on the unpromoted LSCNC, only the La_2O_3 phase was observed for Na-LSCNC, and the La_2SrO_x phase for K-LSCNC. The diffraction peaks of the LSCNC catalyst matched the standard La_2O_3 phase very well (see Figure 6-3 inset), while the diffraction lines of the Na-LSCNC catalyst were slightly shifted to lower 2θ values.

In addition, multi-metallic phases were detected for all the reduced catalysts. The typical diffraction lines of metallic cobalt (JCPDS-ICDD 15-0806), nickel (JCPDS-ICDD 04-0850) and copper (JCPDS-ICDD 04-0836) are 51.83°, 52.18° and 50.73°, respectively. In Figure 6-3 (right), a diffraction peak was observed between pure

cooper and nickel diffraction lines, located at 51.86° for each catalyst (except Na-LSCNC at 51.60°). In Chapter 5, Section 5.2.2, the Co-Ni alloy that was formed in $La_{0.9}Sr_{0.1}Co_{1-y}Ni_yO_3$ (y=0.1 and 0.5) catalysts during the reduction showed a XRD diffraction peak at 52°. Compared to the Co-Ni alloy, the diffraction peak in this study was slightly shifted to the left, closer to the cobalt diffraction line (even past it for Na-LSCNC catalyst). The shift in 2θ values was due to the incorporation of copper to cobalt and nickel (see Table 6-2), indicating the formation of a tri-metallic alloy in the reduction process. It should be mentioned that the shift in 2θ values between the Co-Ni alloy and the Co-Ni-Cu alloy is small due to the low amount of copper in the catalyst. This can be related to the results of Lua *et al*. who reported that the reduction of Ni-Cu-Co oxalate hydrate produced a Ni-Cu-Co alloy [27].

Figure 6-4 shows the H_2-TPR profiles of the perovskite samples. All the catalysts showed multiple peaks, indicating that multi-step reduction occurred. The reduction of Co^{3+} to Co^{2+}, Ni^{3+} to Ni^{2+} and Cu^{2+} to Cu^0 were responsible for the signal appearing around 340°C [24, 28]. The second peak above 450°C (except for LSCNC, 400°C) can be attributed to the reduction of Co^{2+} to Co^0 and Ni^{2+} to Ni^0 (note that these species were not observed on the XRD spectra, as the reduction was performed at 450°C). For the non-promoted perovskite catalyst LSCNC, the reduction process started at 200°C, which was much lower than that of the LSCN perovskite catalyst (Chapter 5, Section 5.2.2). It was reported that for Cu-Co perovskite precursor, copper acted as a reduction promoter, leading to enhanced cobalt reduction in the catalyst at relatively lower temperatures [13, 28]. Tien-Thao *et al*. hypothesized that copper diffused toward the catalyst surface and acted as a catalyst for hydrogen dissociation under reduction conditions. This caused the decrease of the Co^{3+} reduction temperature, particularly for the cobalt species on the grain boundaries [24, 29]. It is expected that the copper in the tri-metal alloy perovskites should play the same role as reduction promoter and lead to a shift of LSCNC reduction towards lower temperature.

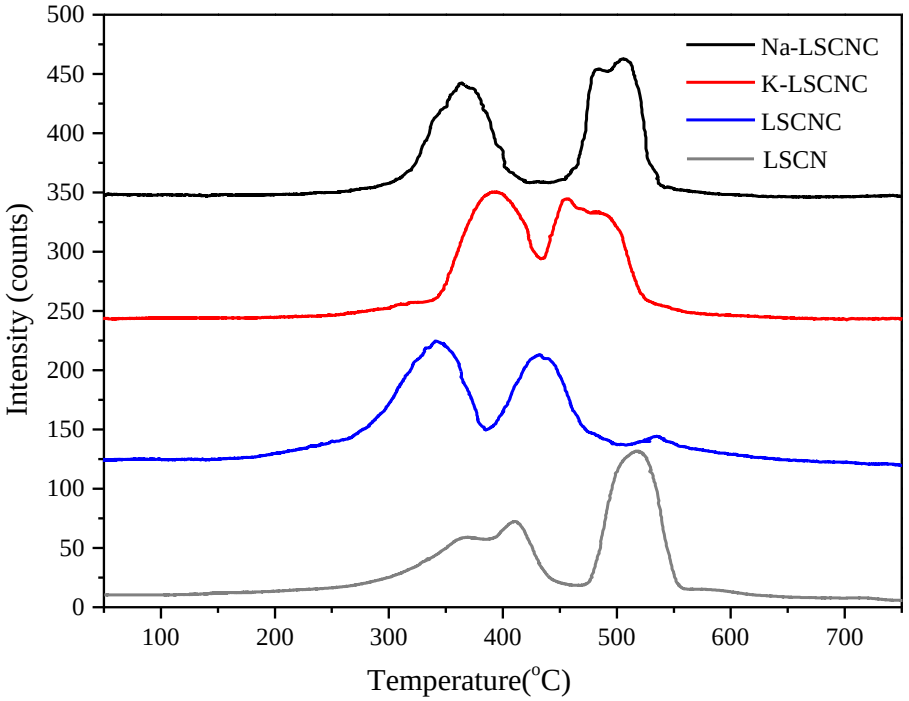

Figure 6-4. TPR profiles of alkali-promoted LSCNC perovskite catalysts.

In contrast, with the presence of alkali elements (sodium and potassium), the catalyst reduction peaks shifted to higher temperatures compared to catalyst LSCNC, as shown in Figure 6-4. The result indicates that the metallic Co^{3+}, Ni^{2+} and Cu^{2+} were more difficult to reduce in the presence of alkali metal. Similar results for bi-metal catalysts were found by Tien-Thao *et al*. [15], Dalmon *et al.* [22] and Sun *et al*. [30]. In addition, the H_2 consumption of the investigated catalysts during the reduction was lower for the alkali-promoted catalysts than for the LSCNC catalyst (Figure 6-5). Therefore, alkali promoters not only increased the catalyst reduction temperature but also decreased the extent of the reduction. Based on the TPR and H_2 consumption results, K-promoted catalyst was easier to reduce than sodium-promoted catalyst.

Alkali metals are considered as electronic promoters, which suppress the H_2 chemisorption on the catalyst surface, resulting in the difficulty of reducing metal oxides species [18, 31]. In other words, the addition of alkali metals tend to prevent the phase transformation of the catalyst [32]. The lower the H_2 consumption, the less metal oxide reduced to form active centre, thus it is expected that CO conversion might be affected with alkali-promoted catalysts.

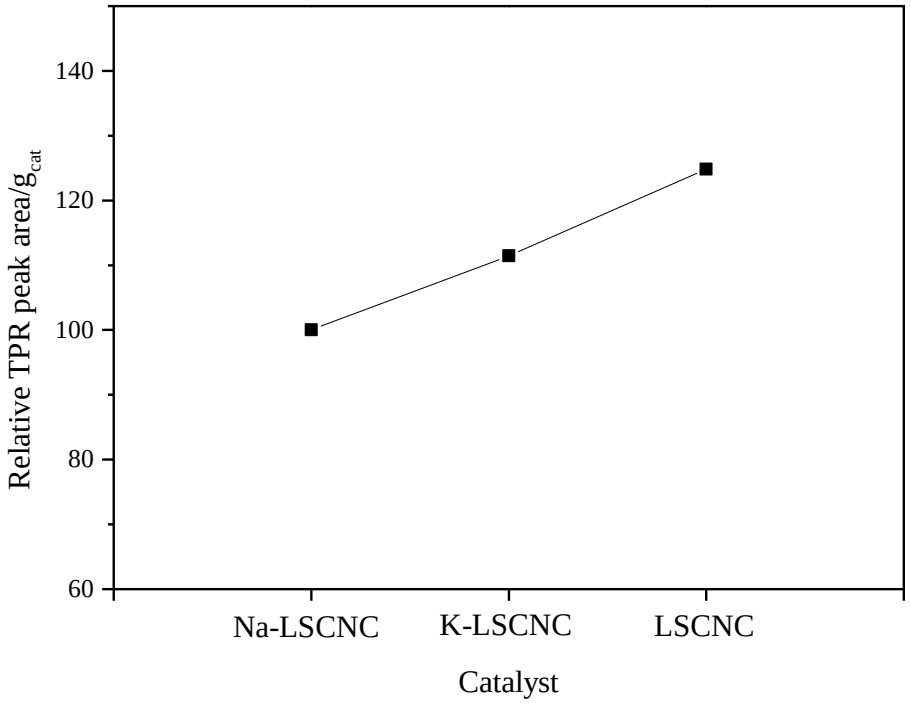

Figure 6-5. Relative total TPR peak area/g_{cat} (TPR peak area of perovskite catalyst/TPR peak area of Na-LSCNC×100, per gram of catalyst).

6.3.2 Effect of Alkali Promoters on Catalytic Activity for HAS

A series of HAS tests at different temperatures between 275 and 340 °C were carried out in 120 h test using the alkali-promoted LSCNC catalysts. After *in-situ* reduction as described in Chapter 3, the promoted catalysts were first tested at the lowest reaction temperature of 275°C, then it was increased by 20°C for each further test (except 310 and 340°C). The results of the CO conversion over the alkali-promoted LSCNC catalysts are given in Figure 6-6.

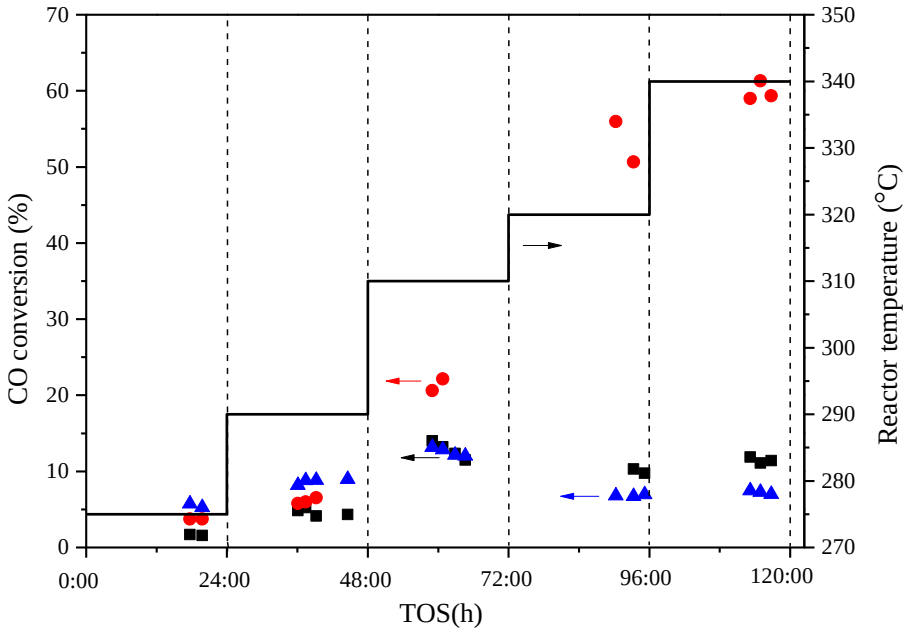

Figure 6-6. CO conversion for HAS with alkali-promoted LSCNC perovskite catalysts, at different temperatures (same reaction conditions as for Figure 6-1): (▲) LSCNC, (■) Na-LSCNC, and (●) K-LSCNC.

As shown in Figure 6-6, CO conversion was strongly depends on the kind of promoters. At low reaction temperatures (<310 °C), Na- and K-promoted LSCNC catalysts displayed lower CO conversions compared to that of the un-promoted catalyst. This result can be explained by the previous observations, that the reduction ability and active centre formation decreased with alkali promotion (see XRD and TPR results in Figure 6-3 and Figure 6-4). However, interesting catalyst behaviours were observed at higher reaction temperatures (≥310°C). CO conversion over the Na-LSCNC catalyst remained constant with increasing temperatures within the range of 310-340 °C. In contrast, CO conversion of K-promoted catalyst increased with increasing temperature and reached the maximum of 60% at 340°C. This is supported by the TPR results, demonstrating that the K-promoted catalyst had a higher reducibility compared to the Na-LSCNC one. As discussed before, the low CO conversion at high temperature observed for the LSCNC catalyst can be attributed to catalyst decay (see Section 6.2). On the other hand, no significant deactivation was observed for the K-LSCNC catalyst within 120 h time on stream, indicating that the addition of potassium prevented the catalyst deactivation, stabilized the catalyst and prolonged the catalyst lifetime.

Alkali-promoted catalysts after reaction at 340°C were also analysed by XRD and the results are given in Figure 6-7.

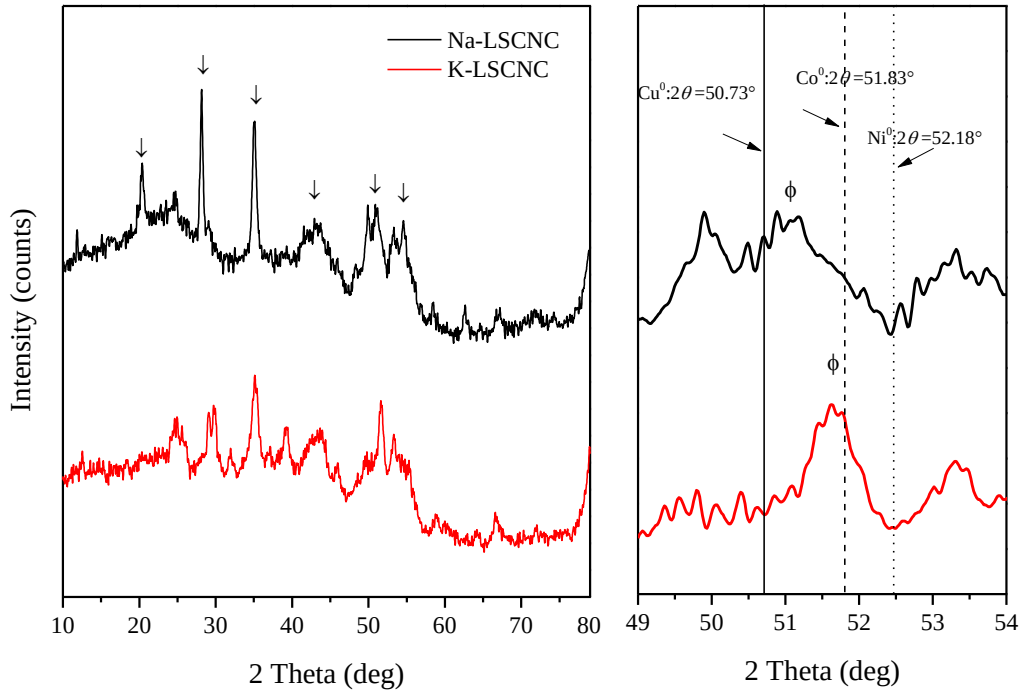

Figure 6-7. X-ray diffraction patterns of alkali-promoted LSCNC perovskite catalysts after reaction (left) full pattern, (right) zoom in on the metallic peak range. Phases: (↓) $LaCO_3OH$ and (ϕ) Co-Ni-Cu.

As with our previous observations, the diffraction peaks of the previously detected La_2O_3 and La_2SrO_x have disappeared in the used catalysts, and are believed to transform into $LaCO_3OH$ (JCPDS-ICDD 26-0815) during the F-T reaction (see Chapter 5, Section 5.3.1). In addition, it was previously observed that for the LSCN catalyst, phase separation occurred after reduction, and Co^0 and Ni^0 peak were observed (see Chapter 5, Figure 5-7). In this instance, no phase separation was observed in the alkali-promoted LSCNC catalysts after reaction. This is consistent with the previous observation that the addition of alkali metals tend to stabilize and prevent the phase transformation of the catalyst [32]. For alkali-promoted catalysts, the diffraction peaks of the Co-Ni-Cu tri-metallic alloy shifted towards lower 2θ value, with a shift more important for Na-LSCNC than for K-LSCNC. Taking the lower activity of the Na-LSCNC catalyst at higher reaction temperatures into account, it is reasonable to assume that the copper species were aggregated inside the Co-Ni-Cu alloy for this catalyst, leading a peak shift towards the metallic copper diffraction line.

The STY of higher alcohols as a function of reaction temperature for all the three investigated catalysts are given in Figure 6-8.

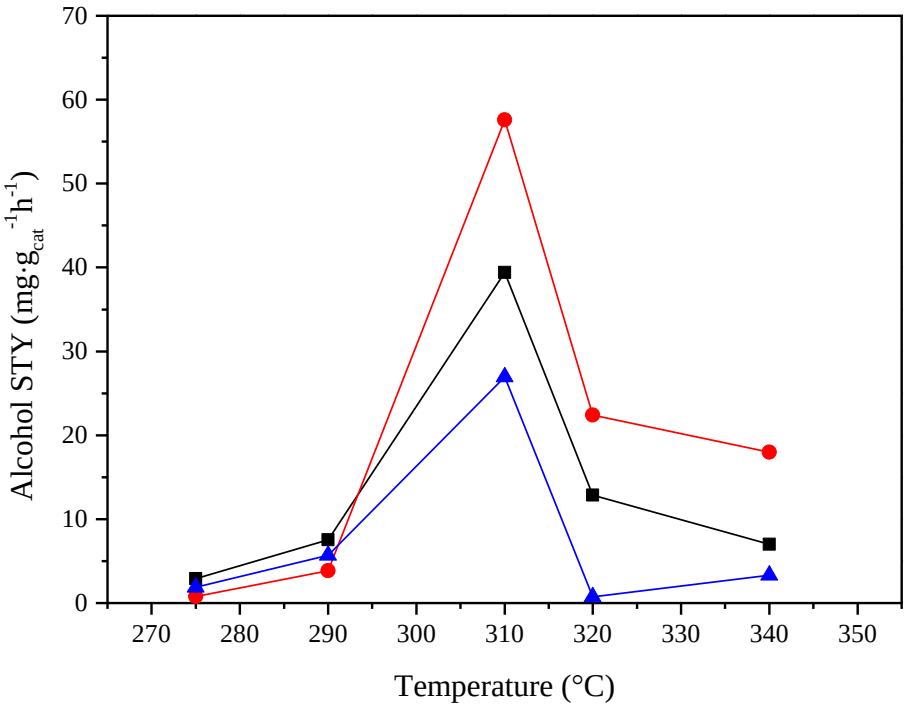

Figure 6-8. Higher alcohol STY for HAS with alkali-promoted LSCNC perovskites (same reaction conditions as for Figure 6-1): (■) Na-LSCNC, (●) K-LSCNC and (▲) LSCNC catalysts.

The higher alcohol STY of all catalysts were very low at 275°C and increased with increasing reaction temperatures to 310°C, where they reached a maximum. The maximal higher alcohol STY remained constant during the 24 h test at this temperature. In order to study the sensitivity of higher alcohol formation to reaction temperature, the reaction temperature was increased further to 320°C. A big drop of higher alcohol STY was detected for all catalysts and beyond this temperature, a gradual decrease was observed with further increasing temperatures. As previously noted in this work (see Chapter 5, Section 5.4) and by previous authors [15, 33], the formation of higher alcohols from syngas over multi-metals catalysts is very sensitive to the temperature and optimum yields occurred in a narrow temperature range.

In addition, the kind of alkali metals used to promote LSCNC catalyst affects the higher alcohol STY. As shown in Figure 6-8, at lower reaction temperatures (< 310 °C), the K-promoted catalyst K-LSCNC has the lowest higher alcohol STY compared to the other catalysts, likely due to the lower reducibility level and less active centres formed after *in-situ* reduction at 450°C before the catalyst performance test, as

explained in Section 6.3.1. As the reaction temperatures increased (≥310°C), the alkali-promoted catalysts displayed higher $C_{2+}OH$ STY than the un-promoted LSCNC catalyst. It can be assumed that these catalysts were further reduced under reduction environment during the F-T reaction to form more active centres, whereas the LSCNC catalyst was decayed at high temperature, as mentioned before. At the reaction temperature of 310°C, the K-promoted catalyst has the highest $C_{2+}OH$ STY, confirming that potassium is an essential promoter for maintaining the Co-Ni-Cu active centre (see Figure 6-7), which is responsible for higher alcohol selectivity improvement in HAS process. Tien-Thao *et al*. reported a similar effect of potassium promoter on alcohol formation over bi-metal Co-Cu catalysts [33].

At low temperature (≤310°C), the three investigated catalysts showed similar methane yields, increasing with reaction temperatures (see Figure 6-9). At higher temperatures (>310°C), different catalysts behave differently. As discussed in session 6.2, the un-promoted LSCNC perovskite catalyst decayed at high temperature due to sintering, resulting in low CO conversion and alcohols and methane formation. For Na-promoted LSCNC catalyst, only a small increase in methane formation can be detected within the temperature range of 310 °C to 340°C. This result is supported by the previous finding suggesting that Na-LSCNC catalyst was not sensitive to the reaction temperature (see Figure 6-6). In contrast, the K-promoted LSCNC catalyst was very active and methanation became predominant as expected at higher temperature range (see Figure 6-9).

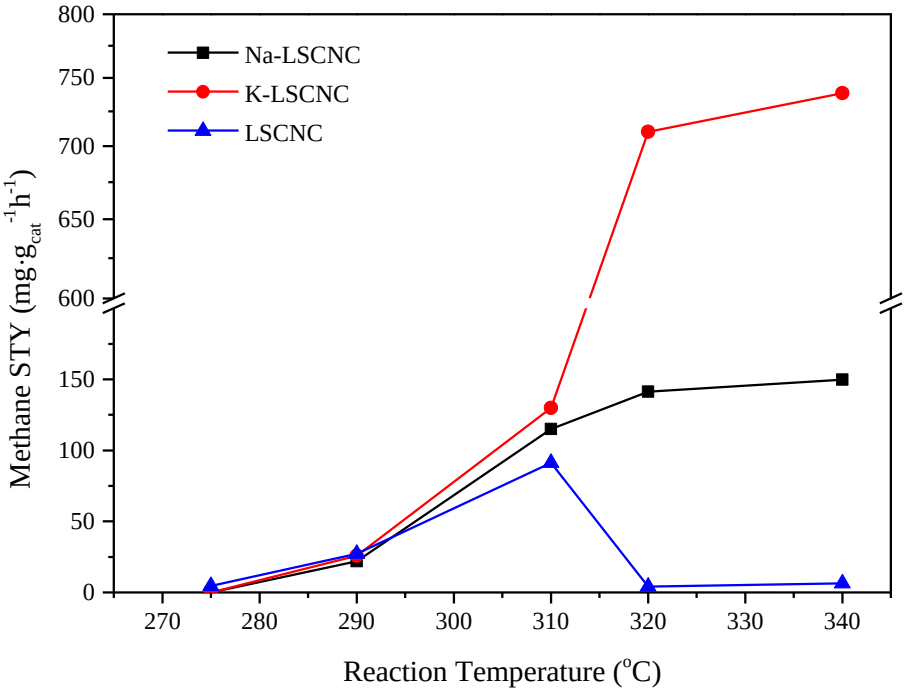

Figure 6-9. Methane STY as a function of reaction temperature for HAS with alkali-promoted LSCNC perovskite catalysts (same reaction conditions as for Figure 6-1).

Given the unpromoted catalyst decay at high temperature, the catalysts' performances at the optimal temperature of 310 °C was used for further discussion in this chapter. The measured results obtained under steady state conditions are summarized in Table 6-3.

Table 6-3. Performance of alkali-promoted LSCNC perovskite catalysts in HAS at 310 °C.

Catalyst	CO conv. %	ROH STY mg·g$_{cat}^{-1}$·h^{-1}	Alcohols Distribution (C atom %)				CO_2 Selectivity %
			C_1OH	C_2OH	C_3OH	$C_{4+}OH$	
Na-LSCNC	12.8	68.7	33.6	45.7	11.2	9.6	18.4
K-LSCNC	21.4	83.1	22.9	49.4	14.0	13.6	16.7
LSCNC	12.6	53.2	40.0	42.5	9.7	7.8	12.1

The results in Table 6-3 show that not only the STY of total alcohols obtained for the K-LSCNC catalyst was much higher than that of the Na-LSCNC and LSCNC perovskite catalysts, but also a very different alcohol distribution can be observed. The ethanol and higher alcohol percentage were 49.4% and 77.1%, respectively, which were much higher than those for the other catalysts. A positive change with the Na-promoted catalyst was also observed but it appears less markedly. The XRD analysis results in Figure 6-3 has indicated that with the modification of alkali metals, the active

centres of Na-LSCNC and K-LSCNC catalysts were the Co-Ni-Cu alloy, similar to that of the un-promoted LSCNC catalyst. As mentioned in Chapter 2, although alkali metals are not active for alcohols formation, they can effectively lead to a change in the alcohol distribution, which might be due to the basicity of the alkali metal that improves the stability of the CH_x intermediate species to prolong the carbon chain [15, 34].

6.4 Further investigations into K-Promoted Tri-metallic Co-Ni-Cu Catalyst for HAS

6.4.1 Effect of Reaction Temperatures on Higher Alcohol Product Distribution

As discussed in Section 6.3.2, K-LSCNC perovskite catalyst displayed a better higher alcohol selectivity and yield among all the tested catalysts. To provide further insights into the K-LSCNC catalyst, the effect of reaction temperature on the synthesis of higher alcohols was investigated. In this section, the reaction temperature was varied between 275°C and 340°C, and the experiments were carried out using the same operating conditions in Section 6.2 (P=3.0 MPa, GHSV=10995 h^{-1} and H_2/CO=2:1).

The results in Figure 6-10 show that at lower reaction temperatures (275-290 °C), methanol was the main product among all the alcohols (84.1% and 64%, respectively). When the temperature was increased to 310°C, the higher alcohol percentage increased from 36% to 77.1%. Especially, a significant increase in ethanol was detected (from 28.3% to 49.4%). At higher reaction temperatures (>310 °C), the ethanol amount remains fairly constant. The amount of propanol and $C_{4+}OH$ alcohols increased clearly with increasing temperature within the range 310°C to 340°C. The highest higher alcohol fraction reached approximately 83.5% at 340°C. This suggests that high reaction temperature favours the formation of higher alcohols from syngas over tri-metallic K-LSCNC catalyst. A similar temperature effect was also found by Liu and co-workers when they studied alcohols formation from syngas over Cu/Zn/Al catalyst [35]. Based on their finding, they proposed that high temperature facilitates the cleavage of C-O bonds, so that it enhances higher alcohol formation. Though high reaction temperatures shifted the alcohol distribution to $C_{2+}OH$ (320°C and 340°C), the alcohol yield was much lower than that at 310°C (see Figure 6-8). Thus, 310 °C is the optimal temperature for higher alcohol production over K-LSCNC catalyst.

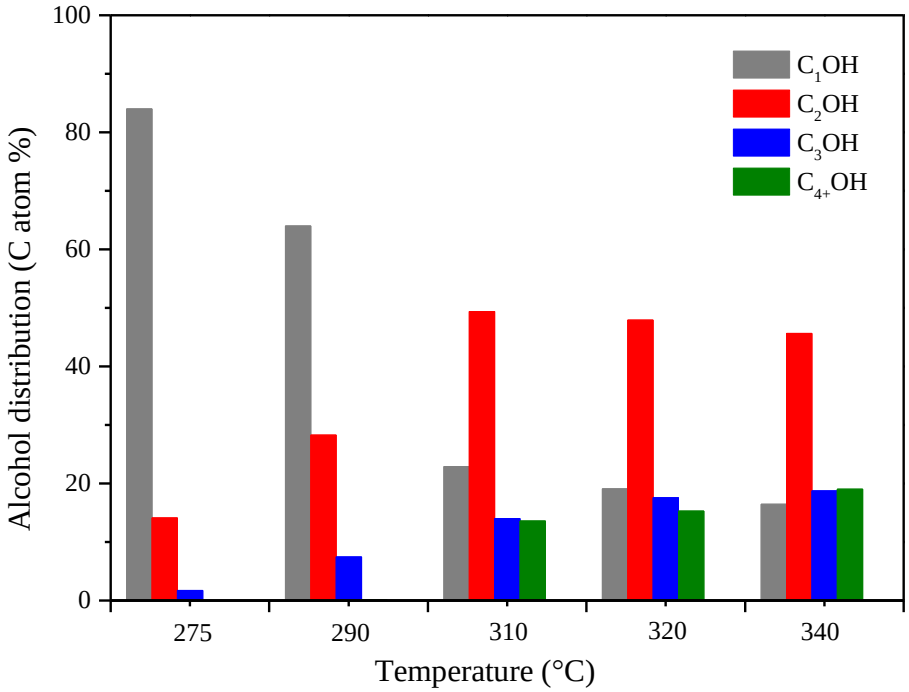

Figure 6-10. Alcohol distribution as a function of reaction temperatures for the K-LSCNC perovskite catalyst Reaction conditions: 275-340 °C, 3.0 MPa, GHSV=10995 h^{-1}, and H_2/CO=2:1.

6.4.2 Effect of H_2/CO ratio on Higher Alcohol Product Distribution

Apart from reaction temperature, H_2/CO ratio is also recognised as an important reaction parameter that has pronounced influence on HAS from syngas [34]. In this section, three experiments were carried out at different H_2/CO ratio of 1.5, 2 and 3. The reactions were kept at stable conditions for at least 12 hours for each condition (310°C, 3.0 MPa, and GHSV=21990 h^{-1}) before the product samples were analysed. The analysis results are given in Table 6-4.

Table 6-4. Effect of H_2/CO ratio on higher alcohol synthesis over K-LSCNC catalyst at 310°C, 3.0 MPa, and GHSV=21990 h^{-1}.

H_2/CO Ratio	CO conv. %	ROH STY[1]	Alcohols Distribution (C atom %)				CH_4 sel. %	CO_2 sel. %
			C_1OH	C_2OH	C_3OH	$C_{4+}OH$		
1.5	9.9	5.4	44.9	46.0	9.0	0.0	10.1	3.8
2	10.1	20.4	33.1	44.2	10.6	12.1	22.9	6.1
3	15.3	7.6	46.2	43.7	8.3	1.8	29.8	3.5

[1] ROH STY: $mg.g_{cat}^{-1}h^{-1}$

As expected, the CO conversion increased with increasing H_2/CO ratio. The catalyst performance at H_2/CO ratio of 1.5 was very low as the targeted alcohol product

STY only reached 5.43 $mg \cdot g_{cat}^{-1} \cdot h^{-1}$, much lower than that of the other tests. With the H_2/CO ratio of 3, CO conversion reached the highest level in this experiment series. Unfortunately, a substantial increase in the selectivity to methane was detected. Similar results were observed by other researchers for HAS from syngas over $LaCo_{0.7}Cu_{0.3}O_3$ perovskite catalyst [33]. According to Equation (2-8) in Chapter 2, an H_2/CO ratio of 2 is ideal for alcohol formation. With the H_2/CO ratio of 2, the total alcohol STY reached the highest level and methanol fraction was much lower than for other ratio. Mechanistically, with a lower H_2/CO ratio (below 2) the partial pressure of CO is higher, which favours CO insertion and carbon chain growth, thus heavier products formation [36, 37]. However, the low H_2/CO ratio also promotes coke formation, which is not ideal for HAS. With increasing H_2/CO ratio (above 2), the partial pressure of H_2 increased, resulting in the formation of C_1 product, such as methane and methanol [38]. Consequently, the H_2/CO ratio of 2 was the optimal ratio for higher alcohol production.

6.4.3 Catalytic Stability of K-LSCNC Perovskite

As discussed above in this chapter, K-LSCNC perovskite catalyst displayed the highest targeted product selectivity and yield among all the tested catalysts at optimal reaction temperature of 310°C, and H_2/CO ratio of 2. The results in section 6.3.2 showed that the K-promoted catalyst had unnoticeable catalyst deactivation within a 120 h reaction time in a bench scale reactor system (Spider 3F-T instrument; Chapter 3, Section 3.5.1.2). As mentioned in Chapter 2, Cu-containing catalysts have a high potential to deactivate because of copper sintering. In order to investigate the stability of K-LSCNC perovskite catalyst ($K\text{-}La_{0.9}Sr_{0.1}Co_{0.8}Ni_{0.1}Cu_{0.1}O_3$) in HAS, long-term experiments were carried out in a larger gas processing rig (Syncat Facility Gas Processing Rig (CSIRO); Chapter 3, Section 3.5.1.3) at 310° C, 3.0 MPa and H_2/CO ratio at 2. The stability of the K-LSCNC perovskite catalyst was examined after the initial induction period of approximately 14 h.

The CO conversion at different GHSV (4970-15420 h^{-1}) during a 245 h test and the corresponding catalytic bed temperature (middle of the catalytic bed) are presented in Figure 6-11. The 24 h cyclic variations observed on the catalytic bed temperature (and to a lower extent on the CO conversion) were due to variations in the feed gases temperatures, as the feed gases were stored outside and no pre-heater was used prior

to the reactor, hence some variation between night and day temperatures (the experiment was conducted in winter). However, for each stage of the experiment, these variations remained within ±3°C.

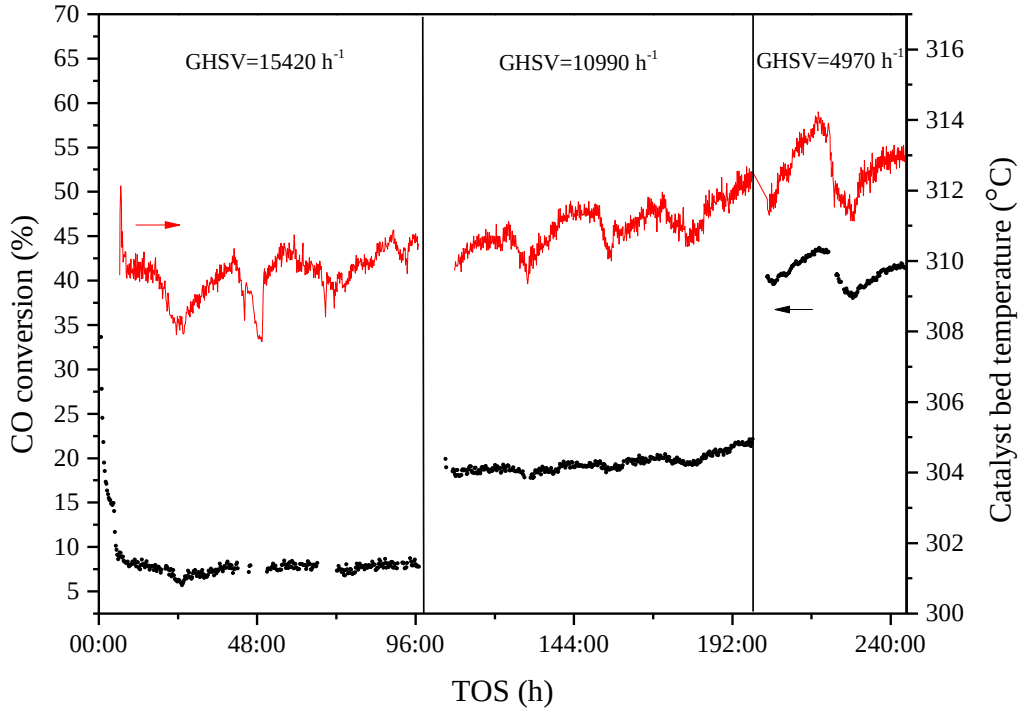

Figure 6-11. CO conversion and varication of catalyst bed temperature over K-LSCNC perovskite catalyst as a function of time on stream. Reaction condition: T=310°C, P=3.0 MPa, and H_2/CO =2:1.

The catalyst stability test started at a high GHSV (15420 h^{-1}). No catalyst deactivation could be observed within the first 97 h of the run, as the measured CO conversion was *ca*. 8% and remained within ±1% throughout this period. Following the first stage, the second stage was carried out at a lower GHSV (10990 h^{-1}) for another time period of 103 h. As expected, with the decrease of the GHSV, the CO conversion jumped to 20%±2%. It should be noted that there was a small increase of about 2% of CO conversion at the end of the second test, due to a slight temperature increasing of the catalyst bed. After the second stage, the feed flow rate was further reduced in the final stage (GHSV=4970 h^{-1}) and CO conversion reached 40.8±3% (average over the period). During this 48 h stage, similar CO conversion cycles were observed. In this stage, cyclic variations in the feed gases temperatures had a more pronounced cyclic effect on the variations in the catalytic bed temperature due to the lower GHSV, and hence on the CO conversion. The results in this section demonstrated that the catalyst did not deactivated after a 245 h test. Furthermore, the

catalytic activity of K-LSCNC catalyst is very sensitive to the GHSV and reaction temperature.

The non-condensable CH_4 and CO_2 gases were analysed during the 245 h test. In order to minimise the unavoidable fluctuation errors, at least 40 samples were analysed and the average values are given in Figure 6-12. The selectivity for both CH_4 and CO_2 remained almost constant for each GHSV, during each stage of the experiment. The decrease of feed gas flow rate (GHSV) resulted in a gradual increased contact time, which led to an increase in CO conversion and CH_4 selectivity [33]. However, CO_2 selectivity showed an opposite trend. The results of alcohol products were not presented due to their low amount, too small for accurate analysis.

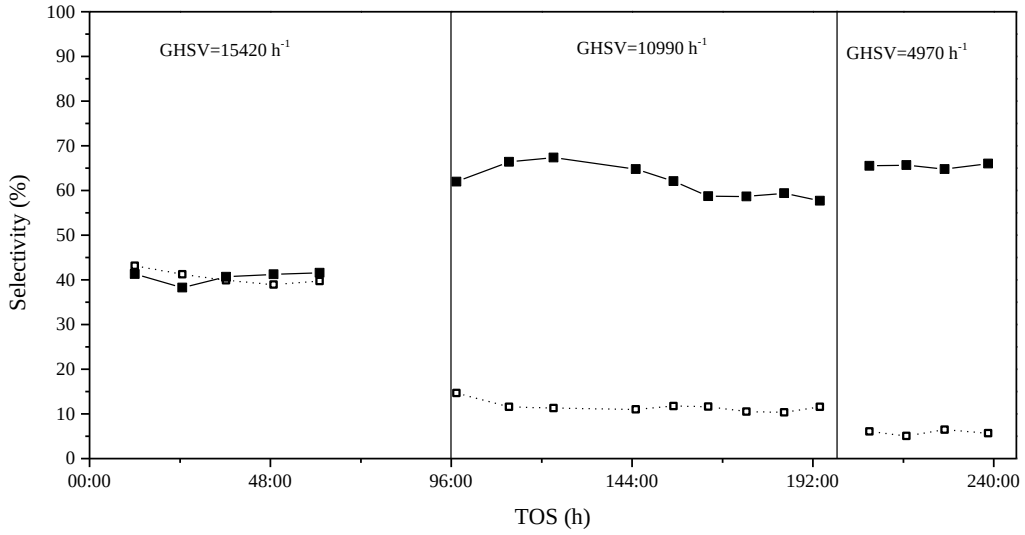

Figure 6-12. Higher alcohol STY and CH_4, CO_2 selectivity over K-LSCNC perovskite catalyst as a function of time on stream under different GHSV (same reaction conditions as for Figure 6-11): (--■--) CH_4 selectivity and (••□••) CO_2 selectivity. Each point represent the average of about 40 samples (~10 h).

6.5 Conclusion

In this chapter, the HAS over tri-metallic $La_{0.9}Sr_{0.1}Co_{0.8}Ni_{0.1}Cu_{0.1}O_3$ (LSCNC) perovskite catalyst was investigated. With the addition of copper, CO conversion and alcohol STY over tri-metallic Co-Ni-Cu catalyst was lower than that of Co-Ni catalyst in F-T reaction and catalyst decay occurred beyond 310°C. Addition of copper to the catalyst reduced its CO dissociation ability, hence the decreased activity of the tri-metallic LSCNC catalyst. However, the synergetic effect between the three metals had

a positive effect on increasing ethanol distribution, indicating that tri-metallic LSCNC catalyst has the potential to produce $C_{2+}OH$ at optimal conditions.

Two alkali metals (sodium and potassium) were used to promote the LSCNC perovskite catalyst. The effect of these promoters on the active centre properties and catalytic activities were studied carefully. The addition of alkali metals reduced the catalyst reducibility. The introduction of sodium in the tri-metallic catalyst did not improve the catalytic activity and prevented catalyst decay. In contrast, the addition of potassium improved the higher alcohol selectivity and yield in the F-T process significantly. Furthermore, the potassium promoter stabilized the catalyst and potentially prevented catalyst deactivation during the reaction, which was responsible for improving the higher alcohol formation. In addition, reaction temperature is one of the key parameters affecting the alcohol production not only quantitatively but also qualitatively. The effect of other reaction conditions, such as H_2/CO and GHSV were also investigated in this study. K-LSCNC perovskite catalyst showed excellent reaction stability for HAS from syngas, with no deactivation observed after more than 240 h TOS, suggesting that potassium is not only a promoter for HAS but also a catalyst stabiliser.

References

[1] V.S. Dorokhov, M.A. Kamorin, N.N. Rozhdestvenskaya, V.M. Kogan, Comptes Rendus Chimie, 19 (2016) 1184-1193.

[2] K. Fang, D. Li, M. Lin, M. Xiang, W. Wei, Y. Sun, Catalysis Today, 147 (2009) 133-138.

[3] K. Xiao, X. Qi, Z. Bao, X. Wang, L. Zhong, K. Fang, M. Lin, Y. Sun, Catalysis Science & Technology, 3 (2013) 1591-1602.

[4] K. Xiao, Z. Bao, X. Qi, X. Wang, L. Zhong, K. Fang, M. Lin, Y. Sun, Chinese Journal of Catalysis, 34 (2013) 116-129.

[5] J. Su, Z. Zhang, D. Fu, D. Liu, X.-C. Xu, B. Shi, X. Wang, R. Si, Z. Jiang, J. Xu, Y.-F. Han, Journal of Catalysis, 336 (2016) 94-106.

[6] W. Mao, H. Ma, H. Zhang, Q. Sun, W. Ying, D. Fang, Catalysis Letters, 142 (2012) 1098-1106.

[7] V.R. Surisetty, A.K. Dalai, J. Kozinski, industrial & Engineering Chemistry Research, 49 (2010) 6959-6963.

[8] H. Guo, H. Zhang, F. Peng, H. Yang, L. Xiong, C. Huang, C. Wang, X. Chen, L. Ma, Applied Clay Science, 111 (2015) 83-89.

[9] H. Guo, L. Xiong, X. Chen, C. Luo, Y. Chen, Acta Physica Sinica -Chinese Edition- 27 (2011) 2632-2638.

[10] A. Kiennemann, A. Barama, S. Boujana, M.M.Bettahar, Applied Catalysis A: General, 99 (1993) 175-194.

[11] Y. Fang, Y. Liu, L. Zhang, Applied Catalysis A: General, 397 (2011) 183-191.

[12] G. Liu, Y. Geng, D. Pan, Y. Zhang, T. Niu, Y. Liu, Fuel Processing Technology, 128 (2014) 289-296.

[13] T. Niu, G.L. Liu, Y. Chen, J. Yang, J. Wu, Y. Cao, Y. Liu, Applied Surface Science, 364 (2016) 388-399.

[14] R. Suárez París, V. Montes, M. Boutonnet, S. Järås, Catalysis Today, (2014) 294-303.

[15] N. Tien-Thao, M. Hassanzahediniaki, H. Alamdari, S. Kaliaguine, Journal of Catalysis, 245 (2007) 348-357.

[16] L. Tan, G. Yang, Y. Yoneyama, Y. Kou, Y. Tan, T. Vitidsant, N. Tsubaki, Applied Catalysis A: General, 505 (2015) 141-149.

[17] V.R. Surisetty, A.K. Dalai, J. Kozinski, Applied Catalysis A: General, 393 (2011) 50-58.

[18] A.-M. Hilmen, M. Xu, M.J.L. Gines, E. Iglesia, Applied Catalysis A: General, 169 (1998) 355-372.

[19] Y. Yang, X. Qi, X. Wang, D. Lv, F. Yu, L. Zhong, H. Wang, Y. Sun, Catalysis Today, 270 (2015) 101-107.

[20] K. Xiao, Z. Bao, X. Qi, X. Wang, L. Zhong, K. Fang, M. Lin, Y. Sun, Journal of Molecular Catalysis A: Chemical, 378 (2013) 319-325.

[21] V.R. Surisetty, A.K. Dalai, J. Kozinski, Applied Catalysis A: General, 404 (2011) 1-11.

[22] J.A. Dalmona, P. Chaumetteb, C. Mirodatosa, Catalysis Today, 15 (1992) 101-127.

[23] K. Shimura, T. Miyazawa, T. Hanaoka, S. Hirata, Journal of Molecular Catalysis A: Chemical, 407 (2015) 15-24.

[24] N. Tien-Thao, H. Alamdari, M.H. Zahedi-Niaki, S. Kaliaguine, Applied Catalysis A: General, 311 (2006) 204-212.

[25] N.D. Subramanian, G. Balaji, C.S. Kumar, J.J. Spivey, Catalysis Today, 147 (2009) 100-106.

[26] M. Ao, G.H. Pham, V. Sage, V. Pareek, Journal of Molecular Catalysis A: Chemical, 416 (2016) 96-104.

[27] A.C. Lua, H.Y. Wang, Applied Catalysis B: Environmental, 156-157 (2014) 84-93.

[28] A. Glisenti, M. Pacella, M. Guiotto, M.M. Natile, P. Canu, Applied Catalysis B: Environmental, 180 (2015) 94-105.

[29] N. Tien-Thao, H. Alamdari, S. Kaliaguine, Journal of Solid State Chemistry, 181 (2008) 2006-2019.

[30] J. Sun, S. Wan, F. Wang, J. Lin, Y. Wang, Industrial & Engineering Chemistry Research, 54 (2015) 7841-7851.

[31] M. Ding, J. Tu, M. Qiu, T. Wang, L. Ma, Y. Li, Applied Energy, 138 (2015) 584-589.

[32] W. Mross, Catalysis Reviews Science and Engineering, 25 (1983) 591-637.

[33] N. Tien-Thao, M.H. Zahedi-Niaki, H. Alamdari, S. Kaliaguine, Applied Catalysis A: General, 326 (2007) 152-163.

[34] M. Gupta, M.L. Smith, J.J. Spivey, ACS Catalysis, 1 (2011) 641-656.

[35] Y. Liu, C. Liu, C. Li, W. Huang, Catalysis Communications, 76 (2016) 29-32.

[36] P. Chaumette, P. Courty, Topics in Catalysis, 2 (1995) 117-126.

[37] X. Xu, E.B.M. Doesburg, J.J.F.Scholten, Catalysis Today, 2 (1987) 125-170.

[38] V.R. Surisetty, J. Kozinski, A.K. Dalai, International Journal of Chemical Reactor Engineering, 9 (2011) 1-18.

Chapter 7 Conclusions and Recommendations

7.1 Introduction

This chapter summarizes the key findings from this PhD research study. The work carried out in this thesis dealt with the catalytic conversion of syngas into higher alcohols over perovskite catalysts. The main focus has been on the development of a series of $LaCoO_3$ based perovskite catalysts to improve the activity and selectivity towards higher alcohols. Firstly, this research reported the role of strontium in Fischer-Tropsch (F-T) catalysts for the first time. Secondly, the effect of nickel substitution on the B site of $LaCoO_3$ perovskite catalyst for higher alcohol synthesis from syngas (HAS) was investigated. Thirdly, alkali promoted tri-metallic Co-Ni-Cu-based perovskite oxides were used as catalysts for HAS from syngas. The effect of alkali promoters and reaction conditions were studied carefully, and catalytic stability tests were carried out over the selected catalyst. In parallel, fundamental understanding of the perovskite structure and properties were achieved in this study, which is of great importance for the enhancement of catalytic performance for HAS. In addition, based on the conclusions from this research, several recommendations are suggested for future work to improve the knowledge in this research area.

7.2 Conclusions

Perovskites (ABO_3) are excellent catalyst precursor structures for HAS from syngas, as they can be easily formed by precipitation method. This makes perovskites suitable for catalyst development research, as accurate and specific catalyst design and preparation can be performed by changing and/or substitution of A and B site easily. As a consequence, the activities of many metals can be tested as active centres for HAS.

7.2.1 Perovskite Catalysts Structure and Characteristics

- Perovskite structure led to a good dispersion of active centres on the surface of the catalyst after reduction, so that it improved the activities of the catalyst significantly.

- Partial substitution at the A and B sites of the perovskite catalysts had different effects on the perovskite structure of $La_{1-x}Sr_xCo_{1-y}Ni_yO_3$.
    - At the A site, increasing the partial substitution level of lanthanum with larger strontium element (x>0.1) distorted the rhombohedral perovskite structure and led to a less stable cubic symmetry, which in turn promoted the catalyst reducibility.
    - However, the substitution of cobalt by nickel at the B site had less effect on the perovskite structure due to their smaller atomic radius. What's more, only a limited amount of nickel ions can enter into the perovskite structure. With higher nickel substitution level (x=0.5), metallic nickel also formed and existed outside of the perovskite framework.

7.2.2 $La_{1-x}Sr_xCo_{1-y-z}Ni_yCu_zO_3$ Perovskite Activity in HAS

- Substitution at the A site improved syngas conversion, but the effect on higher alcohol selectivity could not be observed. In contrast, the substitution at the B site was effective in improving higher alcohol production.
- Partial substitution at the B site of cobalt by nickel and copper promoted the formation of bi- and tri-metal active centres after reduction. Higher alcohol selectivity of the multi-metal catalysts was much higher than that of mono-metal. Synergistic effects of the metals in bi-metal alloy were responsible for the targeted product selectivity improvement.
- The catalytic activity of perovskites was very sensitive to the substitution level of the A and B site. It was found in this work that a low substitution of A and B site led to a positive effect in HAS, but beyond a limit, a reverse effect occurred.
    - Strontium substitution level at the A site has an inverse effect on F-T synthesis over $La_{1-x}Sr_xCoO_3$ perovskite catalysts: at low strontium substitution level (x = 0.1), the catalytic activity in the F-T reaction was improved compared to un-substituted $LaCoO_3$ perovskite due to the improvement in reducibility. At high strontium substitution levels ($x \geq 0.2$), the catalytic activity of $La_{1-x}Sr_xCoO_3$ perovskites decreased because of the negative effect on Co^0 active site dispersion and

sintering, as well as the formation of inactive $SrCO_3$ during the reaction.

- Due to the highly dispersed bimetallic Co-Ni alloy and the lower concentration of extra-lattice metallic nickel, the $La_{0.9}Sr_{0.1}Co_{0.9}Ni_{0.1}O_3$ catalyst showed the highest selectivity toward the higher alcohol formation.

- Alkali metals, which are the important promoters for higher alcohol catalysts, can be introduced into the perovskite catalysts easily.
  - Potassium showed an excellent effect not only on alcohol selectivity but also on the catalyst stability, by preventing catalyst deactivation and protecting the Co-Ni-Cu alloy during the reaction.
- The optimal temperature for HAS from syngas is between 310°C and 320°C for multi-metal Co-Ni and Co-Ni-Cu catalysts. This temperature is slightly higher than that of the traditional temperature of F-T synthesis for HAS (between 270°C and 290°C). The higher alcohol formation occurs in a very narrow reaction temperature range.

7.3 Recommendations

On the basis of the outcome of this PhD project, the following future research is suggested to close the research gaps in this area:

1. It has been proved in Chapter 5 and 6 that the synergistic effect of multi-metal is the key factor for HAS from syngas. According to previous literature on HAS and the effect of some metal elements (see Chapter 2, Section 2.4), future work on the effects of metal elements such as iron, manganese and molybdenum in the B site of $LaCoO_3$ based perovskites could be envisaged to improve the targeted products selectivity .
2. Multi-metal catalysts should be excellent candidates for the HAS process, but this complicated class of catalyst might suffer from catalyst deactivation. Thus, a precise research on catalyst reduction, induction period (catalyst stabilisation time) and promoter for this catalyst should be performed.
3. According to HAS process review, catalyst activity and selectivity are very much dependent on the catalyst support and surface area, to promote the distribution of the active centres and influences the interaction between active

elements and support. As perovskites have very low surface area, they could benefit from being supported, thus improving the overall surface area of the perovskite catalyst and their activity and selectivity towards higher alcohols. Further research is needed to investigate different kinds of supports such as alumina and carbon nanotubes for perovskite catalysts for HAS from syngas. Another option would be to introduce a templating agent during the perovskite synthesis process which could also be a means to increase surface area.

4. The kinetic study of the HAS process is very important because it is not only essential for optimizing reaction parameters, but also a prerequisite for the industrial practice. However, few works have been reported in detail to model the kinetics of this reaction system. Therefore, the next important step would be to study the kinetics of HAS from syngas over perovskite catalysts prepared in this thesis.
5. The characterisation techniques used in the study, while useful and insightful, were very standard. Greater depth in understanding the material, both before and after reaction, could be gained by utilising additional characterisation techniques such as TPD (with selected probe molecules), XPS, HR-TEM (including elemental mapping) and perhaps others. They could provide a more complete picture and lend further support to some of the conclusions regarding the catalyst (and the changes it undergoes) itself.
6. To this date, there is no suitable and well proven theory available for catalyst design, with all results mainly based on empirical work, resulting in long catalyst development time. Thus fundamental knowledge on reaction mechanism and synergistic effect of the metals in multi-metals catalysts should be improved to shorten catalyst development time.

Appendix Copyright Permission Statements

A. Chapter 4, reprinted with permission from (Min Ao, Gia Hung Pham, Valérie Sage, Vishnu Pareek, Structure and activity of strontium substituted $LaCoO_3$ perovskite catalysts for syngas conversion. *Journal of Molecular Catalysis A: Chemical* 2016, 416, 96–104.)

ELSEVIER LICENSE TERMS AND CONDITIONS

Mar 29, 2017

This Agreement between Min Ao ("You") and Elsevier ("Elsevier") consists of your license details and the terms and conditions provided by Elsevier and Copyright Clearance Center.

License Number	4072890212364
License date	Mar 20, 2017
Licensed Content Publisher	Elsevier
Licensed Content Publication	Journal of Molecular Catalysis A: Chemical
Licensed Content Title	Structure and activity of strontium substituted LaCoO3 perovskite catalysts for syngas conversion
Licensed Content Author	Min Ao,Gia Hung Pham,Valérie Sage,Vishnu Pareek
Licensed Content Date	15 May 2016
Licensed Content Volume	416
Licensed Content Issue	n/a
Licensed Content Pages	9
Start Page	96
End Page	104
Type of Use	reuse in a thesis/dissertation
Intended publisher of new work	other
Portion	full article
Format	both print and electronic
Are you the author of this Elsevier article?	Yes
Will you be translating?	No
Order reference number	
Title of your thesis/dissertation	Catalyst Development for Higher Alcohol Synthesis (HAS)
Expected completion date	Jan 2017
Estimated size (number of pages)	160
Elsevier VAT number	GB 494 6272 12
Requestor Location	Min Ao 23 copeland drive,redcliffe Perth, WA 6104 Australia Attn: Min Ao
Total	**0.00 AUD**
Terms and Conditions	

B. Chapter 5, reprinted with permission from (Min Ao, Gia Hung Pham, Valérie Sage, Vishnu Pareek, Selectivity enhancement for higher alcohol product in Fischer-Tropsch synthesis over nickel-substituted $La_{0.9}Sr_{0.1}CoO_3$ perovskite catalysts. *Fuel* 2017, 206, 390–400.)

Copyright Clearance Center RightsLink®

Home | Account Info | Help

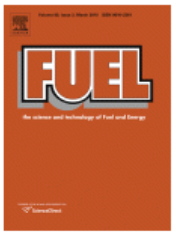

Title: Selectivity enhancement for higher alcohol product in Fischer-Tropsch synthesis over nickel-substituted La0.9Sr0.1CoO3 perovskite catalysts

Author: Min Ao,Gia Hung Pham,Valérie Sage,Vishnu Pareek

Publication: Fuel

Publisher: Elsevier

Date: 15 October 2017

Logged in as:
Min Ao
Account #:
3001085636
LOGOUT

Order Completed

Thank you for your order.

This Agreement between Min Ao ("You") and Elsevier ("Elsevier") consists of your license details and the terms and conditions provided by Elsevier and Copyright Clearance Center.

Your confirmation email will contain your order number for future reference.

Printable details.

License Number	4138641306140
License date	Jun 30, 2017
Licensed Content Publisher	Elsevier
Licensed Content Publication	Fuel
Licensed Content Title	Selectivity enhancement for higher alcohol product in Fischer-Tropsch synthesis over nickel-substituted La0.9Sr0.1CoO3 perovskite catalysts
Licensed Content Author	Min Ao,Gia Hung Pham,Valérie Sage,Vishnu Pareek
Licensed Content Date	Oct 15, 2017
Licensed Content Volume	206
Licensed Content Issue	n/a
Licensed Content Pages	11
Type of Use	reuse in a thesis/dissertation
Portion	full article
Format	both print and electronic
Are you the author of this Elsevier article?	Yes
Will you be translating?	No
Order reference number	
Title of your thesis/dissertation	Catalyst Development for Higher Alcohol Synthesis (HAS)
Expected completion date	Jan 2017
Estimated size (number of pages)	160
Elsevier VAT number	GB 494 6272 12
Requestor Location	Min Ao 23 copeland drive,redcliffe Perth, WA 6104 Australia Attn: Min Ao
Total	0.00 AUD